AD NUMBER

AD894675

LIMITATION CHANGES

TO:

Approved for public release; distribution is unlimited.

FROM:

Distribution authorized to U.S. Gov't. agencies only; Test and Evaluation; FEB 1972. Other requests shall be referred to Air Force Aero Propulsion Lab., Wright-Patterson AFB, OH 45433.

AUTHORITY

AFRPL ltr 3o Jun 1975

AFAPL-TR-72-4

INVESTIGATION OF COMBUSTION INSTABILITY IN A TURBOFAN MIXED-FLOW AUGMENTOR

George E. Smith
NORTHERN RESEARCH AND ENGINEERING CORPORATION
and
Robert E. Henderson
AIR FORCE AERO PROPULSION LABORATORY

TECHNICAL REPORT AFAPL-TR-72-4

April 1972

Air Force Aero Propulsion Laboratory
Air Force Systems Command
Wright-Patterson Air Force Base, Ohio 45433

NOTICE

When Government drawings, specifications, or other data are used for any purpose other than in connection with a definitely related Government procurement operation, the United States Government thereby incurs no responsibility nor any obligation whatsoever; and the fact that the government may have formulated, furnished, or in any way supplied the said drawings, specifications, or other data, is not to be regarded by implication or otherwise as in any manner licensing the holder or any other person or corporation, or conveying any rights or permission to manufacture, use, or sell any patented invention that may in any way be related thereto.

Copies of this report should not be returned unless return is required by security considerations, contractual obligations, or notice on a specific document.

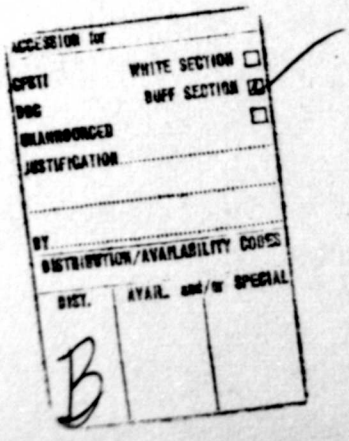

(18) (19) AFAPL-TR-72-4

(6) # INVESTIGATION OF COMBUSTION INSTABILITY IN A TURBOFAN MIXED-FLOW AUGMENTOR.

(10) George E./Smith Robert E./Henderson

(9) Final technical rept. 30 Jun 70-31 Dec 71,

(11) Apr 72 (12) 219p. (14) NREC-1161-1

(15) F33615-70-C-1669

(16) AF-3066 (17) 306605

1473

260 350

mt

FOREWORD

This report describes work accomplished in the program, "Mixed-Flow Augmentor Stability Investigation", conducted under USAF Contract F33615-70-C-1669, Project 3066, Task 306605. The work was accomplished in the period from 30 June 1970 to 31 December 1971 by Northern Research and Engineering Corporation; the experimental part of the program was conducted in-house by the Air Force Aero Propulsion Laboratory under the direction of Mr. R. E. Henderson, TBC. The report was submitted on 31 December 1971.

The program was sponsored by the Air Force Aero Propulsion Laboratory, Wright-Patterson Air Force Base, Ohio. Lt. Michael G. Johnson, TBC, Turbine Engine Division, was the Project Engineer. The program was initiated with FY 1970 Aero Propulsion Laboratory Director's Funds.

Publication of this report does not constitute Air Force approval of the report's findings or conclusions. It is published only for the exchange and stimulation of ideas.

Ernest C. Simpson
Director, Turbine Engine Division

ABSTRACT

An analytical and experimental investigation was conducted of combustion instability in a TF-30-P1 augmentor. A sustained oscillation was observed with a fuel zone combination which does not occur during normal engine operation. On cold days oscillation amplitudes above 35 per cent (peak-to-mean) were observed, but on hot days the amplitudes dropped below 10 per cent. NREC's previously developed combustion instability model correctly predicted an instability with the same frequency as that observed. Once the individual zones of combustion of the TF-30-P1 augmentor were modelled properly, the analysis correctly indicated the fuel zone combination during which the oscillation becomes most severe. The analytical model also correctly predicted the trends which were observed when engine geometry was modified, when AVGAS replaced JP-4, and when the engine inlet temperature was low. But to correlate predicted and observed amplitude levels, a stabilizing turbulent mixing effect had to be hypothesized to supplement the droplet vaporization effects which excite the instability.

TABLE OF CONTENTS

TABLE OF CONTENTS (CONTINUED)

TABLE OF CONTENTS (CONTINUED)

TABLE OF CONTENTS (CONTINUED)

LIST OF ILLUSTRATIONS

LIST OF ILLUSTRATIONS (CONTINUED)

LIST OF ILLUSTRATIONS (CONTINUED)

LIST OF TABLES

LIST OF ABBREVIATIONS AND SYMBOLS

Symbol	Description
A	Boundary acoustic admittance ratio
a	Fraction of fuel remaining in droplet form at the flame-front
b	Fraction of design combustion time not taken up by droplet evaporation
C_o	Sonic velocity
$\tilde{C}_1$	Coefficient relating $T'/\bar{T}$ to $P'/\bar{P}$
$\tilde{C}_3$	Coefficient relating $E'/\bar{E}$ to $P'/\bar{P}$
$\tilde{C}_4$	Coefficient relating $E'/\bar{E}$ to $(\mu'/\bar{\mu})_{INJECTOR}$
$\tilde{C}_5$	Coefficient relating $E'/\bar{E}$ to $(P'/\bar{P})_{INJECTOR}$
$\tilde{C}_6$	Coefficient relating $T'/\bar{T}$ to $(\mu'/\bar{\mu})_{FLAMEHOLDER}$
$\tilde{C}_7$	Coefficient relating mean droplet evaporation time to mean evaporation time without fluid oscillations
E	Energy content of the fluid, per unit mass, at the flame-front
F_n	Radial component of acoustic mode shape
F_y	Axial component of acoustic mode shape
F_θ	Tangential component of acoustic mode shape
f_o	"Acoustic" frequency, without flow and unsteady combustion
f	Frequency
h	Function defining effects of unsteady combustion, through-flow and special boundary losses
j	$\sqrt{-1}$
k_i	Wave number in Chamber
k	Constant

Symbol	Description
M	Mach number
$\dot{m}_f$	Fuel flow rate
P	Pressure
q_c	Heat of combustion
R_o	Outer radius of augmentor
Re_d'	Droplet Reynolds number based on sonic velocity
r	Nondimensionalized radius: R/R_o
T	Temperature
t	Time
U'	Function defining through-flow effects
u	Velocity
w_c	Heat release rate per unit volume
x	Nondimensionalized axial distance (with respect to R_o)
Θ'	Function defining special boundary effects
γ	Ratio of specific heats
δ	Logarithmic decrement of mode
η	Peak-to-mean pressure ratio:
θ	Circumferential variable
ρ	Fluid density
τ	Characteristic time of combustion
ω	Angular velocity of oscillation

Subscripts

a	Pertaining to outer boundary
b	Pertaining to inner boundary
c	Pertaining to chemical kinetics

Subscripts	Description
d	Designates combustion without fluid oscillations
c	Pertaining to droplet evaporation
c_o	Pertaining to droplet evaporation without fluid oscillations
fh	Designates flameholder position
ℓ	Pertaining to nozzle boundary
o	Pertaining to upstream boundary
T	Pertaining to turbulent mixing
Superscripts	
η	Designates a fuel zone
$'$	Designates oscillatory component
$\bar{}$	Designates mean component
$\hat{}$	Designates complex conjugation

CHAPTER I

INTRODUCTION

BACKGROUND

NREC, under contract to the USAF Aero Propulsion Laboratory, first studied combustion instability in aircraft engine augmentors as part of a more general issue: what unsteady flow phenomena, intrinsic to turbojet and turbofan components, tend to initiate engine surges? Combustion instability appears as a sustained pressure oscillation in augmentors; physically it is an acoustic resonance driven by a small fraction of energy from the heat release process. Acoustically treated liners have conventionally been used to suppress such oscillations to levels below those causing mechanical damage to the tailpipe. In the case of turbofans the oscillations can impinge on the fan, thus potentially leading to a fan/compressor surge margin smaller than that of the fan/compressor tested without the augmentor. NREC approached the problem of analytically modelling combustion instability with several questions in mind:

1. What factors contribute to increasing the amplitude of the sustained oscillations?

2. Is suppression from liners sufficient to eliminate the need for integrated fan-augmentor design?

3. Are there circumstances in which combustion instability is masked in ground testing, only to emerge in some extreme flight condition?

The goal was not simply to develop an analytical model providing insights into these questions. The long-range goal was the more ambitious one of an analytical tool which permits more effective elimination or control of augmentor instability as a mechanism which limits the flight envelope of aircraft engines.

The approach taken to modelling combustion instability began with a thorough review of the analytical and experimental research in liquid rocket engine instability (Reference 1). Based on this review, an analytical model was formulated which satisfied three engineering requirements:

1. The model was mathematically simple enough to be tractable, but not so simple as to preclude development toward greater detail.

2. The model, at least in principle, recognized all effects thought to be pertinent to augmentor instability; but all parameters were strictly physically interpretable.

3. The model formally predicted sustained oscillation amplitudes, so that the practical questions of residual oscillation amplitudes and of instabilities requiring large initial disturbances could be examined.

The model was formally developed in the first year of NREC's effort, and a computer program producing numerical results was written in the second year (References 2 and 3). A summary of the model is given in Appendix VIII below.

A parametric study of two conventional turbojet afterburners was the final step in NREC's initial study of augmentor instability. The results of the study (reported in References 2, 3, and 4) confirmed the qualitative validity of the analytical model in that trends predicted were consistent with trends observed. The parametric study had the further benefit of indicating which among the model parameters tended to have the most dramatic effects on the predicted oscillation amplitudes. The chief limitations of this parametric study stemmed first from the limited instability information available for the two afterburners and second from the somewhat dated straight turbojet afterburner designs. In particular, no data were available on oscillation amplitudes in either afterburner, not to mention data on the trends the instability displayed with design variations (other than perforated liners). Equally restrictive was the failure of the parametric study to consider augmented turbofan configurations which are typical of current aircraft designs. Given these shortcomings of the scope of the original parametric study, it was only logical to recommend a joint experimental and analytical study of a mixed-flow augmentor configuration like that of the TF-30, the only augmented turbofan engine currently operational in the USAF. The spirit in which this study was undertaken was very much a continuation of that of the original parametric study: having formulated a model, the first thing to do before making it more complicated is to establish its essential consistency with the facts.

Very little augmentor combustion instability experience has found its way into the literature since acoustic liners were discovered to be an adequate fix against mechanical failures. As a result, the original parametric evaluation of the model was necessarily limited to gross qualitative trends. The current analytical study of the TF-30 was initially suggested to parallel an experimental program conducted by NASA-Lewis on the TF-30-P3 engine. Unfortunately no sustained instabilities were successfully initiated in the NASA tests. In the meantime the Aero Propulsion Laboratory initiated tests on a TF-30-P1, the original engine of the F-111A. The engine tested at APL did exhibit clear instabilities so that data correlation with analytical predictions became possible.

PROBLEM STATEMENT

NREC's combustion instability analysis is in two steps: an acoustics analysis of the augmentor duct defines three-dimensional resonant mode shapes (Program HLMHLT); the energy supplied to and extracted from these modes by the heat release process, by the through-flow, and by screech liners is then calculated (Program REFINE). The self-sustaining amplitude is finally determined when the energy supplied to and extracted from an acoustic mode is in equilibrium. The distribution of the resonant acoustic wave in the augmentor duct is physically altered by the unsteady heat release, by the through-flow, and by absorption at the liners. The NREC

analysis does not currently take into consideration the fact that the natural acoustic mode becomes distorted. The analysis instead assumes that the purely acoustic mode shape is an acceptable approximation to the unstable mode shape. In principle, the analysis can be extended to allow for higher order approximations of the unstable mode shape, but this added complexity has yet to be justified. Other simplifications in the analysis, both in the acoustics and in the instability parts, may well merit critical attention.

THE ACOUSTICS ANALYSIS

The acoustics analysis requires a rather idealized representation of augmentor ducts. The analysis recognizes only purely annular and cylindrical ducts. The duct is divided into two chambers by a flame-front. In each chamber the sonic velocity is uniform, but a step change in sonic velocity at the flame-front is accounted for. Thus schematically HLMHLT can recognize only the following model of an augmentor:

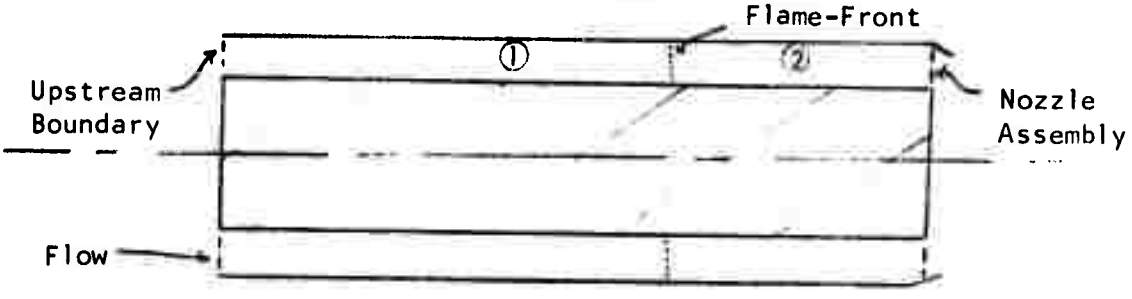

HLMHLT also handles the special case in which the inner radius of the annulus becomes zero.

A turbofan mixed-flow augmentor does not lend itself readily to the HLMHLT restrictions. Using the same reasoning which led to a two-chamber model of conventional afterburners, a mixed-flow augmentor would appear to involve four chambers-- four regions in which the sonic velocity assumes distinctive values:

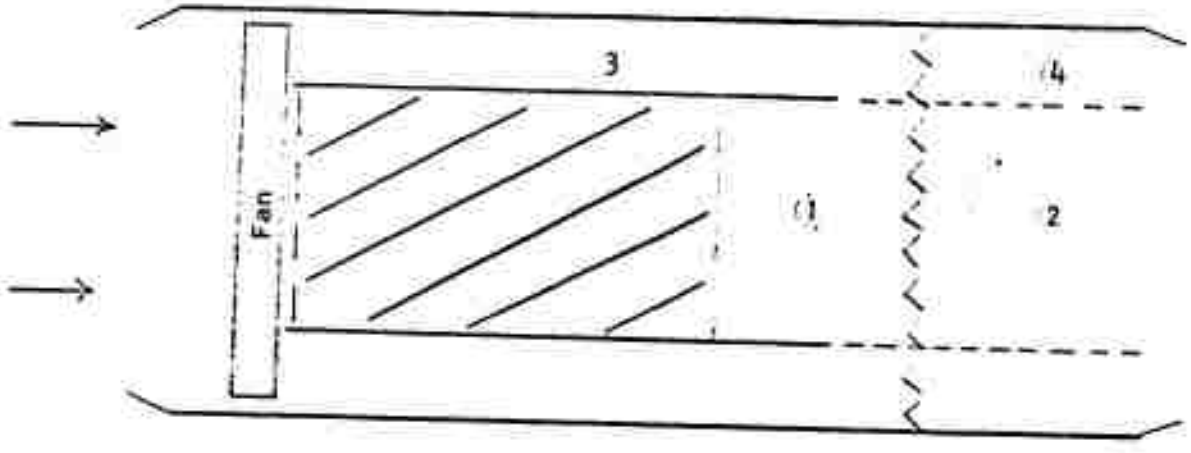

The turbine and fan discharge streams (Chambers 1 and 3 in the sketch) have quite disparate sonic velocities; the two combustion chambers can have marked differences when the augmentor is operating with most of the fuel being injected into the fan or the turbine stream.

The first basic question addressed in the TF-30 augmentor analysis concerns the proper acoustics analysis of mixed-flow ducts. Four alternatives suggest themselves:

1. Model the mixed-flow afterburner as a conventional cylindrical afterburner with an unusual upstream boundary located at the turbine discharge:

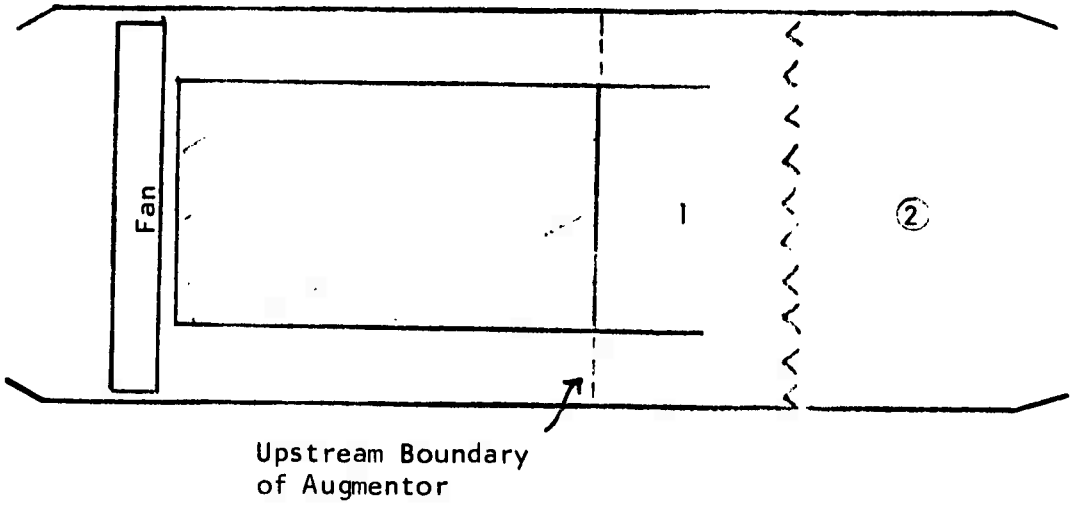

The sonic velocities assumed in Chambers 1 and 2 represent averages of the core and fan streams. The upstream boundary admittance represents an average of the open fan duct and of the turbine choked nozzles.

2. Model the mixed-flow afterburner as a conventional ductburner with an unusual inner boundary:

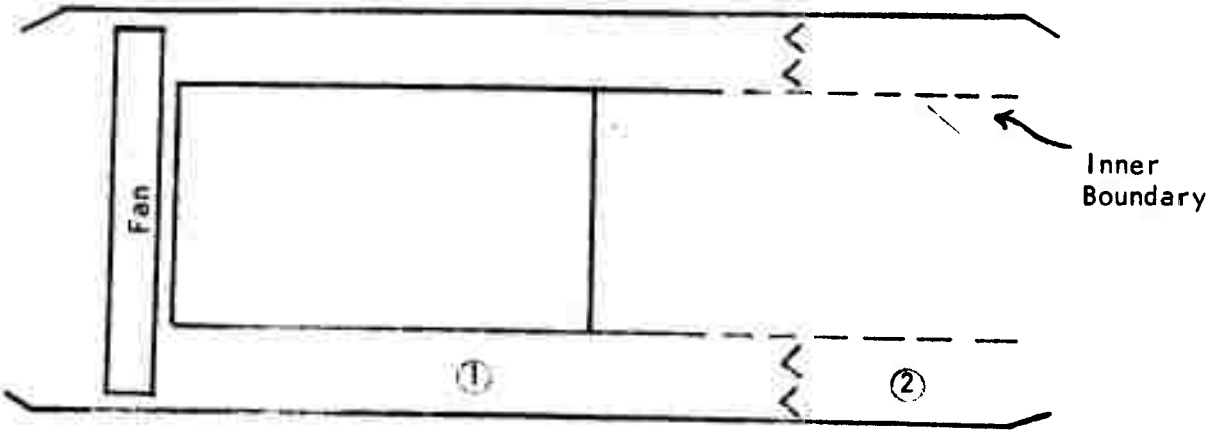

The fan stream is simply isolated from the core stream except for the boundary admittance ratio representing the inner boundary of the idealized ductburner.

3. Treat the core augmentor as a cylindrical afterburner and the fan augmentor as an annular ductburner, and match the solutions along the common interface between the two streams. This approach is not practical with the current Programs HLMHLT and REFINE since the cost of a single solution will increase by about a factor of 10.

4. Write a new acoustics analysis computer program which is capable of treating a four-chamber augmentor duct.

Obviously, the last two alternatives represent a major effort and hence are not warranted until results from the current analysis indicate a need for such refinements. The first basic question of the present study was to decide whether either (or both) of the first two alternatives provide adequate results for mixed-flow augmentors. To put the matter differently, the issue is the best way to use HLMHLT, as presently constituted, to analyze mixed-flow augmentor acoustics.

THE COMBUSTION ANALYSIS

While all of the parameters used in the steady and unsteady heat release analyses are, strictly speaking, physically identifiable, precise numerical values for some of the parameters remain unclear. In the earlier parametric study (cf. Reference 3) estimated input values for these more elusive parameters were used, but the lack of data on the instabilities in the afterburner precluded any evaluation or refinement of these estimates. Ideally what is needed in order to gain a clearer understanding of the input values is a comparison between predicted and observed oscillation amplitudes over a continuous range of augmentor operating conditions. While such a comparison between analysis and experiment is unlikely to resolve all questions pertaining to the combustion model input, it will at least identify which among the input parameters require the most attention in future research. Thus the second basic question in the study of the TF-30 concerns the determination of input values for the heat release parameters. A parametric study of the TF-30, in conjunction with a test program making corresponding changes to the engine, should indicate what input values are needed to correlate analytical and experimental trends.

A review of NREC's earlier parametric study will quickly indicate model parameters for which no clear-cut rules are established for calculating values (see Appendix VIII). The most important of these are indicated below:

1. $\bar{\tau}$, the mean time required for combustion, is known to depend on chemical kinetic, turbulent mixing, and fuel droplet evaporation and burning mechanisms. The mean time is also known to decrease as oscillation amplitudes increase. The relative contributions of

the various mechanisms and their individual variation with oscillation amplitude is not so clear. Moreover, $\bar{\tau}$ is a scalar quantity, representing an "average" combustion time across the normal flow area. In the case of a mixed-flow augmentor the combustion processes in the fan and core streams can be sufficiently distinct that choosing a value for $\bar{\tau}$ is problematic.

2. Coefficients ($\tilde{C}_1$ and $\tilde{C}_6$) which relate oscillations in the time required for combustion to oscillations in pressure and velocity again depend on chemical kinetic, turbulent mixing, and fuel droplet evaporation and burning mechanisms. The comments made above on $\bar{\tau}$ are equally pertinent here.

3. The radial variation of the mean energy content of the fluid ($\bar{E}$) at the flameholder plane obviously depends on the fuel injection system and on the flow pattern between the injectors and the flameholders. The unsteady heat release distribution is sensitive to variations of $\bar{E}$, but without test data it remains unclear how to define $\bar{E}$, given only the fuel flow rates in each injector spray ring.

4. Fluctuations in the energy content of the fluid at the flameholder plane (E') are caused by pressure and velocity fluctuations at the injectors and in the region between the injectors and the flameholders. The amount of fuel which is vaporized upon injection and the fluctuations in the radial distribution of the fuel-air ratio are difficult to define.

5. The combustion instability analysis treats the flameholder assembly only in a highly idealized fashion: a single plane is identified as the flame-front, downstream of which the heat release rate decays exponentially along the length of the augmentor. Provision is made for acoustic energy loss across the flameholders, but this option was ignored in the earlier parametric studies. Given a complicated flameholder assembly, the question of where to define the flame-front in the combustion instability analyses remains open to debate.

6. The parametric study of the two conventional afterburners indicated some potentially dramatic effects of the acoustically treated liners. In one afterburner the residual oscillation amplitude after suppression was predicted to be above 8 per cent; in the other afterburner the liner tended to mask one unstable mode by increasing the threshold level needed to initiate it without reducing the resulting sustained amplitude. While these results are potentially of great engineering interest, they remain conjectural pending supportive experimental evidence. Thus the suppression effectiveness of the liners remains a topic requiring further attention.

All of these parameters require further investigation in conjunction with more thorough experimental data.

THE EFFECTS OF INLET DISTORTION

The previous parametric study of two conventional afterburners indicated that circumferential variations of the fuel distribution in an axisymmetric flow field had minor effects on the self-sustaining amplitudes of unstable modes. For a first tangential mode only a 1 per rev type fuel distortion will have any consequence. The effects of a steady circumferential flow distortion transmitted from the inlet into the augmentor by the fan were not investigated. Since steady inlet distortion is a necessary by-product of flight maneuvers of many airplanes (e.g., F-111A), the sensitivity of augmentor instability to non-axisymmetric flow fields is an issue requiring attention. The third basic question of the current TF-30 study concerns the effects of engine inlet distortion. Unfortunately, the failure to obtain combustion instability data with inlet distortion ultimately eliminated this question from the study. Data could not be obtained because of repeated engine surges encountered when attempting augmentation with distortion screens placed in the inlet.

THE DEVELOPMENT OF TEST EXPERIENCE

While the aircraft engine companies have doubtlessly gained much experience in experimental determination of combustion instability in augmentors, very little information of recent origin is available in the literature. In particular, test experience in which oscillation amplitudes are monitored over a continuous range of augmentor operation has simply not been described in the literature. Thus the fourth basic question of the TF-30 study concerns the effective generation and analysis of augmentor instability amplitude data. This question dominated the Aero Propulsion Laboratory's effort in the program.

SUMMARY OF PROGRAM OBJECTIVES

The study of combustion instability in the TF-30 augmentor represented a direct, logical extension of NREC's earlier study of two conventional turbojet afterburners. The current program differed sallently from the former on two counts: first, the augmentor studied is of recent design and from a turbofan engine; second, an experimental program paralleled the analytical study. The objectives of the current study were as follows:

1. Establish the most effective use of NREC's analytical model for evaluating combustion instability amplitudes in mixed-flow augmentors.

2. Develop improved procedures for calculating values of the parameters used in the combustion instability model by conducting a parametric study and correlating the analytical results with experimental data.

3. Use the model to determine the effects of engine inlet distortion on combustion instability.

4. Establish engine test and data reduction procedures for obtaining combustion instability amplitude data to be used in conjunction with NREC's analytical model.

Only the third objective was abandoned as a consequence of repeated engine surges whenever testing the augmentor with engine inlet distortion.

PROGRAM ORGANIZATION

TEST PROGRAM

A TF-30-P1 was tested in-house by the Aero Propulsion Laboratory. A test matrix involving ten engine test "configurations" was developed by allowing for the following variations:

1. Alternate screech liners.
2. Alternate flameholders.
3. AVGAS as well as JP-4 fuel.
4. Engine inlet with and without distortion screens.

High response pressure oscillation data were obtained for most of these test "configurations" with a variety of fuel zones in operation (including fuel zone combinations which do not occur in normal engine operation). The high response data was put through a spectral density analysis to identify the principal frequencies in the sustained oscillations. Climatic conditions over the period of the engine testing happened to introduce an additional parameter which proved unusually salient, namely engine inlet temperature.

ANALYTICAL PROGRAM

The analytical study was divided into three basic tasks, each of which was further subdivided into an initial analysis subtask and a correlation with experimental data subtask. The three tasks were as follows:

Task I: Mixed-Flow Augmentor Analysis

Task II: Evaluation of Model Parameters

Task III: Evaluation of Inlet Distortion Effects

The third task was eliminated from the program because of the inability to obtain relevant test data.

The first task involved a thorough analysis of the combustion instability characteristics of the nominal design of the TF-30 augmentor.

Ten acoustic modes were examined at five different augmentor fuel zone operating conditions. The complete analysis was conducted using both a cylindrical afterburner and an annular ductburner model of the mixed-flow configuration. The objective of the task was to identify how NREC's combustion instability analysis should be adapted to mixed-flow augmentors. Correlation of analytically predicted with observed oscillation frequencies and amplitudes provided the basis for meeting this objective.

The second task involved a parametric examination of the TF-30 augmentor. Variations considered included the flameholder design, the screech liner, the fuel used, the augmentor inlet temperature, and the fuel flow rate and distribution. Attention in the parametric study centered on those acoustic modes found to be most significant during Task I. The objective of the second task was to clarify the numerical values of the parameters in the NREC model. Again correlation of analytical and experimental oscillation amplitudes provided the basis for evaluating how the parameters in the model are best treated.

CONTENTS OF THE REPORT

The remainder of the main body of the technical report consists of three major chapters. Chapter III describes the TF-30 test program and the augmentor instability results; Chapter IV describes the basic analytical study of the augmentor (Task I above); Chapter V describes the parametric study of the augmentor. The main body ends with a chapter summarizing conclusions and recommendations from the study.

The report includes ten appendices. The first five provide details on the TF-30-P1, its augmentor components, and the modelling of its geometry, through-flow, and combustion. The sixth and seventh appendices give background on the instrumentation and data reduction used in the test program. The eighth appendix reviews NREC's instability model, with particular attention given to unsteady combustion inputs. The ninth appendix describes modifications and corrections to Programs HLMHLT and REFINE, and the tenth appendix provides up-to-date listings of the Fortran source decks of the two programs.

CHAPTER II

SUMMARY

This report describes an experimental program, conducted by the USAF Aero Propulsion Laboratory, and an analytical program, conducted by Northern Research and Engineering Corporation, on the combustion instability characteristics of mixed-flow augmentors, using the TF-30-P1 as a test vehicle. The study is a logical outgrowth of previous APL-sponsored, NREC studies of analytical models of augmentor instability.

The TF-30-P1 was tested at APL. Its augmentor was instrumented with high response Kistler transducers to monitor pressure oscillations at the liner. Several configuration changes were tested, including a blocked screech liner, an alternate flameholder, some blocked fuel zones, and an alternate fuel.

The test program revealed a clear oscillation at roughly 385 Hz, but the oscillation reaches significant amplitudes only when operating with a combination of fuel zones that does not occur during normal engine operation. Variations of the screech liner and the flameholder had negligible effects on the oscillation. Changing from JP-4 to AVGAS practically eliminated it. Variations of engine inlet temperature had the most dramatic effect: when testing on warm summer days, oscillation amplitudes remained below 10 per cent (peak-to-mean); on a cold spring day the amplitude was measured to be 37 per cent.

The analytical effort included first, an analysis of the nominal augmentor to determine how mixed-flow configurations are best approximated within NREC's previously developed instability model; and second, a parametric study of engine design variations to evaluate procedures for calculating some of the more elusive model parameters. In each part of the study NREC's combustion instability model was used to predict oscillation frequencies and amplitudes, and these predictions were then correlated with test data in order to refine the model input values.

The basic analysis of the augmentor correctly indicated its first tangential mode to be strongly unstable, with a frequency between 370 and 400 Hz. The initially predicted amplitude level was in excess of 25 per cent for warm day conditions. With proper modelling of the steady combustion characteristics of the five-zone augmentor, the analysis correctly identified the fuel zone combination during which the oscillation is most severe. The good correlation of predictions with data authorized the conclusion that the observed instability is driven by droplet vaporization and burning mechanisms in the fan stream.

The parametric study correctly predicted the negligible effects of the liner and flameholder modifications, as well as the elimination of the instability when AVGAS is substituted for JP-4. The trend toward more severe instability on cold days was also qualitatively predicted. However, to correlate the predicted and the observed amplitude differences on warm and

cold days, it was necessary to hypothesize a turbulent mixing effect which tends to stabilize the oscillation.

The over-all study provided the first empirical confirmation of NREC's engineering model of combustion instability. The study displayed the usefulness of the model as it stands, and it also showed that the model is likely to be more effective once better treatments of turbulent mixing and droplet mechanisms are developed via proper experiments.

CHAPTER III

TF-30-P1 AUGMENTOR TESTS

The analytical study of mixed-flow augmentor instability, described in Chapters IV and V, was supported with test data provided under an Air Force Aero Propulsion Laboratory (AFAPL) in-house test program. The test vehicle was a TF-30-P1 augmented turbofan engine, employing a mixed-flow type augmentor. A description of the engine is given in Appendix I. The specific engine tested had operated for 219 hours prior to this program, in which almost 80 additional hours were accumulated. The engine had flown in an F-111A aircraft.

The test program had some specific objectives to be satisfied in support of the analytical program. First, a crucial achievement was to establish a repeatable, sustained oscillation in the augmentor. Second, data were needed on how the sustained oscillation amplitude varies with different engine modifications (particularly fuel type, screech liner, and flameholder variations). Third, data were needed on how engine inlet distortion affected the instability characteristics of the augmentor, if at all. The test program had the additional objective of putting into the literature a description of the type of augmentor test procedures and instrumentation needed in support of NREC's analytical model.

The present chapter describes the basic results of the test program and offers general observations made during the test program relative to engine stability, performance, and general operating characteristics. Some additional details on the engine test configurations can be found in Appendices I through V, and the instrumentation and data reduction are described in detail in Appendices VI and VII, respectively.

ENGINE TEST CELL INSTALLATION

The test engine was installed in Test Stand "C" at the AFAPL. This stand is a ground level "U-type" stand. Air enters a large inlet plenum chamber room through the ceiling at one end of the cell. The engine was mounted on a 40,000 pound thrust stand at the center of this room, the exhaust of which was directed into a large water cooled ejector. Behind the ejector was an acoustically treated exhaust plenum which directed the cooled gases through the roof at the opposite end of the cell, thus the U-type airflow path. A schematic of this test cell is shown in Figure 1. No airflow preconditioning was made in this test cell.

In addition to various steady-state instrumentation which provided detailed information on engine operation, the augmentor was instrumented with six high response, Kistler Model 603L transducers which monitored the oscillatory component of the pressure at the outer diameter of the augmentor. The six high response transducers were located as follows:

1. Channels 1, 3, and 7 were located approximately in the plane of the vee-gutter flameholder at roughly 0, 90, and 135 degrees

around the circumference (in fact, at 14, 103, and 146 degrees).

2. Channels 2, 4, and 8 were located approximately 19 inches downstream of the first set, in the same circumferential positions respectively; this axial position coincides with the downstream end of the perforated screech liner.

These channel designations are used below in describing the data obtained.

Several times during the test program, recirculation of the test cell exhaust gases occurred. This phenomena is not uncommon with U-type test cells when the prevailing winds pass across the cell from exhaust to inlet. Of course, a condition such as this could not be tolerated during a record run. Re-ingestion of exhaust products resulted in wide fluctuations in engine performance and critical operating parameters. Recirculation could be easily monitored through the engine inlet temperature sensors which showed broad temperature excursions (as much as 30-40 deg F) during exhaust gas ingestion. When this condition was observed, the test was terminated.

TEST PLAN

A detailed test plan was established at the start of the program defining the matrix of augmentor test configurations and operating conditions to be examined during the program. A principal objective of this in-house program was to establish at least one controlled unstable operating condition within the augmentor and document its oscillatory activity using high response Kistler pressure instrumentation. The various test configurations and operating conditions defined in the test plan (Table I) were identified as potential approaches to establishing this unstable condition. The TF-30-P1 engine, although found to be sensitive at certain operating conditions, had a very stable afterburner system. The basic changes made to this augmentor in an attempt to alter its stability included:

1. Blocking 70 per cent of the conventional screech liner damping holes to eliminate or significantly reduce its damping characteristics.

2. Substituting a modified flameholder assembly for the conventional assembly.

3. Altering the fuel distribution characteristics of the augmentor fuel injection system.

4. Imposing flow distortion at the engine inlet using distortion screens.

5. Substituting Aviation Gasoline (AVGAS) for the conventional jet fuel-- JP-4.

The test plan matrix (Table I) distinguishes among ten engine test configurations in which the following distinctions dominate:

1. Tests 1 and 6 correspond to the nominal engine (with Test 1 using a blocked screech liner).

2. Tests 7 and 8 employed a modified flameholder.

3. Tests 9 and 10 used AVGAS.

4. Tests 2, 3, 4, and 5 employed circumferential distortion screens at the inlet of the engine.

The TF-30-P1 augmentor has five fuel injection zones, numbered in the sequence in which they become activated. Zones 1 and 5 are in the core stream, zones 3 and 4 are in the fan stream, and zone 2 employs a combined aerodynamic flameholder and premixed fuel-air-jet-injector near the outer diameter of the fan stream. Augmentor oscillation data were taken with two standard and four extraordinary fuel zone combinations:

1. Z4: all zones operating except zone 5 in the core stream.

2. Z5: max augmentation (all zones).

3. Z6: all zones except zone 2 at the outer diameter.

4. Z7: zone 1 in the core stream and zone 3 in the fan stream.

5. Z8MIN: zones 1 and 3 and minimal fuel from zone 4 in the fan stream.

6. Z8MAX: zones 1 and 3 and maximal fuel from zone 4 in the fan stream.

The details of the fuel zone combinations and the injector positions can be found in Appendix V. The fuel zone combinations other than Z4 and Z5 do not occur during normal engine operation. In the present study they have the effect of producing some unusual radial fuel distributions.

Because the test program extended from the spring to the summer of 1971, an additional test variable emerged as a result of changing climatic conditions, namely engine inlet temperature. Some of the most striking augmentor instability results were obtained in cold day tests in the early part of the test program. Subsequent attempts to repeat these tests at the end of the test program could not be carried through as a result of an engine failure.

ESTABLISHING AN AUGMENTOR INSTABILITY

Most of the configuration changes identified above had little effect on the stability of the augmentor. However, during a fuel redistribution test an audible screech was identified. First observation was made while examining the fuel zone condition Z8MAX. This condition initiated a 400 Hz

oscillation which was audible within the control room and caused an increase in the level of turbine vibration from 1.2 to 2.8 mils. This condition was subsequently verified by the high response pressure instrumentation installed in the afterburner case (see Appendix VI). Further substantiation was provided by high speed film taken with a Fastax camera installed in the exhaust ejector viewing into the afterburner through the engine exhaust nozzle.

The unstable operating condition described above was a controlled condition in that it did not achieve catastrophic proportions (often a result of severe combustion instability) and could be repeated at any time. Thus, a full detailed analysis of this instability could be accomplished.

A typical oscillograph trace of the pressure oscillation during the audible instability is shown in Figure 2. This record corresponds to the nominal engine (Test 6) at the Z8MAX fuel condition; the data is taken from Channel 4. A power spectral density analysis of this oscillation reveals (see Figure 3) a prominent spike at roughly 370 Hz, and a lesser spike at roughly 190 Hz. For simplicity these two prominent components of the oscillation will henceforth be referred to as the 400 Hz and the 200 Hz components, respectively. The power spectral density analysis indicates no other frequencies with large activity below 5000 Hz. In terms of peak-to-mean pressure oscillation amplitudes, the 400 Hz component of Figure 3 represents almost 7 per cent. By way of contrast, Figure 4 shows a PSD plot of the same channel in the same engine test, but for the Z5 fuel condition (full augmentation) at which no audible instability occurred. Spikes just below 400 Hz and 200 Hz are still the distinguishable features of the PSD analysis, but the lower frequency component is now more prominent than the higher frequency. In terms of peak-to-mean amplitudes the 400 Hz component of Figure 4 is at 1.44 per cent, while the 200 Hz component is at 2.67 per cent. These two peaks appear consistently throughout the PSD analysis of the high response test data. Only the 400 Hz component reaches large amplitudes, and these occur only in the Z8MAX fuel condition.

EFFECTS OF ALTERNATE CONFIGURATIONS

Several afterburner configurations were examined during the tests. However, only one repeatable unstable condition was identified regardless of configuration tested-- the 400 Hz instability at condition Z8MAX.

The screech liner, blocked or standard, had no effect on initiating or damping the oscillation. The standard TF-30-P1 screech liner, however, was not tuned for a screech condition of 400 Hz and, therefore, was virtually ineffective as a damping device for this condition.

Flameholder configuration seemed to have little or no effect on the 400 Hz condition.

Substituting AVGAS for JP-4 fuel appeared to have some effect on augmentor stability. The 400 Hz response was still present with AVGAS at the Z8MAX condition, but the amplitudes were consistently low in spite of the audibility of the oscillation.

Flow distortion effects could not be examined due to high sensitivity of the test engine to imposed distortion.

Only fuel distribution changes seemed to have a dramatic effect on augmentor combustion stability. At Z8MAX, the instability was strong; at Z8MIN and Z5 the instability ceased, amplitude levels returning to low, virtually negligible values.

INLET TEMPERATURE EFFECTS

The stability test program was conducted over a period of six months from early spring to late summer. Consequently, a spread in engine inlet temperature from a low of 25 degrees F to a high of 85 degrees F was observed. This temperature spread appeared to have some influence on the amplitude of the oscillatory instability described above. When the 400 Hz activity was first observed, inlet temperature to the engine was 35 degrees F, resulting in an audible response. However, later in the test program at higher inlet temperatures the amplitude level of the 400 Hz oscillation decreased. This phenomenon was consistent throughout the program-- the cooler the engine inlet temperature the higher the pressure amplitude. In fact, during a period of engine calibration testing when the test cell temperature dropped to approximately 25 degrees F, the instability became of sufficient magnitude to contribute to, if not directly cause, a failure of a fuel injector ring splash-plate and of an exhaust nozzle actuator pressure line. Subsequent analysis of the failed parts showed a vibration fatigue failure possibly caused by the instability. The failure occurred during an extended afterburning run at Z8MAX (approximately 15 minutes duration). Oscillatory overpressures during this run could have been of sufficient magnitude to overstress these parts. Furthermore, the engine manufacturer, Pratt and Whitney Aircraft, indicated that the flameholder and fuel injector hardware have a natural response at approximately 400 Hz and, therefore, warned that a failure of these parts could result. The flameholder, however, remained in excellent condition throughout the program.

Figure 5 displays a power spectral density analysis of channel 7 during the Z8MAX condition on a relatively cold day of testing (engine inlet temperature was 35 degrees F). The spike at 385 Hz is substantially more prominent than that shown in Figure 3. In terms of the peak-to-mean pressure oscillation amplitude, the value indicated for 385 Hz is 37.4 per cent. On this same day significantly greater activity was observed even at the Z4 condition (Figure 6), where a sustained peak-to-mean amplitude of 9 per cent was recorded. A detailed discussion of the inlet temperature effect can be found in Chapter V.

SUMMARY OF OBSERVED AMPLITUDES

From the point of view of NREC's augmentor instability analysis, the preferred form of the pressure oscillation test data is that of peak-to-mean amplitude: $p'/\bar{p}$. The results of the various power spectral density

analyses, which indicate the RMS value of the oscillatory pressure component, have been reduced to peak-to-mean form. Tables II through VII show the peak-to-mean amplitudes (as percentages) for the 400 Hz oscillation in the various test configurations and fuel zone combinations. Tables VIII through XIII give the corresponding results for the 200 Hz oscillation. In some test configurations the 400 Hz oscillation appeared as a double peak in the PSD plots, but the data shown in the tables represents the highest amplitude value within 400 Hz $\pm$50 Hz. Blanks in the tables represent failures to obtain data, usually because of improperly functioning charge amplifiers (see Appendix VI). The data tabulated has guided the analytical efforts of the program.

THE 400 HZ COMPONENT

Some basic trends in the tabulated data deserve comment. The 400 Hz oscillation consistently shows a marked increase in amplitude as maximum fuel flow in zone 4 is reached in the Z8 condition. Amplitude levels are rather low, with no distinctive patterns in all other fuel zone combinations. Even in Z8MIN the amplitude of the 400 Hz component does not differ markedly from its value without any augmentation. It should be noted that even without augmentation the PSD plots indicate a concentration of activity in the 400 Hz area, so that the Z0 amplitudes in the tables do not represent pure noise. The conclusion, then, is that specifically with the Z8MAX fuel combination an intermediate level instability becomes sustained in the TF-30-P1 augmentor. The instability is considered intermediate or moderate in severity because in general the amplitude levels observed remained below 10 per cent. The prominent exception, of course, was the 37 per cent level observed on a cold day-- an amplitude level which is severe. The second conclusion, then, is that the moderate instability in the Z8MAX condition becomes severe when the engine inlet temperature is low.

Comparing amplitude levels from channel to channel indicates that the 400 Hz oscillation has a dominent tangential component since the circumferential variation in each instrumentation plane is marked. Whether the oscillation has a significant longitudinal component remains unclear from the tabulated data. Since the highest amplitude point moves circumferentially from the flameholder plane to the plane at the end of the screech liner, the oscillation appears to be winding like a cork-screw along the length of the augmentor. The Fastax movies of the instability indicate a sloshing mode with primary oscillation activity at the outer diameter, as is characteristic of a tangential mode. The movies also indicate that the oscillation is a first tangential in that only two hot spots, 180 degrees apart, stand out alternately.

Changing the flameholder and the screech liner-- at least in hot day testing-- produced no distinctive trends in the 400 Hz oscillation characteristics. The only marked peak continued to occur at Z8MAX, and the level remained moderate. Switching to AVGAS fuel, however, caused the oscillation level to drop in all fuel zone combinations (see Tests 9 and 10 in Tables II through VII). The relative prominence of the Z8MAX condition also diminished. Still, the PSD plots show a clear spike in the 400 Hz range even with AVGAS.

THE 200 HZ COMPONENT

The 200 Hz oscillation persists over a broad range of augmentor operating conditions, but never exhibits markedly significant amplitude levels. None of the fuel zone combinations-- not even Z8MAX-- have marked effects on the 200 Hz amplitude. The maximum observed amplitude of 5.35 per cent happens to occur in the lightly augmented Z7 condition. This oscillation is more prominent than the 400 Hz resonance during zero augmentation, so that it might be driven by some energy source other than the augmentor heat release process.

Unlike the 400 Hz resonance, the 200 Hz component does not appear to be sensitive to engine inlet temperature. The modified flameholder, however, appears to increase its characteristic amplitudes for all augmentor operating conditions. The screech liner, tuned to a much higher frequency, shows no pattern of effect. AVGAS reduces the amplitudes, but not so pronouncedly as in the case of the 400 Hz component.

TURBINE DISCHARGE TEMPERATURE EFFECTS

Contrary to the above discussion relative to higher inlet temperature effects, it was noted that higher turbine discharge temperatures seemed to increase oscillatory activity at Z8MAX. During one such examination a Z8MAX condition was established with the engine trimmed to military specification. The 400 Hz instability was noted. When the engine was then uptrimmed, resulting in increased turbine discharge temperatures, the unstable condition became more pronounced-- increased audibility in the control room and higher pressure amplitude levels from the Kistler instrumentation. Based on the observation described above and the effect of increased turbine discharge temperature discussed herein, it would appear that the unstable condition at 400 Hz is sensitive to the temperature difference between the fan stream and core stream. In both instances, an increase in this temperature difference increased the oscillatory activity within the augmentor.

INLET DISTORTION TESTS

As the test plan indicates, a series of inlet flow distortion tests were planned to assess the effects a distorted flow condition imposed at the engine inlet might have on the combustion stability of the augmentor. Two distortion conditions were originally planned subject to engine stall sensitivity-- a 180 degree screen over the fan inlet (Figure 7) and a 90 degree screen (later reduced to 72 degrees, Figure 8). The screens where $\frac{1}{2}$-inch square mesh of 0.072 inch wire. It was expected that this wide, uniform mesh screen (normally used as the base support screen for attaching more complex distortion patterns) would provide some inlet distortion but not of such magnitude to disturb severely the normal operating characteristics of the engine. Unfortunately, distortion screens from 180 degrees-coverage to 72 degrees-coverage were found to be too severe for the engine. The engine

would surge when attempting to light the afterburner for every screen configuration examined. Consequently, no test data could be acquired relative to the effect of inlet distortion on augmentor stability. Although the engine underwent several severe compressor surges (a condition during which the airflow through the engine is suddenly reversed causing burner pressures to drop to near starting pressure levels, and often resulting in combustion gases to be expelled out the front of the engine), the engine's structural integrity was virtually unaffected, permitting completion of nearly all testing planned under the program. Turbine durability was of prime concern during a surge condition since turbine inlet temperatures momentarily exceed structural design limits. No severe turbine damage was noted, however; engine performance remained consistent, with little or no deterioration throughout the duration of the program. In-house testing of this TF-30 engine was eventually terminated as a result of a major turbine failure and fuel control problem during a retest of some selected points of interest under cold day conditions. All test data of significance had been recorded prior to this failure.

SPECIAL TESTS

Several special tests beyond those defined in the test plan were also conducted to permit examination of other conditions of interest not identified early in the program. These special tests are listed below.

Test No. 1: Two special test conditions were included in the report of this test to show the significant effect inlet air temperature had upon the stability characteristics of the augmentor. The basic test series of Test 1 was conducted at inlet temperatures of 49 to 51 degrees F. The two special tests were conditions Z4 and Z8MAX, but were conducted at inlet temperatures of 35 degrees F. An order of magnitude increase in pressure amplitude was observed in the two special tests.

Test No. 6: At the conclusion of this test, a special test was conducted to examine an afterburning condition in which fuel zones 1, 2, and 5 were on while zones 3 and 4 were off. This condition would provide a high temperature core (zones 1 and 5) and outer wall stream (zone 2) while the mid, splitter stream would remain relatively cool in the vicinity of the flameholder. No severe oscillation was observed, although the 400 Hz and 200 Hz spikes still appeared in the PSD analysis.

Test No. 9: At the conclusion of this test using AVGAS fuel, two conditions were repeated-- Z8MAX and Z4. These repeat conditions were conducted, however, at higher turbine discharge temperature to investigate a similar effect of increased augmentor instability activity as observed on JP-4 fuel at elevated turbine discharge temperature levels. Turbine discharge temperatures were increased 50 to 60 degrees during these special tests by uptrimming the engine to a higher operating level.

Test No. 10: Two special tests were conducted at the conclusion of this test to examine the change of stability characteristics as a result

of afterburner fuel change (AVGAS to JP-4). The first special test was conducted at elevated turbine discharge temperature levels using AVGAS as the primary afterburner fuel. The second special test was conducted at essentially the same operating conditions but using JP-4 as the primary afterburner fuel. This provided a back-to-back test of both fuels at equal operating conditions. Some variation in augmentor stability was observed but not as much as expected. It is possible the high engine inlet temperature existing during these tests (67 degrees F) may have significantly suppressed any possible activity.

CHAPTER IV

BASIC INSTABILITY ANALYSIS OF THE TF-30-P1 AUGMENTOR

This chapter describes the Task I study of the nominal TF-30-P1 augmentor design. The task was conducted in two parts: first, the NREC combustion instability analysis was used to predict the oscillatory combustion characteristics of the augmentor; these predictions were then correlated with the experimental results, described in the preceding chapter, and approaches for attaining better agreement between theory and test were adduced. This basic study of the augmentor ranges over a large number of potentially unstable acoustic modes and over several fuel zone combinations. Three objectives were kept in mind:

1. To determine the preferred approach for using NREC's analysis for mixed-flow augmentors: whether they are best modelled as cylindrical afterburners or as annular ductburners.

2. To compare predicted and observed instability characteristics in order to check the applicability of NREC's augmentor analysis as it currently stands.

3. To identify which model parameters are most effectively varied to improve agreement between analysis and experiment, and hence which parameters merit most attention in the future development of NREC's model.

The chapter reviews in sequence the ground rules for the analysis, the results of the initial analysis, the comparison with experiments, and the input changes for better correlation.

GROUND RULES

The initial analytical effort of Task I was to produce 100 instability solutions, produced as follows: 5 fuel zone combinations; 10 augmentor duct acoustic modes; and 2 approaches to modelling the mixed-flow configuration. The input for these solutions was selected with little regard for some of the details of the TF-30-P1 augmentor. For the more elusive input parameters the initial analyses used the same values as were used with apparent success in the earlier parametric studies of conventional afterburners. Thus the initial analyses are best viewed as providing a rough benchmark for the TF-30-P1. Comparison of these results with experimental data then led to more refined input values, and hence to more refined analyses.

The five fuel zone combinations which were investigated were identified in the preceding section of the report and are described in detail in Appendix V. The essential characteristics of the five combinations are as follows:

1. Z4: max augmentation in the fan stream.

2. Z5: max augmentation.

3. Z6: max augmentation except for no fuel to Zone 2 at the outer diameter of the fan-- i.e., Z5 without Zone 2.

4. Z7: only Zone 1 (the pilot zone) and Zone 3 in the fan stream operating.

5. Z8MAX: max augmentation in the fan stream except for no fuel to Zone 2 at the outer diameter of the fan-- i.e., Z4 without Zone 2.

The last three combinations are alike in that Zone 2, normally the second zone to be engaged, is assumed to have the fuel blocked off. Zone 2 differs from the other four zones in that its fuel is pre-mixed with compressor discharge air, and hence prevaporized. In the initial analyses the different fuel zone combinations were assumed to affect three of the model input parameters: the step rise in the sonic velocity at the flame-front; the through-flow distribution downstream of the flame-front; and the magnitude and radial variation of the chemical energy content of the fluid entering the combustion chamber. Details of the inputs for each zone combination can be found in Appendix V. The reader should note that in the initial analyses the quality of the fuel (i.e., percent vaporized) at the flame-front was assumed to be the same regardless of the zone which supplied it.

The ten acoustic modes which were selected for analysis were expected to be the most likely to exhibit instability. The ten are described below in terms of their dominant spatial component in the combustion chamber:

1. Mode 1: first longitudinal.

2. Mode 2: second longitudinal.

3. Mode 3: third longitudinal.

4. Mode 4: first tangential.

5. Mode 5: first tangential combined with first longitudinal.

6. Mode 6: first tangential combined with second longitudinal.

7. Mode 7: second tangential.

8. Mode 8: third tangential.

9. Mode 9: first radial.

10. Mode 10: first radial combined with first longitudinal.

While this set extends over a broad frequency range-- 0 to 1100 Hz in the afterburner solutions and 0 to 2400 Hz in the ductburner solutions-- not all acoustic modes within this range are included. Several more longitudinal modes would have to be examined to exhaust the frequency range. The ten that were chosen all have comparatively simple mode shapes, a condition thought to be normal, if not necessary for an instability.

The two methods for modelling the mixed-flow geometry have been identified earlier in terms of the distinction between a cylindrical afterburner and an annular ductburner. In the case of the cylindrical afterburner model the upstream boundary was located at the turbine discharge nozzles, and the remainder of the fan duct upstream of the boundary was represented via an acoustic admittance. In the case of the annular ductburner model, only the fan stream was considered, and the interface between the fan and core streams was assumed to be an acoustically reflective boundary.

A few additional assumptions made in the initial analyses require mention. The idealized augmentor duct dimensions assumed in the acoustics analyses are summarized in Appendix I. Raw estimates of the boundary acoustic admittances were used except in the case of the screech liner; upstream and downstream admittances are discussed in Appendix I, and the liner admittances, in Appendix V. The Mach number levels at the nozzle and at the turbine and fan discharge are sufficiently high as to dominate the acoustic admittances, so that the use of raw estimates for the latter is not thought significant. Through-flow velocities were calculated from correct duct dimensions, but mixing between core and fan streams was ignored; only the axial component of the through-flow was considered. Finally, the representation of the steady and unsteady combustion, as mentioned above, was very simplified in the initial analyses. Since subsequent comparison with experimental data led to more refined combustion representation, it is easier to discuss the input assumptions in the context of correlating analyses with tests.

A brief final preparatory remark is needed on the form of solution produced by NREC's instability analyses. NREC's model is discussed in some detail in Appendix VIII. The solution for any individual acoustic mode ultimately consists of three numbers: its frequency, its sustained amplitude (zero for stable modes), and the threshold amplitude which must be exceeded to trigger it. The solution is developed in three steps:

1. An acoustics analysis (Program HLMHLT) calculates the frequencies, decrements, and mode shapes of the natural acoustic modes of the augmentor duct. The decrement represents the rate at which energy is removed from the mode, and hence represents the rate of decay (or, if negative, the rate of growth) of the mode.

2. An unsteady energy analysis (Program REFINE) calculates refined values of the frequency and decrement for each acoustic mode. These refinements, which vary nonlinearly with pressure oscillation amplitude, account for the energy added or absorbed by the flow and combustion processes and by surface effects ignored in the initial acoustics analysis.

3. The nonlinear variation with amplitude produces results of the following form from Step 2:

$$f^2(amp) = f_o^2 + \Delta f^2(amp)$$

$$\delta^2(amp) = \delta_o^2 + \Delta \delta^2(amp)$$

where the subscript designates purely acoustic results. A graphical procedure, shown below, is finally used to determine the threshold and sustained amplitudes and the sustained frequency of the duct mode under examination. The sustained amplitude is that at which the energy added to and removed from the oscillation is in equilibrium-- i.e., the amplitude at which the decrement is zero and the slope of the decrement versus amplitude curve is positive.

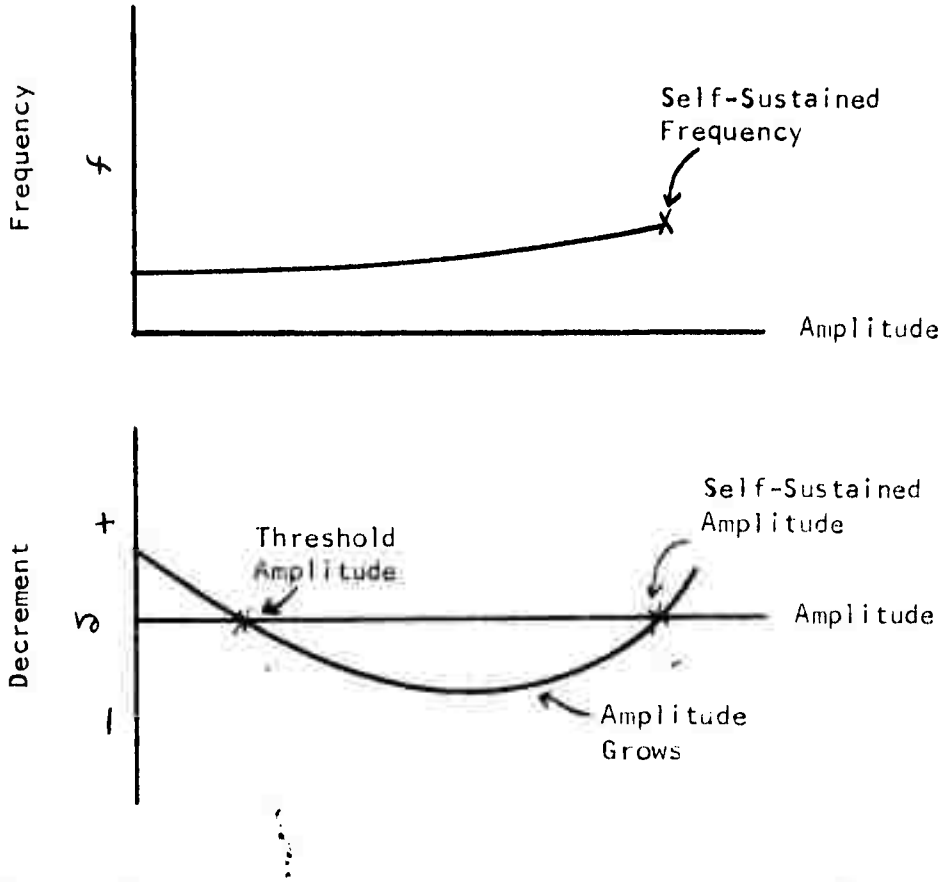

The functions shown are constructed from the results of Step 2. The final solution for any acoustic mode can thus be put in the form of plots like the above. The extent to which the decrement plot becomes negative is a measure of the rate of growth of the oscillation. Modes for which the decrement plots remain positive are simply stable. All other modes are oscillatory, but only those with significant self-sustained amplitudes are termed "unstable". Many of the results of the TF-30-P1 solutions will be presented in this graphical form since it displays so many salient features of the numerical solution in a single picture.

RESULTS OF THE INITIAL ANALYSES

The baseline analyses predicted that many of the ten modes examined are stable for all fuel zone combinations regardless of the representation of the mixed-flow duct. The table below summarizes the predictions for maximum augmentation (i.e., for Z5).

Mode		A/B Results			D/B Results		
No.	Composition	Stable	f	f_o	Stable	f	f_o
1	1st Longitudinal	Yes	49	28	Yes	31	18
2	2nd Longitudinal	Yes	105	166	Yes	48	54
3	3rd Longitudinal	Yes	128	277	Yes	85	115
4	1st Tangential	NO	380	449	Yes	280	316
5	1st Tan, 1st Long	Yes	425	484	Yes	285	352
6	1st Tan, 2nd Long	Yes	430	562	Yes	280	395
7	2nd Tangential	NO	710	762	Yes	590	626
8	3rd Tangential	Yes	1060	1050	NO	840	918
9	1st Radial	Yes	967	959	NO	2600	2666
10	1st Rad, 1st Long	Yes	930	1004	NO	2400	2675

In the table f indicates a typical frequency with flow and with unsteady combustion, and f_o indicates an acoustic frequency of the duct, ignoring flow and unsteady combustion; frequencies are, of course, stated in Hz. The observed instability was at 385 Hz.

For discussing these results in detail it is easiest to distinguish three categories: modes predicted to be stable with both representations, modes predicted to be unstable only in the ductburner solutions, and modes predicted to be unstable only in the afterburner solutions.

MODES PREDICTED TO BE STABLE

The three purely longitudinal modes are predicted to be simply stable, with logarithmic decrements in excess of 1.0. Figure 9 shows the solution for the second longitudinal mode at full augmentation. The large decay rate of the longitudinal modes is primarily a consequence of through-flow effects. The large difference between the acoustic and the "refined" frequencies is also primarily a consequence of through-flow. Since the Mach numbers in the augmentor are highest during full augmentation, the contribution of through-flow in the tabulated results is somewhat greater than at lesser operating conditions. It should be remembered that the analysis ignores flow terms of higher order than Mach number squared. Even without through-flow, however, the three longitudinal modes are predicted to be stable since the unsteady heat release processes themselves are stabilizing for these modes.

The other two modes predicted to be always simply stable in the initial analyses have in common that they consist of the first tangential mode combined with longitudinal components in the combustion zone. Figure 10 shows

the solution for the combined first tangential, second longitudinal mode at full augmentation. Through-flow has a stabilizing effect on these modes, and unsteady heat release excites them. These two modes are stable, while the simple first tangential is unstable, because the longitudinal component of their mode shapes causes the pressure oscillation amplitude level to be low in the region of high steady heat release, just downstream of the flame-front. Unstable Mode 4 has an oscillation amplitude peak just downstream of the flame-front; stable Modes 5 and 6 have their lowest amplitude levels in this region. Figure 11 gives a picture of the mode shape of the stable Mode 6.

MODES PREDICTED TO BE UNSTABLE IN THE DUCTBURNER SOLUTIONS

Three modes are predicted to be unstable in the ductburner solutions and stable in the afterburner solutions: the two radial modes and the third tangential mode. The two radial modes are different only in the presence of a higher order longitudinal component in the second of the two. Figure 12 displays the solution for the radial mode with no longitudinal component downstream of the flame-front. The ductburner solution has a frequency above 2400 Hz and a decrement which barely becomes negative. The afterburner solution has a frequency below 1000 Hz and a positive decrement of about 0.3. The large difference in predicted frequencies between the two solutions is straightforwardly a consequence of the assumptions made for the ductburner: specifically, it is assumed that the interface between the core and fan streams is acoustically perfectly reflective. Thus, in the ductburner solutions the radial wavelength is roughly the annulus height of the fan stream; in the afterburner solutions the wavelength is roughly the outer radius.

The large changes in the frequencies from the acoustic to the refined solutions result from through-flow effects. In particular, the fact that Mode 10 has a lower frequency than the simpler Mode 9 is a consequence of the through-flow terms. This discrepancy suggests that the failure to consider higher order Mach number terms results in an erroneous recalculation of the frequencies with through-flow when the Mach number reaches the levels of the TF-30-P1, namely 0.75.

The fact that no oscillations were observed in the frequency range of 2500 Hz licenses a rejection of the ductburner solutions-- at least, those solutions for the radial modes in which the interface stream surface is assumed to be perfectly acoustically reflective. Why the ductburner radial modes are unstable and the afterburner radial modes are not nonetheless requires some comment. The ductburner predictions of instability are much more pronounced when the liner, which is tuned to a frequency a little below 2000 Hz, is assumed to be blocked. Since the liner has little effect on the 1000 Hz "afterburner" radial mode, the difference in their predicted stability characteristics is greater than that shown in Figure 12 when the liner is blocked. Most of the difference in the decrement plots of Figure 12 results from contrasting effects of through-flow. These effects are calculated to be stabilizing in both the afterburner and the ductburner solutions, but the magnitude of the effect is much larger in the former.

The difference in the through-flow effects is primarily a consequence of the high frequency in the ductburner solutions, with its resultant shorter wave lengths being less affected by through-flow.

The third tangential mode is calculated to be unstable in the ductburner solution and stable in the afterburner solution. Figure 13 shows the solutions for this mode at full augmentation. The difference in the decrement plots of Figure 13 arises primarily from the much larger amount of energy supplied to the pressure oscillation by unsteady heat release in the ductburner solution. This, in turn, results from the fact that the ductburner solution has a pressure oscillation amplitude peak in the region o highest heat release just downstream of the flame-front; the afterburner solution has its peak two-thirds of the way downstream toward the nozzle.

MODES PREDICTED TO BE UNSTABLE IN THE AFTERBURNER SOLUTIONS

Two modes were predicted to be unstable in the afterburner solutions and stable in the ductburner solutions, namely the first and second tangential modes. The second tangential mode, with a frequency slightly above 700 Hz, was calculated to be unstable at full augmentation, but stable at such lesser operating conditions as Z8MAX. Figure 14 shows the afterburner and the ductburner solutions for this mode.

Three features of the solution for the second tangential mode require comment. First, the afterburner solution is predicted to be unstable at Z5 and stable at Z8MAX for two reasons: the through-flow is more stabilizing with the latter zone combination, and the unsteady heat release is calculated to contribute much more energy with the former zone combination. The second significant point is that in the ductburner solutions unsteady heat release is calculated to have a damping, not a driving effect, largely because of the longitudinal variation of the amplitude in the combustion chamber. Finally, the unstable decrement level for the second tangential mode is not severe compared to that of the first tangential mode, to be discussed below. Indeed, the input modifications made to gain good correlation between analysis and experiment for the first tangential mode suffice to make this second tangential mode stable in all solutions with all zone combinations. That is, subsequent refinement of the input, as discussed below, resulted in eliminating the prediction that Mode 7 is unstable at maximum augmentation.

The major predicted instability occurs in the first tangential mode as calculated in the afterburner solution, and the predicted frequency corresponds well with that observed in the tests (i.e., roughly 380 Hz). Figures 15 and 16 show the instability solutions for this mode at full augmentation and at Z8MAX respectively. The decrement levels are substantially negative, with no indication of an equilibrium amplitude level below 30 per cent. Comparison of Figures 15 and 16 indicates that in the initial analyses the first tangential mode is predicted to be more unstable-- in the sense that the mode will grow more rapidly-- in the case of maximum augmentation. Examination of the computer output indicates

that at Z5 the through-flow effect drives rather than damps the mode, as at Z8MAX. Also, much more energy is calculated to be supplied by unsteady heat release at Z5.

The fact that the first tangential mode is predicted to be unstable in the afterburner solutions and stable in the ductburner solutions is important below. The large difference in the decrement levels calculated in the two types of solution results mostly from the stabilizing effect unsteady heat release is calculated to have in the ductburner solutions. In part, this latter difference stems from the calculated mode shapes of the mode, as shown in Figure 17. The peak amplitude in the mode shape in the afterburner solution occurs just downstream of the flame-front, while that in the ductburner solution occurs almost midway to the nozzle.

COMPARISON OF PREDICTED AND OBSERVED AUGMENTOR INSTABILITIES

In summary, comparison of initial predictions with observations indicates one mode with sufficient agreement to serve as a basis for further studies. The principal unstable mode, as calculated by the afterburner solutions, is the first tangential mode. Its calculated frequency of roughly 380 Hz compares well with the observed frequency of 385 Hz. However, the initial analyses predict higher amplitudes than were observed, and they predict that the instability will be worse during maximum augmentation while, in fact, the instability is significant only during Z8MAX operation. These points of comparison will be discussed in more detail below.

First, however, it is necessary to extract some major conclusions from the simple comparison of predictions with observations. The most significant conclusion is to reject the ductburner solutions at least for transverse modes of instability in mixed-flow augmentors. The ductburner solutions failed to give any indication of an instability in the 385 Hz frequency range which was observed. Moreover, those transverse instabilities which were predicted in the ductburner solutions did not appear at all in the test results. No indication of higher oscillatory activity was noticed above 600 Hz. In rejecting the ductburner solution-- and in accepting the afterburner solution-- for transverse modes in mixed-flow augmentors, no additional conclusions should be drawn on the proper solution for longitudinal modes. Experimental data were not sufficient to compare the two types of solution for longitudinal modes.

The initial analyses gave no indication of which augmentor duct acoustic mode is being excited in the 180 Hz range. The fact that some augmentor mode-- presumably longitudinal-- is involved in this oscillatory activity seems obvious. However, the test data, as discussed in an earlier section of the report, suggest that whatever mode is involved in the 180 Hz oscillation, the source of the excitation energy is not unsteady combustion. In other words, this oscillation does not appear to be an instance of combustion instability. Various suggestions have been made as to the source of the excitation-- e.g., vortex shedding from the fan discharge vanes or from the flameholders. However, since it was felt

not to be a combustion instability, this oscillatory component was researched no further in this program. Presumably additional analyses of the augmentor acoustics with through-flow (and without unsteady heat release) should at least indicate which duct mode is being excited, but such analyses were not undertaken in the current effort.

Restricting attention to the afterburner solutions, which predicted instabilities in the first and second tangential modes, does not eliminate all problems since no oscillation was observed in the 700 Hz range of the second tangential mode. As remarked above, the second tangential mode is less unstable than the first. Since the predictions above represent a very naive view of the input to NREC's model, the fact that the second tangential mode was initially predicted to be unstable should not be considered a problem at this stage. Indeed, as will be seen below, input which better correlates the first tangential mode also eliminates the erroneous prediction of instability in the second tangential.

COMPARISON OF PREDICTED AND OBSERVED INSTABILITY FREQUENCY

The remarkably close agreement between the observed instability frequency and that predicted by the afterburner type solution is, of course, very encouraging. This agreement is all the more notable when it is recalled that the purely acoustic frequency of this mode is calculated to be nearly 450 Hz. The 75 Hz reduction in the calculated frequency results from through-flow and unsteady heat release effects, with the former accounting for roughly 60 per cent of the reduction.

The observed oscillation showed some variation in peak frequency from one fuel zone combination to another. In the more high temperature operating conditions, Z5 and Z6, the observed frequency was roughly 10 Hz higher than that observed in Z8MAX, but in some tests this marginal decrease in frequency with Z8MAX was not noted. The analyses showed only a 2 or 3 Hz variation in frequency from one zone combination to another when the oscillation amplitude was assumed to be about 10 per cent.

The main issue in deciding how to model mixed-flow augmentors concerns the acoustics of the duct. Frequency is the best parameter to use to judge the acoustics question. Other mixed-flow augmentor modelling questions--such as mixing between streams, velocity interactions between streams, and interactions between the combustion processes in the two streams-- cannot be answered at all by comparing frequencies. The close agreement in predicted and observed frequency, however, does support the conclusion that tangential modes in mixed-flow augmentors resemble tangential modes in conventional cylindrical afterburners.

COMPARISON OF PREDICTED AND OBSERVED INSTABILITY AMPLITUDE

The basic analyses of the TF-30-P1 augmentor did not explicitly make any assumption regarding engine inlet temperature or augmentor inlet temperature. The latter quantity physically governs the fraction of the fuel which is vaporized upstream of the flame-front. In the basic analysis it

was simply assumed that droplet evaporation and burning occupies 90 per cent of the time required for combustion of a fluid particle. Thus the predicted amplitude levels cannot readily be compared to the levels observed without a more detailed account of the augmentor inlet conditions assumed in the analyses.

The amplitude levels predicted for the 380 Hz instability are quite large-- well above the 0.25 peak-to-mean level at which NREC's model has ceased to be applicable because of lack of treatment of shock losses. The observed amplitude levels, except for the cold day tests, were less than 0.10. Only on a cold day were amplitude levels observed comparable to those predicted in the basic instability analyses. The comparison of amplitudes thus poses a problem since the augmentor instability model was primarily aimed at evaluation of sustained amplitude levels in the 5 to 15 per cent regime. The crux of the problem is a more detailed treatment of the effects of inlet temperature on the various unsteady combustion input parameters. A thorough examination of augmentor inlet temperature effects is a major part of Task II, and is hence postponed for the moment.

COMPARISON OF PREDICTED AND OBSERVED SENSITIVITY TO FUEL ZONE COMBINATIONS

The initial afterburner solutions predicted that the first tangential mode is unstable for all fuel zone combinations examined except Z7. Moreover, the worst condition, in terms of the magnitude of the negative decrement, is Z5, and the least severe unstable condition is Z8MAX. The augmentor tests, however, indicate that the 385 Hz instability is peculiarly sensitive to Z8MAX. Amplitude levels in other fuel zone combinations were consistently small compared to those observed during Z8MAX. Thus the initially predicted sensitivity to fuel zone combinations is directly at variance with observations. This descrepancy is particularly noteworthy since the initial analyses predict that the TF-30-P1 augmentor is unstable during normal operation-- it is not-- and that eliminating Zones 2 and 5 attenuate the instability-- in fact, only by eliminating these zones does the oscillation become severe. Thus even on qualitative grounds the initial predictions conflict with the observed sensitivity to fuel zone combinations.

The initial analyses took a very simple view of the TF-30-P1 augmentor. In particular, the fact that the different zones have different combustion characteristics was ignored. The discrepancy between predicted and observed effects of fuel zoning raises a basic issue: How should zoned augmentors be represented within NREC's instability model? This issue was given a distinctive interpretation in the investigation reported below: what refinements of the input will most plausibly yield good agreement on the relative effects of the different fuel zone combinations. The problem is thus one of constructing a plausible correlation of analysis and experiment.

CORRELATION OF OBSERVED AND PREDICTED FUEL ZONE EFFECTS

The objective is to correlate the calculated and the observed sensitivity

to fuel zone combinations by means of suitable refinements of the inputs used in the instability analyses. As discussed in Appendix V, various physical parameters obviously depend on the fuel zones in operation:

1. The temperature rise and hence the sonic velocity rise in the combustion chamber.

2. The through-flow velocity distribution in the augmentor.

3. The spatial relation of the steady heat release to the pressure oscillation mode.

4. The average quality of the fuel at the flame-front.

The first of these, the sonic velocity increase in the combustion chamber, causes the first tangential mode shape to be slightly different from one fuel zone combination to another. Close inspection of these differences, however, indicate that they are of little significance in determining which fuel zone combination supplies the most energy to the pressure oscillation. The other three physical effects of different fuel zones being in operation are discussed separately below.

THE EFFECTS OF AVAILABLE COMBUSTION DRIVING ENERGY

The gross chemical energy level at which the augmentor operates corresponds essentially with the augmentor fuel flow rate (below stoichiometric conditions). The energy available to drive any particular acoustic mode, however, depends additionally on the distribution of the fuel (radially and circumferentially) relative to the spatial distribution of the acoustic mode in question. In particular, putting more fuel into regions of large pressure oscillation has a more pronounced effect on an acoustic mode than putting more fuel into regions of low pressure oscillation. In mathematical terms we can formalize this feature of the available driving energy by means of the following equation:

$$\text{AVAILABLE DRIVING ENERGY} = \iint r\, \bar{E}\, F_r^2\, F_\theta^2\, dr\, d\theta \qquad (1)$$

where F_r is the radial component of the mode shape, F_θ is the circumferential component, and $\bar{E}$, a function of r and θ, is the mean energy content per unit mass of the fluid at the flame-front. Here the available driving energy, A.D.E., is defined specifically with reference to an acoustic mode and to a mean or steady fuel distribution.

The question, then, is how do the various fuel zone combinations affect the available driving energy for the first tangential mode of the TF-30-P1 augmentor. The table below summarizes the answer to this question, the details of which can be found in Appendix V.

Zone Combination	Zones in Operation	Total Augmentor Fuel Flow (lbm/hr)	Available Driving Energy for Mode 4 ($ft^2/sec^2 \times 10^5$)
Z4	1,2,3,4	27,000	69.5
Z5	1,2,3,4,5	32,000	107.8
Z6	1,3,4,5	33,000	103.5
Z7	1,3	12,000	10.2
Z8MAX	1,3,4	21,000	40.6

The higher total fuel flow in Z6 than in Z5 is caused by the TF-30-P1 fuel control system when Zone 2 is blocked.

The available driving energy for the first tangential mode thus decreases from Z5 to Z6, Z4, Z8MAX, and finally Z7. This sequence is the same as that of the predicted negative decrement values. In other words, the changes in the available driving energy correlate with the initially predicted severity of the instability.

The question is: Can plausible modifications of the radial distribution of $\bar{E}$ lead to Z8MAX having more available driving energy than the other fuel zone combinations? If it can, then the originally predicted sensitivity to fuel zone combinations can be accounted for in terms of erroneous assumptions as to the fuel distribution at the flame-front. A quick glance at the preceding table, however, indicates that no such plausible modification can be made. The assumed fuel distributions may be somewhat in error, but not so much that Z8MAX can have more available driving energy than Z5 or Z6. The answer to the fuel zone sensitivity problem must be found elsewhere. The differences in the available driving energy, rather than solving the problem, indicate how difficult the solution will be.

THE EFFECTS OF THROUGH-FLOW VELOCITY

Different features of the through-flow velocity distribution in the combustion chamber have different effects. In particular, higher acceleration rates in the combustion chamber theoretically stabilize, but higher average velocities in the combustion chamber tend to drive tangential modes. These theoretical trends must be viewed with caution, however, since they are derived by ignoring higher order Mach number terms-- i.e., they assume low Mach number levels. The TF-30-P1, at least at high levels of augmentation has high Mach number levels. Thus the manner in which NREC's model accounts for through-flow effects may be suspect for such high augmentation levels as Z4, Z5, and Z6.

The different through-flow velocity distributions with different fuel-zone combinations are described in Appendix V. The consequences of these different distributions are indicated in the table on the following page.

Fuel Zone Combination	Mach No. at Nozzle Inlet	~Δ Decrement from Through-flow	Decrement w/o Unsteady Combustion
Z4	0.72	+0.04	0.05
Z5	0.82	-0.08	-0.02
Z6	0.78	-0.12	-0.02
Z7	0.46	+0.20	0.28
Z8MAX	0.63	+0.13	0.12

The main point of this table is that through-flow excites the first tangential mode during Z5 and Z6; damps the mode during Z7 and Z8MAX; and has little net effect on the mode during Z4. Indeed, the right-hand column indicates that the first tangential mode is predicted to be unstable even when unsteady combustion effects are entirely ignored.

It is at least plausible that the initial erroneous prediction that Z5 is the worst operating condition results from an erroneous estimate of the through-flow effects at Z5. The claim would be that NREC's model ignores flow terms of higher order than Mach number squared; but in the TF-30-P1 such higher terms need to be taken into account. The correctness of this claim is difficult to decide without a more powerful analysis of the through-flow effects. Since revisions of the model to account for higher order flow terms was far outside the scope of the contracted effort, this possible explanation of the fuel zone combination sensitivity was examined no further. It remains a hypothesis for future investigations.

THE EFFECTS OF FUEL QUALITY

The fuel supplied by the five fuel zones of the TF-30-P1 does not vaporize at a uniform rate. Three vaporization characteristics can be distinguished:

1. The fuel from Zone 2 is pre-vaporized prior to injection into the fan stream.

2. The liquid fuel from Zones 1 and 5 is injected into the hot core stream and vaporizes quite rapidly.

3. The liquid fuel from Zones 3 and 4 is injected into the cold fan stream and vaporizes more slowly.

In the initial analyses of the TF-30-P1 augmentor, droplet vaporization and burning mechanisms were the only coupling mechanisms taken into account. These necessarily are very sensitive to the rate of vaporization of the fuel. NREC's model, however, can recognize only a single rate across the entire face of the augmentor. Thus, in the case of a zoned augmentor it is necessary to specify a single vaporization characteristic which represents an "average" over the various zones. The

question of how to define this average occupies the remainder of this section of the report. The background of the question will be reviewed first, then the question will be resolved.

NREC's instability model has been developed in terms of two key combustion parameters: E , the chemical energy content (per unit mass) of the fluid at the flame-front; and τ , the characteristic time required for combustion. How these parameters fit into the over-all model is discussed in detail in Appendix VIII. Suffice it to say here that while E and τ are physically interpretable, they cannot simply be assigned values from standard augmentor design information. Properly designed experiments are needed to characterize E and τ in terms of augmentor design variables. In particular, E and τ need to be characterized in three ways:

$$\frac{E'}{\bar{E}} = f_{E'}\left(\frac{p'}{\bar{p}}, \frac{\mu'}{\bar{\mu}}\right)$$

$$\frac{\tau'}{\bar{\tau}} = f_{\tau'}\left(\frac{p'}{\bar{p}}, \frac{\mu'}{\bar{\mu}}\right) \qquad (2)$$

$$\bar{\tau} = f_{\bar{\tau}}\left(\frac{p'}{\bar{p}}, \frac{\mu'}{\bar{\mu}}\right)$$

That is, the oscillatory components of E and τ and the mean component of τ are all thought to be sensitive to pressure and velocity oscillations. The three functions indicated define the effects of coupling mechanisms on E and τ . Likely candidates for coupling mechanisms in augmentors are droplet atomization, vaporization, and burning, chemical kinetics, and turbulent mixing. NREC's instability model was not formulated to include such functions as $f_{E'}$, etc., specifically because it was felt that the likely coupling mechanisms are not amenable to a theoretical analysis.

In order to perform calculations with NREC's instability model some specific functions must be chosen, however crude and hypothetical. In the initial analyses of the TF-30-P1, NREC assumed a very simple model of droplet vaporization to provide, as it were, working hypotheses for these functions. The fluctuating component of E was defined as follows:

$$\frac{E'}{\bar{E}} = -\frac{a}{\gamma}\frac{p'}{\bar{p}} - \frac{(1-a)}{2}\left[\frac{\mu_3'}{\bar{\mu}_3} + \frac{1}{\gamma}\frac{p'}{\bar{p}}\right]_{INJECTOR} \qquad (3)$$

where a is the fraction of the fuel remaining in droplet form at the flame-front (here it is assumed that all vaporization between the injectors and the flame-front takes place instantaneously at the injectors). The components of τ are defined as follows:

$$\frac{\tau'}{\bar{\tau}} = \tilde{C}_1 \frac{p'}{\bar{p}} \qquad \text{and} \qquad \bar{\tau} = \tilde{C}_7 \tau_d \tag{4}$$

where τ_d is the "design" characteristic time-- the time without fluid oscillations. The two coefficients, $\tilde{C}_1$ and $\tilde{C}_7$, vary nonlinearly with the amplitude of the pressure oscillation as follows:

$$\tilde{C}_1 = - \frac{0.15\, R_{ed}'^{1/2} \left| p'/\bar{p} \right|^{1/2}}{1.0 + 0.3\, b\, R_{ed}'^{1/2} \left| p'/\bar{p} \right|^{1/2}} \tag{5}$$

$$\tilde{C}_7 = \frac{1.0 + 0.3\, R_{ed}'^{1/2} \left| p'/\bar{p} \right|^{1/2} b}{1.0 + 0.3\, R_{ed}'^{1/2} \left| p'/\bar{p} \right|^{1/2}} \tag{6}$$

where R_{ed}' is the droplet Reynolds number based on the sonic velocity, and b is the fraction of the design time not taken up by droplet evaporation; i.e.,

$$b = \left(1.0 - \frac{\tau_e}{\tau_d}\right) \tag{7}$$

where τ_e is the time required for evaporation without pressure oscillations.

Three variables must accordingly be assigned values in order to compute the stability of the TF-30-P1 augmentor: a, the fraction of the fuel remaining in droplet form at the flame-front; b, the fraction of the design time not taken up by droplet vaporization; and R_{ed}', the droplet Reynolds number based on sonic velocity. All three of these parameters pertain to steady or mean combustion.

In the initial analyses of the TF-30-P1 these variables were simply assigned the same values as were used in the earlier parametric studies of conventional afterburners (Ref 2). The fact that the TF-30-P1 augmentor is zoned was simply ignored, and the values were thought to remain the same regardless of the zone combination in operation. The values assigned were as follows:

$$a = 0.5$$

$$b = 0.1$$

$$R_{ed}' = 10^4$$

The results described above were computed with these values assumed in all solutions: for all modes, for all zone combinations, and for

afterburner and ductburner models. This approach is obviously faulty since it fails to recognize the gross differences in the fuel vaporization characteristics from zone to zone. The need to account for the effects of individual zones was accordingly hypothesized to be the source of the erroneous prediction that Z5, not Z8MAX would produce the worst instability.

Three steps were taken in constructing a model of the zoned combustion of the TF-30-P1. First, the key combustion coefficients were defined in terms of weighted averages of the coefficients of each zone. That is,

$$\tilde{C}_1 = \left(\sum_{n=1}^{5} \tilde{C}_1^n \dot{m}_f^n\right) \Big/ \sum_{n=1}^{5} \dot{m}_f^n$$

$$\tilde{C}_7 = \left(\sum_{n=1}^{5} \tilde{C}_7^n \dot{m}_f^n\right) \Big/ \sum_{n=1}^{5} \dot{m}_f^n \qquad (8)$$

$$a = \left(\sum_{n=1}^{5} a^n \dot{m}_f^n\right) \Big/ \sum_{n=1}^{5} \dot{m}_f^n$$

where the superscript n designates a zone, and $\tilde{C}^n$ is the combustion coefficient of that zone taken individually; $\dot{m}_f^n$ is the fuel flow rate in the zone. Constructing the model input parameters by such averaging should always be the rule for zoned augmentors.

The second step was to assign values to a, b, and R'_{e_d} in each zone. The droplet Reynolds number was still assumed to be 10^4, and the other two quantities were defined as follows for the hot day tests:

	a	b
Zones 1, 2, 5	0.0	0.0
Zones 3, 4	0.6	0.9

Here it was assumed that the zones do not affect one another; each zone has its unique combustion properties regardless of which other zones are in operation. With these assumptions the instability model predicts that Z5 and Z8MAX produce the same level of instability (the same value of negative decrement), and all other zone combinations are less severe.

The third step is to recognize that the zones do affect one another. Consider the rate of vaporization of fuel injected in Zones 3 and 4 into the fan stream. If only Zones 3 and 4 are in operation, their fuel will vaporize quite slowly. The introduction of Zone 1 increases this rate to that which occurs during Z7 and Z8MAX. This rate further increases when Zones 2 and/or 5 are in operation since they heat the portion of the fan stream into which the fuel from Zones 3 and 4 is injected. These considerations led to the revised values of b for Zones 3 and 4 which are

tabulated below (for hot-day conditions):

$$b^{3,4} = \left(1 - \tilde{T}_c^{3,4}/\tilde{T}_4\right)$$

Z4, Z5, Z6	0.6	
Z7, Z8	0.9	

The point of the diagrams is to indicate that combustion in Zones 2 and 5 accelerates the rate of vaporization in Zones 3 and 4 by heating the fan stream in the region of Zones 3 and 4.

The values of b chosen for Zones 3 and 4 are those needed to achieve qualitative agreement with the observed sensitivity to the fuel zone combinations. That is, with these values the instability solutions of the first tangential mode indicate the instability is severe with Z8MAX and is either markedly less severe or non-existent with the other zone combinations. Figures 18 through 22 show the revised instability solutions for the first tangential mode for Z4, Z5, Z6, Z7, and Z8MAX, respectively.

The results shown in Figures 18 through 22 agree only qualitatively with the observed fuel zone sensivity. None of the solutions yields a value of sustained amplitude. In the tests a low level sustained amplitude was observed in zone combinations other than Z8MAX, while that in the latter combination ranged from 0.10 on hot days to 0.37 on cold days. To account fully for the observed trends it is necessary for the model's solution for amplitude to be improved. This effort will be discussed in the next section, as part of the parametric studies. Subject to the provision that all the decrement curves of Figures 18 through 22 are misshapen (in that they don't turn back toward the zero decrement axis), the revised treatment of the TF-30-P1 zoned configuration is considered to correlate with the observed zone combination sensitivity.

These changes to the input procedures for the TF-30-P1 augmentor have an additional felicitous consequence. The second tangential mode was originally calculated to be unstable at full augmentation. Once the individual zones are treated separately, however, and interactions among zones are taken into account, this mode is predicted to be stable. Figure 23 shows the instability solution for the second tangential mode with the revised Z5 unsteady combustion input. The fact that this mode is now predicted to be stable removes the major discrepancy between predicted and observed oscillation frequencies in the case of the afterburner solutions.

CONCLUSIONS OF THE BASIC STUDIES

Three major conclusions were reached-- two about NREC's model and one about the TF-30-P1-- during the basic studies:

1. At least for transverse modes the cylindrical afterburner model should be used to calculate the stability of mixed-flow augmentors. No conclusions are warranted on longitudinal modes at this time.

2. In calculating combustion parameters for zoned augmentors, each zone should be treated individually, and the input parameters should be obtained by averaging over the zones according to the amount of fuel in each. In calculating combustion parameters for the individual zones, the effects of other zones must be taken into consideration; the individual zones should not be treated as if they are isolated from one another. In general, the basic studies of the TF-30-P1 suggest that more accurate representations of the steady combustion lead to more accurate predictions of instability trends.

3. The key reason for the observed instability becoming significant only in Z8MAX is that only with this fuel zone combination are two conditions met: the available driving energy is great enough, and the rate of vaporization of the liquid fuel in Zones 3 and 4 is slow enough. This insight into the basis for the observed instability is, of course, a conjecture deduced from the analyses, not an established experimental fact.

CHAPTER V

PARAMETRIC STUDY OF INSTABILITY IN THE TF-30-P1 AUGMENTOR

The TF-30-P1 augmentor tests included three modifications of the nominal augmentor in order to examine the effects of design changes on augmentor instability:

1. 70 per cent of the perforated screech liner was blocked off.
2. An alternative flameholder was used, in which the middle vee-gutter ring is 9 inches farther downstream than that of the standard flameholder.
3. AVGAS was used in the augmentor rather than JP-4.

Instability analyses were conducted in parallel with these changes.

Other variables worth examining parametrically came to light during the test program. First, engine inlet temperature was noted to have a dramatic inverse effect on the instability amplitude sustained during Z8MAX operation. Second, the core stream temperature was increased to see whether it too would reduce the amplitude level in a manner analogous to an increased engine inlet temperature. Finally, a Z8MIN condition was tested to see how sensitive the instability is to the fuel flow rate in Zone 4.

Comparison of hot and cold days and of AVGAS and JP-4 revealed more clearly what problem is behind the poor correlation between the observed and the initially predicted sustained amplitude levels. The final effort of Task II was devoted to an examination of the mechanisms and parameters which govern the sustained amplitude level of the 385 Hz instability. The Task II parametric study thus included four sensitivity investigations.

1. Sensitivity to Augmentor Geometry Modifications.
2. Sensitivity to Fuel Type and Flow Rate Variations.
3. Sensitivity to Augmentor Inlet Temperature.
4. Factors Governing Sustained Amplitude Levels.

These four are discussed in separate sections below after review of the ground rules of the studies.

GENERAL RULES FOR THE PARAMETRIC STUDIES

As in the Task I basic study of the augmentor, the effort in the parametric study was divided into two parts: first, an analysis of the modified augmentor served to predict the oscillation amplitude and

frequency changes; these predictions were then compared with the test results, and modifications of the input data were examined in pursuit of better agreement between calculated and observed trends. The parametric study concentrated on the dominantly unstable first tangential mode. Typical longitudinal and radial modes were also examined to see if engine modifications were predicted to affect the stability of these modes. Since the afterburner type solution was established to provide the best approximation of the mixed-flow augmentor, this solution alone was used in treating the transverse modes. Input was prepared with recognition of the separate fuel zones of the TF-30-P1, as described in the preceding chapter. In particular, all unsteady combustion parameters were calculated by averaging over the zones, and the coefficients of individual zones were calculated initially by means of droplet vaporization formulas as presented in the preceding chapter (see Appendix VIII for a full discussion).

The correlation between analysis and experiment in the parametric study concentrated initially on the trends which result from engine parameter modifications. Efforts to correlate the absolute levels of predicted and observed amplitude were postponed until the final stage of the parametric study. The reasons for this postponement should be clearly understood. Although NREC had previously examined two turbojet afterburners, the TF-30-P1 provided the first opportunity to check instability predictions against thorough test data. Since NREC's model is recognized to require experimental development of coupling mechanism models, the study of the TF-30-P1 further provided the first opportunity to check on what sort of coupling mechanism models are required for acceptable amplitude predictions in the case of current augmentors. Thus, in addition to the goal of checking the instability model's usefulness in evaluating design changes, the parametric study also took note of the goal of a better insight into the unsteady combustion mechanisms which govern augmentor instability.

SENSITIVITY TO AUGMENTOR GEOMETRY MODIFICATIONS

Two geometry modifications were examined. Neither the blocked liner nor the alternate flameholder was calculated to affect the stability characteristics of the TF-30-P1. This predicted lack of effect compares favorably with experimental evidence, since neither of the geometry changes appear to affect the observed instability frequency, amplitudes, and sensitivity to fuel zone combinations. Details of the geometry studies are discussed below.

SENSITIVITY TO SCREECH LINER LENGTH

Three of the six engine tests had the perforations blocked off along the upstream 70 per cent of the screech liner. In analytical terms this represented a 70 per cent reduction of the screech liner length. In the nominal configuration the screech liner is 33 inches long, 6 inches of which extend upstream of the center vee-gutter ring. The liner of this engine is designed for maximum absorption at a frequency near 2000 Hz,

and the blocking of the perforations did not alter the liner frequency. The details of the liner geometry can be found in Appendix III.

In the NREC analysis the screech liner is represented by an acoustic admittance ratio (a complex number, the real part of which pertains to damping) which varies with oscillation amplitude and frequency. The acoustic admittance of the TF-30-P1 screech liner is discussed in Appendix III. In the parametric analyses the liner modification was assumed to make the outer wall perfectly reflective except over the short portion of the screech liner where the perforations remained unblocked.

The reduction in the length of the screech liner was calculated to have no effect on the 385 Hz first tangential instability (see Figure 24). The frequency of the instability was changed by only 1.3 Hz, and the decrement was decreased by only 0.06 for a 10 per cent and by 0.03 for a 25 per cent peak-to-mean amplitude level. Given the high amplitude levels predicted for this unstable mode, the liner was found to have no effect on the self-sustaining amplitude and only a slight effect on the threshold amplitude (an increase of 1 per cent).

Tests 1, 8, and 9 used the partially blocked screech liner, and Tests 6, 7, and 10 used the standard liner. Examination of the amplitude data shows no particular trend with the reduction of the liner length. Some channels have a lower 400 Hz amplitude with the complete liner, but others have a larger amplitude. The variation from test to test is similarly inconclusive. Since no cold day tests were conducted with the complete liner, the effect of reducing the liner length on high amplitude oscillations was not determined.

In summary, the TF-30-P1 liner turns out to be irrelevant to the oscillations which were successfully sustained in the augmentor. Future studies will be needed to determine how well NREC's instability model accounts for changes in screech liner design.

SENSITIVITY TO FLAMEHOLDER MODIFICATIONS

The alternate flameholder, tested in Tests 7 and 8, differs in two ways from the standard TF-30-P1 flameholder:

1. The outer vee-gutter ring is perforated in such a way as to introduce a small component of swirl around its circumference.

2. The central vee-gutter ring is roughly 9 inches farther downstream than in the standard vee-gutter:

Both flameholders use the same size vee-gutter elements and the same number of radial elements between rings.

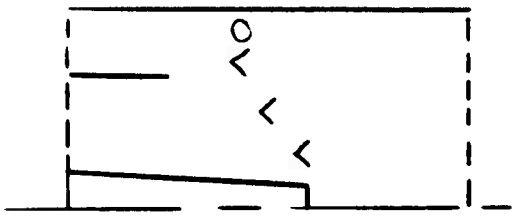

Standard
Flameholder

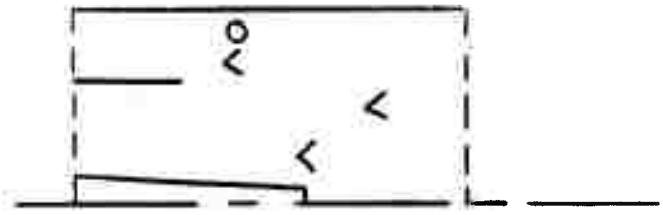

Modified
Flameholder

NREC's augmentor instability analysis was originally developed to permit the flameholder to be accounted for in three ways: in terms of the flame-front position, of the flameholder acoustic impedance, and of the vortex shedding from the vee-gutters. To date, however, no techniques for calculating flameholder impedance and vortex shedding inputs have been devised. All instability calculations to date, both for the two turbojet afterburners and for the TF-30-P1 augmentor, have ignored the flameholder geometry except insofar as it governs the axial position of the flame-front.

The instability analyses positioned the flame-front, rather arbitrarily, midway between the upstream and the downstream vee-gutter rings. The consequence is that the modified flameholder produces a roughly 5 inch downstream shift of the flame-front position. This change in the input affects both the acoustic modes and the instability calculations. Nevertheless, the over-all instability characteristics of the augmentor were calculated to be insensitive to this shift of the flame-front. The principal unstable mode has a relatively flat longitudinal component, so that no effect should be anticipated. The longitudinal and radial modes examined in the parametric study incur little change in the longitudinal component-- less change than occurs with variation of fuel zone combinations.

The test results using the modified flameholder similarly displayed no effects on the principal unstable mode. Again the variations in the data from Test 1 to Test 8 and from Test 6 to Test 7 have no pattern, and hence are more likely to be produced by other differences from test to test. The predicted and observed trends with the alternative flameholder thus compare favorably, but this fact in itself is inconclusive. The study cannot clarify how important a more thorough, detailed model of the flameholder is to the accurate prediction of instabilities. More radical changes of flameholder design than those examined in the current program will doubtlessly be required if sensitivities to flameholder geometry are to become obtrusive.

SENSITIVITY TO FUEL TYPE AND FLOW RATE VARIATIONS

NREC's model of the unsteady heat release distribution is stated in terms of four parameters, two of which (density and convection velocity) depend only on fluid flow conditions, but the other two of which (E and τ) depend also on the properties and the distribution of the fuel. Since E

(the energy content of the fluid) and τ (the characteristic time of combustion) are the parameters which are least susceptible to a thorough theoretical definition, the TF-30-P1 test program included some unusual variations specifically aimed at highlighting the effects of fuel on an instability. The various zone combinations which were tested have already been discussed in the preceding chapter. Once an instability was observed with full fuel flow in Zones 1, 3, and 4 (i.e., during Z8MAX), data were also recorded with Zone 4 barely in operation (i.e., during Z8MIN) to see how sensitive the instability is to the Zone 4 fuel flow rate. Similarly, the presumption that droplet vaporization and burning mechanisms are likely to be significant in the augmentation of fan streams encouraged examination of different fuel volatility. The engine was tested with AVGAS in the augmentor to see how a more volatile fuel affects the observed instability. The parametric studies described below parallel these two test variations. In general terms, the analyses predict that negligible oscillatory activity will occur in the augmentor during Z8MIN operation and during all operation with AVGAS. The analytical predictions thus correspond precisely to the results observed in the tests.

SENSITIVITY TO ZONE 4 FUEL FLOW RATE

Since the 400 Hz oscillation showed a significant increase in amplitude at the Z8MAX condition as compared to the Z7 condition, an intermediate fuel zone condition was tested. The Z8MIN condition has less fuel flow than the Z8MAX condition in each fuel zone. Compared to the Z7 condition, the Z8MIN has 92 per cent of the fuel flow in Zones 1 and 3.

The analysis of the Z8MIN condition involved only an alternative radial distribution of E, the mean energy content of the fluid. The other parameters affected by the zoning-- the sonic velocity rise and the axial velocity distribution-- do not differ from those of Z7 sufficiently to warrant a completely separate set of input for Z8MIN. The analytical results for Z8MIN indicate that the principal tangential mode is simply stable. The level of the unsteady combustion driving of this mode is not sufficient to overcome the damping produced by through-flow effects until the Zone 4 fuel flow rate approaches its maximum value.

The test data for Z8MIN generally show a slight increase in 400 Hz oscillation amplitude over that of Z7. Typically, Z8MIN amplitudes are a factor of 2 greater than those of Z7, while Z8MAX amplitudes are a factor of 4 greater than those of Z8MIN. The analysis thus compares well with the test results.

The study of the Z8MIN fuel zone combination enhanced the understanding of the conditions which govern the 385 Hz instability observed in the test program. The analyses indicate that three conditions must be satisfied for this instability to occur:

1. The available driving energy for the first tangential mode must

be sufficient to overcome the inherent damping of the mode produced by losses at the nozzle and, at some operating points, by through-flow.

2. The fuel supplied by Zones 3 and 4 into the fan stream must not be completely vaporized upstream of the flame-front.

3. The rate of fuel vaporization downstream of the flame-front in Zones 3 and 4 must not exceed some limits (the exact rate of vaporization at which the instability amplitude becomes negligible cannot be defined with confidence at this time).

The study indicates that at Z8MIN the available driving energy for the first tangential mode is not sufficient to produce an instability. There is simply not enough fuel flow to drive the instability. It will later be seen that in the case of AVGAS the second condition is not satisfied. In the preceding chapter it was noted that failure to satisfy the third condition explains why the instability is minor during Z4, Z5, and Z6 operation.

SENSITIVITY TO AVGAS

Tests 9 and 10 were conducted with AVGAS rather than JP-4. Because of fuel pump limitations, the Z5 and Z6 conditions could not be tested with AVGAS, and some doubt remains whether Z8MAX was fully achieved, though the Z8MAX fuel flow rates are essentially the same as with JP-4. The precise question in the study of AVGAS is what effect the more volatile fuel has on the Z8MAX sustained oscillation. In the tests, as described in Chapter III, the effect was to eliminate the oscillation for practical purposes. The amplitude level never exceeded 2 per cent during operation with AVGAS.

The comparative volatilities of AVGAS and JP-4 are discussed in detail in Appendix IV. They differ in two crucial respects. First, for a two atmosphere vapor pressure the boiling point of AVGAS is 185 deg F, and that of JP-4 is 260 deg F. Second, the distillation band of JP-4 is much wider than that of AVGAS: specifically a 200 deg F temperature rise is required to go from 10 per cent to 90 per cent distillation of JP-4, while a 100 deg F rise is required in the case of AVGAS. In other words, AVGAS begins vaporizing at a roughly 75 deg F lower temperature, and it is completely vaporized at a roughly 175 deg F lower temperature than JP-4 when the augmentor is operating at 2 atmospheres.

During most JP-4 tests and during all AVGAS tests "warm day" conditions prevailed. In particular, during Tests 6 (with JP-4) and 10 (with AVGAS) the fan discharge temperature for Z8MAX testing was 210 deg F. The fan stream is heated by convection along the core engine length and by mixing with the core stream in the region immediately upstream of the flameholders. It was accordingly assumed that during Tests 6 and 10 the vaporization of the Zone 3 and 4 fuel upstream of the flame-front is

governed by a roughly 300 deg F fluid temperature. At this temperature AVGAS is essentially 100 per cent vaporized upstream of the flame-front, and JP-4 is only 40 per cent vaporized.

The instability analyses for AVGAS therefore assumed a value of 0.05 for α in Equations 5 and 6 of the preceding chapter, so that Zones 3 and 4 do not differ markedly from Zones 1, 2, and 5 when AVGAS is used. The results of the analyses for Z8MAX with AVGAS are indicated in Figure 25. The first tangential mode is predicted to be simply stable. The predictions agree with the data.

The experimental and analytical comparison of JP-4 and AVGAS proved particularly instructive on the question of what mechanism governs the 385 Hz instability. Three coupling mechanisms are considered likely to govern unsteady combustion in augmentors: turbulent mixing, chemical kinetics, and droplet vaporization (including atomization and burning). Changing from JP-4 to AVGAS should have negligible effects on turbulent mixing and on chemical kinetics. The only mechanism likely to be affected is droplet vaporization and burning. The fact that both the experiments and the analyses showed a dramatic reduction in the instability when AVGAS replaces HP-4 is persuasive evidence that the 385 Hz oscillation depends on droplet mechanisms for its driving energy. Substituting AVGAS for JP-4 in a conventional turbojet afterburner, with turbine discharge temperatures above 1000 deg F, would not be expected to affect instabilities. But since the fan discharge temperature is in the distillation range of AVGAS and just below the boiling point of JP-4, droplet mechanisms should simply be expected to play a large role in the TF-30-P1 fan stream augmentation.

SENSITIVITY TO AUGMENTOR INLET TEMPERATURE

By chance, one set of TF-30-P1 tests were conducted during the early spring of 1971-- early enough that the engine inlet temperature was comparatively low. These tests were conducted with the objective of finding some operating condition at which the augmentor becomes unstable. On that cold day when the severe oscillation was discovered during Z8MAX operation, data were recorded. These data were largely ignored at the time, however, since the engine was to be thoroughly tested again with the zone combinations examined in a planned sequence. When the "official" testing began and the data were reduced, the level of instability proved to be disappointingly low. Examination of the cold day tests revealed a decrease in amplitude level from roughly $\pm$10 psi to roughly $\pm$3 psi in going from cold days to warm days. All of the remaining tests were conducted during the summer. An effort to conduct additional cold day testing during the late fall had to be abandoned following an engine failure. The one set of cold day results thus stand alone, unsupported by additional test data.

Once it was recognized that augmentor inlet temperature has a dramatic effect on the TF-30-P1 instability, some special tests were conducted to see whether an increase in turbine discharge temperature alone has any effect.

Parametric studies were conducted of both the fan and the turbine discharge temperatures. In summary, the instability model predicted that lower fan discharge temperature would intensify the first tangential instability, but that higher turbine discharge temperature would have negligible effect in the range tested. These predictions agree qualitatively with the test data. Efforts to secure a more quantitative agreement, in terms of the amplitude levels sustained on cold and warm days, are discussed later in the chapter.

SENSITIVITY TO HIGHER TURBINE DISCHARGE TEMPERATURE

The special tests conducted in Tests 9 (with AVGAS) and 10 (with JP-4) had a 50 to 70 deg F increase in turbine discharge total temperature--e.g., from 1180 to 1250 deg F. In Test 9 with AVGAS a roughly 5 per cent increase in the amplitude level of the 358 Hz oscillation was observed. The test with JP-4 indicated no clear trend when compared with the comparable Z8MAX run of Test 6. A slightly more pronounced increase of the 200 Hz oscillation was observed in both cases with the higher temperature.

Increasing the turbine discharge temperature would appear to influence only two model parameters. The Mach number in the combustion chamber is slightly increased, and the rate of vaporization of the liquid fuel in Zones 3 and 4 is somewhat increased because of greater heating of the fan stream by the hotter core stream. But the 60 degree temperature increase actually achieved in the tests is simply too small to warrant revisions of the parameter values in question. The uncertainty with which these values are known exceeds any change in them from the higher turbine discharge temperature. Thus the analytical examination of this engine test variation proved inconclusive. This result does not really differ from that of the experimental examination.

SENSITIVITY TO REDUCED FAN DISCHARGE TEMPERATURE

As remarked in connection with AVGAS, the fan stream temperatures of the TF-30-P1 tests fall quite close to the boiling point of JP-4. Since JP-4 has a wide distillation band, variations in fan discharge temperature are likely to produce significant variations in the fraction of JP-4 from Zones 3 and 4 which is vaporized upstream of the flame-front. Thus on purely heuristic grounds the increase in oscillation amplitude from 10 to 37 per cent on cold days is not counterintuitive.

The cold day tests have a fan discharge temperature of 178 deg F, which is 25 deg F below that of the corresponding warm day tests. In the parametric analyses the fan stream temperature at the flameholders was assumed to be 270 deg F on cold days and 300 deg F on warm days. The key parameter which changes is a, the fraction of the fuel remaining in droplet form at the flame-front. In analyzing the warm day condition 60 per cent of the fuel from Zones 3 and 4 was assumed to be unvaporized; for analyzing the cold day condition, the value of a for Zones 3 and 4 was assumed to be 1.0. The latter value may be a slight exaggeration since

the boiling point of JP-4 at two atmospheres is about 260 deg F, but for purposes of the parametric studies greater accuracy is not needed.

The increase in the liquid fraction of Zones 3 and 4 produces a proportional increase in the oscillatory energy produced by droplet vaporization mechanisms. In terms of NREC's model the coefficients governing E' and τ' are both affected:

$$\frac{E'}{\bar{E}} = -\frac{a}{\gamma}\frac{P'}{\bar{P}} - \frac{1-a}{2}\left[\frac{\mu_j'}{\bar{\mu}_j} + \frac{1}{\gamma}\frac{P'}{\bar{P}}\right]_{INJECTOR} \tag{10}$$

$$\frac{\tau'}{\bar{\tau}} = \left[\frac{\sum_{n=1}^{5} a^n C_f^n \dot{m}_f^n}{\sum_{n=1}^{5} \dot{m}_f^n}\right]\frac{P'}{\bar{P}} \tag{11}$$

where the average liquid fraction, a, is obtained from the values of the individual zones:

$$a = \left[\sum_{n=1}^{5} a^n \dot{m}_f^n\right] \Big/ \sum_{n=1}^{5} \dot{m}_f^n \tag{12}$$

An increase in a thus increases the amplitude of $\tau'/\bar{\tau}$, but its effect on $E'/\bar{E}$ depends on the comparative importance of fluid oscillations at the flame-front and at the fuel injectors. Since $\tau'/\bar{\tau}$ is usually the dominant term governing the oscillatory heat release rate, the above equations indicate that increasing the liquid fraction of the fuel will in general produce a greater oscillatory heat release rate for a given pressure oscillation. But whether the oscillatory heat release rate drives or damps the pressure oscillation depends on the phase lag between them. Thus, increasing the liquid fraction does not necessarily make a mode more unstable. The rest of the NREC model is needed to determine whether the resulting intensification of the heat release rate oscillation drives or damps each mode.

The point here is that it is <u>not</u> a trivial consequence of NREC's model that on cold days the TF-40-P1 is predicted to have a more severe 385 Hz oscillation than on warm days. As Figure 26 shows, the model does predict a significantly more negative decrement on cold days. The results shown in the figure are for Z8MAX. The comparable result for Z4 on a cold day similarly shows a more negative decrement. Indeed, Z4 on a cold day has a negative decrement which is roughly 75 per cent of that of Z8MAX on a warm day. In other words, the instability solutions yield two qualitative predictions:

1. The 385 Hz oscillation is more intense on cold days than on warm

days. The intensification holds for each fuel zone combination, but it is most dramatic in the case of Z8MAX, for which Zones 3 and 4 play a dominant role.

2. On a cold day the 385 Hz oscillation is intensified during Z4 operation to the point that it approaches the level predicted for Z8MAX on warmer days.

A glance at the data, shown for example in Table VI, indicates that these two qualitative trends predicted by the model are precisely the trends which were observed. On a cold day the Z8MAX instability is much more severe, and the Z4 oscillation reaches the order of severity of the Z8MAX instability on a warm day. The Z4 zone combination was chosen for the comparison because it is the only one other than Z8MAX for which cold day data are available.

The conclusion, then, is that NREC's instability model, supplemented by simple droplet vaporization formulas, does predict the direction of the effect of a reduced fan discharge temperature. The solutions in Figure 26, do not, however, predict sustained amplitude levels, so that comparison must be made in terms of a physically more elusive variable, viz. the negative decrement or growth rate of the oscillation. Since the analytical solutions do not determine a sustained amplitude, we have not predicted what was observed, namely a reduction of sustained amplitude levels as fan discharge temperature increases. The problem of predicting amplitude levels rather than just oscillation growth rates is discussed in the remainder of this chapter.

PREDICTING THE SUSTAINED AMPLITUDE LEVELS

The problem is easy to define. The observed amplitude level during Z8MAX operation was below 10 per cent on warm days and above 35 per cent on cold days. The calculations, based on a simple droplet vaporization model, predict that the amplitude level-- whatever it may be-- exceeds 30 per cent on both warm and cold days. The key fault in the calculated results is not simply their failure to predict the lower amplitude of the warm day tests. The key fault is that the graphical solutions for the instability show no sign whatever of producing a sustained amplitude number. Regardless of the augmentor inlet temperature, the decrement curve is calculated to have the following shape:

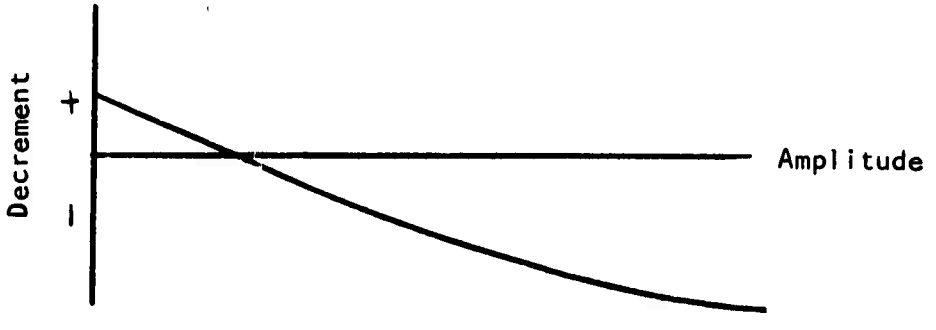

For the largest amplitude examined, the instability is not simply still growing, it is growing even faster than at lower amplitudes. For the instability analysis to predict a sustained amplitude, the decrement curve must turn back toward the axis:

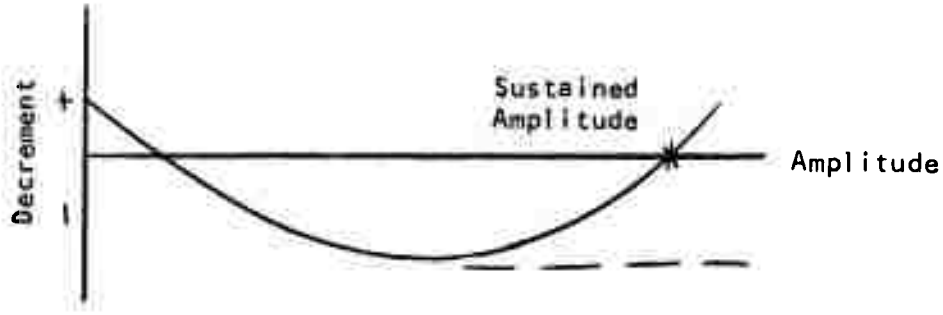

The solutions using the simple droplet vaporization model, rather than turning back, all appear to be asymptotic to some minimim value of the decrement.

Two questions require examination. First, why does the analysis fail to produce decrement curves of the shape anticipated? Second, what type of revision of the analysis is necessary for the decrement curves to be of the correct shape? These two questions are addressed in the next section. The succeeding section will then indicate what sort of correlation between predicted and observed amplitudes can be achieved by following a logical line of revision of the analyses.

FACTORS GOVERNING THE SUSTAINED AMPLITUDE LEVEL

The decrement calculated in the instability analysis is a consequence of a number of effects, some of which add positively to it (i.e., stabilize the mode) and others, negatively:

1. The upstream and downstream boundary effects damp the instability.
2. In the case of Z8MAX, the through-flow damps the instability.
3. The screech liner damps the instability, but only slightly, and even then less at high amplitude.
4. The oscillatory heat release drives the instability, and its contribution to the calculated negative decrement increases with amplitude.

The through-flow and upstream and downstream boundary effects are assumed not to vary with amplitude: the contributions they make to the decrement are constant. Accordingly, increasing these effects will not produce the desired effect of reshaping the calculated decrement curve; it will only shift the curve:

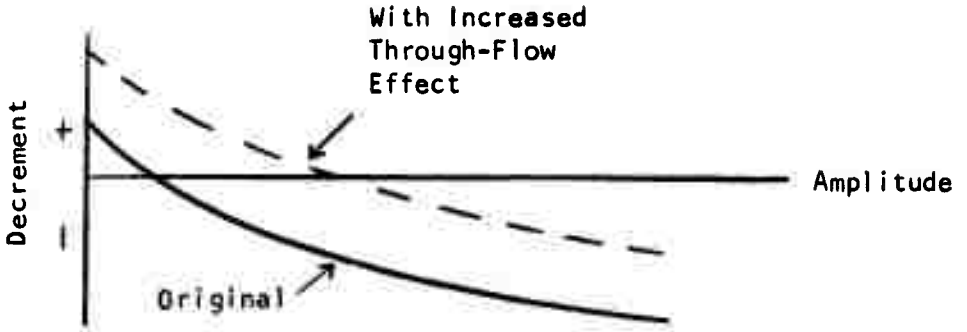

In NREC's earlier parametric studies of conventional afterburners amplitude levels below 10 per cent were predicted, but only as a consequence of large screech liner acoustic absorption. The test data clearly show that the liner is not governing the amplitude level sustained in the TF-30-P1 augmentor. Thus, although the liner effect varies nonlinearly, in the case of the TF-30 oscillation at 385 Hz it is not significant.

NREC's instability analysis intentionally ignored shock losses in its calculation of the contribution of through-flow to the decrement. Shock losses vary sharply nonlinearly with the amplitude of the oscillation insofar as the velocity oscillation must be sufficient for the local flow to reach sonic values before shocks appear. During Z8MAX operation, the mean or steady velocity in the augmentor does not exceed a Mach number of 0.75. Thus shock losses cannot be governing the instability amplitude level on warm days when the pressure fluctuations are below 10 per cent amplitude. Shock losses should become significant for the Z8MAX instability only as amplitude levels in excess of 25 per cent are reached. The shock losses may govern the cold day amplitude levels, but they are not the mechanism which the initial analyses of the TF-30-P1 have crucially failed to consider.

The oscillatory heat release rate is thus the mechanism which most significantly controls the sustained amplitude level in the TF-30-P1 at least for the warm day conditions. NREC's treatment of the oscillatory heat release has four distinct components:

1. For Z8MAX, oscillations in the convection velocity governing combustion have a very small damping effect on the 385 Hz instability. The extent of the damping increases slightly with increasing amplitude.

2. Local density oscillations drive the instability significantly, and the extent of their effect increases somewhat, but not markedly, with the amplitude level.

3. Oscillations in the energy content of the fluid entering the combustion chamber have a slight driving effect, which increases somewhat with the amplitude level.

4. Oscillations in the characteristic time of combustion make, by a factor of 2, the largest driving contribution at large amplitude, but at small amplitudes their contribution is negligible.

The first two contributions to the unsteady heat release, those resulting from the convection velocity and the density, are essentially independent of coupling mechanisms. Their contribution to the decrement varies slightly nonlinearly only because the mean time for combustion is calculated to decrease at larger amplitude levels. Neither of these contributions will suffice to reshape the decrement curve. Similarly, the effect of the energy content is too small to be significant in governing the sustained amplitude level, particularly since it is essentially constant with amplitude.

Attention thus centers on the effects of the characteristic time of combustion. For practical purposes all other mechanisms which are thought to be relevant make a constant contribution to the unstable decrement curve of Z8MAX. Only the $\tau'/\bar{\tau}$ effect varies sufficiently strongly nonlinearly that it can govern the sustained amplitude level by governing the shape of the calculated decrement curve. The reason that the analyses fail to predict sustained amplitude levels is to be found in the modelling of the $\tau'/\bar{\tau}$ dependence on amplitude level.

The decrement calculations were made assuming that droplet vaporization is the only coupling mechanism of significance. In particular, the relation between τ and the fluid oscillations was assumed to be as follows (see Equations 5 and 6):

$$\tau'/\bar{\tau} = \tilde{C}_1 \, p'/\bar{p} \qquad (13)$$

$$\bar{\tau} = \tilde{C}_7 \, \tau_d$$

Here $\tilde{C}_1$ and $\tilde{C}_7$ both vary nonlinearly with amplitude, and they also depend on the droplet Reynolds number and on the fraction of the nominal design time required for droplet vaporization (i.e., $b = \tau_e / \tau_d$). Figure 27 displays typical curves for $\tilde{C}_1$ and $\tilde{C}_7$ as a function of these parameters. Both $\tilde{C}_1$ and $\tilde{C}_7$ are asymptotic in these curves. In particular, $\tilde{C}_1$ keeps increasing with increasing amplitude. Thus, the unfortunate shape of the decrement plots is a direct result of the shape of the $\tilde{C}_1$ curve, which corresponds to a simple droplet vaporization model. Within this simple view of droplet vaporization increasing amplitudes of pressure oscillation will invariably result in increasing amplitudes in the oscillation of the time required for combustion. The relationship between $\tau'/\bar{\tau}$ and $p'/\bar{p}$ based in this way on droplet vaporization cannot produce a self-sustained amplitude prediction.

There remain three approaches by which the analyses may yet predict sustained amplitude levels. One suggestion, discussed in NREC's earlier studies (Ref 2), is that if the mean time of combustion, $\bar{\tau}$, becomes sufficiently small, the contribution of $\tau'/\bar{\tau}$ becomes small:

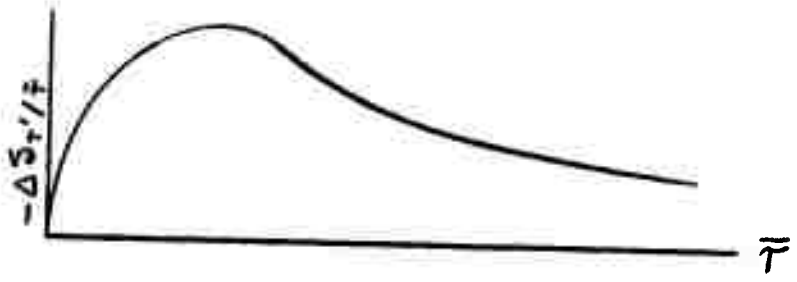

In physical terms, when the combustion is concentrated in a short enough length of the augmentor, the contribution of $\tau'/\bar{\tau}$ becomes zero, and the decrement curve turns back toward the axis. In the case of the TF-30-P1 all combustion has to be concentrated in less than 10 inches of the augmentor before a sustained amplitude can be reached. Turbulent mixing requirements preclude such a concentrated combustion zone. Moreover, amplitude levels in excess of 25 per cent are needed for the mean droplet vaporization times to become so small, even should turbulent mixing be ignored.

The second approach is to argue that the droplet vaporization model is too naive in that it ignores secondary effects which, when taken into account, will produce the preferred shape of the $\tilde{C}_1$ plot in Figure 27. This suggestion may ultimately be vindicated by more detailed experimental studies of droplet mechanisms. NREC resists it at this point in the belief that the gross features of instability should not require consideration of secondary effects.

The third approach is to examine coupling mechanisms other than droplet evaporation. Droplet burning, chemical kinetics, and turbulent mixing are mechanisms thought to be significant in augmentors. In simple terms, they couple fluid conditions to the time required for combustion as follows:

$$\begin{aligned} &\text{Droplet Burning:} && \tau \sim k_1 / (1 + k_2 p^{1/2}) \\ &\text{Chemical Kinetics:} && \tau \sim k_4 e^{E_a/RT} / p^2 \\ &\text{Turbulent Mixing:} && \tau \sim k_3 / \mu_{th} \end{aligned} \qquad (14)$$

In other words, chemical kinetic and droplet burning mechanisms have the same type of effect as droplet vaporization; so that if the latter in fact drives an instability, so will the former. Turbulent mixing, by varying with velocity, is out-of-phase with the others, and hence will tend to stabilize when the others tend to drive. Therefore, the most plausible approach to predicting sustained amplitudes is to introduce supplementary stabilizing effects by hypothesizing a model of oscillatory turbulent mixing.

HYPOTHESIZING THE REQUIRED TURBULENT MIXING EFFECT

The problem is to devise a simple account of turbulent mixing in

unsteady flow which will enable prediction of low levels of sustained amplitude for operation at Z8MAX on warm days. Ideally, the added effect of turbulent mixing will also produce predicted sustained amplitudes below 5 per cent for Z4 etc., even on cold days. Developing a detailed theoretical account is beyond the scope of this study. We shall instead adopt a simple view of the physical mechanism and deduce the level of effect required from it for predictions to correlate with the TF-30-P1 observations.

Program REFINE includes provision for a turbulent mixing effect in that it allows for a coefficient, $\tilde{C}_6$, as follows:

$$\frac{\tau'}{\bar{\tau}} = \tilde{C}_1 \frac{p'}{\bar{p}} + \tilde{C}_6 \left(\frac{u_3'}{\bar{u}_3} \right)_{\text{flame holder}} \tag{15}$$

where the velocity oscillation is defined at the flameholders. The problem, then, is to determine $\tilde{C}_6$ as a nonlinear function of amplitude level.

If both turbulent mixing and droplet vaporization are taken into account, the expression for characteristic time of combustion must be made somewhat more complicated:

$$\frac{\tau'}{\bar{\tau}} = \frac{\bar{\tau}_T}{\bar{\tau}} \left(\frac{\tau'}{\bar{\tau}} \right)_T + \frac{\bar{a}\,\bar{\tau}_e}{\bar{\tau}} \left(\frac{\tau'}{\bar{\tau}} \right)_e \tag{16}$$

$$\bar{\tau} = \bar{\tau}_T + \bar{a}\,\bar{\tau}_e \tag{17}$$

where, again, a is the fraction of fuel remaining in droplet form, and the subscripts e and T refer respectively to evaporation and turbulent mixing. What is required are formulas for $\tilde{C}_1$ and $\tilde{C}_6$ of the following form:

$$\tilde{C}_1 \frac{p'}{\bar{p}} = \frac{\bar{a}\,\bar{\tau}_e}{\bar{\tau}} \left(\frac{\tau'}{\bar{\tau}} \right)_e \tag{18}$$

$$\tilde{C}_6 \left(\frac{u_3'}{\bar{u}_3} \right)_{fh} = \frac{\bar{\tau}_T}{\bar{\tau}} \left(\frac{\tau'}{\bar{\tau}} \right)_T \tag{19}$$

Here it is assumed that $\tilde{C}_1$, as presented in Figure 27, is adequate for present purposes.

The time required for turbulent mixing varies inversely with the velocity at the flameholders (ignoring secondary effects):

$$\tau_T = k_3 / \mu_{fh} \tag{20}$$

Using standard perturbation techniques, the fluctuation in time can be defined as follows:

$$\left(\frac{\tau'}{\bar{\tau}}\right)_T = -\frac{k_T}{1 + (\mu_3'/\bar{\mu}_3)_{fh}} \left(\frac{\mu_3'}{\bar{\mu}_3}\right)_{fh} \tag{21}$$

where the factor k_T should theoretically be 1.0, but is here left as a parameter to enable adjustment of the level of effect of turbulent mixing. The other term in Equation 19, $\bar{\tau}_T/\bar{\tau}$, also varies nonlinearly with amplitude simply because $\bar{\tau}_c/\bar{\tau}$ varies nonlinearly. That is, assuming $\bar{\tau}_T$ is constant with amplitude, decreasing the mean time required for droplet evaporation will increase $\bar{\tau}_T/\bar{\tau}$, the fraction of the mean time taken up by turbulent mixing.

There are thus two factors contributing to $\tilde{C}_6$. One factor $(\tau'/\bar{\tau})_T$, introduces an inverse variation of $\tilde{C}_6$ with amplitude. The increased role of turbulent mixing, $\bar{\tau}_T/\bar{\tau}$, on the other hand, introduces a nonlinear factor which varies directly with amplitude. The net effect is as follows:

$$\tilde{C}_6 = -\left[\frac{\bar{a}\,\bar{\tau}_T + (1-\bar{a})\tilde{C}_7\,\bar{\tau}_{e_0}}{\bar{a}\,\bar{\tau}_T + \tilde{C}_7\,\bar{\tau}_{e_0}}\right] \frac{k_T}{1 + (\mu_3'/\bar{\mu}_3)_{fh}} \tag{22}$$

where $\bar{\tau}_{e_0}$ is the mean time required for droplet vaporization without pressure oscillations, and $(\tilde{C}_7 \cdot \bar{\tau}_{e_0})$ is the mean time required with oscillations. Since $\tilde{C}_7$ varies nonlinearly with the pressure oscillation amplitude, so will $\tilde{C}_6$. Figure 28 shows a typical variation of $\tilde{C}_6/k_T$ with amplitude level when $\tilde{C}_7$ is assumed to vary in the manner also shown in Figure 28. What the figure shows is that $\tilde{C}_6$ increases with amplitude when reasonable assumptions are made about the ratio of the characteristic times of evaporation and mixing in Zones 3 and 4. Since $\tilde{C}_6$ increases with amplitude, it can in principle serve as the stabilizing factor needed for the analyses to predict some sustained amplitude level. Such a superficial treatment of turbulent mixing is scarcely conclusive. It only shows that including the effects of turbulent mixing will produce the type of modification of the calculated decrement curves which we need.

Using the curve for $\tilde{C}_4/k_T$ shown in Figure 28, a value of k_T can be selected which will specifically produce the result of a 10 per cent amplitude level sustained in Z8MAX on a warm day. Figure 29 shows such a revised warm day solution. With this same value of k_T, the cold day amplitude for Z8MAX continues to exceed 30 per cent, as again shown in Figure 29. Moreover, as shown in Figure 30, with this same value of k_T the sustained amplitude level predicted for Z4 becomes less than 5 per cent on both warm and cold days. The level of the turbulence effect has accordingly been chosen to correlate predicted and observed amplitude levels on warm days in Z8MAX. The fact that when this somewhat arbitrary choice is made, correlation of predicted and observed amplitudes at other operating conditions is achieved confirms qualitatively that turbulent mixing is the stabilizing mechanism. In other words, the analysis ultimately claims that the TF-30-P1 augmentor instability involves a delicate balance between an exciting droplet vaporization mechanism and a damping turbulent mixing mechanism.

CONCLUSIONS OF THE PARAMETRIC STUDIES

1. In both the analyses and the tests the geometry variations of the liner and flameholder which were examined were found to have negligible effects on the first tangential instability.

2. The predicted trends with more volatile fuel and lower fan discharge temperature agreed qualitatively with the trends observed: the instability essentially disappears with AVGAS, and it becomes more severe with reduced fan temperature. These trends indicate that the crucial mechanism driving this instability is droplet evaporation in the colder fan stream.

3. In order to obtain any predictions of sustained amplitude level from the instability analysis, it is necessary to hypothesize a stabilizing effect from turbulent mixing. If the level of this effect is stipulated on the basis of observed warm day amplitudes, the analyses will yield qualitatively correct predictions of sustained amplitudes for cold days and when operating at Z4 rather than Z8MAX. Thus turbulent mixing in conjunction with droplet evaporation appears ultimately to control the sustained amplitude level.

CHAPTER VI

CONCLUSIONS AND RECOMMENDATIONS

CONCLUSIONS PERTAINING TO THE INSTABILITY MODEL

1. At least for predominately transverse modes, mixed flow augmentors are best modelled as conventional cylindrical afterburners with unusual upstream boundaries. No conclusions were reached on predominately longitudinal modes.

2. NREC's heat release model, which uses lumped-parameters to define local heat release rates, is adequate even for multiple zoned augmentors with significantly different combustion properties in different zones. However, for such zoned augmentors the combustion input parameters should be calculated by averaging over the individual zones, and the effects of each zone on the steady combustion of others should be taken into account.

3. The instability model correctly predicted the qualitative trends which result from the liner and flameholder modifications, from the substitution of AVGAS for JP-4, from the blocking of individual fuel zones, and from reductions in engine inlet temperature. However, better "submodels" of droplet vaporization and burning, chemical kinetics, and turbulent mixing are needed for the model to predict sustained amplitude levels with even rough accuracy.

CONCLUSIONS PERTAINING TO THE ENGINE TESTS

1. The instability observed in the TF-30-P1 augmentor requires three conditions to be satisfied before its amplitude levels become significant:

   a. The augmentation level must be sufficient; specifically, at least Zones 1, 3, and 4 must be in operation.

   b. The fuel supplied by Zones 3 and 4 into the fan stream must not be mostly vaporized upstream of the flameholders.

   c. The rate of droplet vaporization and burning downstream of the flameholders in the fan stream must not exceed some upper limit.

   The first condition explains why there is no instability during Z7 and Z8MIN operation; the third condition explains why there is no instability during Z4, Z5, and Z6 operation; and the second condition explains why the instability disappears with AVGAS and is less severe on warm days.

2. During a sustained 37 per cent amplitude oscillation at 385 Hz in the augmentor, the TF-30-P1 fan/compressor did not surge.

3. The high response pressure instrumentation used in the test program provided effective data to be used in conjunction with the NREC combustion instability model.

RECOMMENDATIONS

1. The general augmentor instability model previously developed by NREC should be used in augmentor development programs, and its further development via systematic comparison of predictions and observations should be pursued with vigor.

2. Longitudinal modes in mixed-flow augmentors should be examined analytically and experimentally to determine how to apply NREC's model to them. The prerequisite is an augmentor with a significant longitudinal instability.

3. Studies should be made of the preferred representation of the steady combustion in augmentors within the context of NREC's instability model. In particular, interactions of core stream and fan stream combustion zones require more reliable modelling.

4. Improved models of coupling mechanisms in augmentors, including their interactions and their nonlinear dependence on oscillation amplitude, should be pursued in order to increase the quantitative effectiveness of the instability model.

5. Future engine test programs, possibly even on the TF-30, should examine how augmentor instability is affected by steady inlet distortion in turbofan engines.

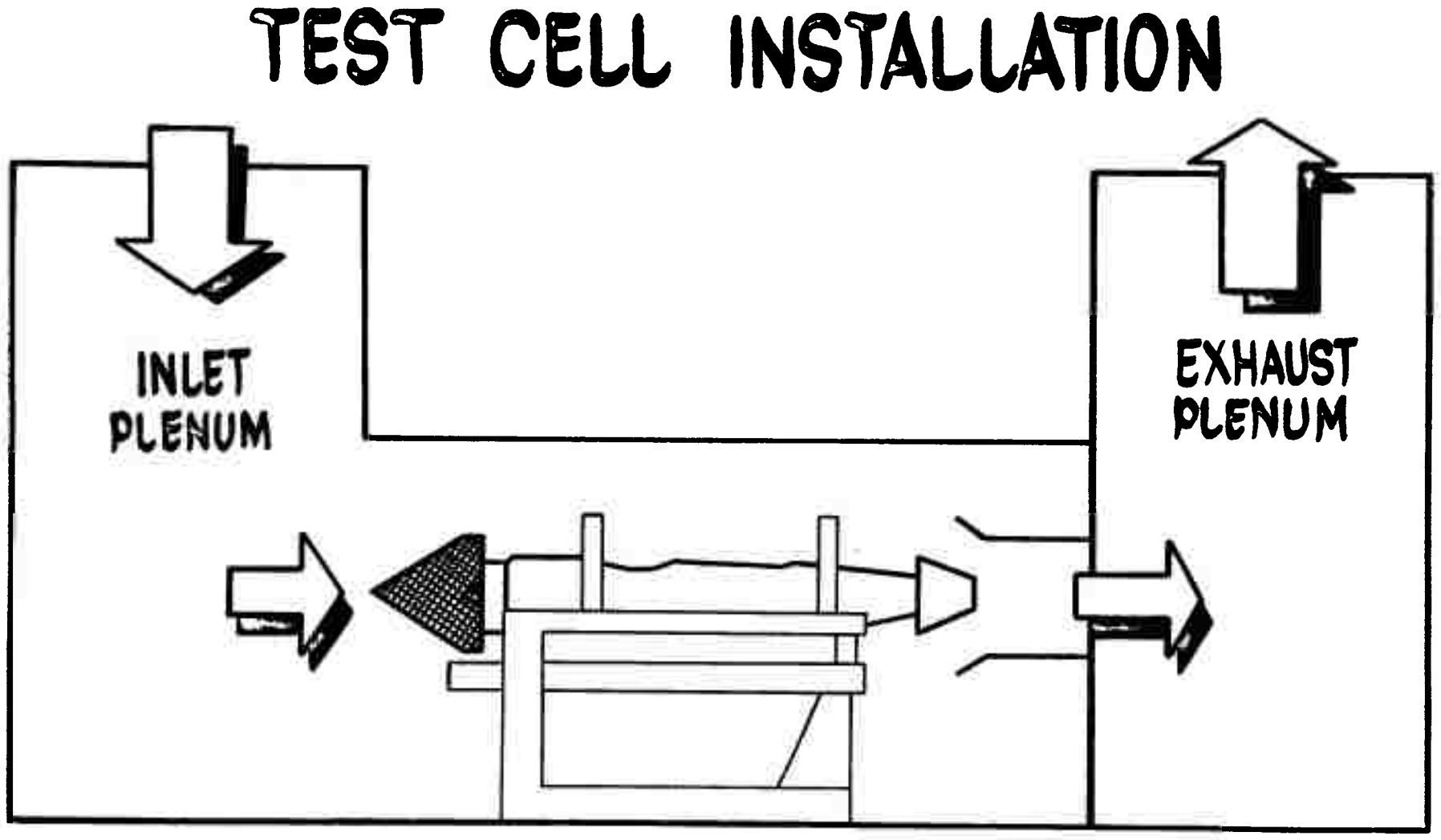

FIGURE 1 - SCHEMATIC OF TEST CELL INSTALLATION

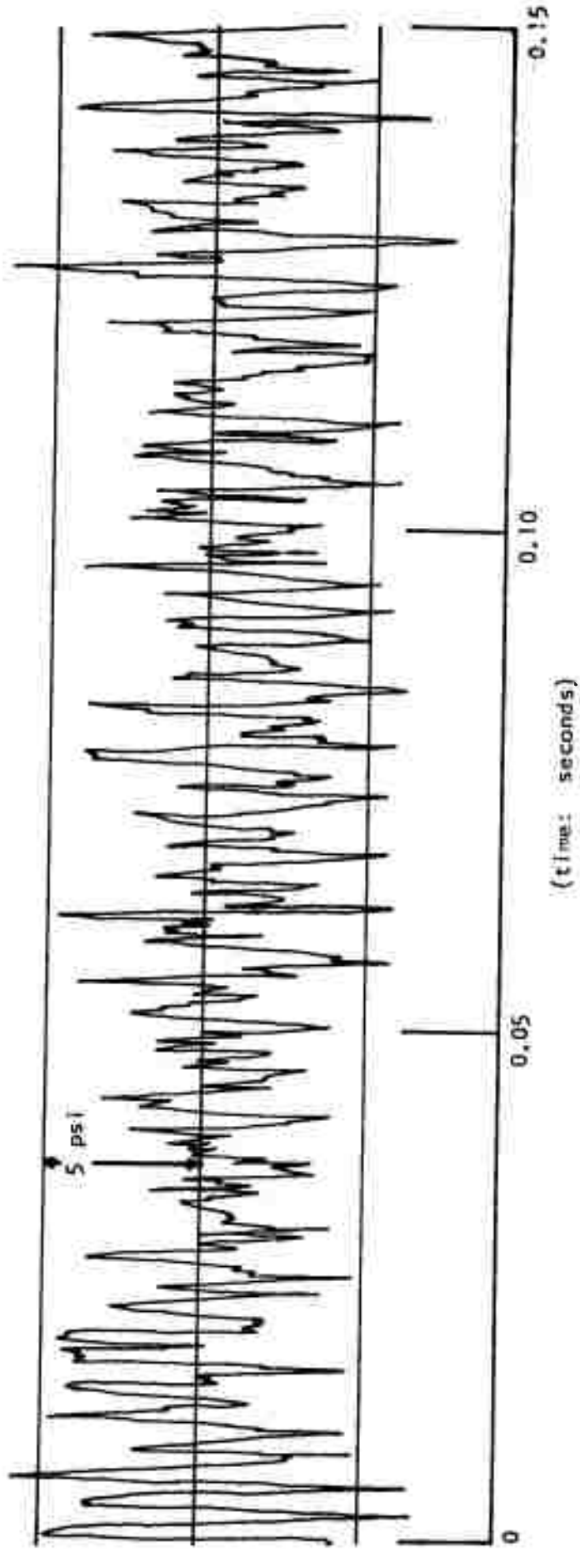

FIGURE 2 - PRESSURE OSCILLATION TRACE, CHANNEL 4, TEST 6, Z8MAX

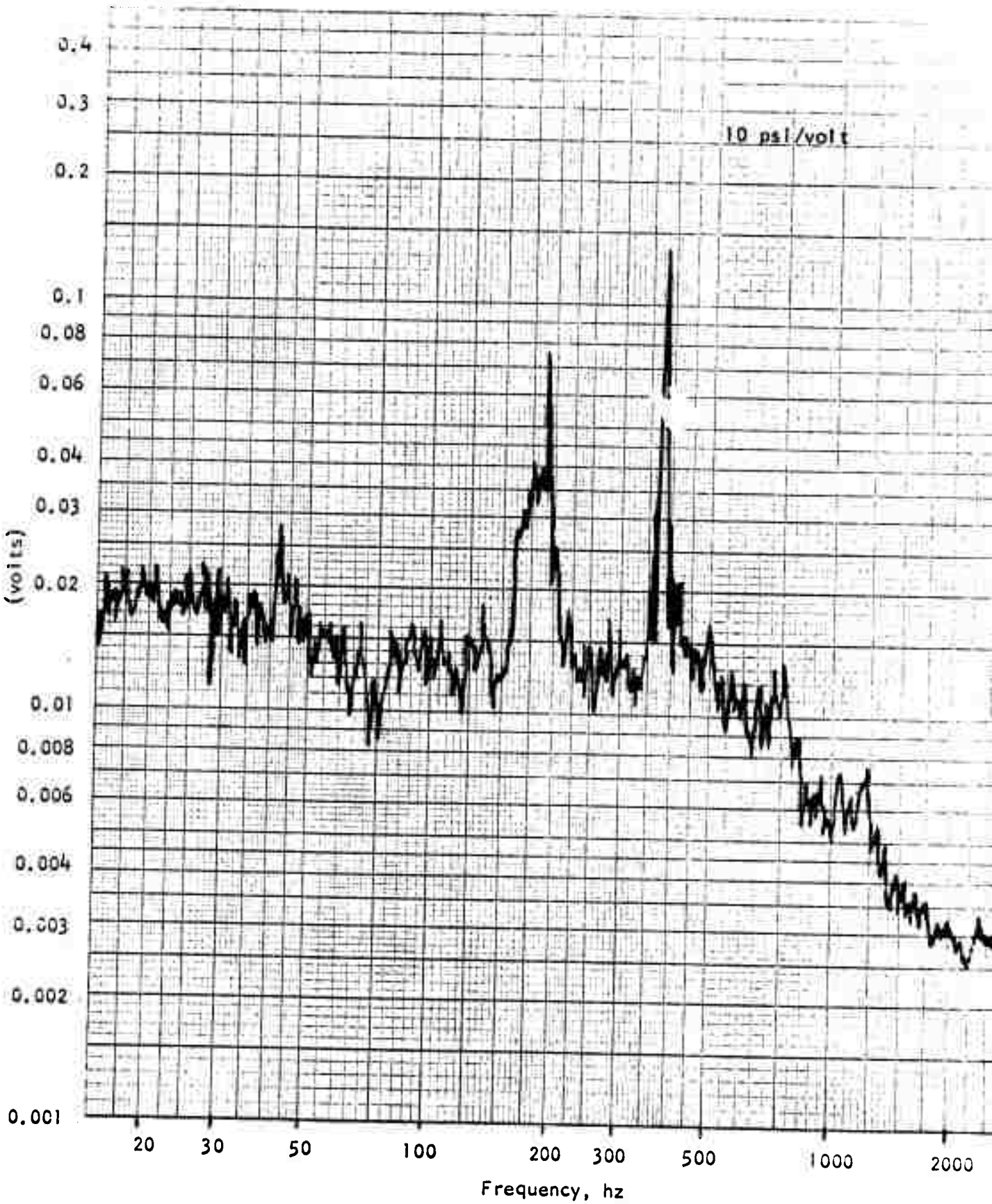

FIGURE 3 - PSD OF PRESSURE OSCILLATION, CHANNEL 4, TEST 6, Z8MAX

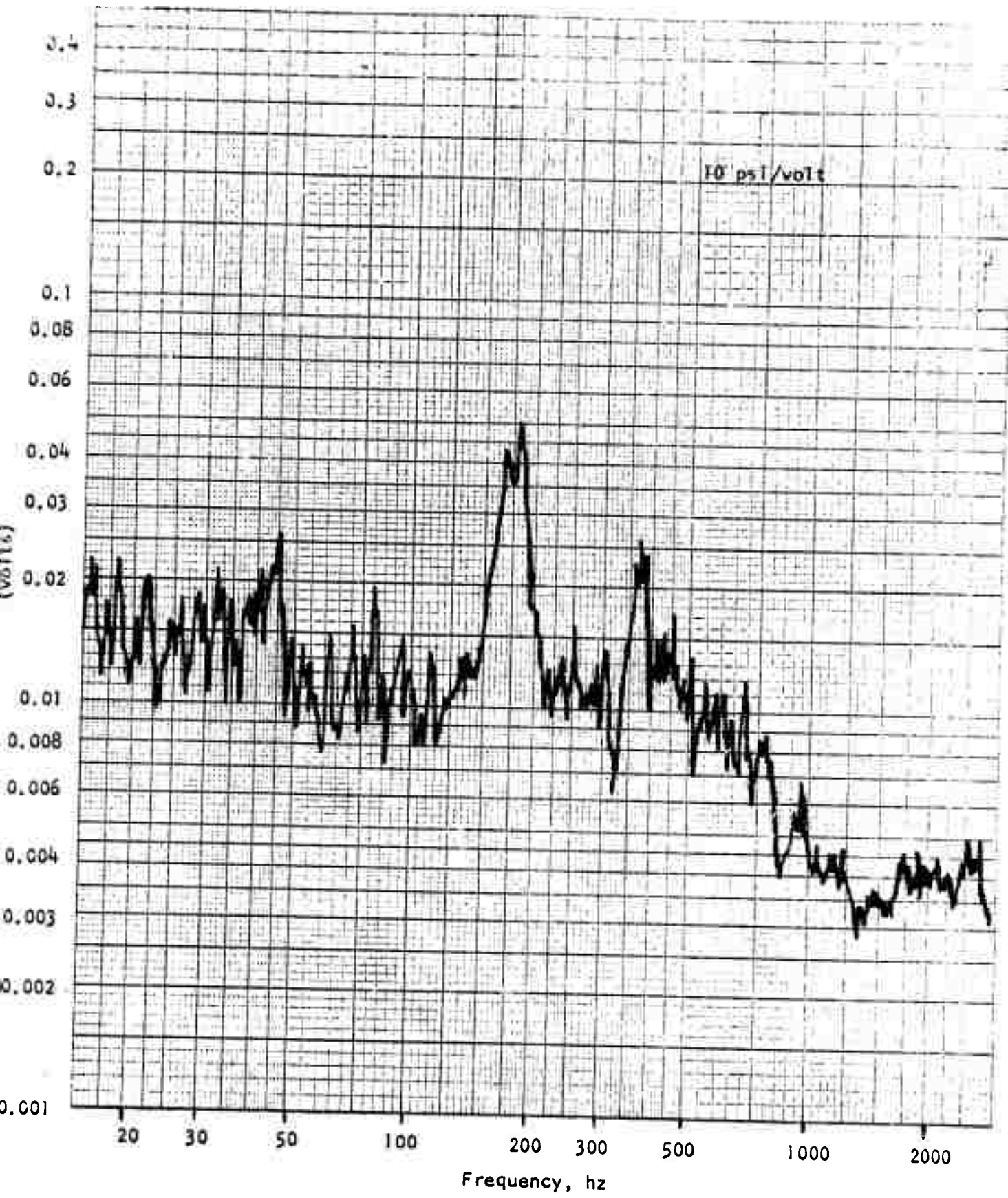

FIGURE 4 - PSD OF PRESSURE OSCILLATION, CHANNEL 4, TEST 6, Z5

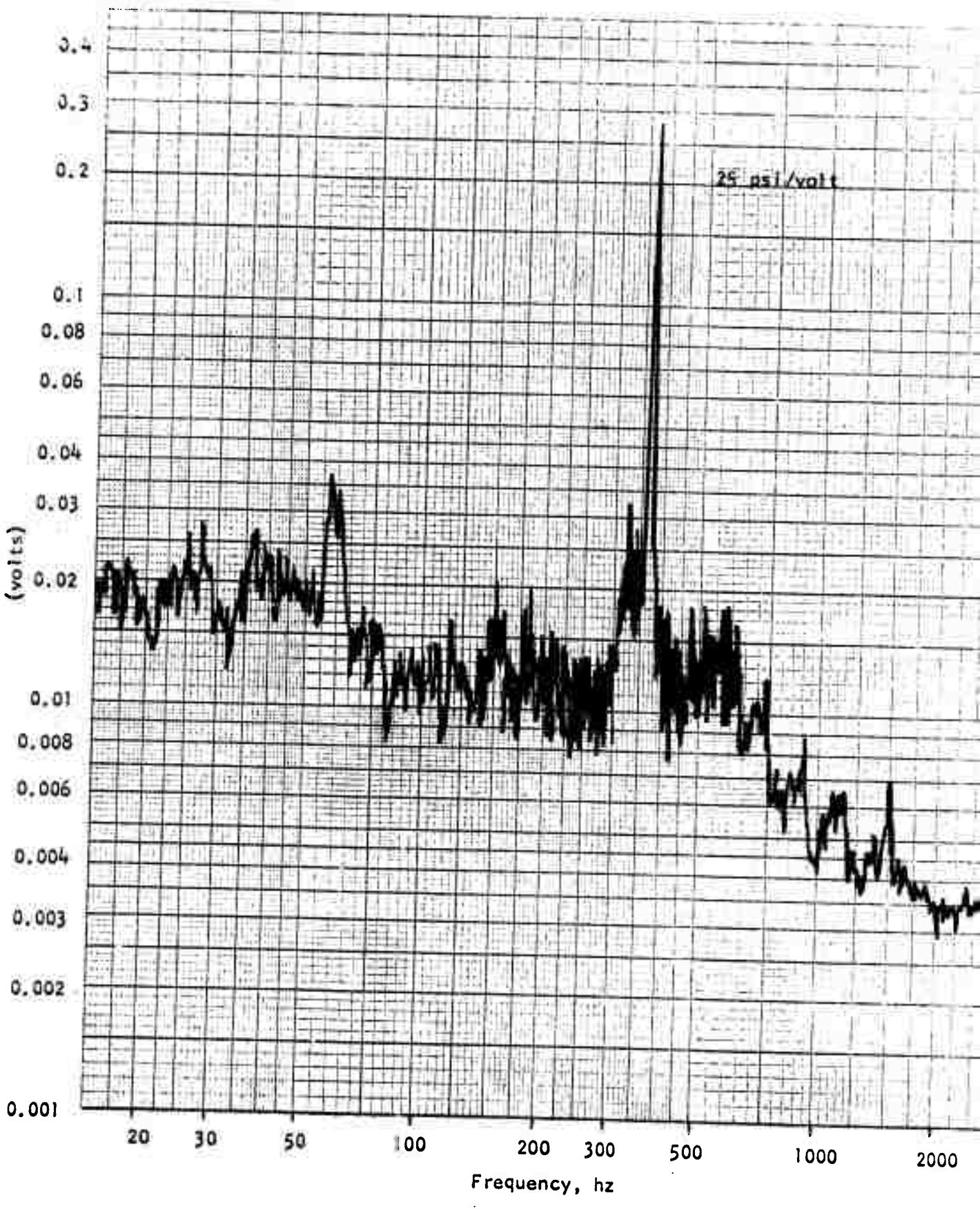

FIGURE 5 - PSD OF PRESSURE OSCILLATION, CHANNEL 7, TEST 1, Z8MAX (COLD DAY)

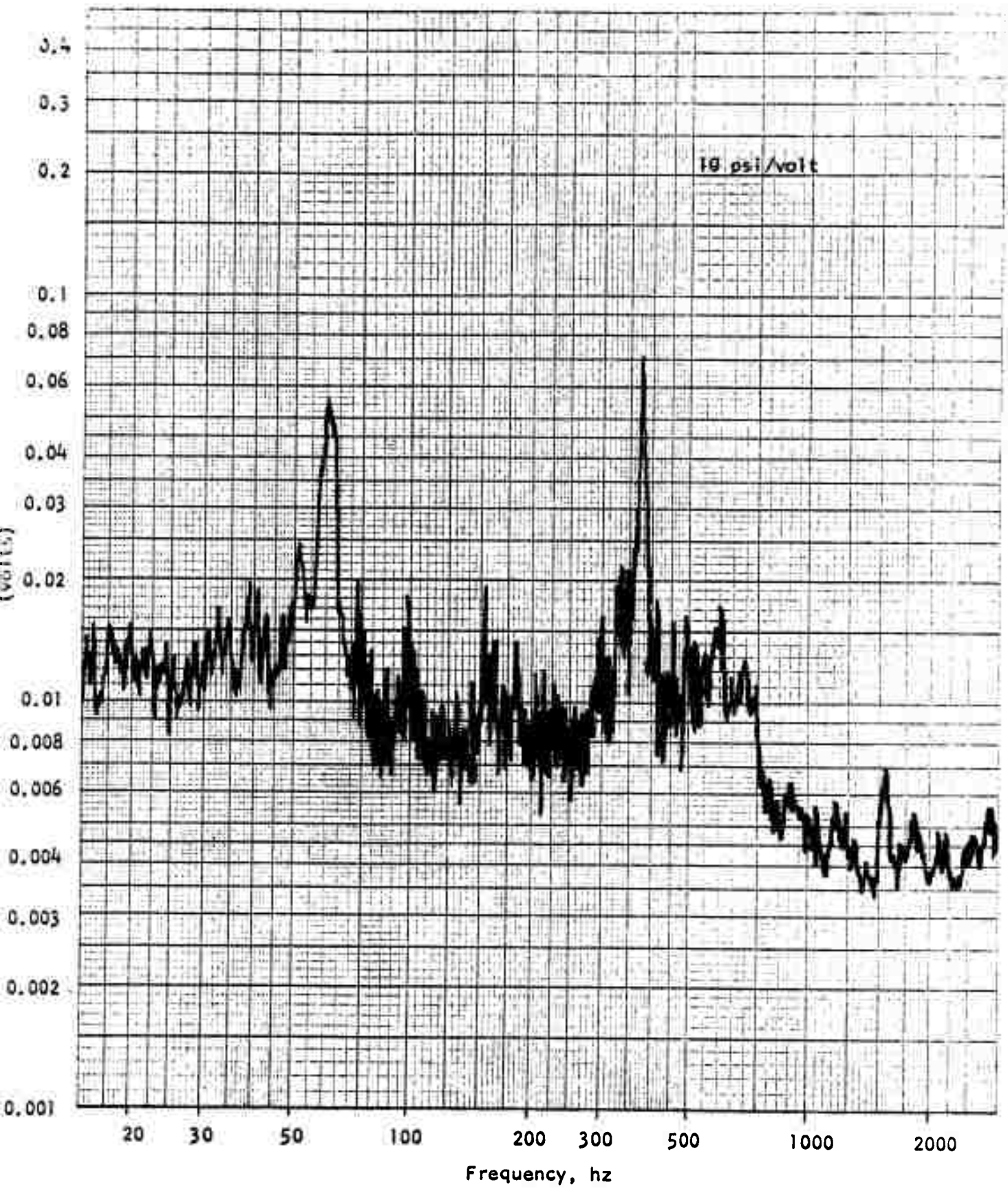

FIGURE 6 - PSD OF PRESSURE OSCILLATION, CHANNEL 7, TEST 1, Z4 (COLD DAY)

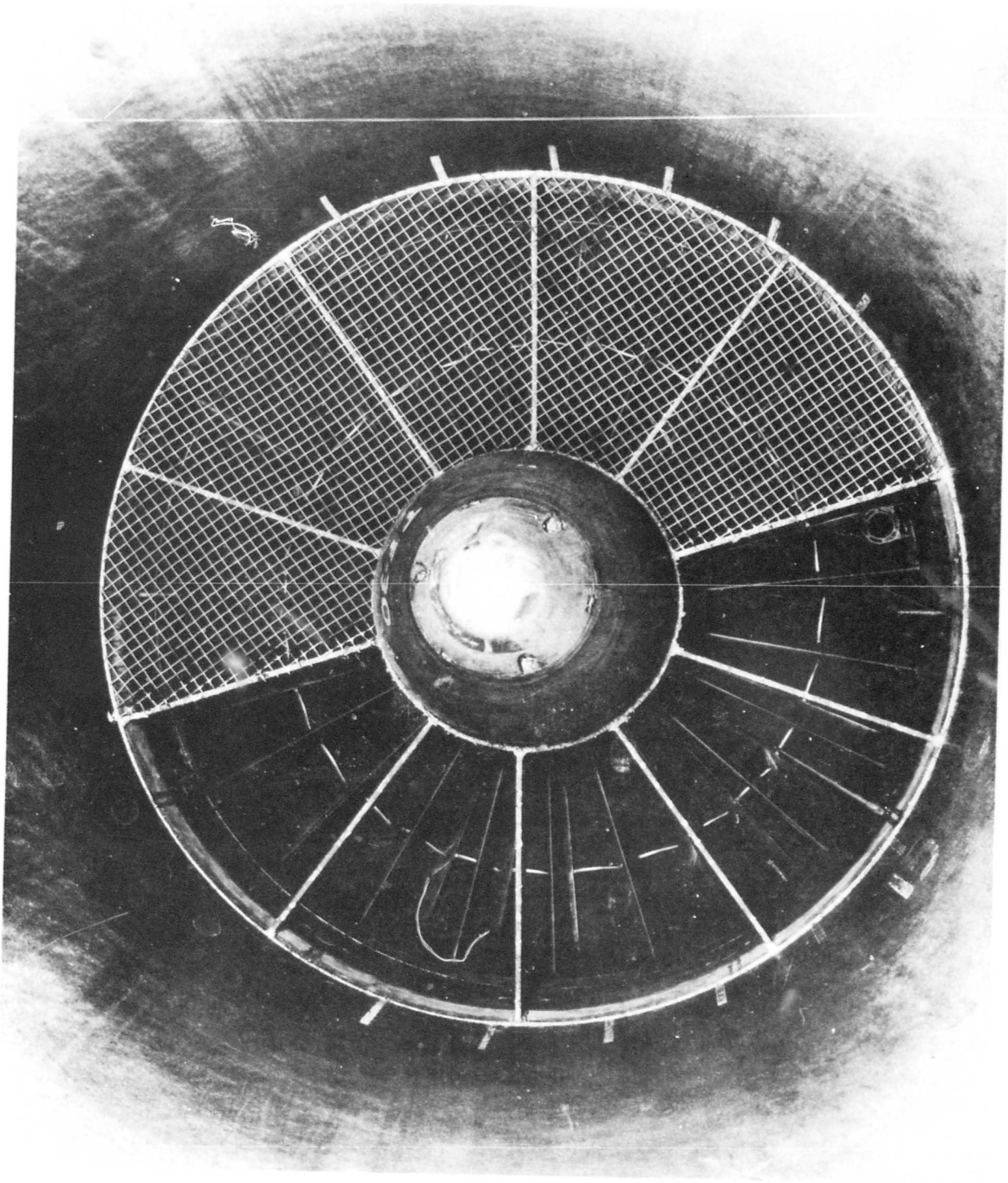

FIGURE 7 - FAN INLET DISTORTION SCREEN: 180 DEGREES

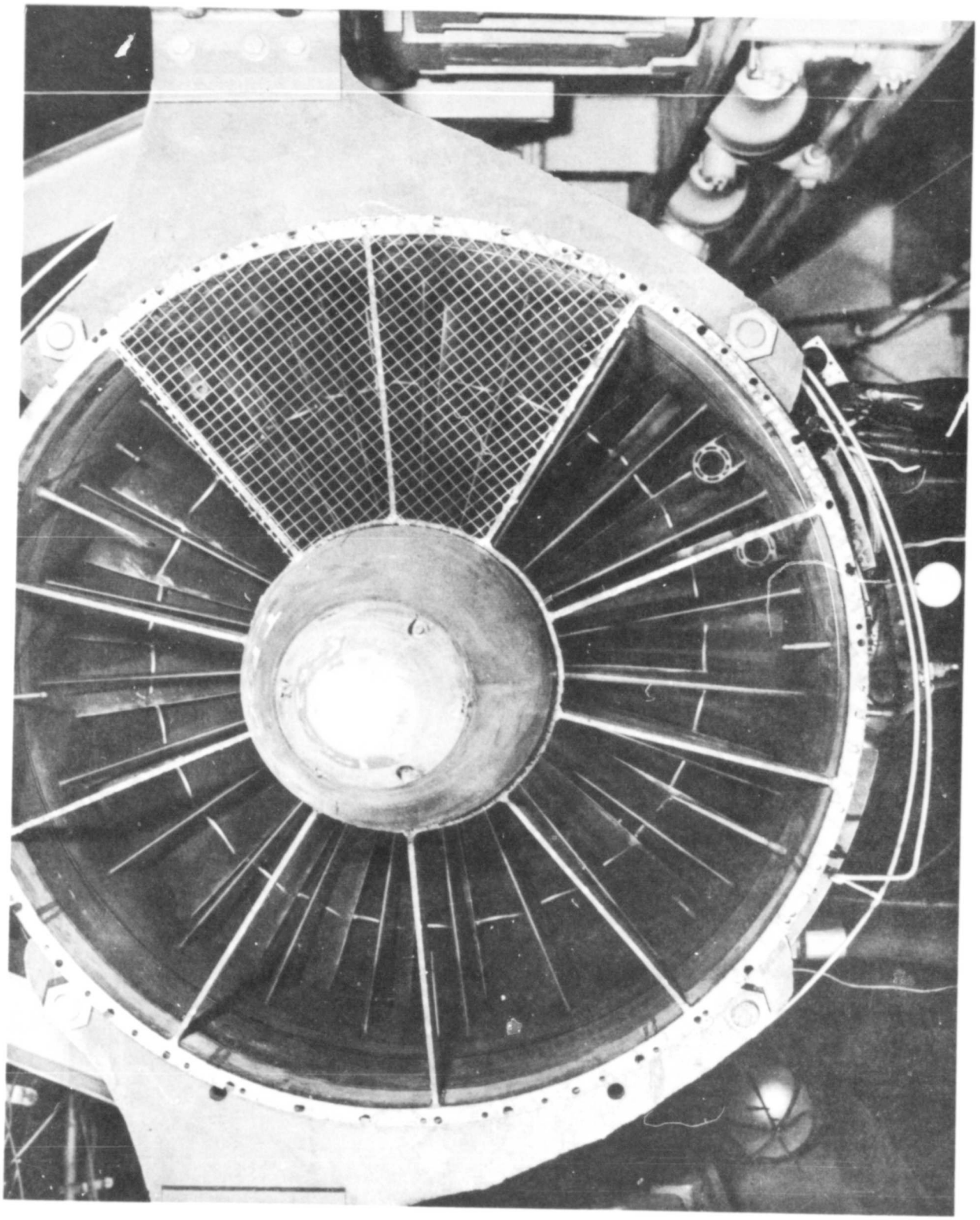

FIGURE 8 - FAN INLET DISTORTION SCREEN: 72 DEGREES

Mode 2:

2nd Axial
0th Tangential
0th Radial

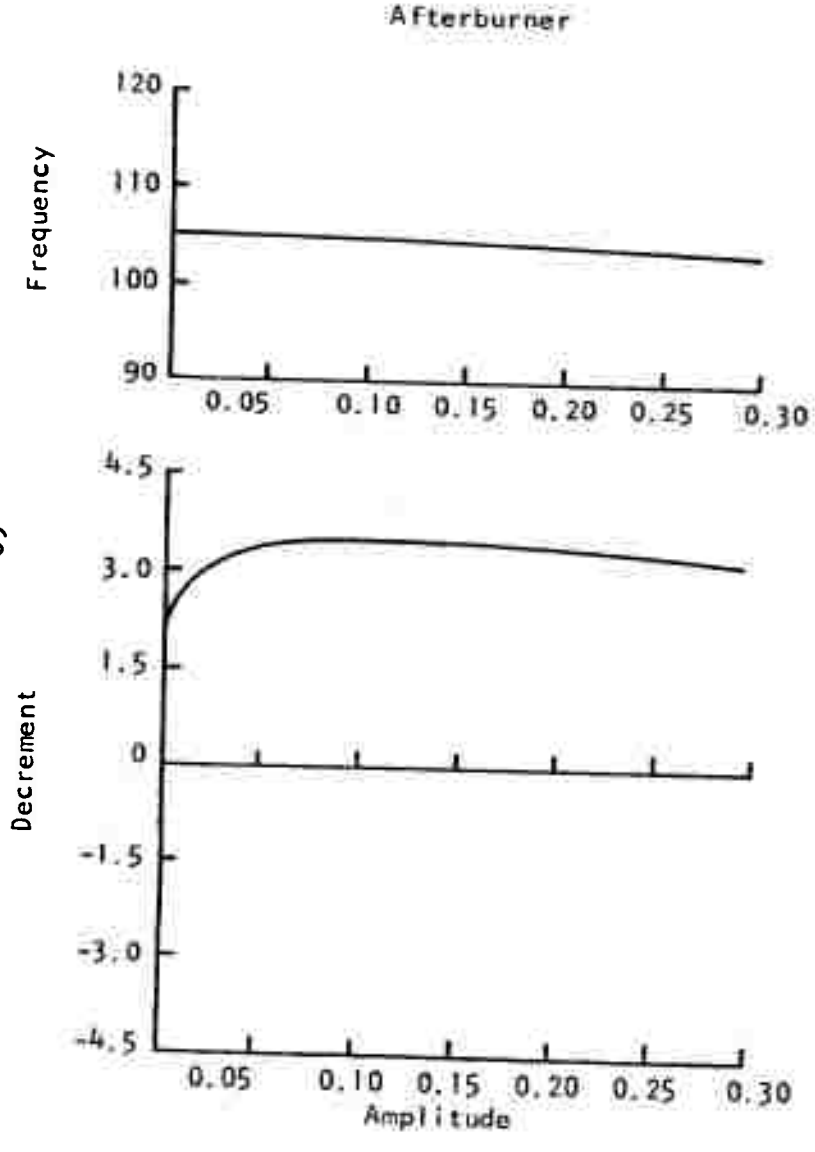

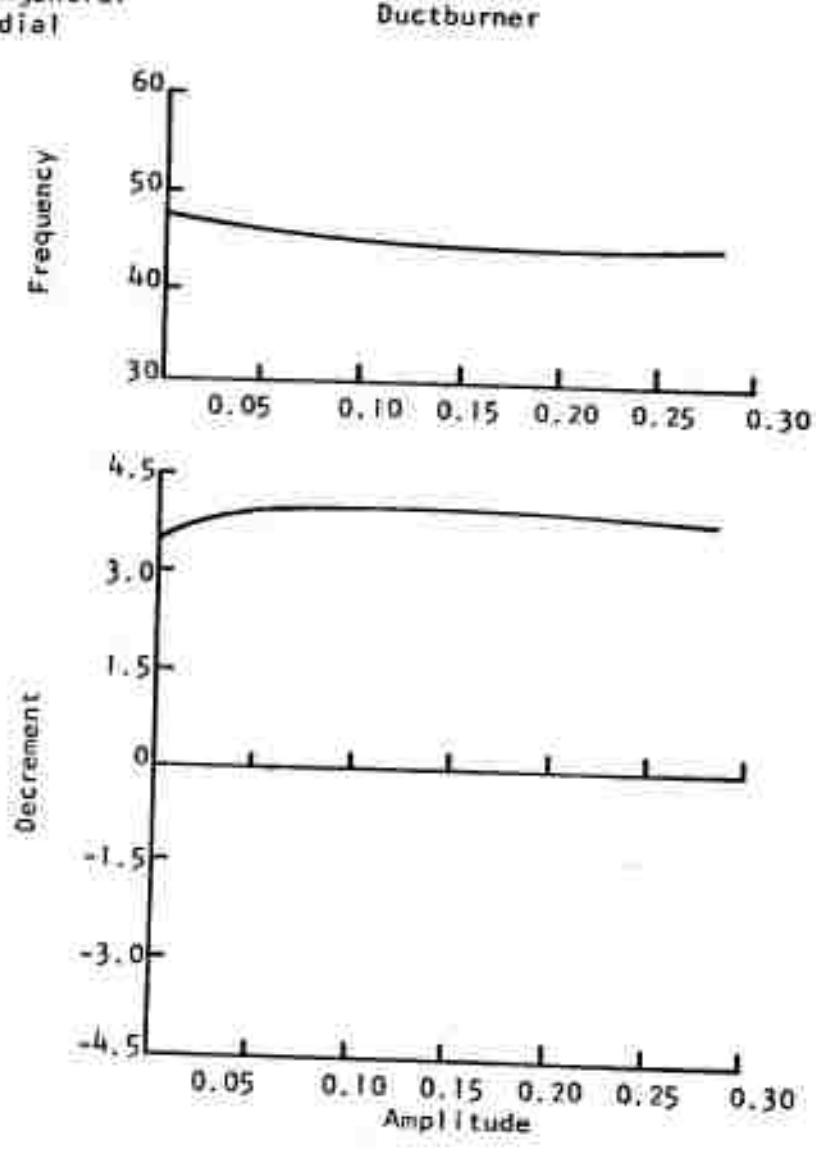

Mode 6:

2nd Axial
1st Tangential
1st Radial

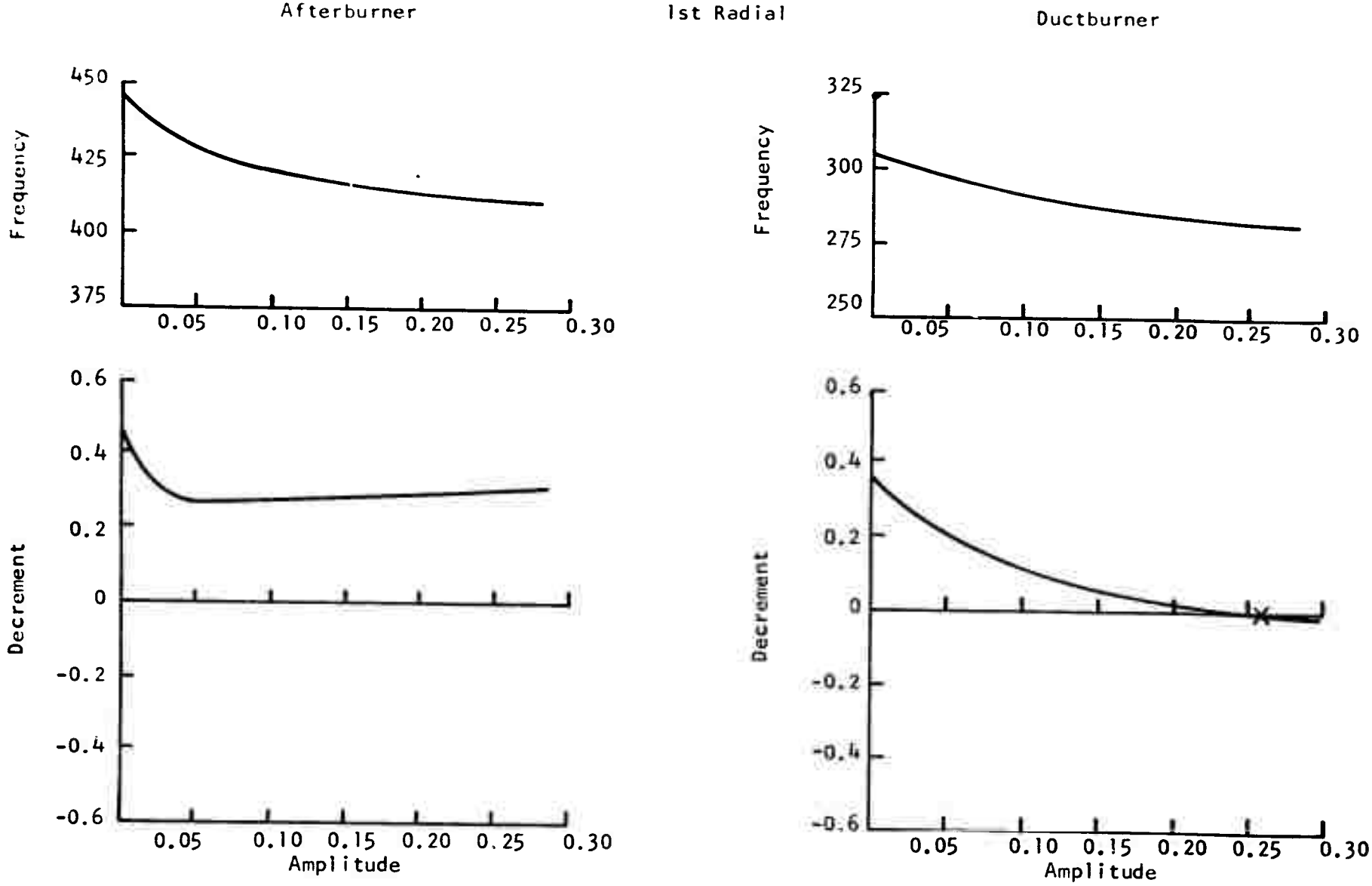

FIGURE 10 - INSTABILITY SOLUTION FOR A COMBINED TANGENTIAL-LONGITUDINAL MODE: MODE 6 AT Z5

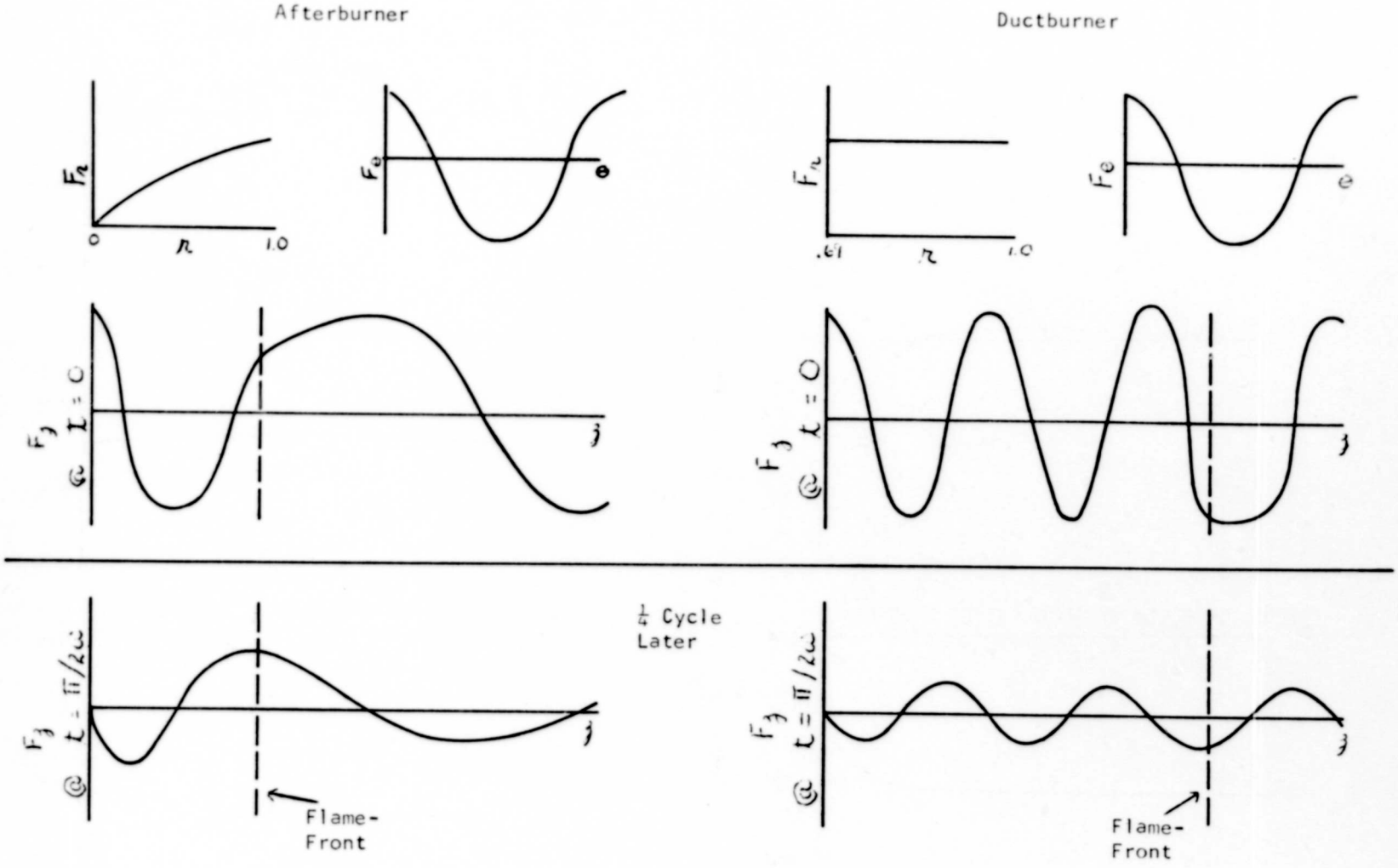

FIGURE 11 - MODE SHAPE OF MODE 6 AT Z5

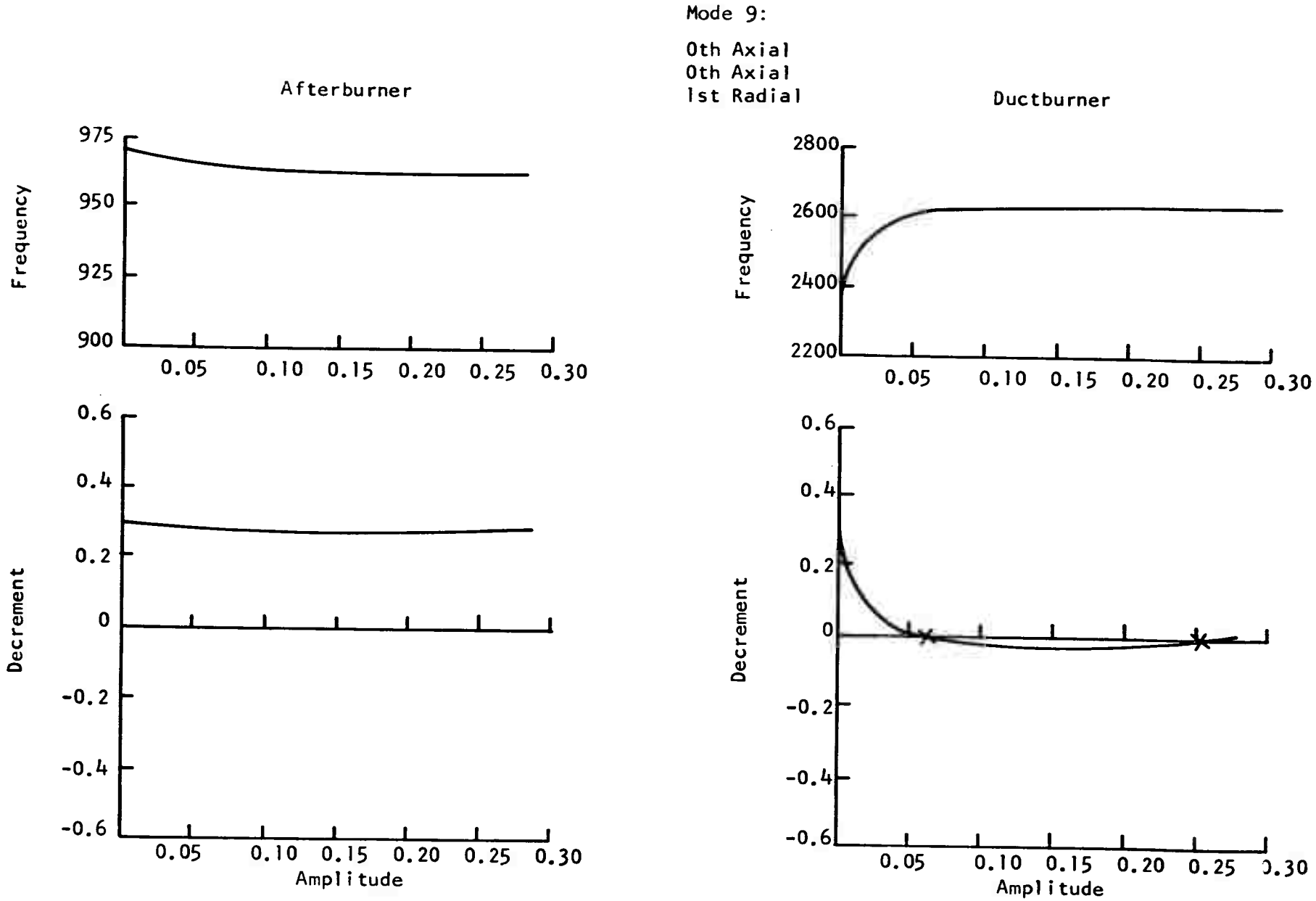

FIGURE 12 - INSTABILITY SOLUTION FOR THE FIRST RADIAL MODE: MODE 9 AT Z5

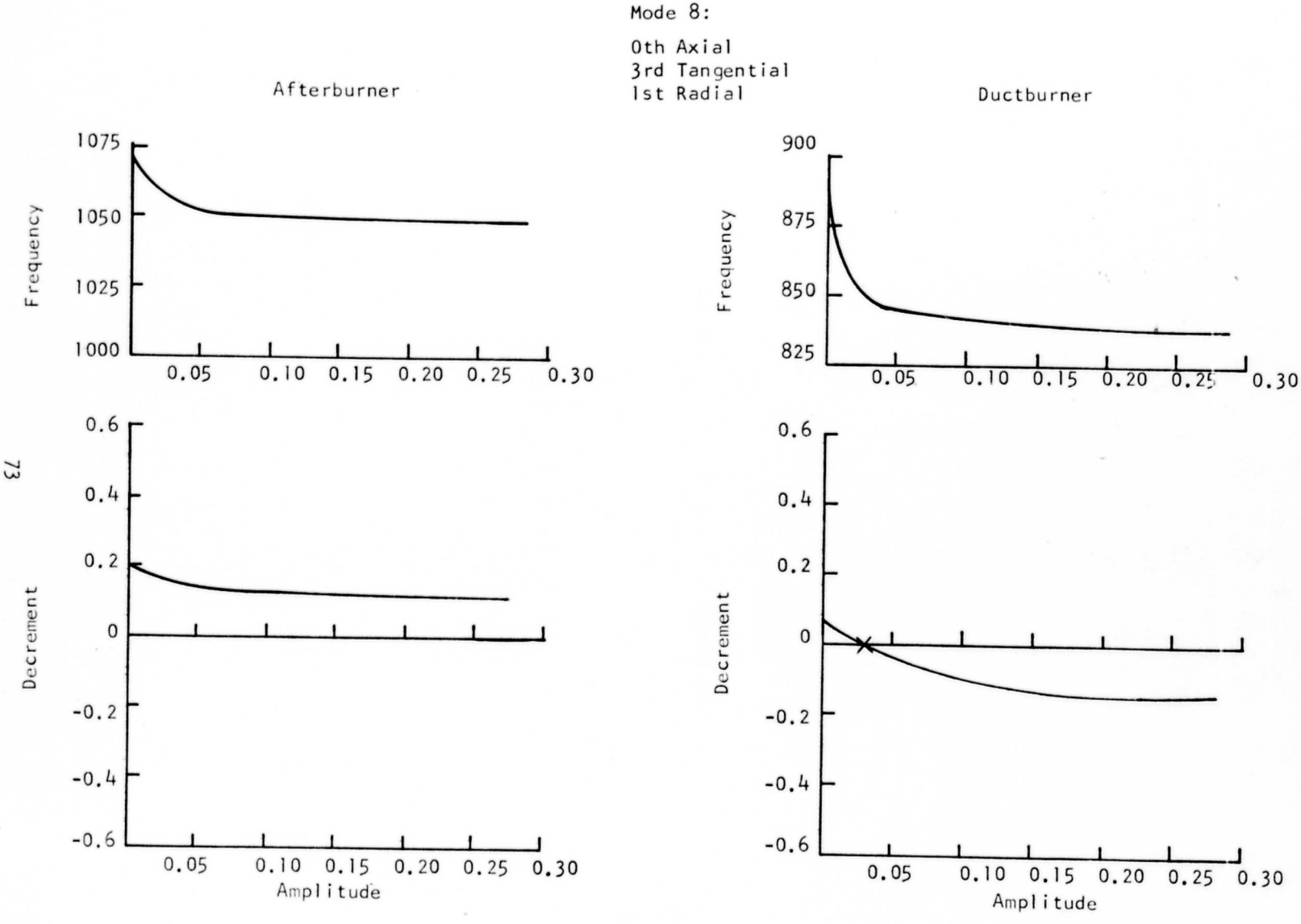

FIGURE 13 - INSTABILITY SOLUTION FOR THE THIRD TANGENTIAL MODE: MODE 8 AT Z5

Mode 7:

0th Axial
2nd Tangential
1st Radial

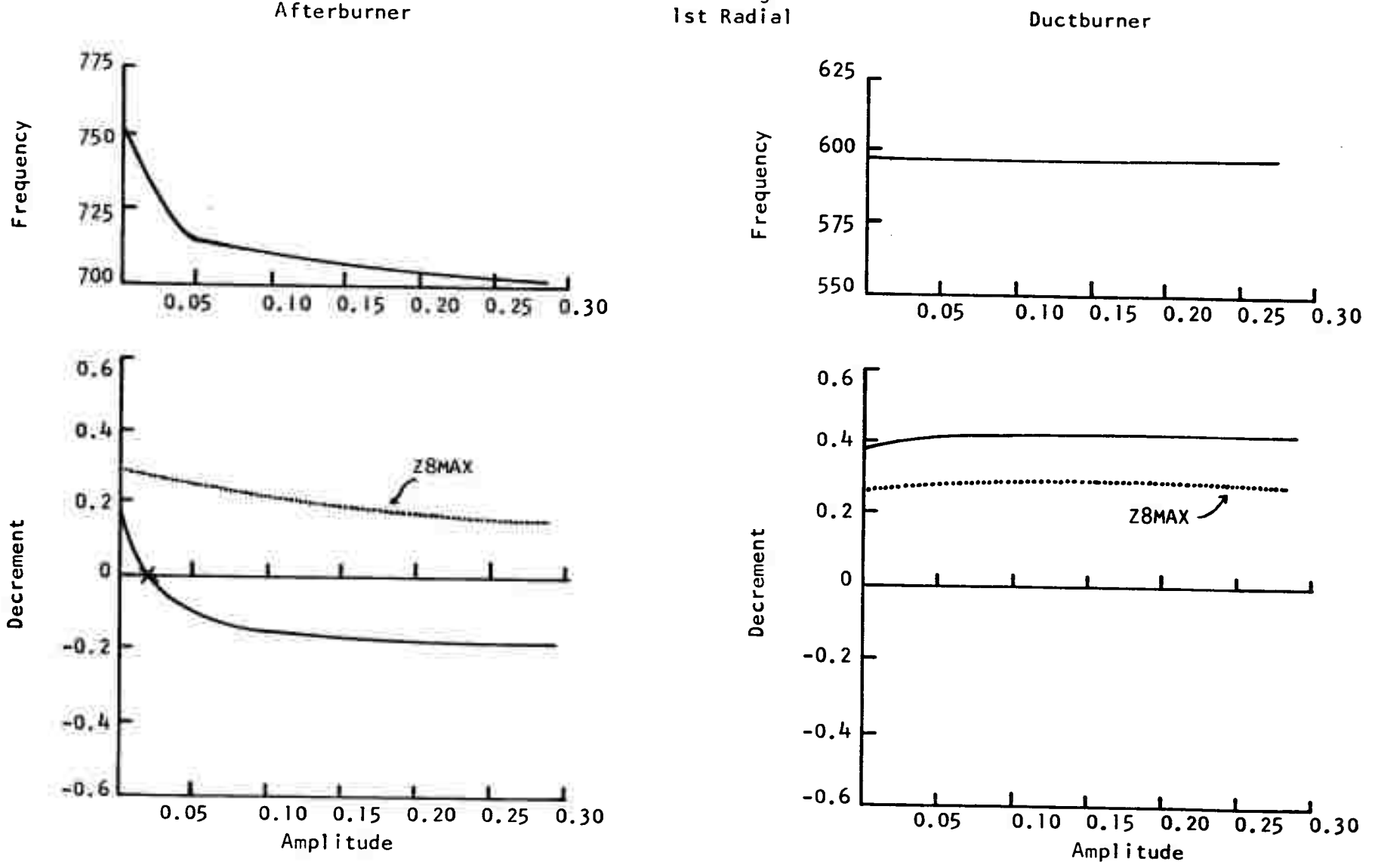

FIGURE 14 - INITIAL INSTABILITY SOLUTION FOR THE SECOND TANGENTIAL MODE: MODE 7 AT Z5 AND AT Z8MAX

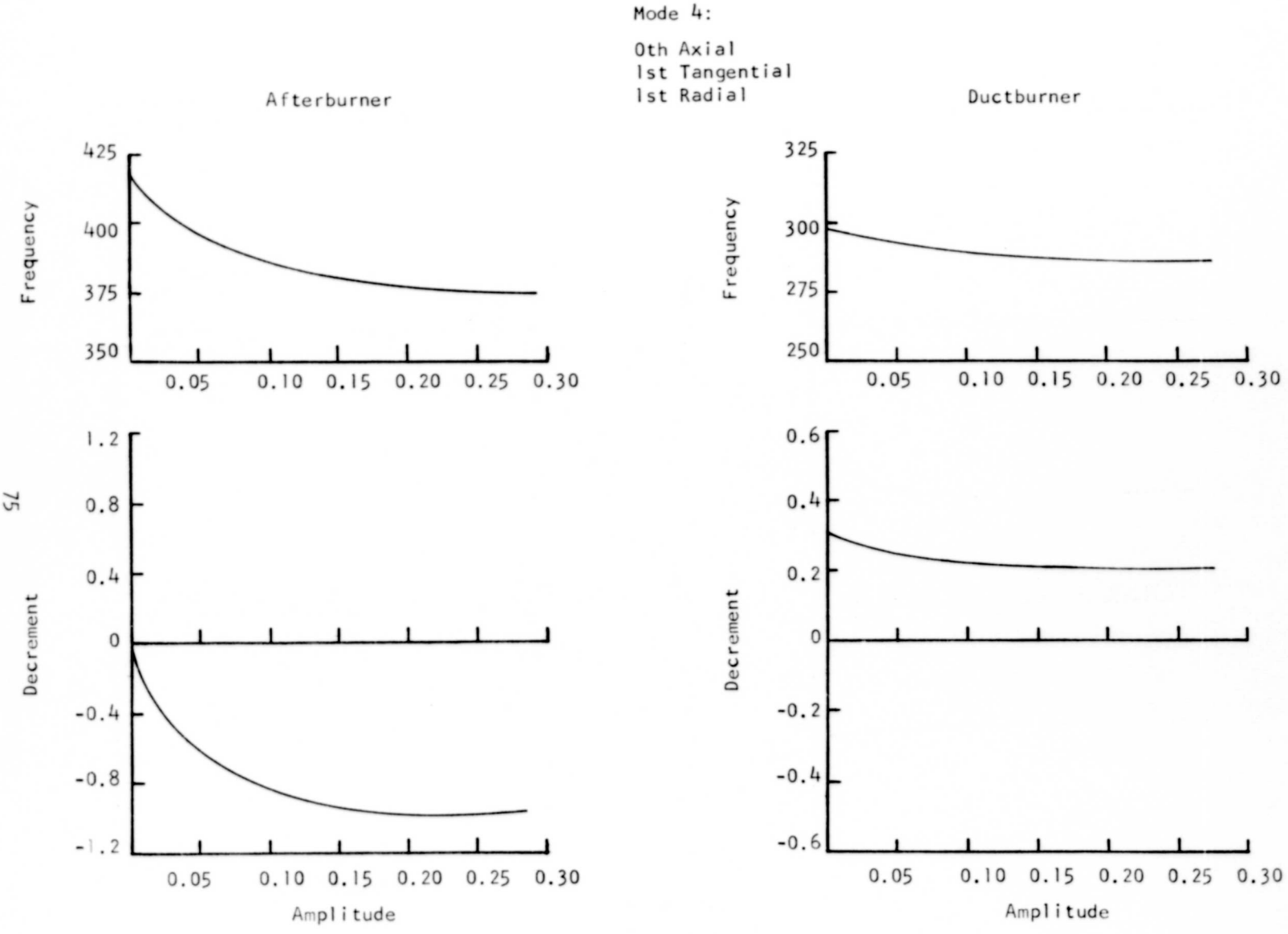

FIGURE 15 - INITIAL INSTABILITY SOLUTION FOR THE FIRST TANGENTIAL MODE: MODE 4 AT Z5

Mode 4:

0th Axial
1st Tangential
1st Radial

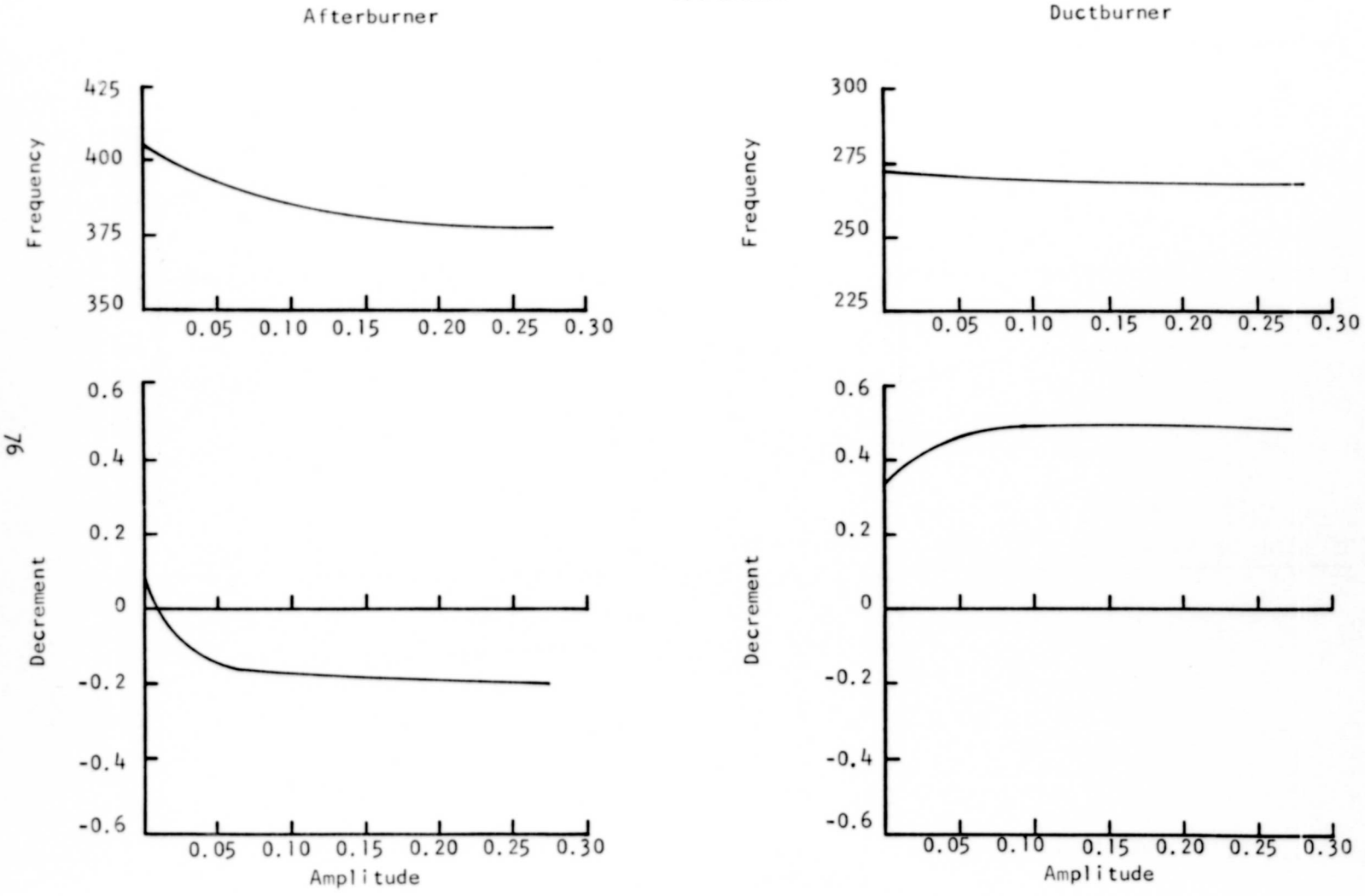

FIGURE 16 - INITIAL INSTABILITY SOLUTION FOR THE FIRST TANGENTIAL MODE: MODE 4 AT Z8

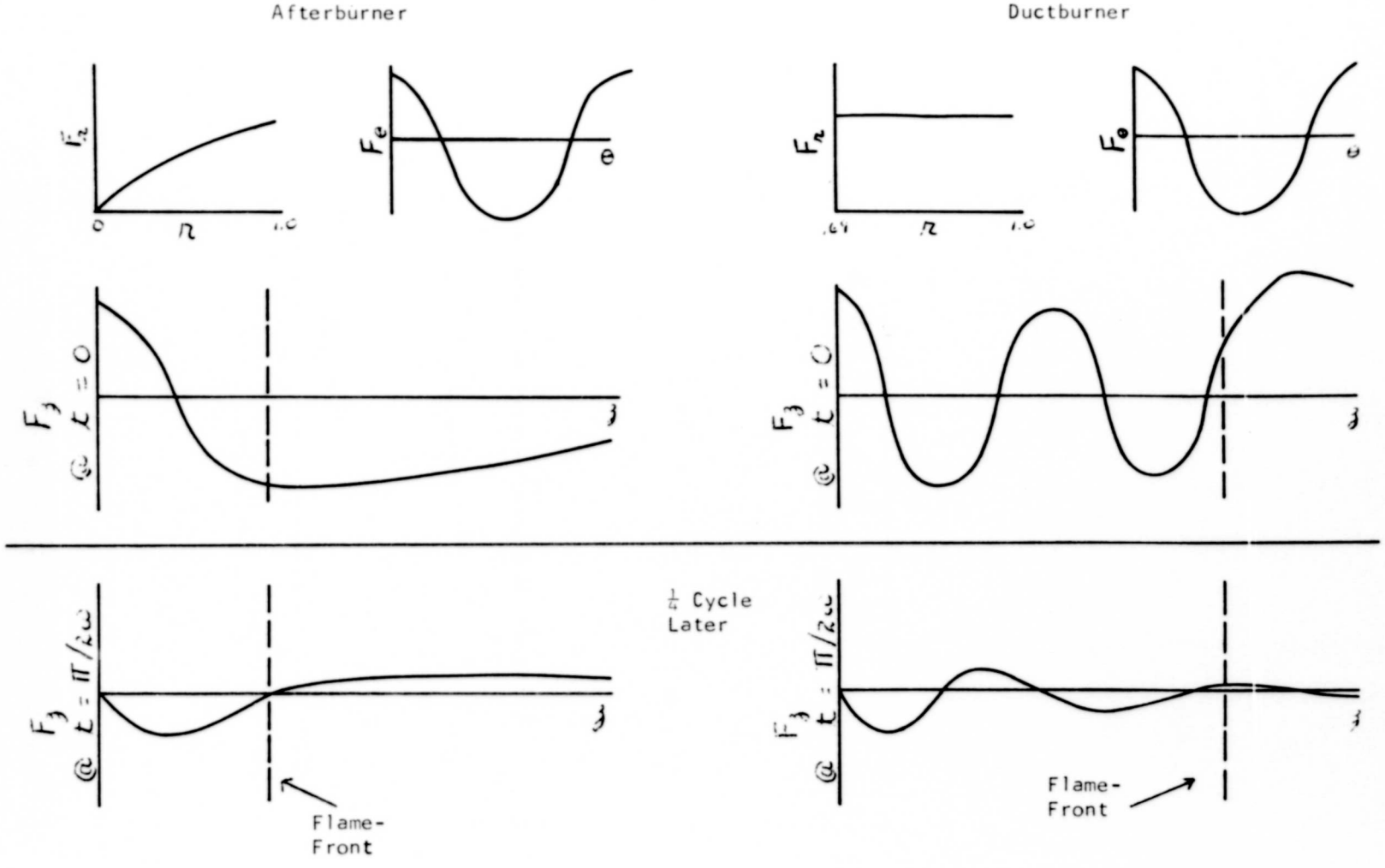

FIGURE 17 - MODE SHAPE OF MODE 4 AT Z5

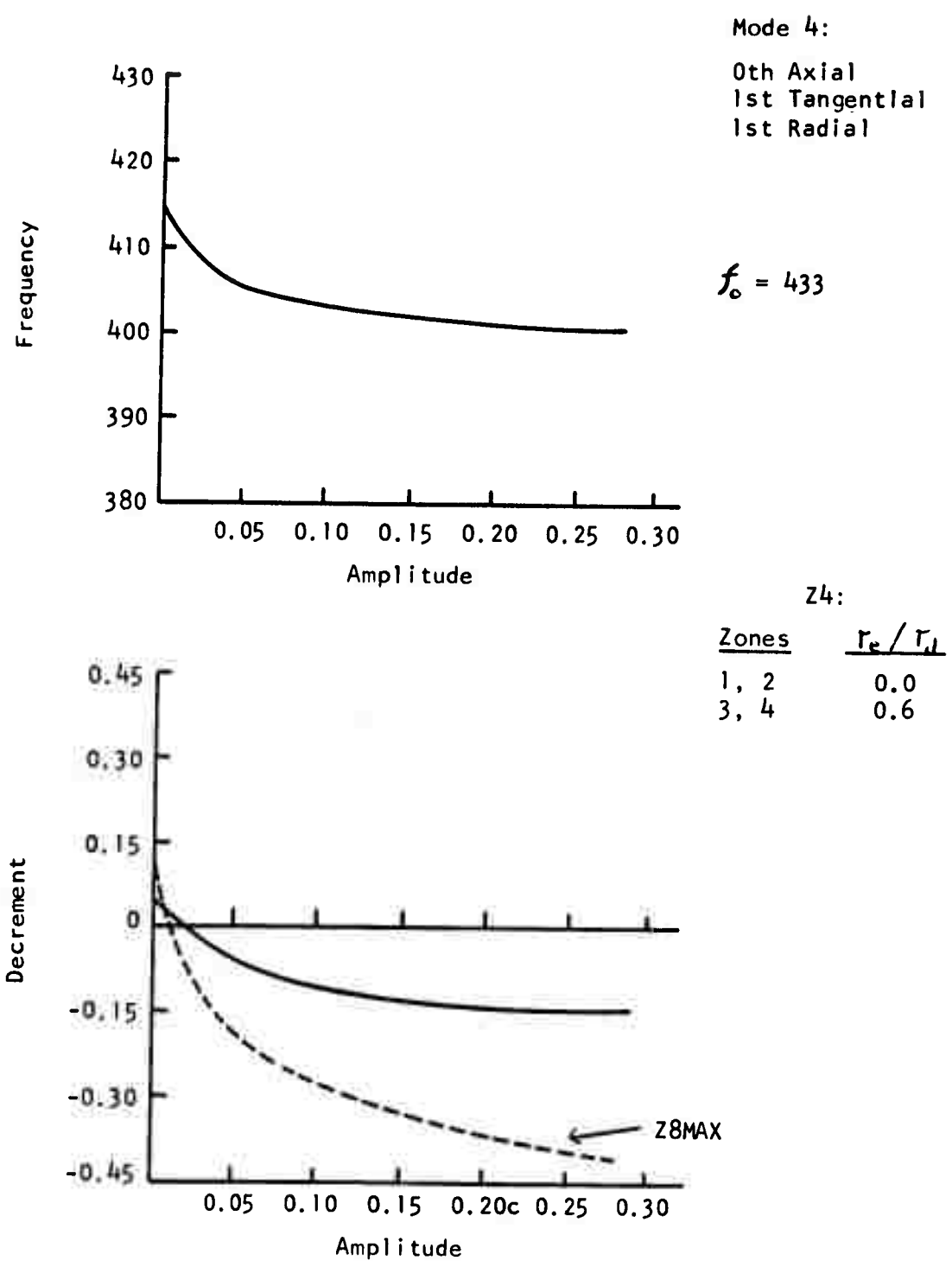

FIGURE 18 - REVISED INSTABILITY SOLUTION FOR THE FIRST TANGENTIAL MODE: MODE 4 AT Z4

Mode 4:

0th Axial
1st Tangential
1st Radial

f_o = 449

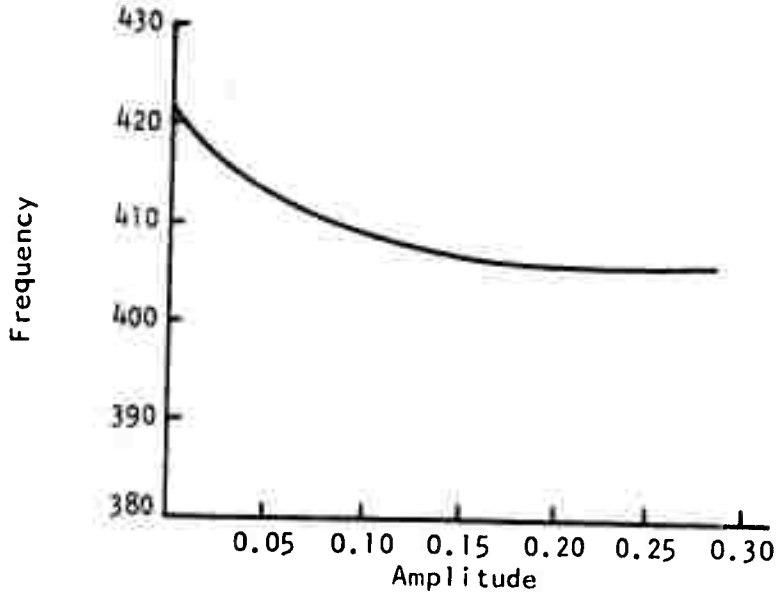

Z5:

Zones	τ_o / τ_a
1, 2, 5	0.0
3, 4	0.6

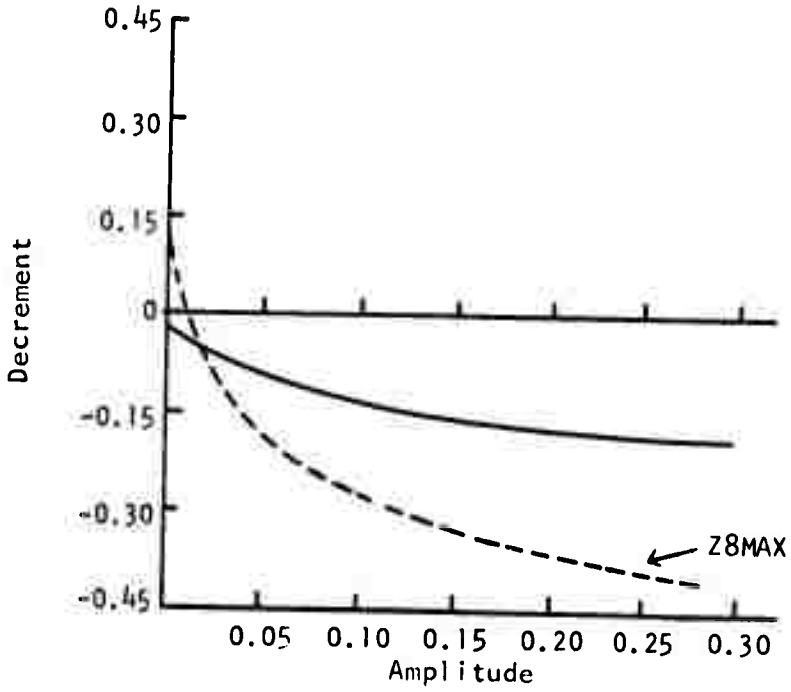

FIGURE 19 - REVISED INSTABILITY SOLUTION FOR THE FIRST TANGENTIAL MODE: MODE 4 AT Z5

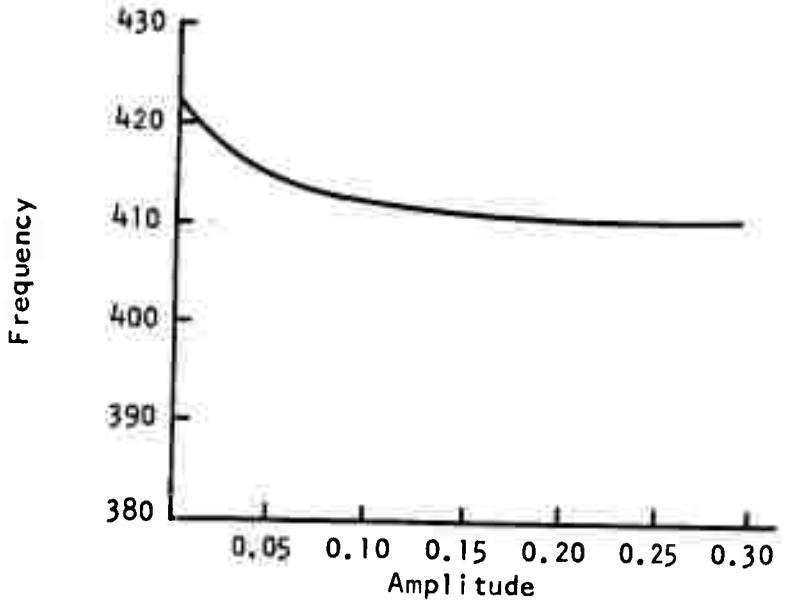

Mode 4:

0th Axial
1st Tangential
1st Radial

f_c = 453

Z6:

Zones	r_c / r_d
1, 5	0.0
3, 4	0.6

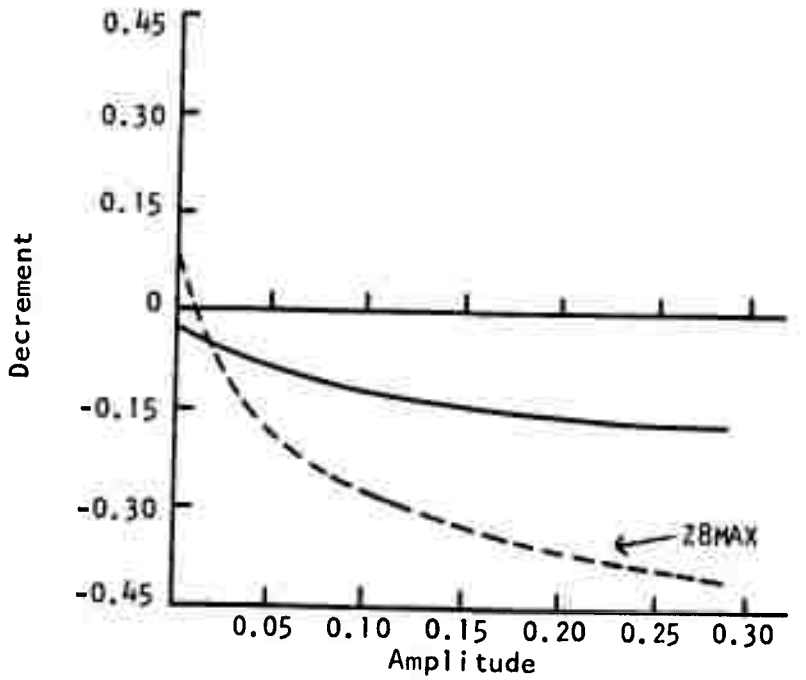

FIGURE 20 - REVISED INSTABILITY SOLUTION FOR THE FIRST TANGENTIAL MODE: MODE 4 AT Z6

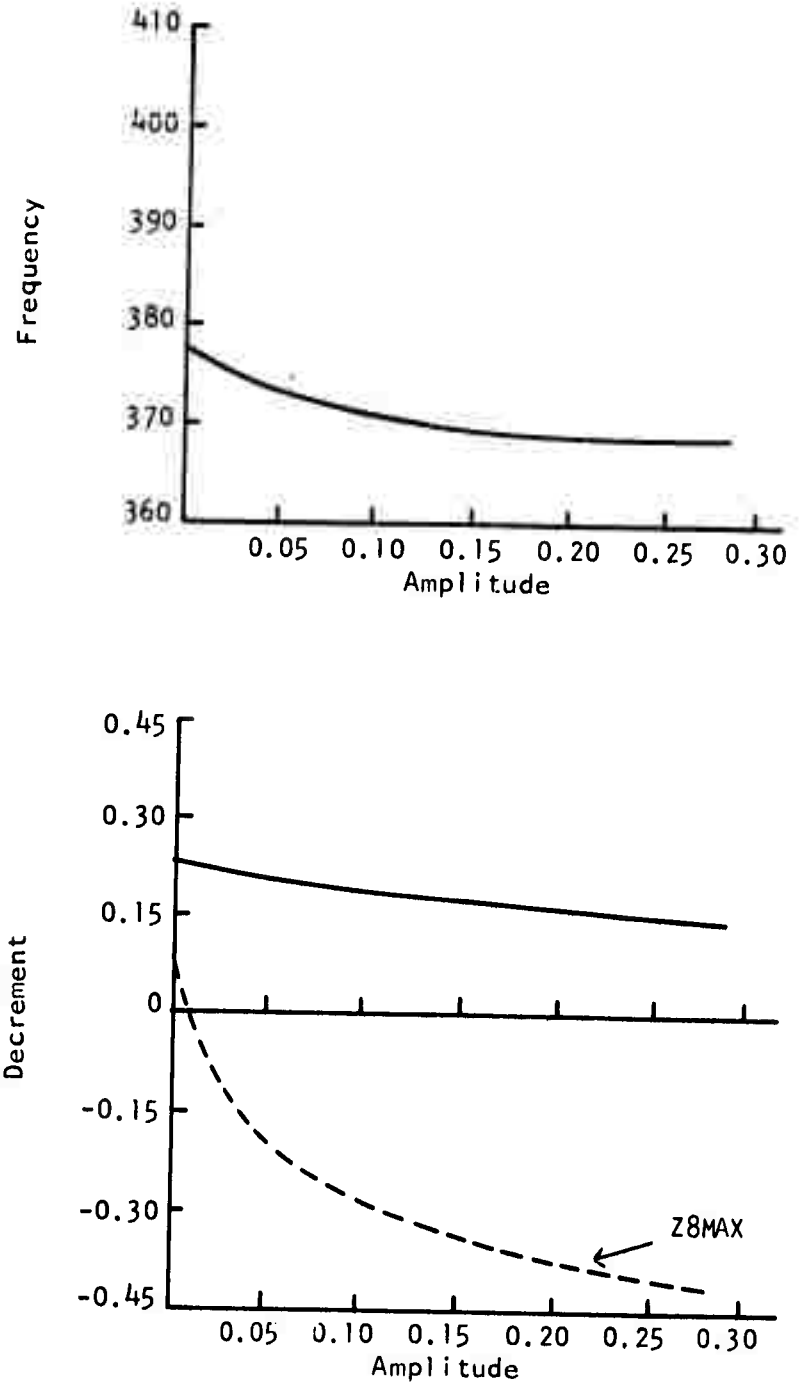

FIGURE 21 - REVISED INSTABILITY SOLUTION FOR THE FIRST TANGENTIAL MODE: MODE 4 AT Z7

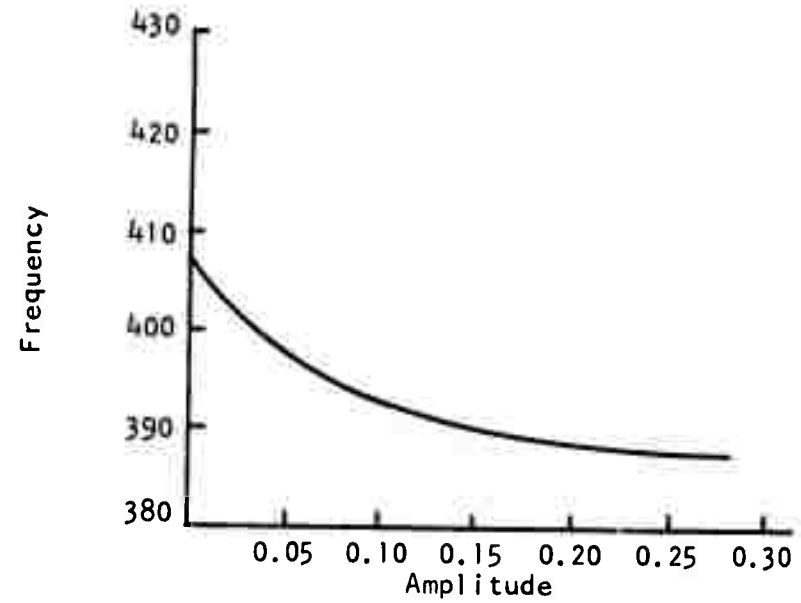

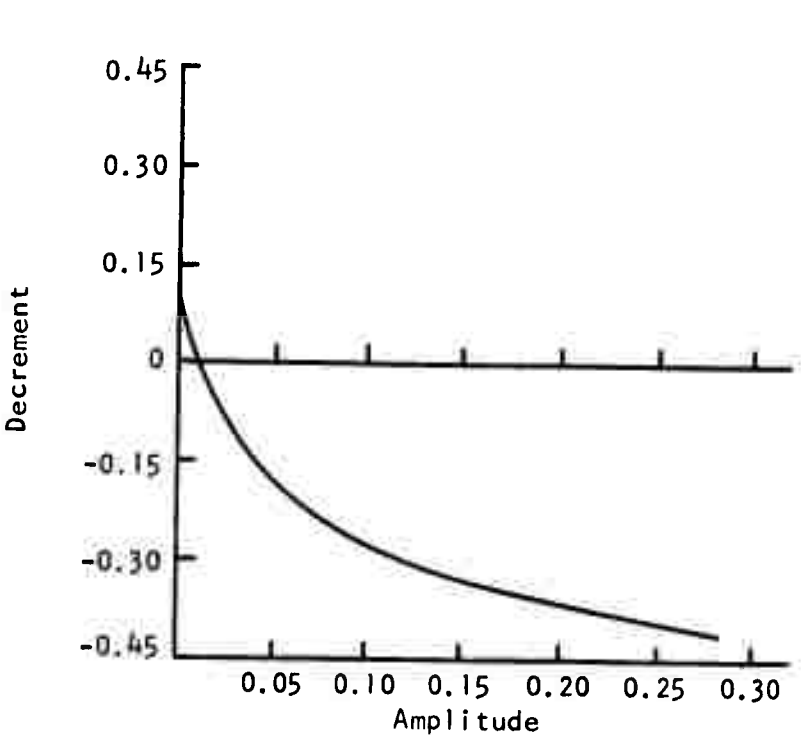

FIGURE 22 - REVISED INSTABILITY SOLUTION FOR THE FIRST TANGENTIAL MODE: MODE 4 AT Z8MAX

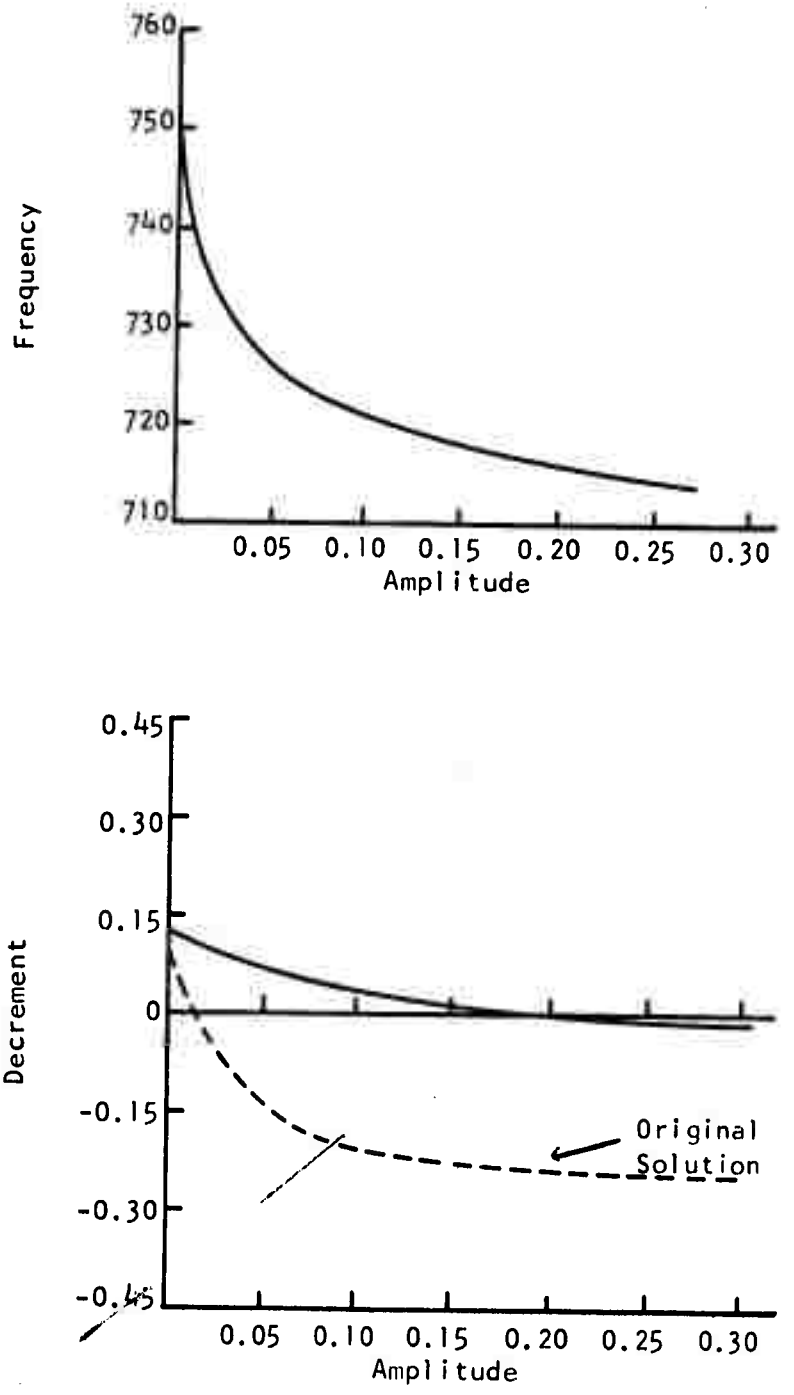

FIGURE 23 - REVISED INSTABILITY SOLUTION FOR THE SECOND TANGENTIAL MODE: MODE 7 AT Z5

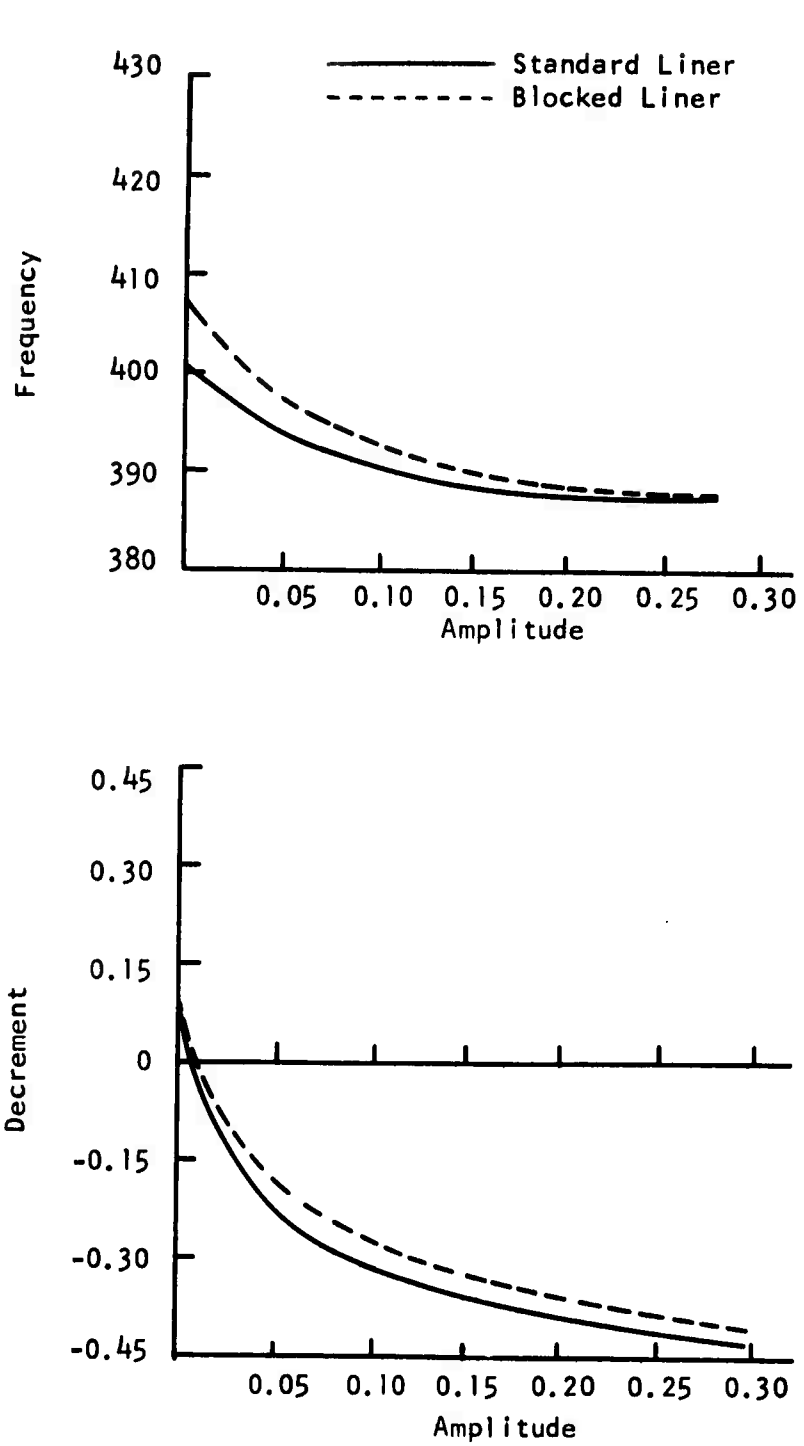

FIGURE 24 - INSTABILITY SOLUTIONS FOR THE FIRST TANGENTIAL MODE WITH TWO LINER LENGTHS: MODE 4 AT Z8MAX

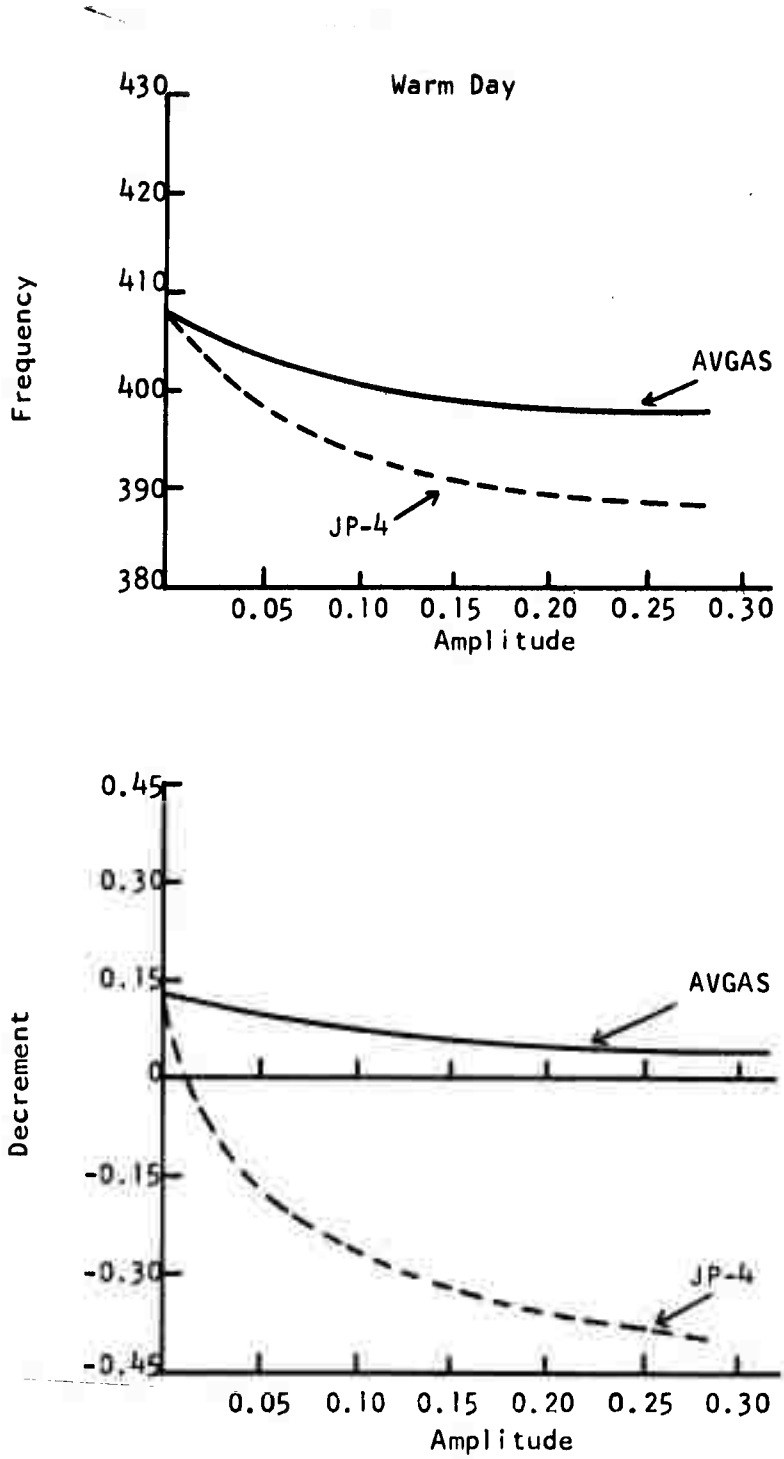

Mode 4:

0th Axial
1st Tangential
1st Radial

f_c = 419

Z8 with AVGAS:

Zones	r_e / r_i
1	0.0
3, 4	0.1

FIGURE 25 - INSTABILITY SOLUTIONS FOR THE FIRST TANGENTIAL MODE WITH AVGAS AND JP-4: MODE 4 AT Z8MAX

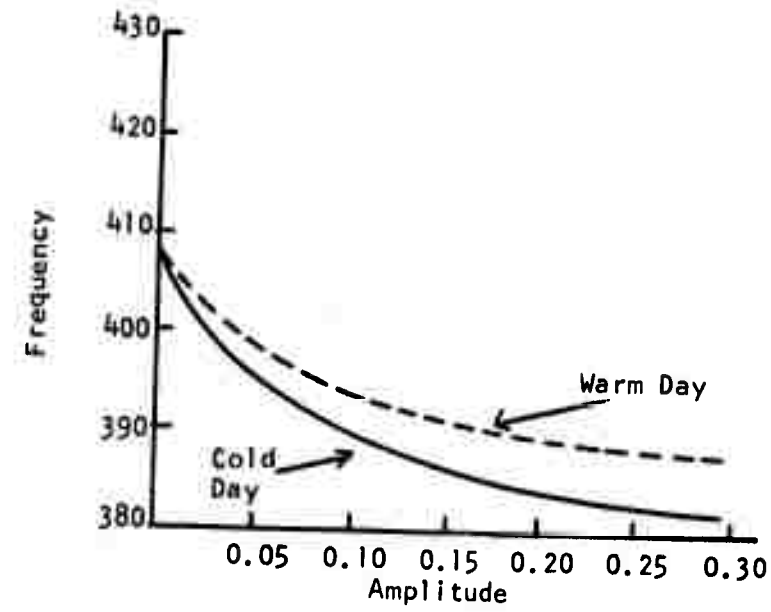

Z8: a

Zones	Cold	Warm
1	0.0	0.0
3, 4	1.0	0.6

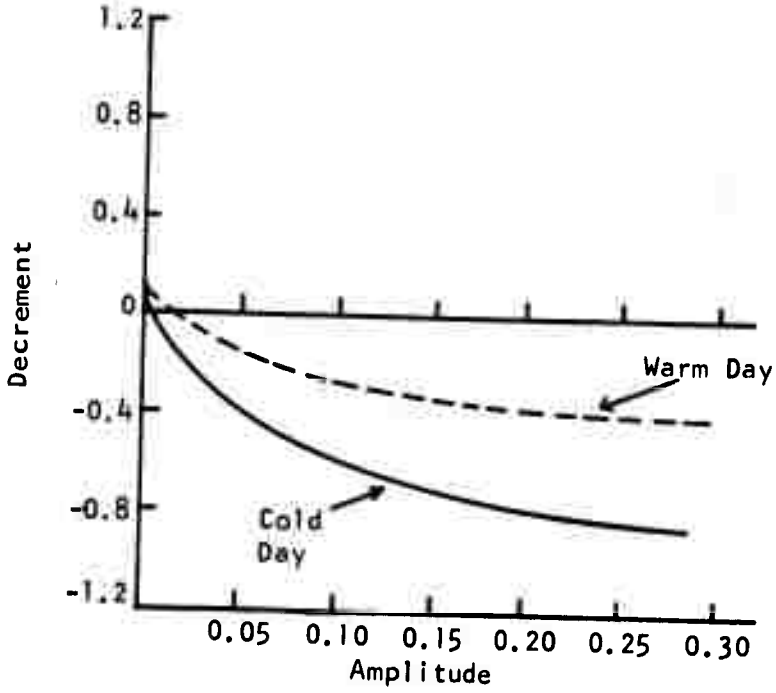

FIGURE 26 - INITIAL COMPARISON OF INSTABILITY SOLUTIONS FOR COLD DAY AND WARM DAY CONDITIONS: MODE 4 AT Z8MAX

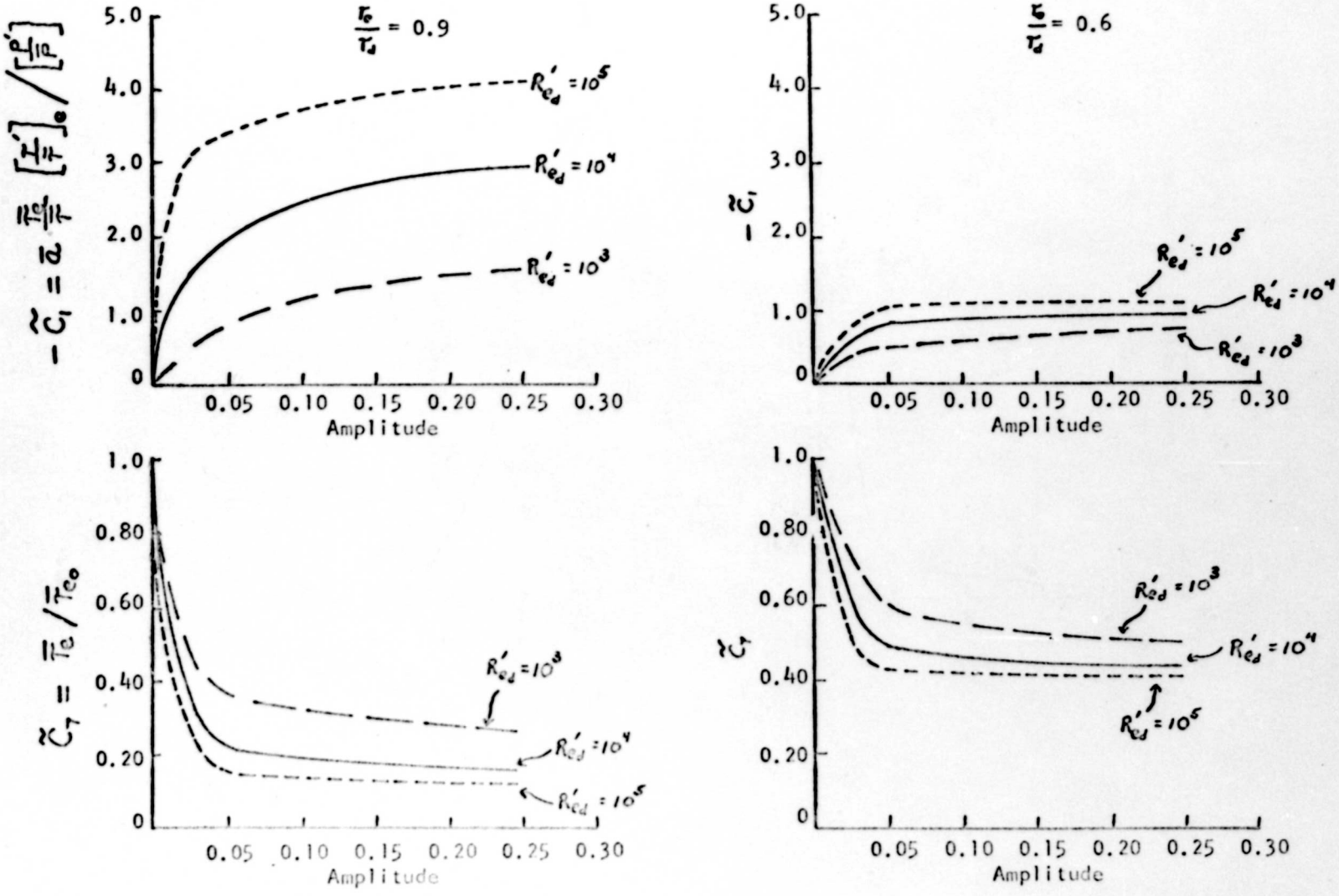

FIGURE 27 - NONLINEAR VARIATION OF $\tilde{T}$ AS A CONSEQUENCE OF UNSTEADY DROPLET EVAPORATION

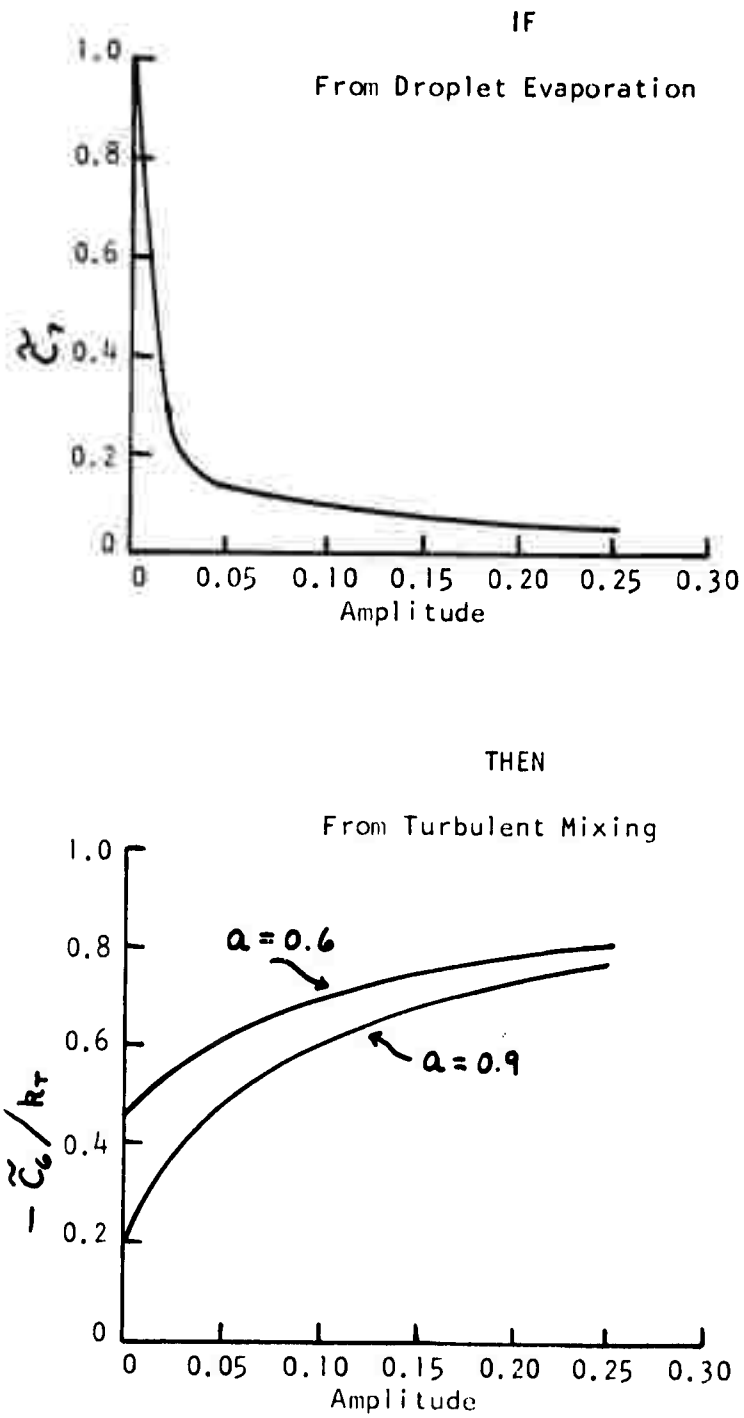

FIGURE 28 - HYPOTHESIZED NONLINEAR VARIATION OF τ AS A CONSEQUENCE OF UNSTEADY TURBULENT MIXING

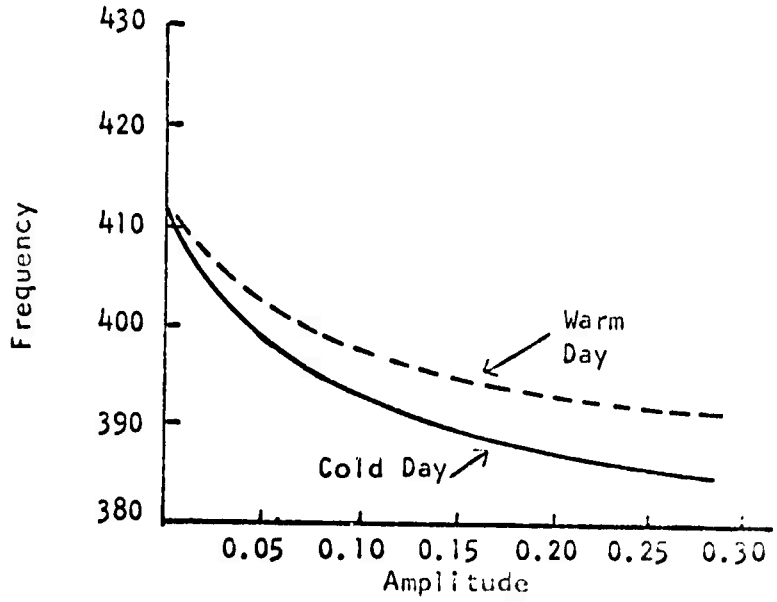

Zones	Z8: Cold	Warm
1	0.0	0.0
3, 4	1.0	0.6

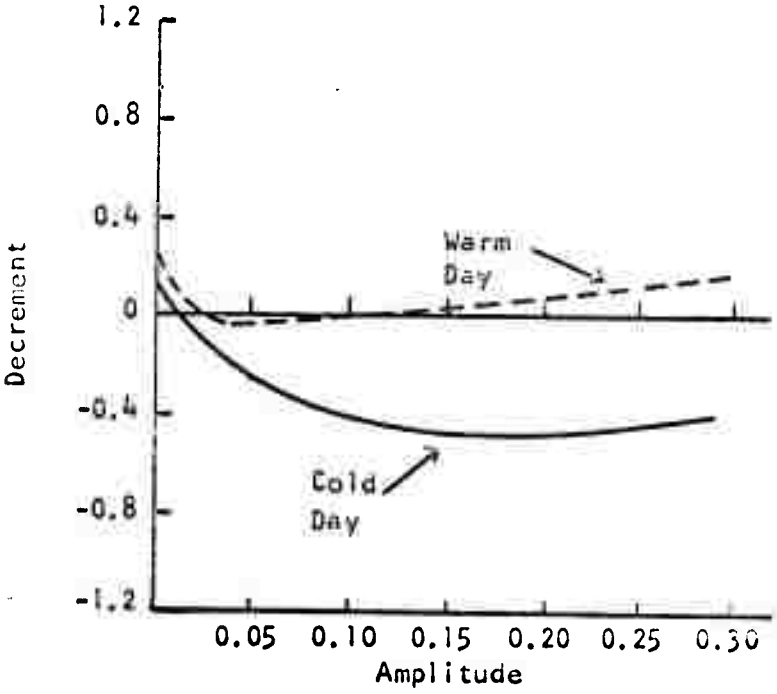

FIGURE 29 - REVISED COMPARISON OF INSTABILITY SOLUTIONS FOR COLD DAY AND WARM DAY CONDITIONS: MODE 4 AT Z8MAX

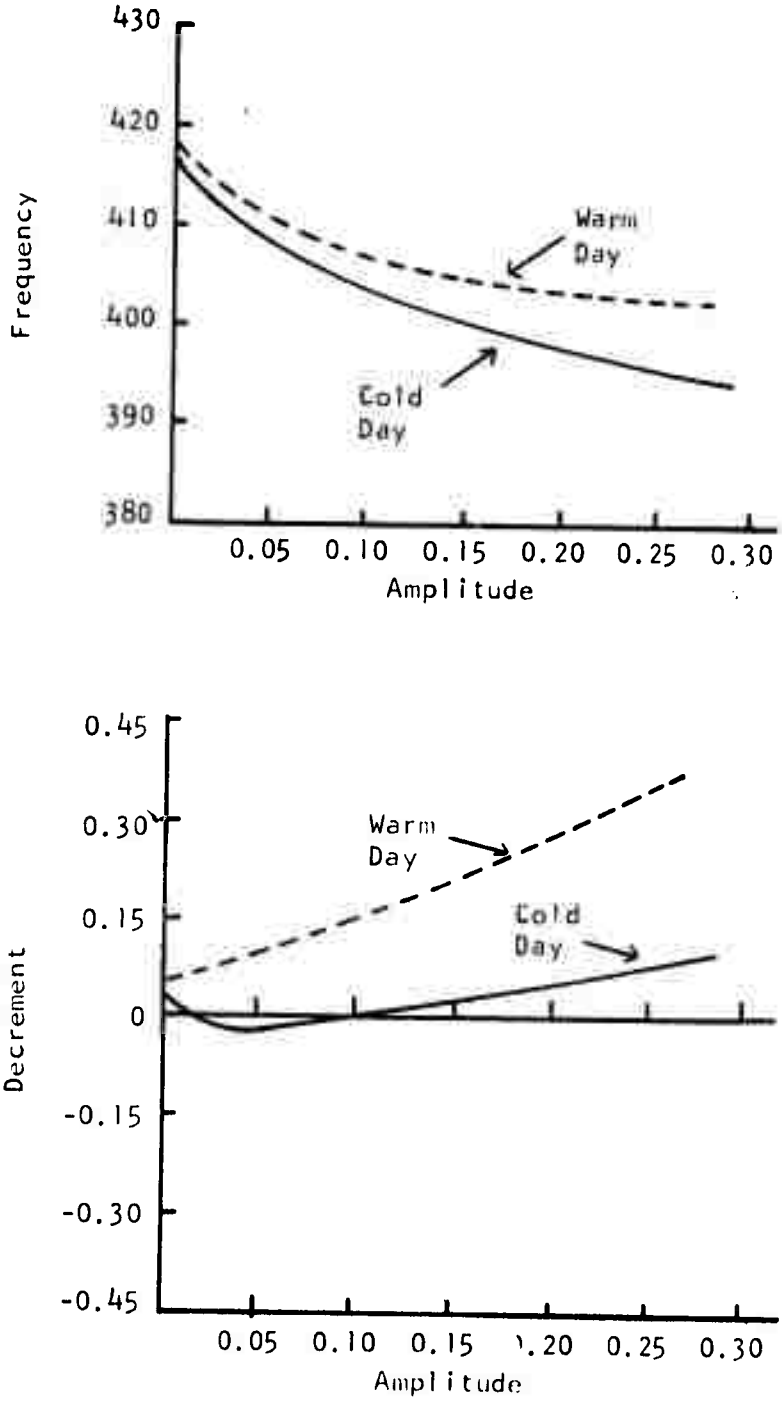

FIGURE 30 - COMPARISON OF INSTABILITY SOLUTIONS FOR COLD DAY AND WARM DAY CONDITIONS: MODE 4 AT Z4

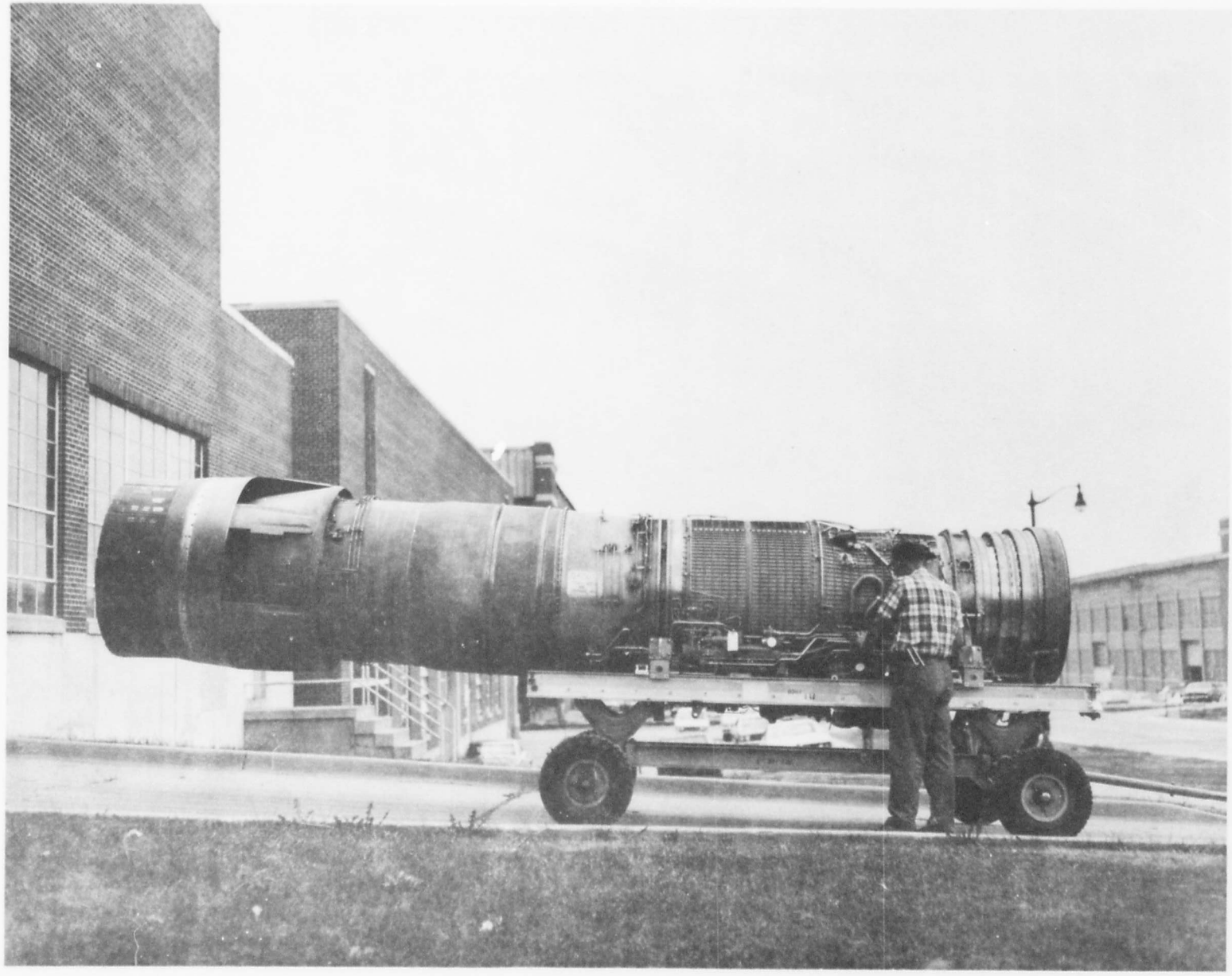

FIGURE 31 - TF-30-P1 TURBOFAN ENGINE

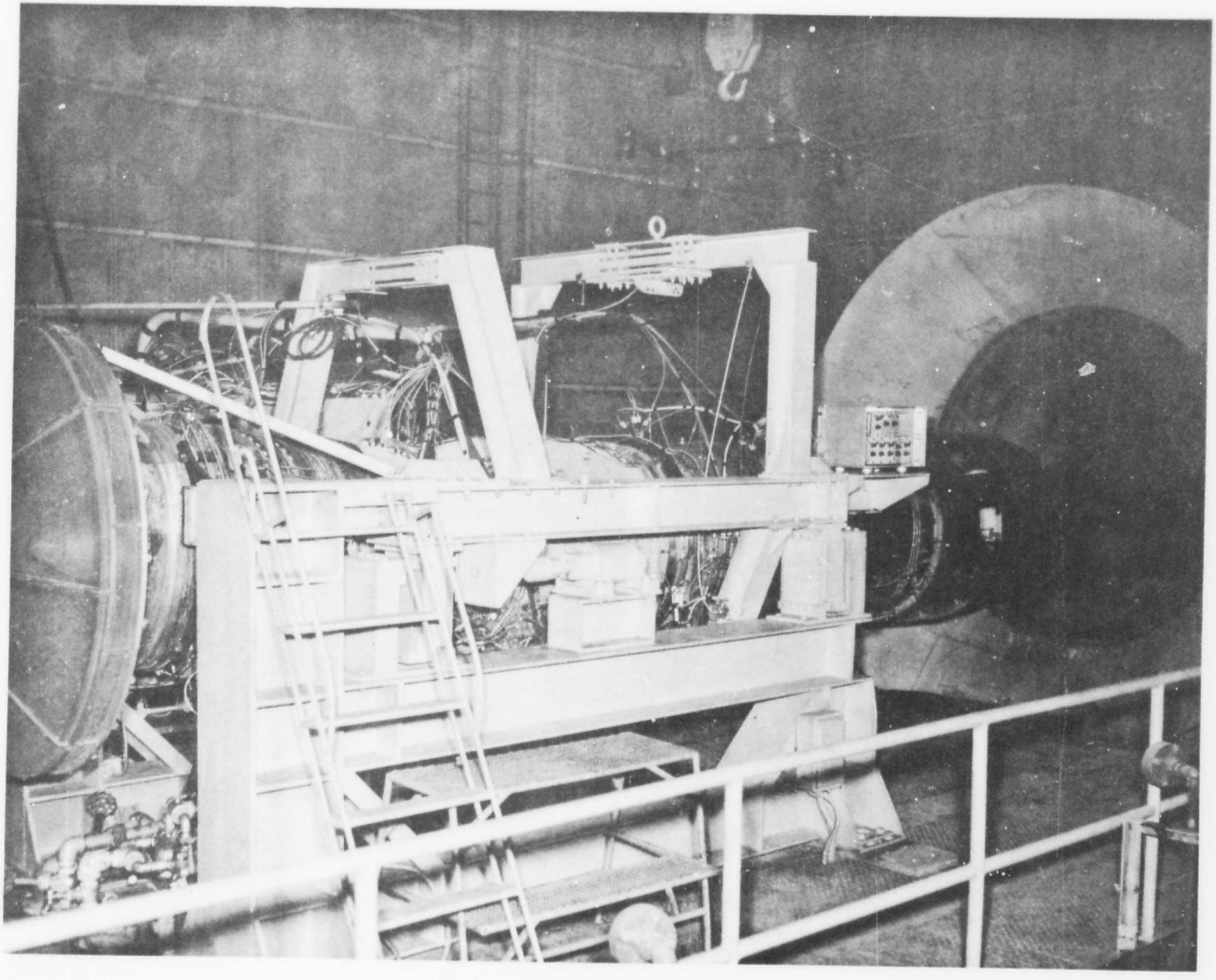

FIGURE 32 - TF-30-P1 INSTALLED IN TEST STAND

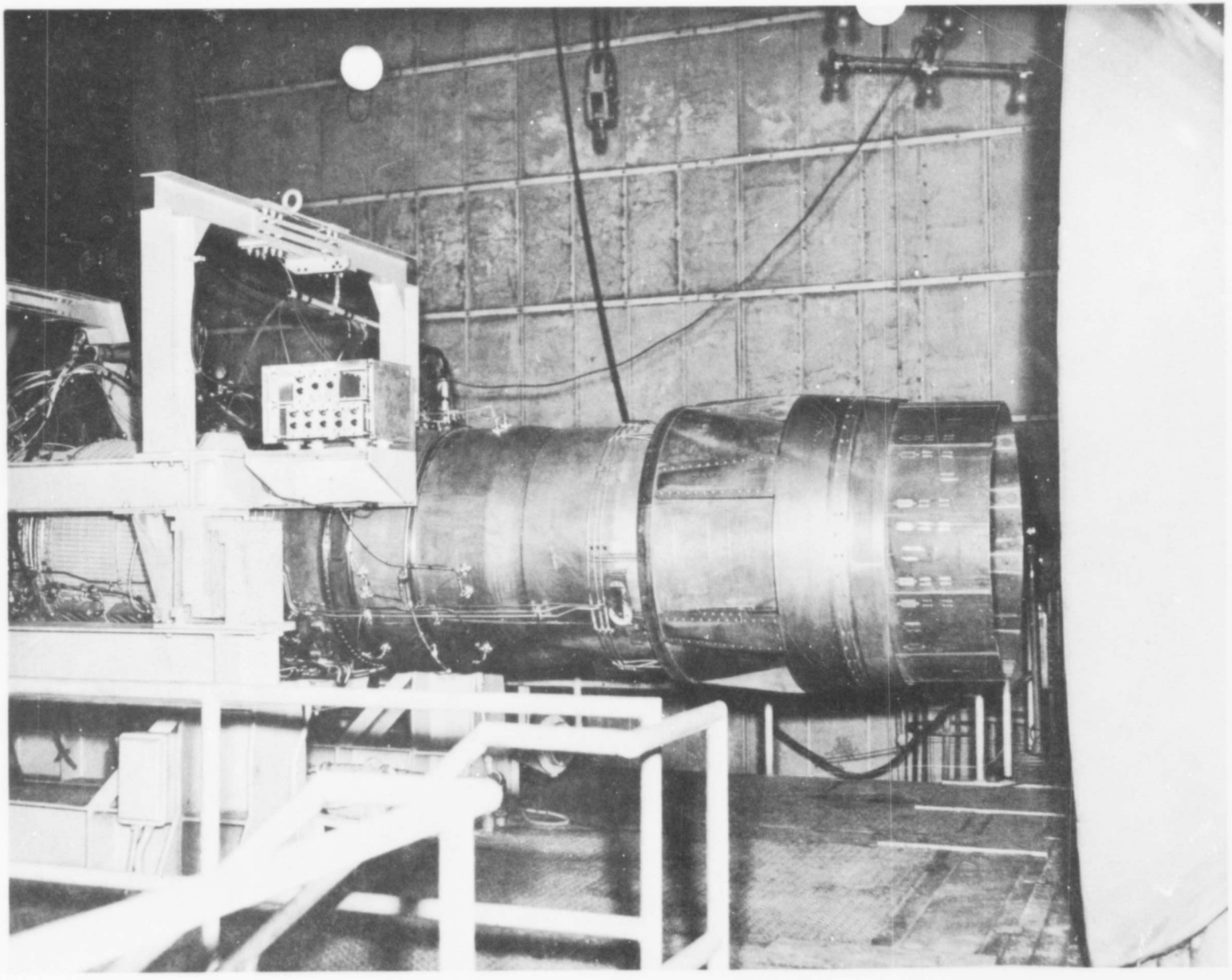

FIGURE 33 - TF-30-P1 AUGMENTOR AND NOZZLE

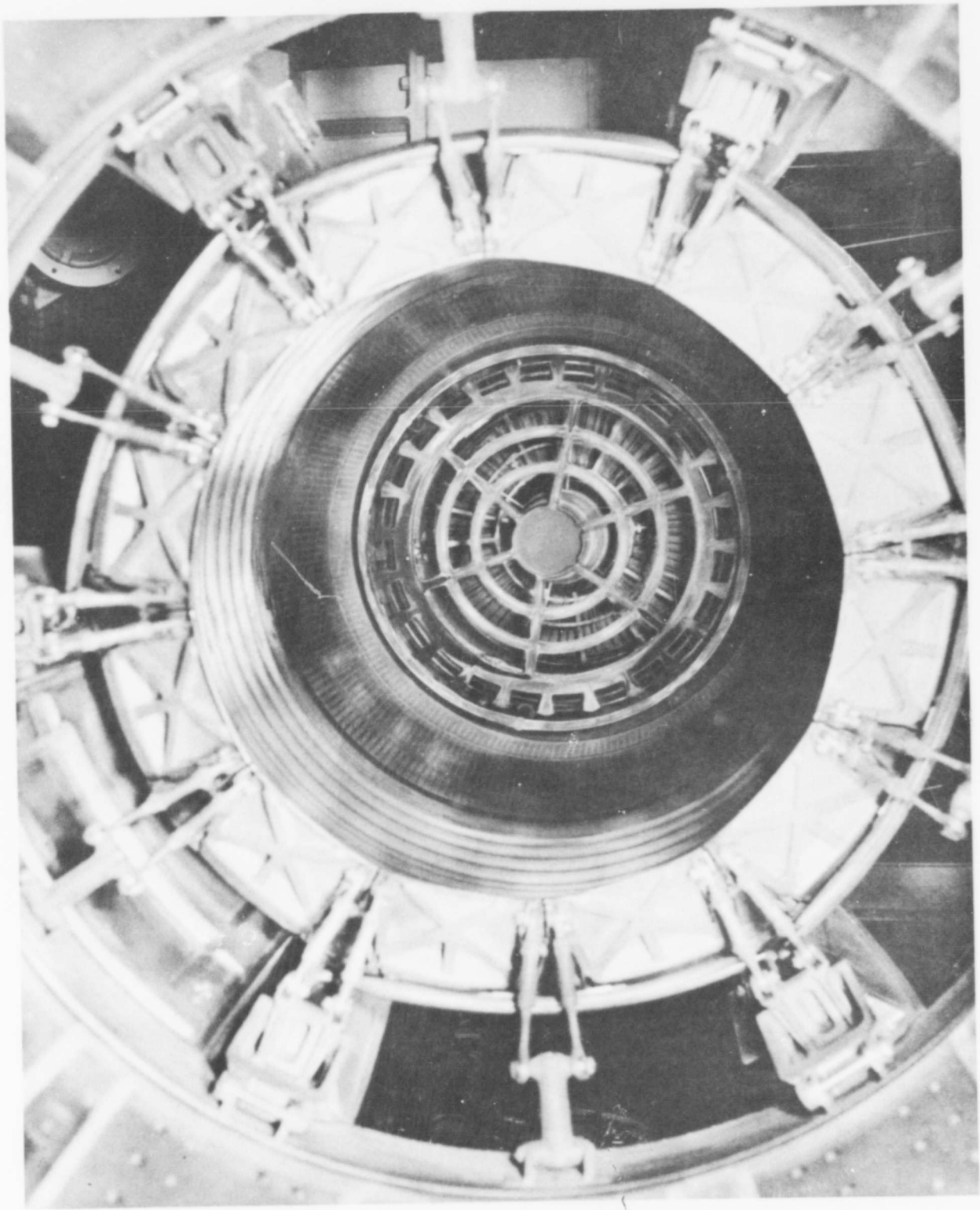

FIGURE 34 - TF-30-P1 AUGMENTOR (REAR VIEW)

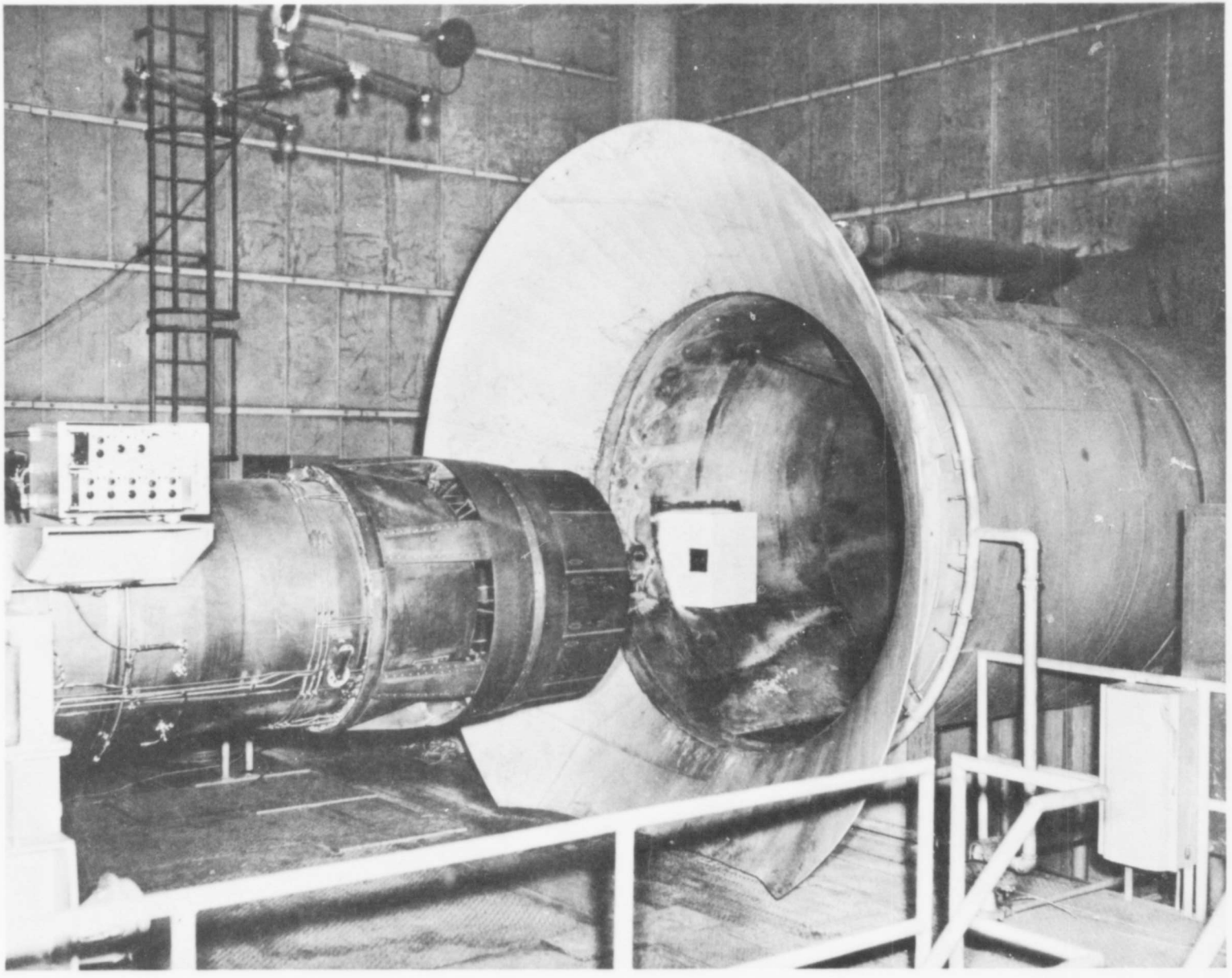

FIGURE 35 - TF-30-P1 EJECTOR NOZZLE

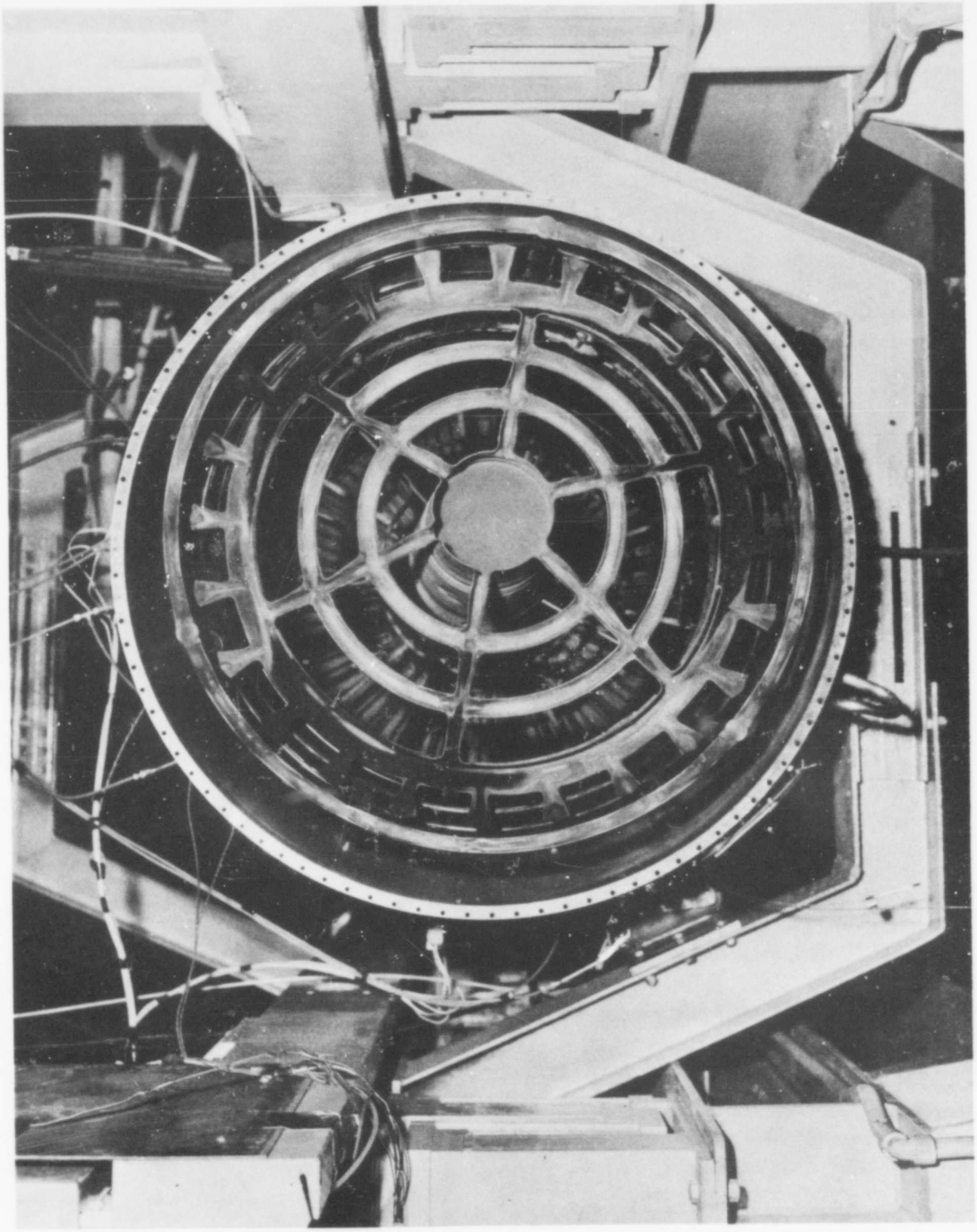

FIGURE 36 - TF-30-P1 AUGMENTOR ZONES AND STABILIZERS

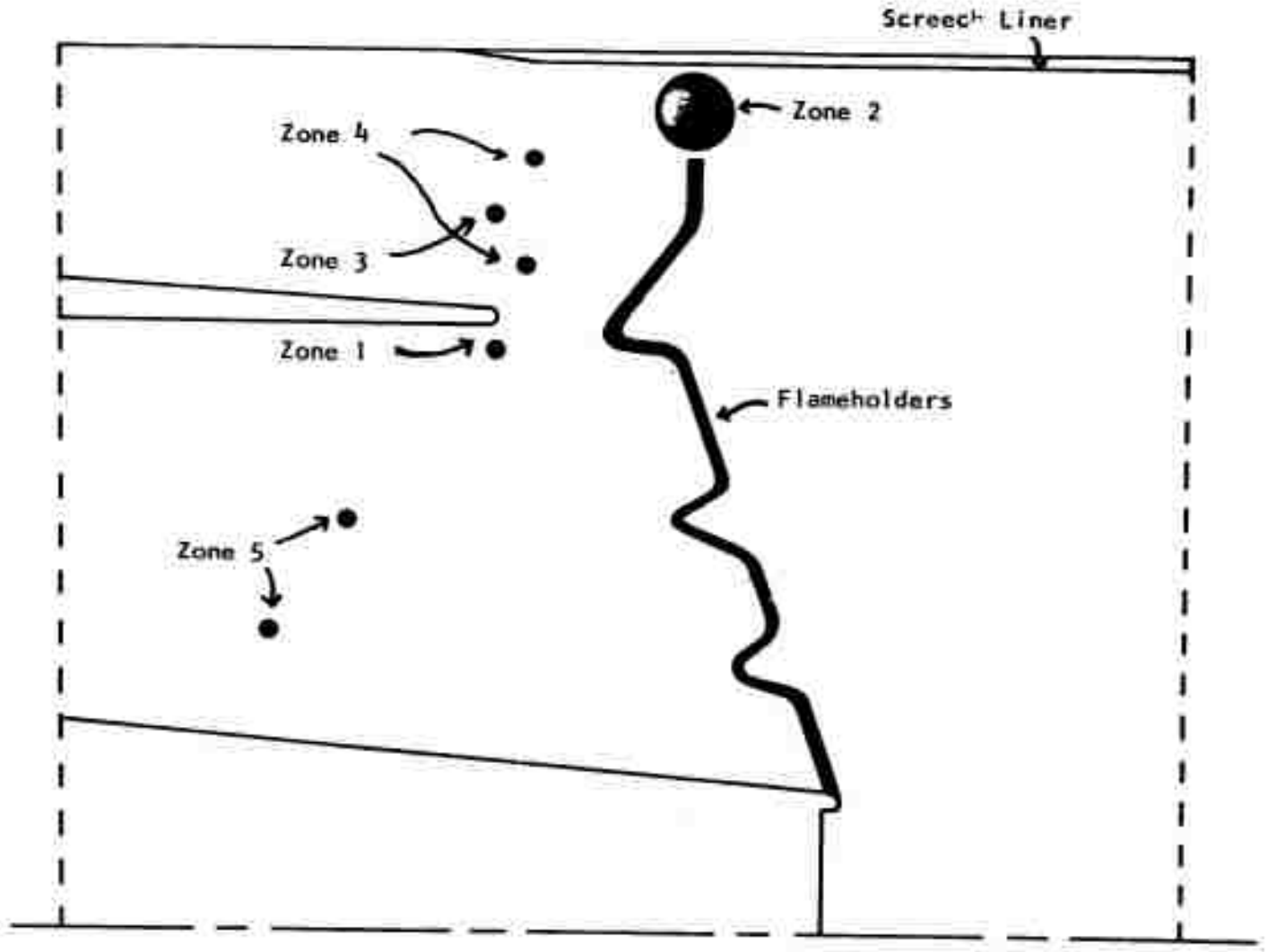

FIGURE 37 - SCHEMATIC OF AUGMENTOR FUEL INJECTORS AND FLAMEHOLDERS

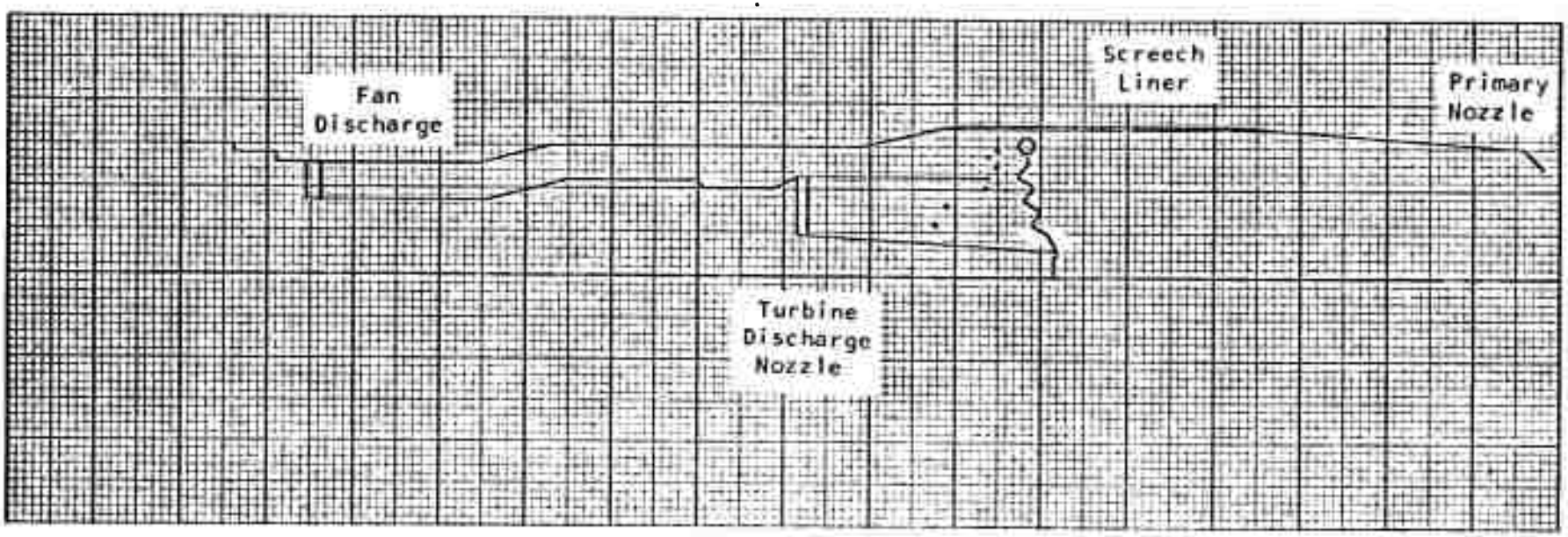

FIGURE 38 - FLOW PATH OF TF-30-P1 AUGMENTOR

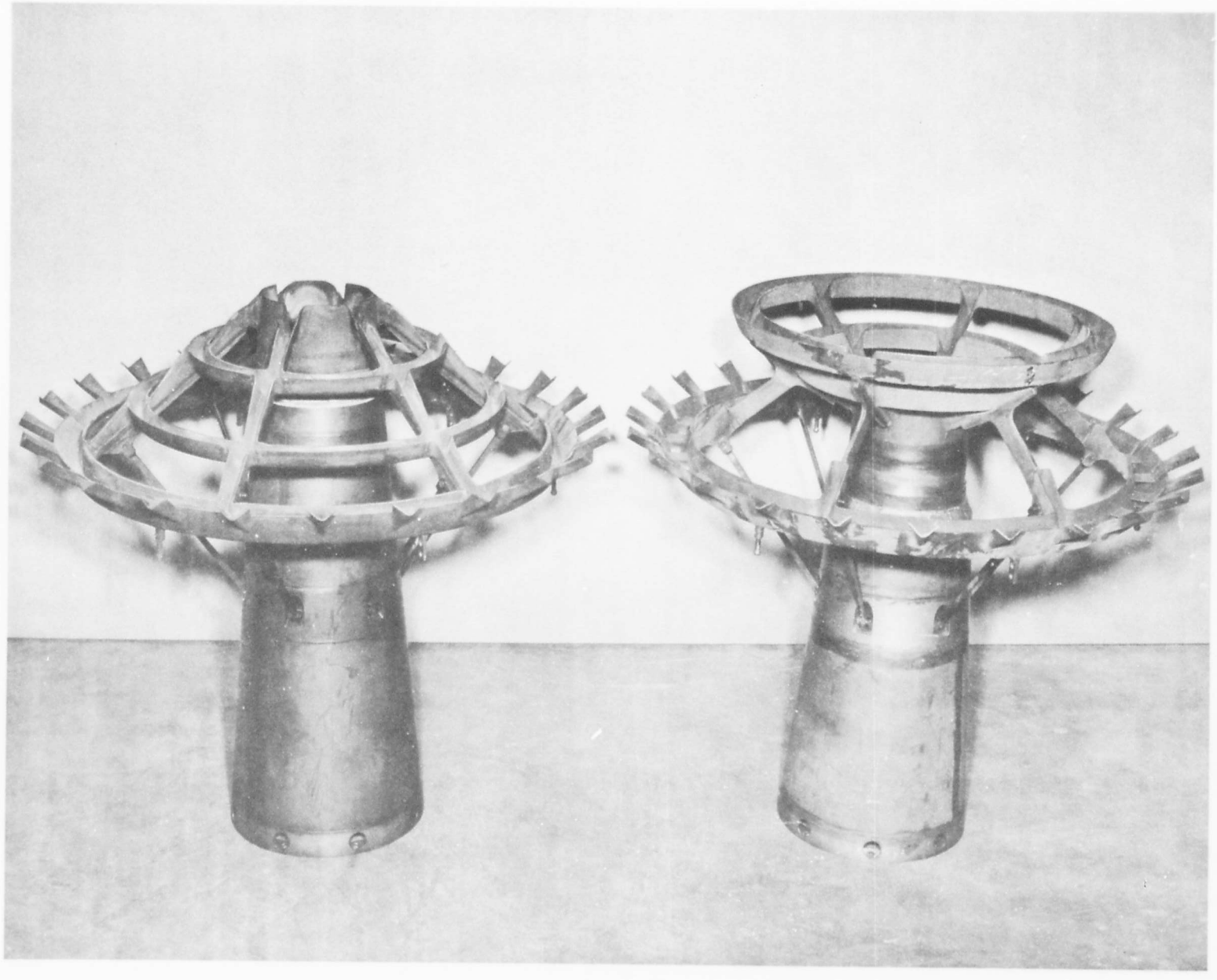

FIGURE 39 - FLAMEHOLDER ASSEMBLIES TESTED

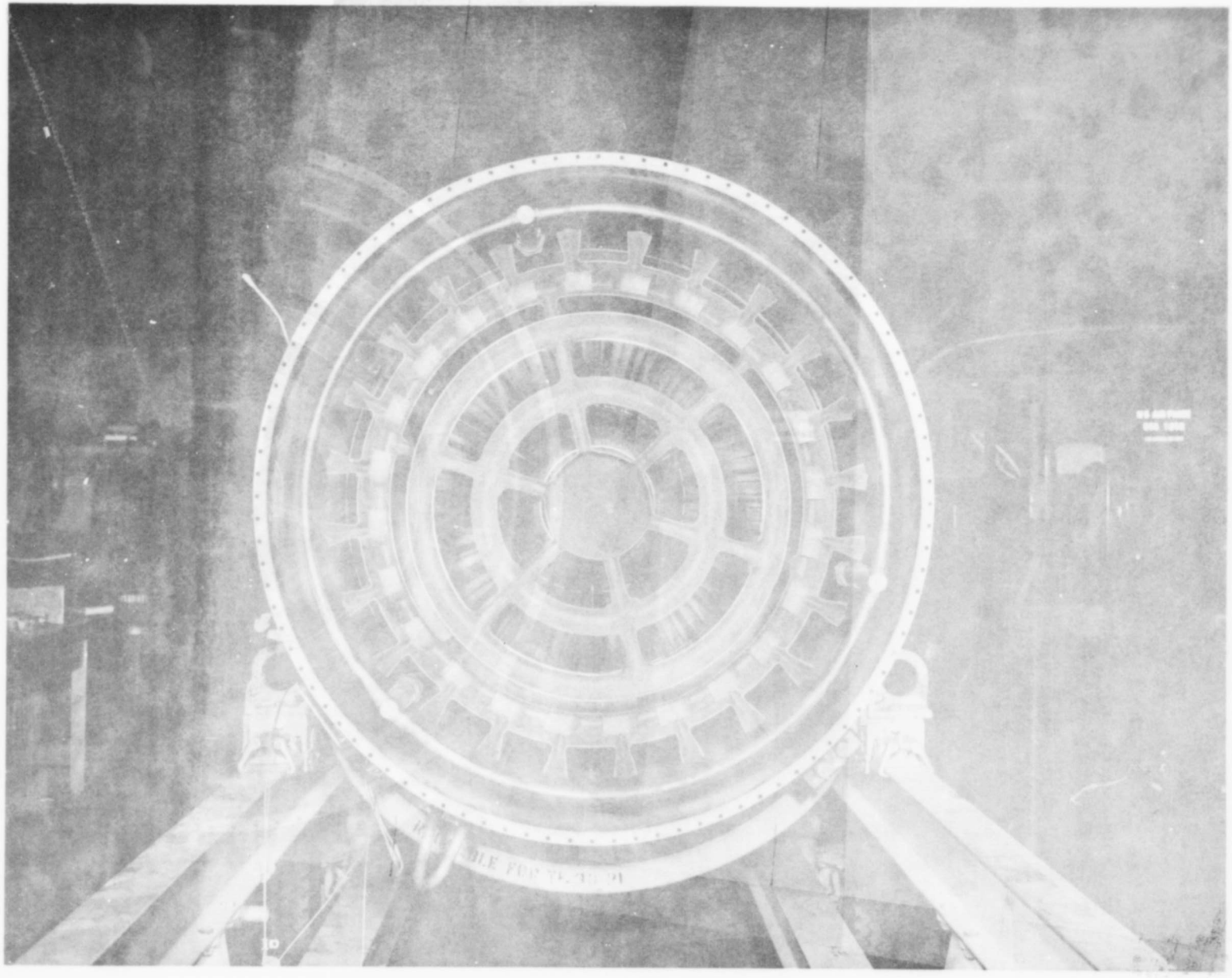

FIGURE 40 - MODIFIED FLAMEHOLDER ASSEMBLY INSTALLED (REAR VIEW)

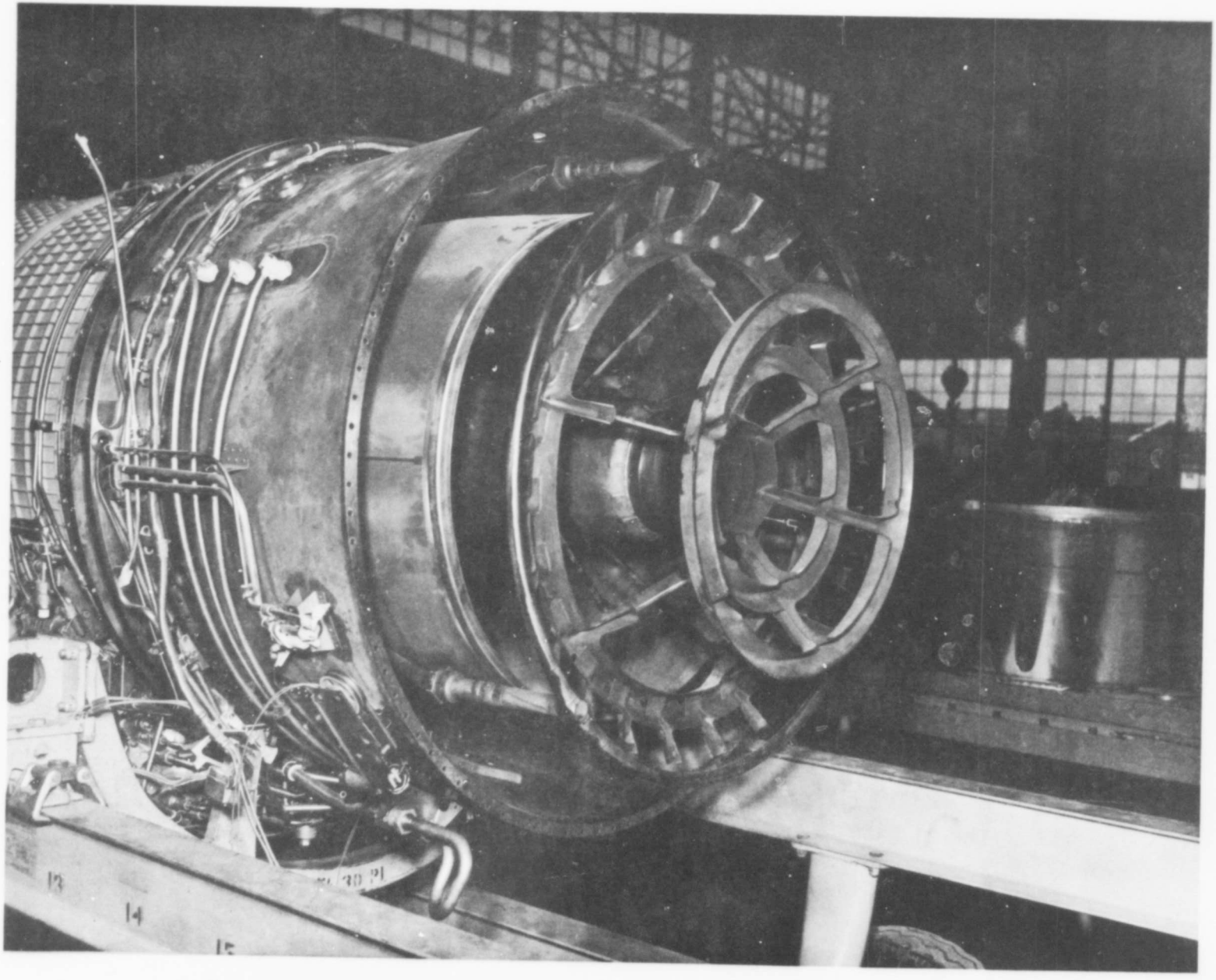

FIGURE 41 - MODIFIED FLAMEHOLDER ASSEMBLY INSTALLED (SIDE VIEW)

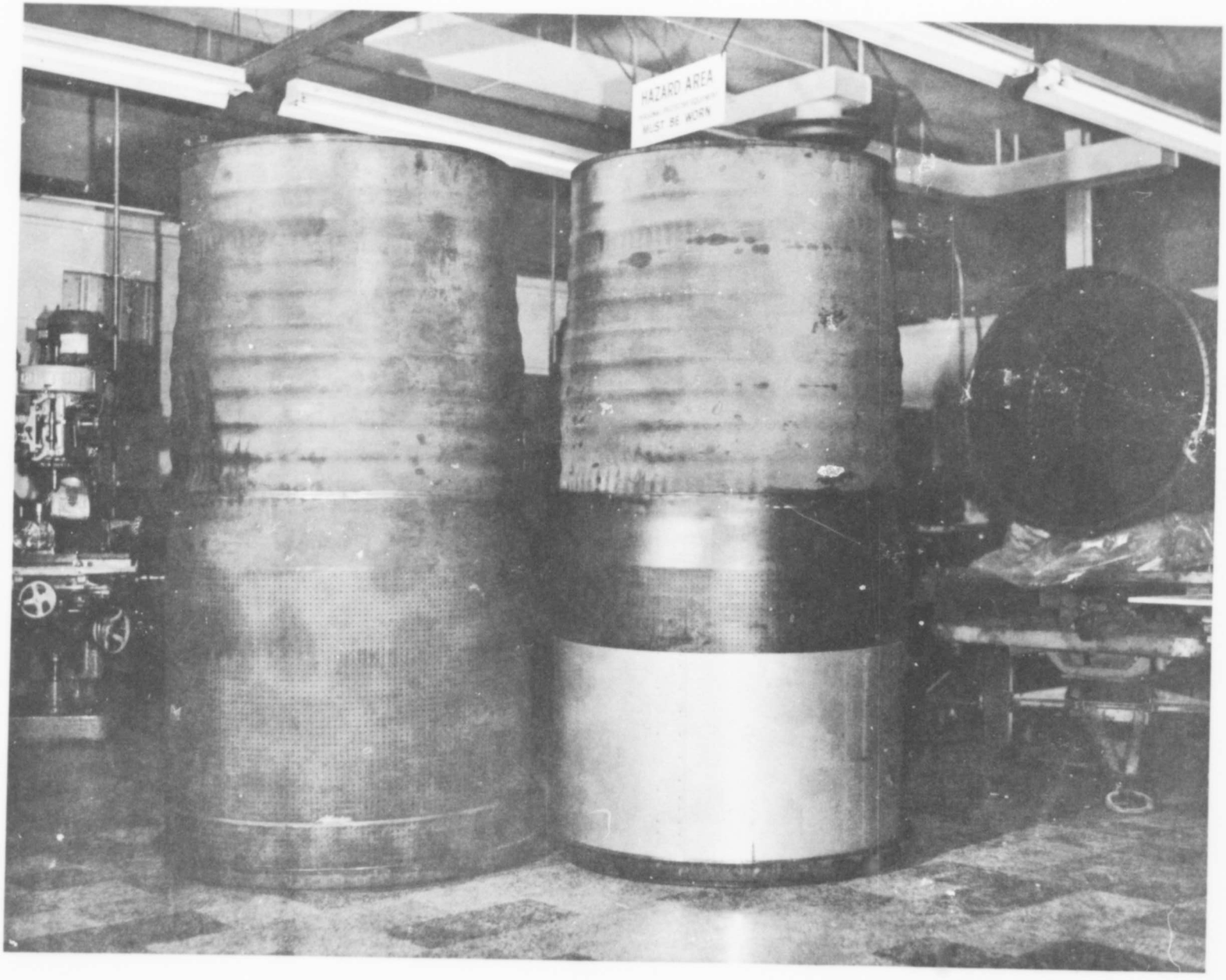

FIGURE 42 - STANDARD AND MODIFIED SCREECH LINERS

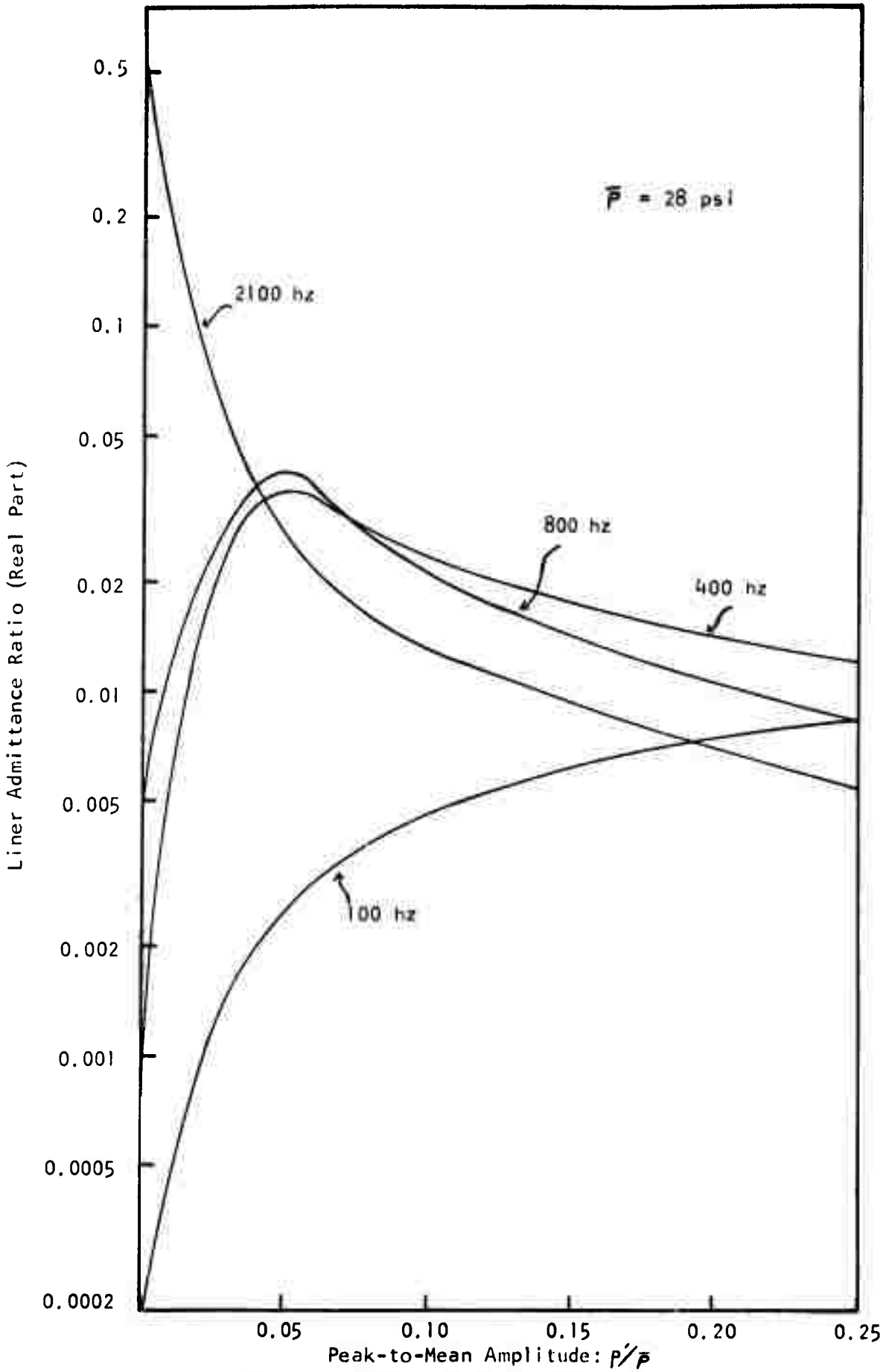

FIGURE 43 - ACOUSTIC ADMITTANCE (REAL PART) OF SCREECH LINER

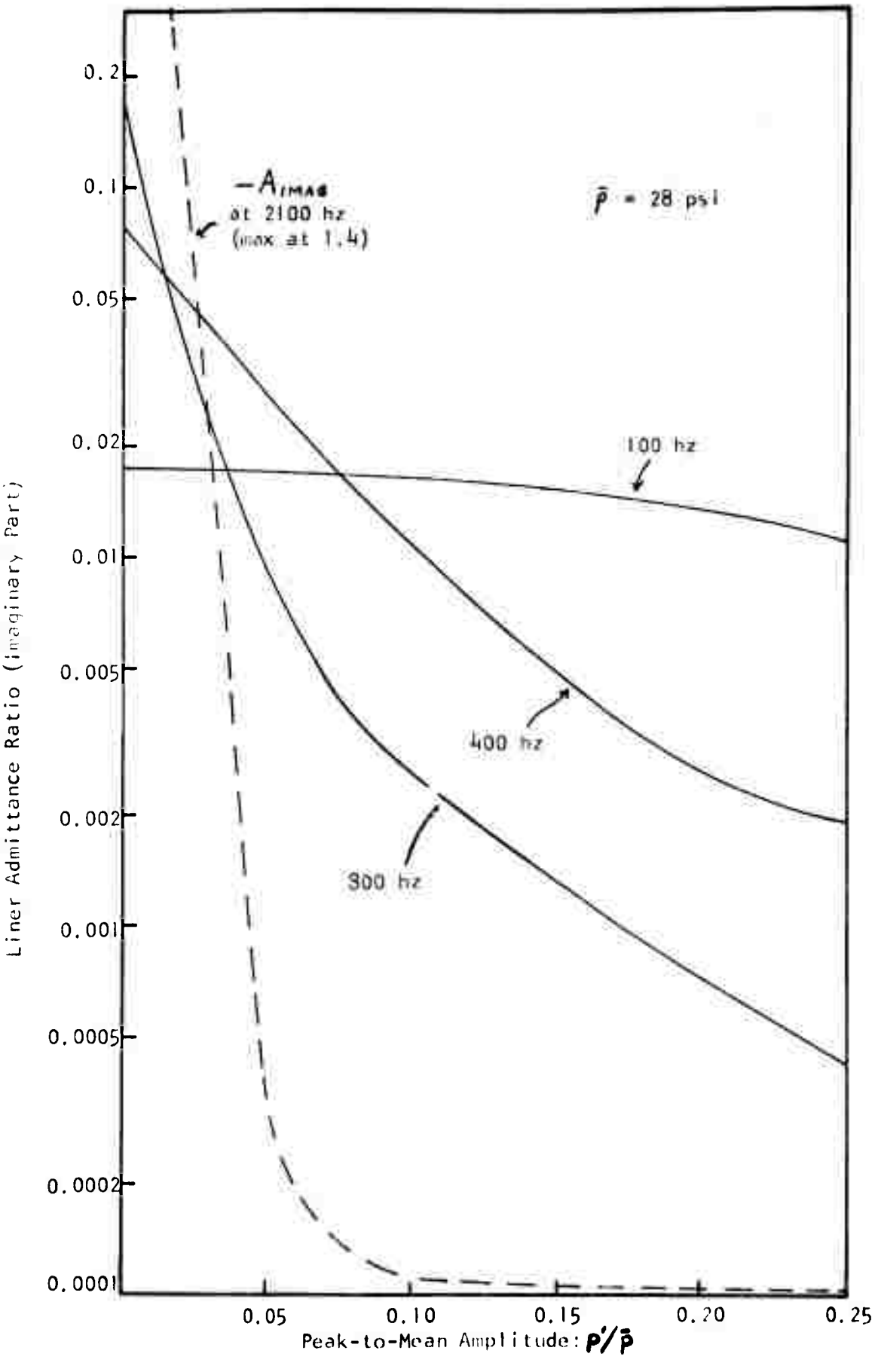

FIGURE 44 - ACOUSTIC ADMITTANCE (IMAGINARY PART) OF SCREECH LINER

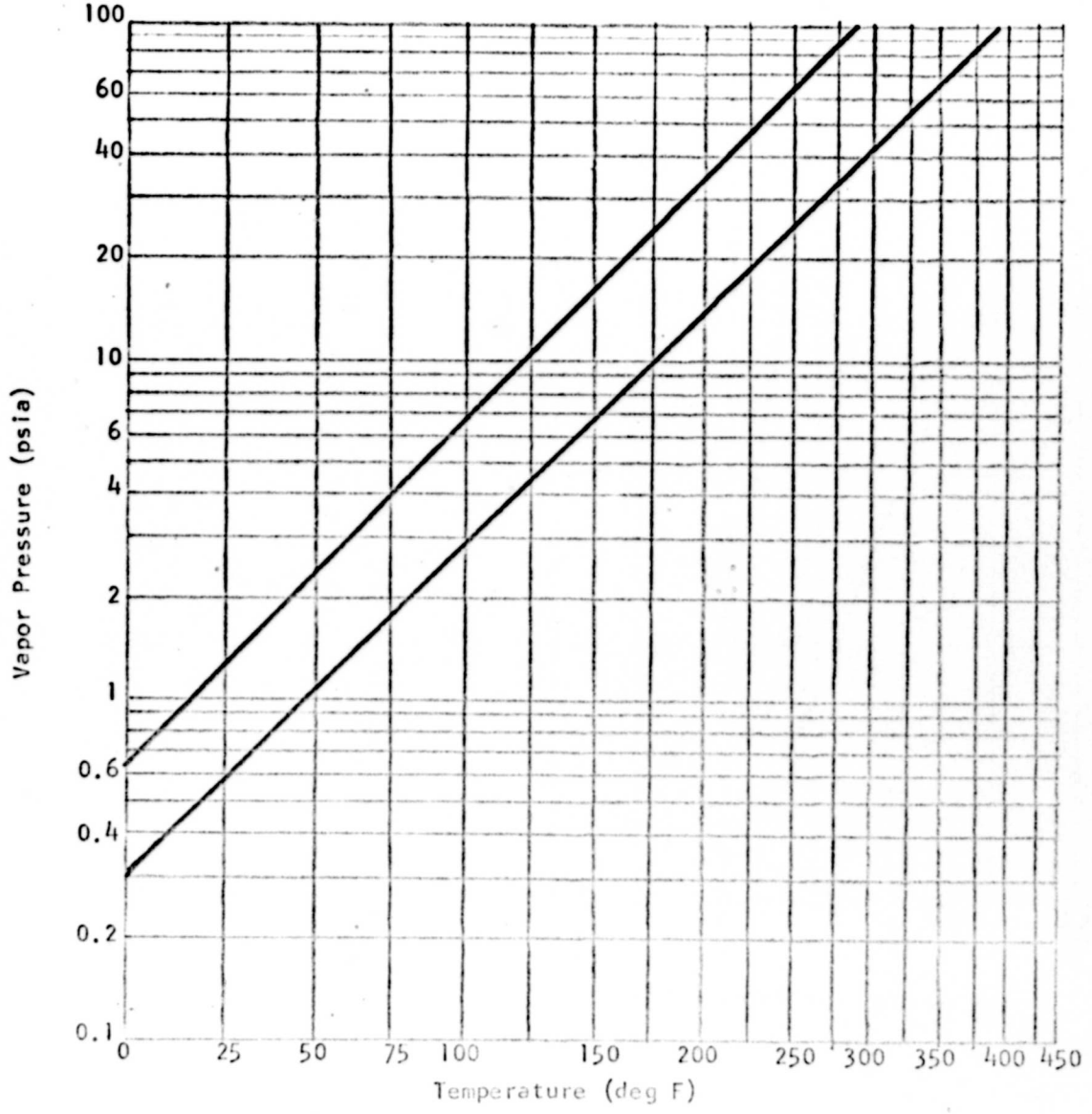

FIGURE 45 - VAPOR PRESSURE VS TEMPERATURE OF AVGAS AND JP-4 (10 PER CENT DISTILLATION)

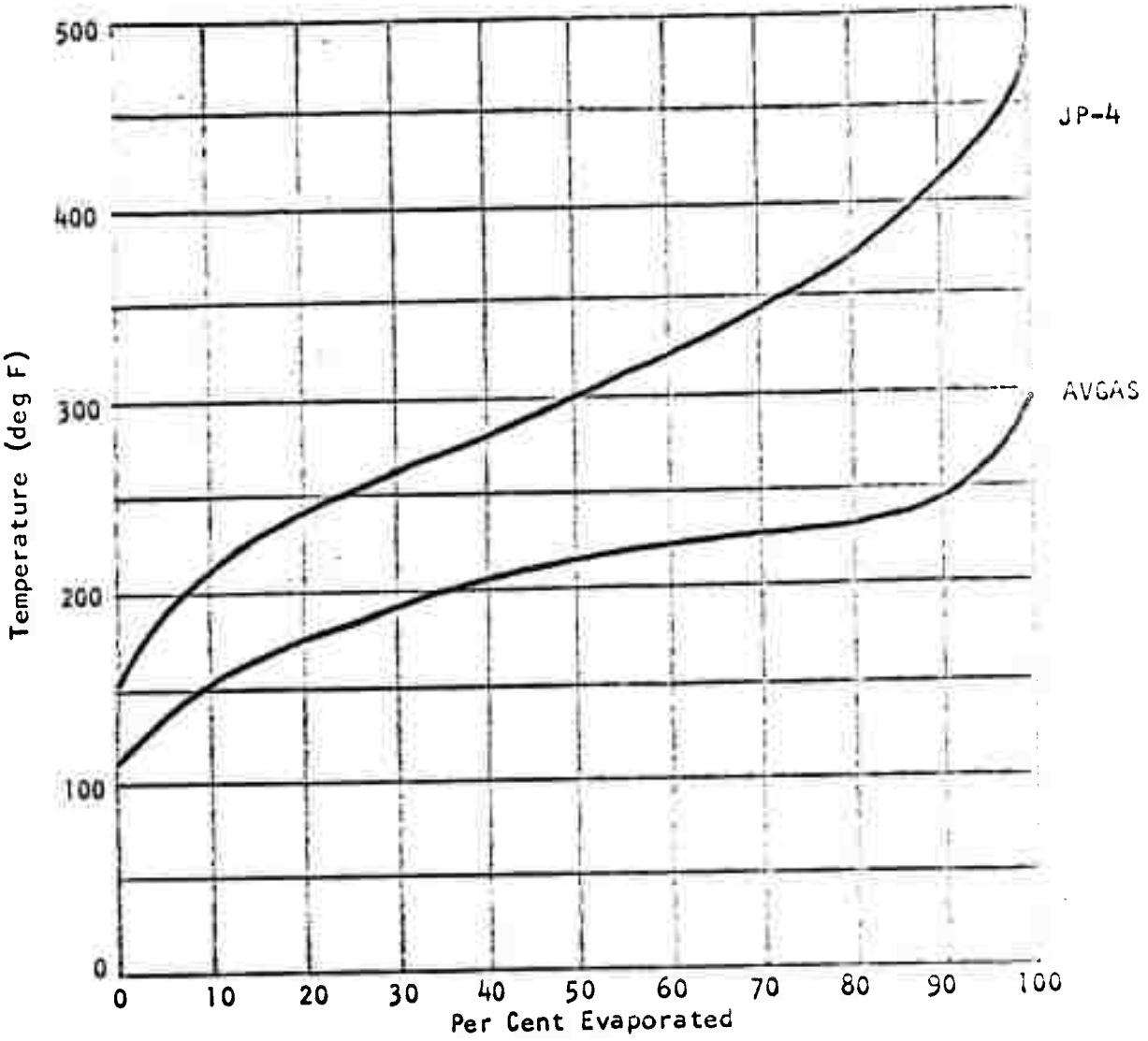

FIGURE 46 - DISTILLATION OF AVGAS AND JP-4 AT ATMOSPHERIC CONDITIONS

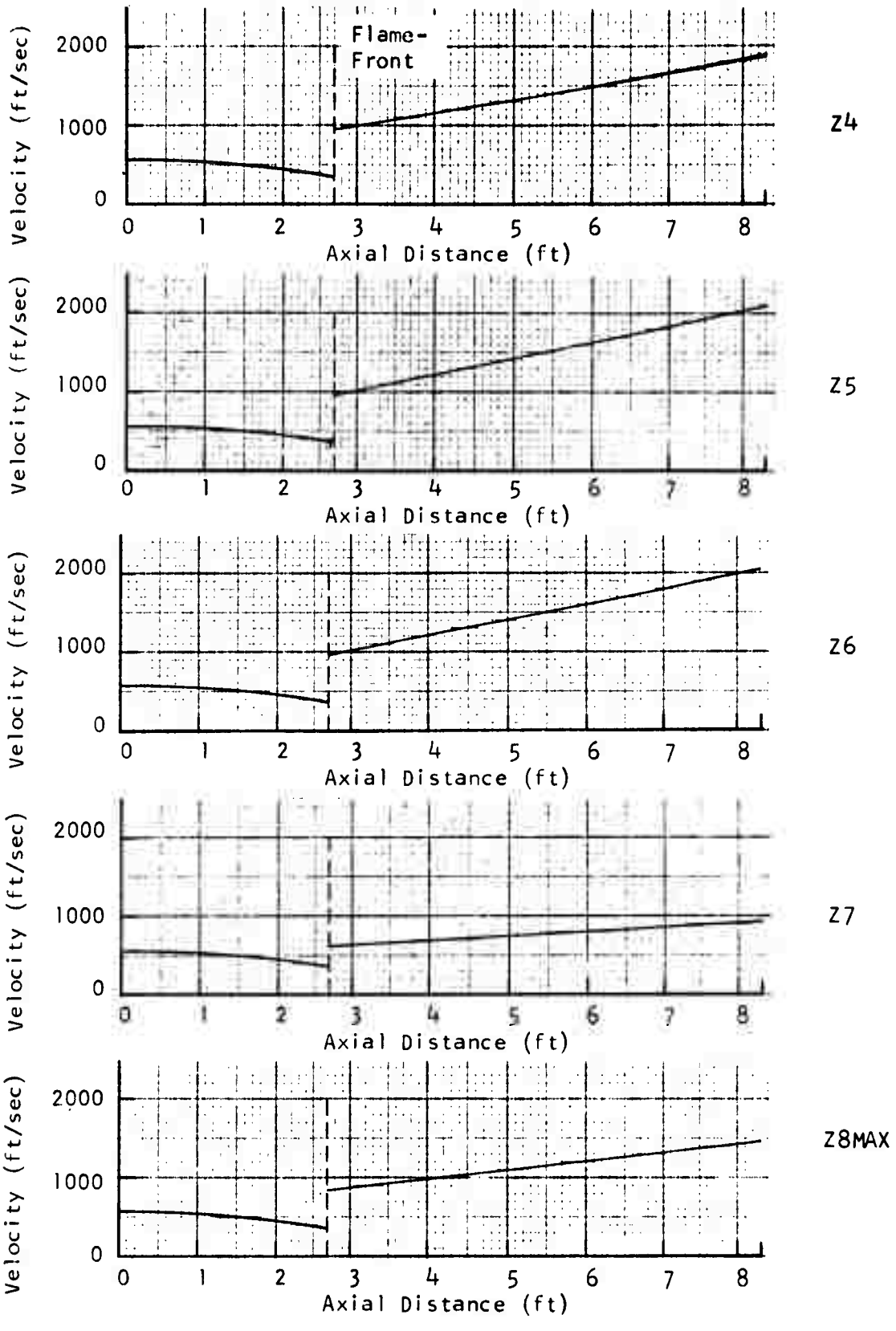

FIGURE 47 - THROUGH-FLOW VELOCITIES ASSUMED IN THE AFTERBURNER SOLUTIONS

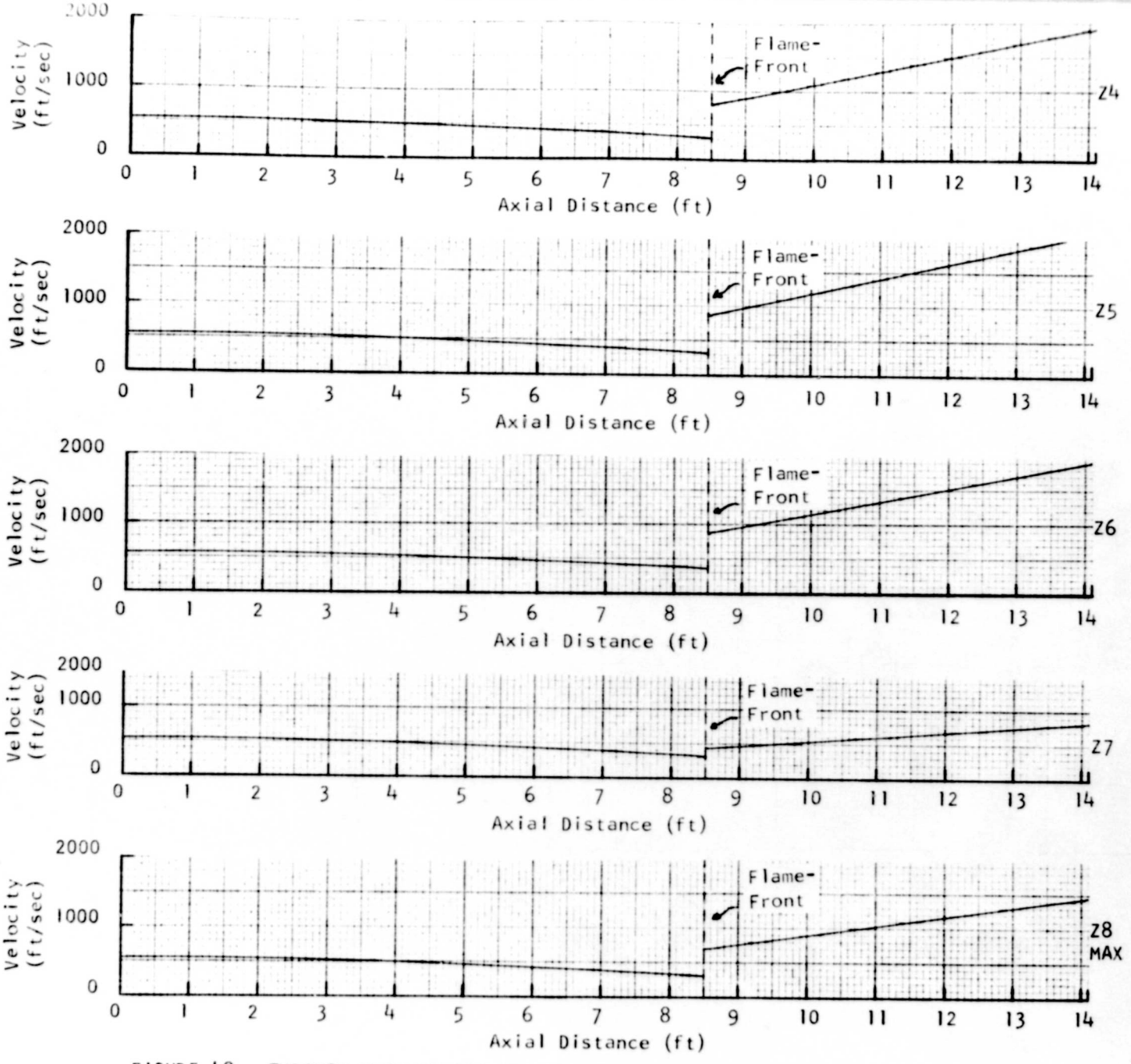

FIGURE 48 - THROUGH-FLOW VELOCITIES ASSUMED IN THE DUCT BURNER SOLUTIONS

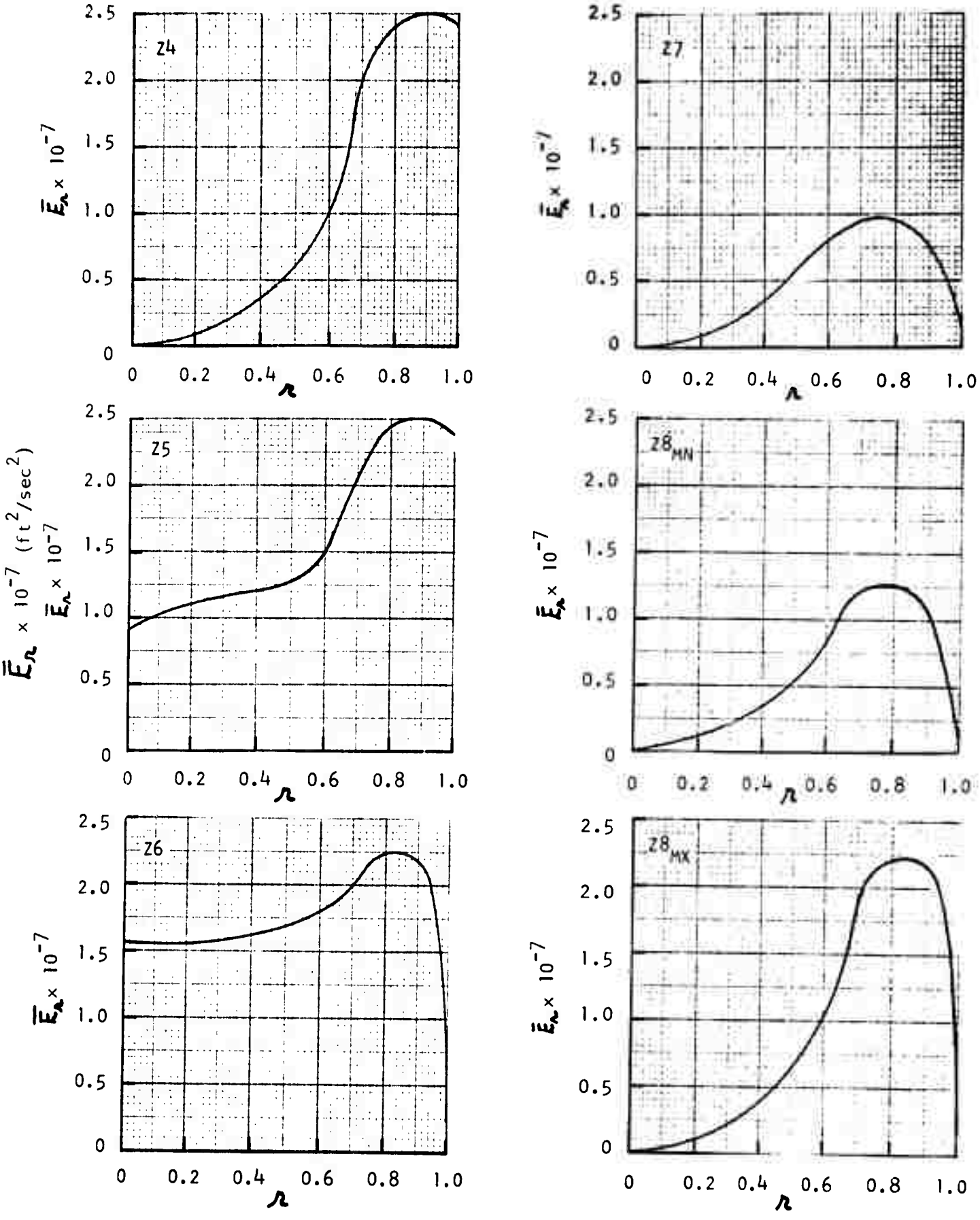

FIGURE 49 - RADIAL VARIATION OF $\bar{E}$ ASSUMED FOR DIFFERENT FUEL ZONE COMBINATIONS

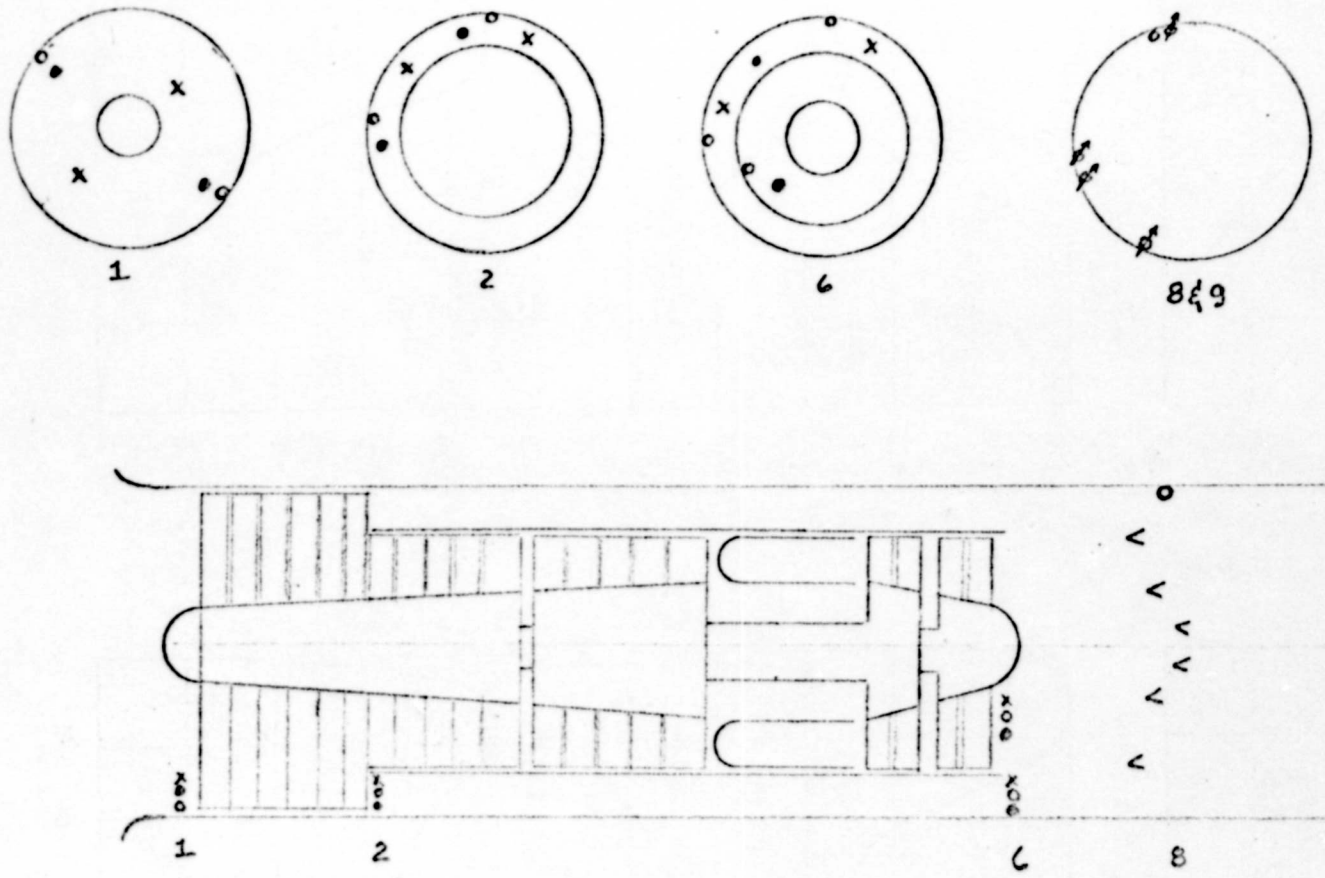

X Total Temperature

o Static Pressure

Total Pressure

Kistler Transducer

FIGURE 50 - SCHEMATIC OF INSTRUMENTATION SENSOR LOCATIONS

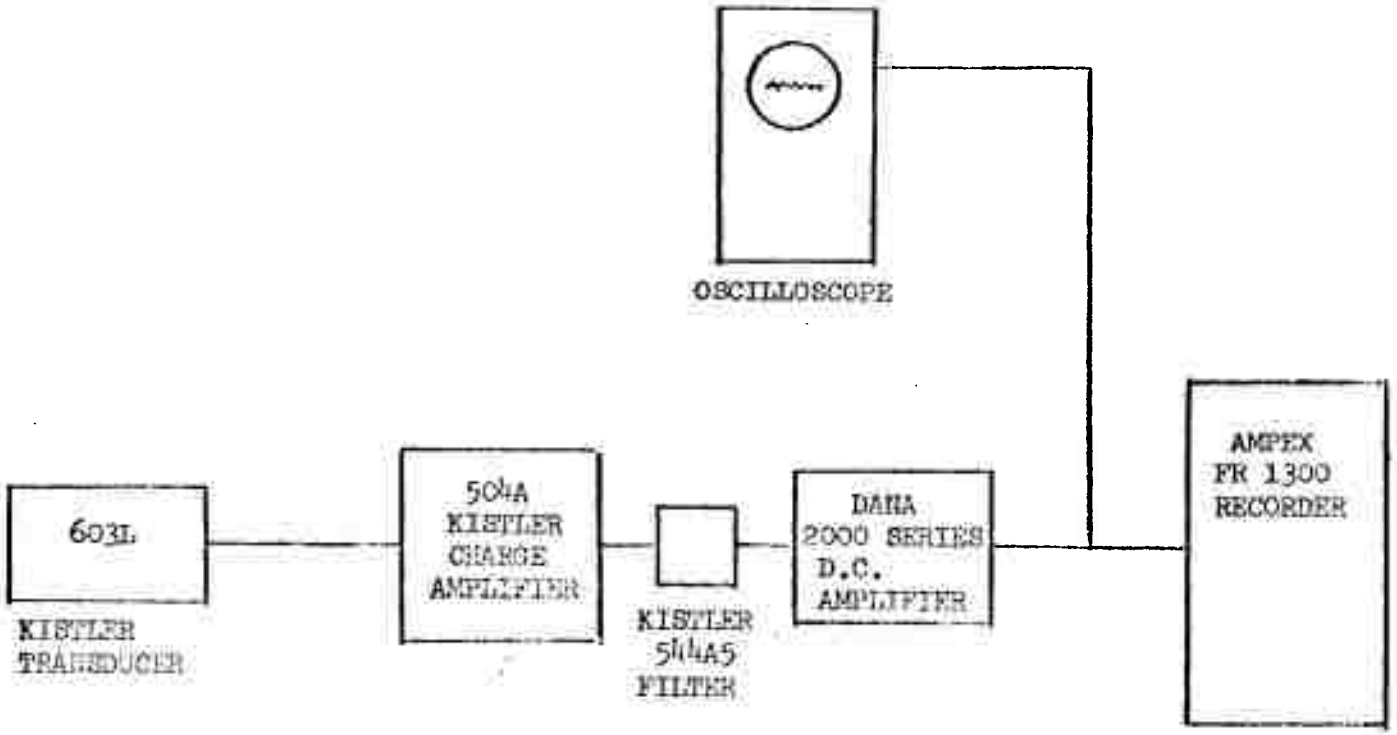

FIGURE 51 - SCHEMATIC OF ANALOG CIRCUITRY

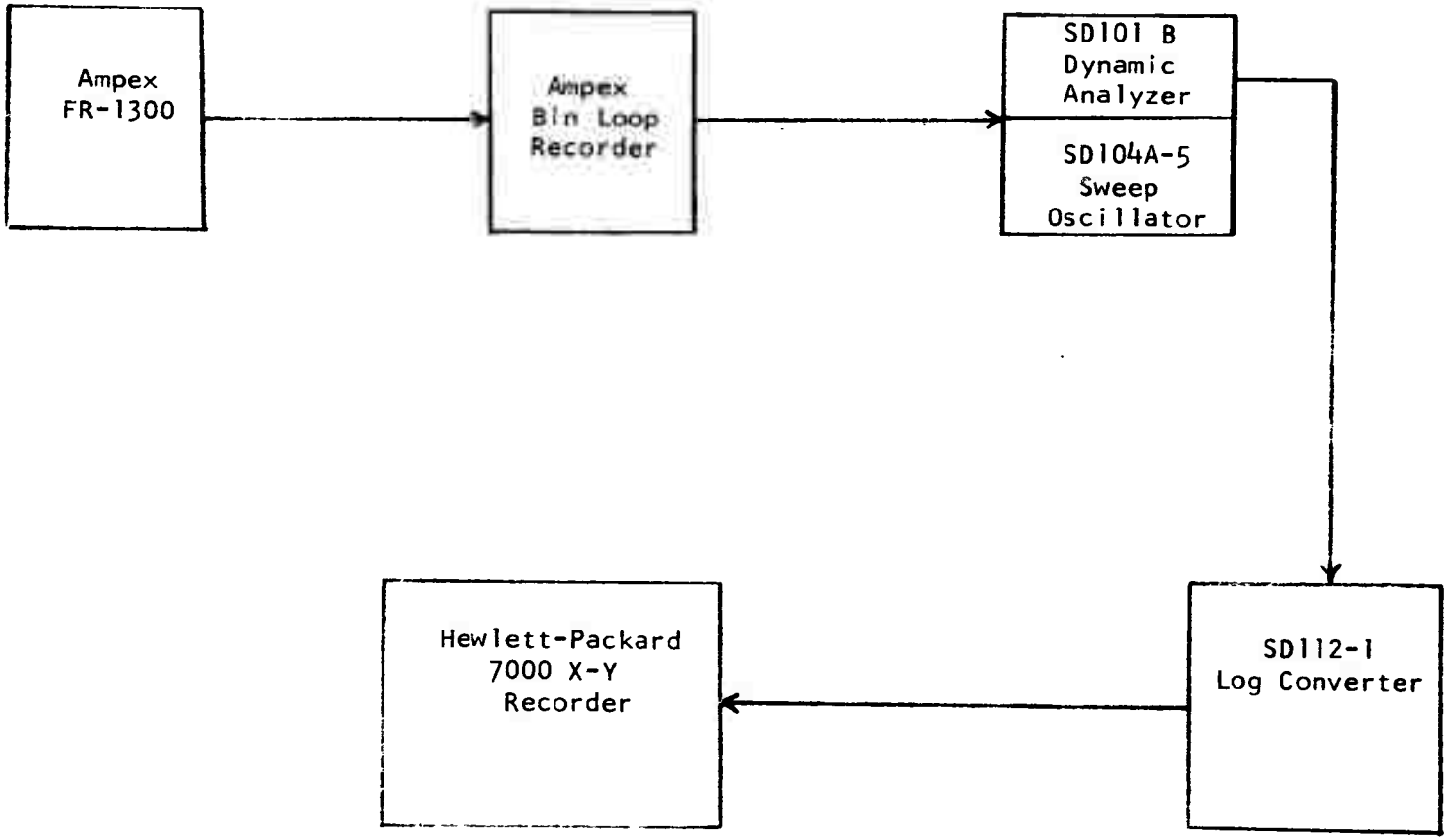

FIGURE 52 - SCHEMATIC OF ANALOG DATA REDUCTION SYSTEM

TABLE I

TF-30-P1 AUGMENTOR INSTABILITY TEST PLAN

	Tests									
	1	2	3	4	5	6	7	8	9	10
Fuel	JP-4	JP-4	JP-4	JP-4	JP-4	JP-4	JP-4	JP-4	AVGAS	AVGAS
Flameholder	Normal	Normal	Normal	Normal	Normal	Normal	Mod	Mod	Normal	Normal
Liner	Blocked	Normal	Normal	Blocked	Blocked	Normal	Normal	Blocked	Blocked	Normal
Distortion	0	180	180	90	90	0	0	0	0	0
Normal Zones	Z4,Z5	Z4,Z5	Z4,Z5	Z4,Z5	Z4,Z5	Z4,Z5	Z4,Z5	Z4,Z5	Z4	Z4
Special Zones	Z6,Z7,Z8	Z6,Z7,Z8	Z6,Z7,Z8	Z6,Z7,Z8	Z6,Z7,Z8	Z6,Z7,Z8	Z6,Z7,Z8	Z6,Z7,Z8	Z7,Z8	Z7,Z8

Zone Combination Legend

Z4: 1, 2, 3, 4
Z5: 1, 2, 3, 4, 5
Z6: 1, 3, 4, 5
Z7: 1, 3
Z8: 1, 3, 4

Note

Tests 2 through 5 could not be executed because of engine surges.

TABLE II

PRESSURE OSCILLATION AMPLITUDES
CHANNEL 1 AT ~400 HZ

	Test 1	Test 6	Test 7	Test 8	Test 9	Test 10
Z0	--	0.97	--	0.43	--	--
Z4	0.38	0.17	--	0.75	0.28	--
Z5	0.36	0.19	--	--	--	--
Z6	0.32	0.21	--	0.24	--	--
Z7	0.45	--	--	--	--	--
Z8 MIN	0.32	--	--	--	--	--
Z8 MAX	1.50	0.30	--	0.30	--	--
Z4*	0.24	--	--	--	--	--
Z8* MAX	4.27	--	--	--	--	--

Note: Amplitudes are peak-to-mean: Values in per cent.

* Cold day tests.

TABLE III

PRESSURE OSCILLATION AMPLITUDES
CHANNEL 2 AT ~400 HZ

	Test 1	Test 6	Test 7	Test 8	Test 9	Test 10
Z0	--	1.60	0.86	1.18	0.33	0.75
Z4	1.54	0.64	1.97	2.67	0.45	1.12
Z5	1.17	0.75	--	--	--	--
Z6	1.57	0.56	2.24	2.57	--	--
Z7	1.33	0.61	2.55	2.46	0.40	1.28
Z8 MIN	1.39	0.67	2.77	2.89	0.48	1.44
Z8 MAX	2.93	4.54	4.31	3.85	0.80	1.07
Z4*	2.66	--	--	--	--	--
Z8* MAX	20.65	--	--	--	--	--

Note: Amplitudes are peak-to-mean: Values in per cent.

* Cold day tests.

TABLE IV

PRESSURE OSCILLATION AMPLITUDES
CHANNEL 3 AT ~400 HZ

	Test 1	Test 6	Test 7	Test 8	Test 9	Test 10
Z0	--	0.59	1.39	2.03	--	--
Z4	0.51	1.29	2.15	0.99	--	--
Z5	0.72	1.07	--	--	--	--
Z6	0.63	1.39	1.82	0.83	--	--
Z7	1.17	1.50	2.03	2.89	--	--
Z8 MIN	1.07	0.88	2.56	1.87	--	--
Z8 MAX	0.83	4.17	2.68	3.23	--	--
Z4*	0.78	--	--	--	--	--
Z8* MAX	1.87	--	--	--	--	--

Note: Amplitudes are peak-to-mean: Values in per cent.

* Cold day tests.

TABLE V

PRESSURE OSCILLATION AMPLITUDES
CHANNEL 4 AT ~400 HZ

	Test 1	Test 6	Test 7	Test 8	Test 9	Test 10
Z0	--	1.23	0.70	0.63	1.07	1.28
Z4	1.07	2.46	2.25	1.18	0.75	1.17
Z5	0.75	1.44	--	--	--	--
Z6	0.78	2.30	1.50	1.77	--	--
Z7	0.75	2.73	2.03	1.23	0.40	0.91
Z8 MIN	0.70	2.25	2.36	2.14	0.46	0.93
Z8 MAX	2.40	6.97	2.72	3.00	1.34	1.17
Z4*	0.70	--	--	--	--	--
Z8* MAX	9.89	--	--	--	--	--

Note: Amplitudes are peak-to-mean: Values in per cent.

* Cold day tests.

TABLE VI

PRESSURE OSCILLATION AMPLITUDES
CHANNEL 7 AT ~ 400 HZ

	Test 1	Test 6	Test 7	Test 8	Test 9	Test 10
Z0	--	--	--	--	0.28	0.22
Z4	0.70	--	--	--	0.53	0.43
Z5	0.80	--	--	--	--	--
Z6	0.71	--	--	--	--	--
Z7	0.56	--	--	--	0.32	0.37
Z8 MIN	1.87	--	--	--	0.37	0.32
Z8 MAX	9.90	--	--	--	0.75	0.54
Z4*	3.63	--	--	--	--	--
Z8* MAX	37.40	--	--	--	--	--

Note: Amplitudes are peak-to-mean: Values in per cent.

* Cold day tests.

TABLE VII

PRESSURE OSCILLATION AMPLITUDES
CHANNEL 8 AT ~ 400 HZ

	Test 1	Test 6	Test 7	Test 8	Test 9	Test 10
Z0	--	0.28	--	--	--	--
Z4	0.23	--	--	1.12	0.23	--
Z5	--	--	--	--	--	--
Z6	0.19	--	0.51	0.59	--	--
Z7	0.21	--	--	--	0.19	0.32
Z8 MIN	0.51	--	--	--	0.27	0.27
Z8 MAX	2.09	--	--	1.07	0.51	0.43
Z4*	1.29	--	--	--	--	--
Z8* MAX	5.60	--	--	--	--	--

Note: Amplitudes are peak-to-mean: Values in per cent.

* Cold day tests.

TABLE VIII

PRESSURE OSCILLATION AMPLITUDES
CHANNEL 1 AT ~200 HZ

	Test 1	Test 6	Test 7	Test 8	Test 9	Test 10
Z0	--	6.97	--	--	--	--
Z4	0.64	0.94	--	--	--	--
Z5	0.75	0.95	--	--	--	--
Z6	0.75	0.75	--	--	--	--
Z7	0.82	1.07	--	--	--	--
Z8 MIN	0.77	0.77	--	--	--	--
Z8 MAX	0.62	0.73	--	--	--	--
Z4*	0.26	--	--	--	--	--
Z8* MAX	0.24	--	--	--	--	--

Note: Amplitudes are peak-to-mean: Values in per cent.

* Cold day tests.

TABLE IX

PRESSURE OSCILLATION AMPLITUDES
CHANNEL 2 AT ~200 HZ

	Test 1	Test 6	Test 7	Test 8	Test 9	Test 10
Z0	--	2.78	1.98	2.64	0.88	0.80
Z4	0.91	1.02	2.57	3.20	0.94	0.83
Z5	0.78	0.86	--	--	--	--
Z6	0.91	0.94	1.87	4.50	--	--
Z7	1.23	0.99	2.57	4.30	0.83	0.91
Z8 MIN	1.34	0.94	2.57	3.01	1.07	0.64
Z8 MAX	0.94	1.07	1.61	3.96	1.76	0.91
Z4*	1.28	--	--	--	--	--
Z8* MAX	1.39	--	--	--	--	--

Note: Amplitudes are peak-to-mean: Values in per cent.

* Cold day tests.

TABLE X

PRESSURE OSCILLATION AMPLITUDES
CHANNEL 3 AT ~ 200 HZ

	Test 1	Test 6	Test 7	Test 8	Test 9	Test 10
Z0	--	0.59	1.97	3.64	--	--
Z4	0.45	1.05	3.64	0.48	--	--
Z5	0.51	1.98	--	--	--	--
Z6	0.41	3.10	2.08	0.62	--	--
Z7	0.54	2.25	1.81	--	--	--
Z8 MIN	0.43	2.67	1.76	1.18	--	--
Z8 MAX	0.75	1.55	2.03	--	--	--
Z4*	0.81	--	--	--	--	--
Z8* MAX	1.07	--	--	--	--	--

Note: Amplitudes are peak-to-mean: Values in per cent.

* Cold day tests.

TABLE XI

PRESSURE OSCILLATION AMPLITUDES
CHANNEL 4 AT ~ 200 HZ

	Test 1	Test 6	Test 7	Test 8	Test 9	Test 10
Z0	--	3.32	1.87	2.45	2.78	5.36
Z4	0.29	3.75	2.67	2.67	0.56	1.23
Z5	0.48	2.67	--	--	--	--
Z6	0.45	2.46	2.35	4.81	--	--
Z7	1.11	3.42	2.67	5.35	0.83	1.65
Z8 MIN	0.48	3.75	4.39	4.91	0.83	1.55
Z8 MAX	0.29	3.95	3.85	4.91	1.20	1.87
Z4*	1.39	--	--	--	--	--
Z8* MAX	1.28	--	--	--	--	--

Note: Amplitudes are peak-to-mean: Values in per cent.

* Cold day tests.

TABLE XII

PRESSURE OSCILLATION AMPLITUDES
CHANNEL 7 AT ~ 200 HZ

	Test 1	Test 6	Test 7	Test 8	Test 9	Test 10
Z0	--	--	--	--	0.83	1.05
Z4	0.53	--	--	--	0.88	1.39
Z5	0.53	--	--	--	--	--
Z6	0.53	--	--	--	--	--
Z7	0.53	--	--	--	0.67	1.17
Z8 MIN	1.71	--	--	--	0.94	0.78
Z8 MAX	2.01	--	--	--	1.34	1.07
Z4*	1.74	--	--	--	--	--
Z8* MAX	2.67	--	--	--	--	--

Note: Amplitudes are peak-to-mean: Values in per cent.

* Cold day tests.

TABLE XIII

PRESSURE OSCILLATION AMPLITUDES
CHANNEL 8 AT ~ 200 HZ

	Test 1	Test 6	Test 7	Test 8	Test 9	Test 10
Z0	--	0.29	--	--	--	--
Z4	0.23	--	--	--	0.43	0.80
Z5	--	--	--	--	--	--
Z6	0.19	--	--	--	--	--
Z7	0.17	--	--	--	0.51	0.94
Z8 MIN	0.49	--	--	--	0.59	0.96
Z8 MAX	0.51	--	--	--	0.64	1.07
Z4*	1.39	--	--	--	--	--
Z8* MAX	1.50	--	--	--	--	--

Note: Amplitudes are peak-to-mean: Values in per cent.

* Cold day tests.

TABLE XIV

FAN DISCHARGE TOTAL TEMPERATURES

	Test 1	Test 6	Test 7	Test 8	Test 9	Test 10
Z0	204	210	250	240	233	210
Z4	205	210	220	242	225	210
Z5	204	210	--	--	--	--
Z6	207	210	240	240	--	--
Z7	204	210	218	240	225	212
Z8 MIN	206	210	220	233	227	210
Z8 MAX	203	212	220	233	225	210
Z4*	178	--	--	--	--	--
Z8* MAX	178	--	--	--	--	--

Note: Temperatures in deg F.

* Cold day tests.

TABLE XV

TOTAL AUGMENTOR FUEL FLOWS FROM TEST POINT TO TEST POINT

	Test 1	Test 6	Test 7	Test 8	Test 9	Test 10
Z0	--	--	--	--	--	--
Z4	27200	26700	25700	24100	28500	23400
Z5	32300	31100	--	--	--	--
Z6	35400	33400	33100	32700	--	--
Z7	11500	12400	12000	11000	11400	12500
Z8 MIN	13800	14100	13200	13700	15600	14100
Z8 MAX	20700	26300	19600	18500	21300	21000
Z4*	28400	--	--	--	--	--
Z8* MAX	21500	--	--	--	--	--

Note: Fuel flow in lbm/hr.

* Cold day tests.

TABLE XVI

ZONE-BY-ZONE REPRESENTATIVE FUEL FLOWS ASSUMED IN THE ANALYSES

	Zone 1	Zone 2	Zone 3	Zone 4	Zone 5	Total AB
Z0	--	--	--	--	--	--
Z4	6500	6000	7000	7500	--	27000
Z5	5500	6500	6500	7500	6000	32000
Z6	6500	--	7500	8500	10500	33000
Z7	6000	--	6000	--	--	12000
Z8 MIN	5500	--	5500	1300	--	14000
Z8 MAX	6500	--	7000	7500	--	21000

Note: Fuel flow in lbm/hr.

TABLE XVII

SONIC VELOCITIES AND TEMPERATURE RISES ASSUMED IN THE ACOUSTICS ANALYSES

Fuel Zone Combination	Afterburner Solutions		Ductburner Solutions	
	Sonic Velocity (ft/sec)	ΔT_o (deg R)	Sonic Velocity (ft/sec)	ΔT_o (deg R)
Z4	2470	1900	2700	3000
Z5	2600	2225	2700	3000
Z6	2630	2300	2545	2550
Z7	2115	935	1940	1100
Z8MAX	2365	1575	2480	2350

Upstream Values in All Cases

Afterburner Solutions		Ductburner Solutions	
Sonic Velocity (ft/sec)	T_o (deg R)	Sonic Velocity (ft/sec)	T_o (deg R)
1600	1150	1260	680

APPENDIX I

TF-30-P1: THE ENGINE STUDIED

THE ENGINE TESTED

The TF-30-P1 (Figures 31 and 32) is a mixed-flow afterburning, dual-spool turbofan engine consisting of a three-stage fan and a six-stage low pressure compressor (low spool), a seven-stage high pressure compressor (high spool), an eight-can can-annular combustion system, a one-stage high pressure turbine (high spool), a three-stage low pressure turbine (low spool), and a mixed-flow afterburner equipped with a fully modulating flap-type convergent primary nozzle and a blow-in door ejector with variable inlet and exhaust areas.

The fan airstream, ducted around the core engine, mixes with the high temperature turbine discharge gases entering the afterburner. Concentric fuel manifolds in the diffuser downstream of the turbine, at the splitter exit plane between the core and fan streams, and in the fan stream inject fuel which is metered by the afterburner fuel control. The afterburner (Figures 33 and 34) contains a circumferential vee-gutter flameholder assembly with radial spikes, a perforated screech liner, and a convection cooled aft liner. The combustion exhaust gases from the afterburner pass through a flap-type convergent primary nozzle and enter a blow-in door ejector secondary nozzle (Figure 35). Primary nozzle area is controlled and monitored by the afterburner fuel control; major area changes occur only during afterburner modulation. The ejector nozzle flaps and blow-in doors are aerodynamically controlled as a function of inside and outside pressure differences.

The afterburner is a fully modulating five-zone system (Figure 36). Zone 1 is the ignition and minimum augmentation zone, consisting of a single circumferential spray ring fuel injector located in the turbine discharge gas stream. Ignition is effected by a "hot streak" system. Zone 2 is a jet-flameholder fuel injection ring, located at the outer diameter of the fan stream. This special spray ring provides aerodynamic flameholding and injects a fuel-air mixture into the fan stream. The air used in this spray ring is taken from the high compressor discharge and is introduced by the fuel control. Zones 3 and 4 consist of a three-ring fuel injector cluster, located at the splitter exit plane between the turbine discharge and fan streams. Zone 5 is a two-ring injector, located in the turbine discharge stream. Figure 37 provides a schematic of the fuel zone and flameholder system of the afterburner. The afterburner is modulated as a function of power lever position from Zone 1 through Zone 5 sequentially. Approximately 72 per cent thrust augmentation is achievable.

The basic performance characteristics of the TF-30-P1 at sea level, maximum power are listed below:

	Military	Max. A/B
Thrust, lbs	10,750	18,500
SFC	0.616	2.29
RPM		
(1) N1	9630	9700
(2) N2	13,770	13,810
Total Airflow, lb/sec	233.1	235.1
Overall Primary Cycle Pressure Ratio	16.32	16.85
Turbine Inlet Temperature, deg F	1839	1918
Turbine Outlet Temperature, deg F	1048	1105
Primary Nozzle Throat Area, sq ft	3.75	7.15
Secondary Nozzle Exit Area, sq ft	8.95	8.95
Bypass Ratio	1.0	1.0

AUGMENTOR INLET CONDITIONS ASSUMED IN THE ANALYSIS

Engine operating conditions varied slightly from test to test. For purposes of augmentor stability analysis the following typical values were assumed to hold at the splitter exit plane during all engine operating conditions (in the initial analyses):

	Core	Fan
Total Temperature: deg R	1560	670
Total Pressure: psi	28.72	28.33
Mach Number	0.281	0.208
Area: sq ft	3.97	4.46

The upstream sonic velocities assumed in the HLMHLT analyses were 1260 ft/sec in the case of a ductburner and 1600 ft/sec in the case of an afterburner.

AUGMENTOR GEOMETRY ASSUMED IN THE ANALYSIS

The combustion instability analysis requires constant duct dimensions for evaluating augmentor acoustics properties, but indirectly recognizes flow area changes via variations in the through-flow velocity. The afterburner dimensions assumed in the HLMHLT analyses are as follows:

	Cylindrical Afterburner	Annular Ductburner
Outer Radius, ft	1.67	1.67
Inner Radius, ft	0.0	1.16
Length of Chamber 1, ft	2.71	8.52
Length of Chamber 2, ft	5.59	5.59

Chambers 1 and 2 are respectively upstream and downstream of the flame-front, so that the above dimensions effectively locate the flame-front. The afterburner exit plane is defined to be at the entrance of the primary nozzle. The upstream plane is defined at the fan exit guide vanes in the case of the ductburner analysis and at the turbine discharge nozzles in the case of the afterburner analysis.

A scale drawing showing the dimensions used in calculating the through-flow velocity distribution is presented in Figure 38. The relevant flow areas are 8.98 sq ft at the flame-front and 7.23 sq ft at the nozzle entrance. The analysis of the velocity distributions treated the fan and core as distinct, concentric streams; the radius of the interface between the streams was varied to maintain equal static pressure on either side of the interface. The resulting velocity distributions are described in Appendix V.

ASSUMED AUGMENTOR INLET AND DISCHARGE ACOUSTIC ADMITTANCES

The augmentor acoustics analysis represents the effects of the discharge nozzle and of the upstream blade rows by means of acoustic admittance ratios. Methods are not yet available for calculating admittances of choked nozzles which are short compared to their outer diameters. The extremely complicated problem of sound wave reflection from fan exit guide vanes and turbine discharge nozzles is even less tractable. Therefore the analyses described in this report made gross assumptions on the upstream and downstream admittances-- assumptions which are educated guesses. Because of the large velocities at the nozzle and upstream boundaries, the values assigned the admittances are not exceedingly critical: a 50 per cent error in admittance represents only a 15 per cent error in the boundary coefficient for longitudinal modes.

The primary nozzle acoustic admittance ratios assumed in the HLMHLT analyses of the TF-30-P1 are as follows:

Predominant Component of Mode	Nozzle Admittance Ratio
Longitudinal	0.20 + j 0.25
Transverse	0.10 + j 0.05

Two sets of upstream boundary admittances were estimated: those for the ductburner represent the fan exit guide vanes; those for the afterburner represent an average between the effects of the turbine discharge nozzle and the effects of the open fan duct. The values used in the HLMHLT analyses are as follows:

Predominant Component of Mode	Upstream Admittance Ratio	
	Afterburner	Ductburner
Longitudinal	0.20 + j 0.25	0.10 + j 0.15
Transverse	0.15 + j 0.10	0.08 + j 0.05

The larger values for the afterburner model assume acoustic energy loss up the fan duct. The upstream boundary of the afterburner is stipulated to be at the turbine discharge nozzles; the fan duct boundary at this point is treated as an open end.

APPENDIX II

FLAMEHOLDERS EXAMINED

FLAMEHOLDER ASSEMBLIES

Two flameholder assemblies, both using three vee-gutter rings, were examined in the experimental program. The standard flameholder on the TF-30-P1, shown on the left in Figure 39, has an essentially conical shape. The outer ring, farthest upstream, is in the fan stream, and the two inner rings are in the core stream. A combination aerodynamic injector and flameholder surrounds this flameholder assembly, as shown in Figure 40.

Tests 7 and 8 were conducted with the modified flameholder assembly, shown on the right in Figure 39, installed in the augmentor. The distinctive characteristic of the modified flameholder is that the middle vee-gutter ring has been placed roughly 9 inches further downstream than is the case with the standard flameholder. Figures 40 and 41 show the modified flameholder installed in the augmentor. As can be seen by comparing Figures 36 and 40, the only difference in the modified flameholder when viewed up the tailpipe is the addition of swirler cups in the outermost vee-gutter ring. Viewed from the side as in Figure 41, however, it can readily be seen that the flame-front structure will be significantly different in the case of the modified flameholder. In particular, since the central vee-gutter ring corresponds to Zone 1, the relative positions of the flame-fronts of Zone 1 and Zones 3 and 4 (the outer ring) are completely different: with the modified flameholder Zone 1 combustion will initiate downstream rather than upstream of the initiation of combustion in Zones 3 and 4. Thus the pair of flameholders tested should indicate whether the spatial structure of the flame-front has a marked effect on any instability in the augmentor.

MODELLING THE FLAMEHOLDERS

Flameholders produce three effects which are pertinent to the instability characteristics of augmentors:

1. The flameholder flow blockage introduces an acoustical impedance between the chambers upstream and downstream of the flameholder.

2. The flameholder axial location in part determines the axial location of the flame-front.

3. The geometry of the flameholder assembly (not that of the individual vee-gutter) determines the spatial distribution of the heat release.

The second and third of these effects are, of course, physically difficult to distinguish, but the distinction is significant in the instability model.

Programs HLMHLT and REFINE contain various parameters which can depend on these effects and hence can depend on the specific flameholder assembly. However, little attention has been given to date to the question of the proper modelling of the flameholder within the overall instability model. The problem of modelling flameholders has simply been considered of minor significance compared to that of modelling the unsteady energy release. Thus the very simplified approach to the flameholder used in the previous parametric studies was continued in the current program. The two flameholder assemblies were modelled as follows:

1. Their acoustic impedance was ignored entirely because of the lack of a method for calculating values of the relevant input parameters of HLMHLT.

2. The flame-front with the standard flameholder was specified, somewhat arbitrarily, to be 3.5 inches downstream of the aerodynamic flameholder ring. With the modified flameholder it was specified to be 8.5 inches downstream. In both cases the rule followed was to locate the flame-front midway between the most upstream and downstream flameholder rings.

3. The different effects of the two flameholders on the heat release parameters (E, τ, and the unsteady combustion coefficients) were ignored.

Future investigations with the NREC instability model will undoubtedly provide far more justifiable approaches to modelling flameholders. Had the instability amplitudes and frequencies observed in the test program differed with the two flameholder assemblies, the current program might have led to more sophisticated modelling techniques, but under the circumstances no reasons for less arbitrary modelling arose.

APPENDIX III

SCREECH LINERS EXAMINED

THE LINERS TESTED

The perforated screech liner of the TF-30-P1 augmentor extends 33 inches downstream from the plane of the splitter lip (see Figure 38). The liner uses a square matrix of 0.094 inch holes spaced 0.587 inches apart; the liner is 0.048 inches thick, and the backing cavity is 0.678 inches deep.

Tests were conducted with two screech liner configurations: first, the nominal screech liner and second, with all but the downstream 12 inches of the nominal liner covered to block off the acoustic perforations. The two liner variations are pictured in Figure 42.

MODELLING THE SCREECH LINER

The combustion instability analysis represents the effects of the screech-liner via an acoustic admittance ratio for the outer boundary. The admittance ratio, which varies with both the amplitude and the frequency of the sustained oscillation, is defined by the following equations (from Reference 3):

$$\{A_a\}_{REAL} = \frac{\{Z_{REAL}\}}{\{Z_{REAL}\}^2 + \{Z_{IMAG}\}^2}$$

$$\{A_a\}_{IMAG} = \frac{-\{Z_{IMAG}\}}{\{Z_{REAL}\}^2 + \{Z_{IMAG}\}^2}$$

The method for calculating Z is then as follows:

$$Z_{REAL} = \frac{4}{\sigma \rho C_o}\sqrt{\frac{\mu \rho \omega}{2g}}\left[1 + \frac{t_a}{d_o} + 1.62\left(\frac{P'}{a}\right)^{.787}\right]$$

$$Z_{IMAG} = \frac{2\pi f_o l_{eff}}{C_o \sigma}\left(\frac{\Omega_o}{f_o} - \frac{f_o}{\Omega_o}\right)$$

where ρ is the fluid density
σ is the open area ratio
μ is the fluid viscosity
C_o is the sonic velocity
ω is the angular frequency

g is the gravitational constant
t_a is the liner thickness
d_a is the aperture diameter

$$\Omega = \omega / 2\pi$$

$$\ell_{eff} = t_a + (.85\Omega)\left[1 - .7\sigma^{1/2}\right] d_a$$

$$f_o = \frac{c_o}{2\pi}\sqrt{\frac{\sigma}{\ell\, \ell_{eff}}}$$

ℓ is the backing distance
P_a' is the RMS pressure amplitude (lbf per ft sq).

The liner in the TF-30-P1 is tuned to a frequency (f_o) of roughly 1900 Hz. Figures 43 and 44 display respectively the real and the imaginary parts of the TF-30-P1 liner admittance ratio as functions of oscillation amplitude and frequency. The real part corresponds to the damping effect of the liner.

APPENDIX IV

FUELS EXAMINED

FUELS TESTED

Current military jet engine requirements list Aviation Gasoline (AVGAS) as an emergency fuel. Therefore, since the vaporization and volatility characteristics of AVGAS are much different from those of more conventional military jet fuels, JP-4 and JP-5, an assessment was made of the resultant effects AVGAS has on the combustion stability of the augmentor. Of the two fuels examined in the test program, the primary fuel was the conventional turbine aviation fuel, Grade JP-4 per MIL-T-5624H. The alternate fuel was AVGAS, Grade 115/145 per MIL-G-5572E.

Because of its high lead content, AVGAS was introduced only into the agumentor fuel system in order to minimize hot part lead deposition. The main combustion system of the core engine was operated continuously on JP-4 throughout the test program.

The effects of AVGAS were examined during Tests 9 and 10 (the former test used the blocked screech liner, and the latter, the conventional screech liner). The highest sustained oscillation levels occurred at Z8MAX with JP-4 fuel. Because of limitations of the fuel supply pump, the fuel flow from the AVGAS tank was restricted to the point that neither the Z5 nor the Z6 condition could be produced; also, the Z8MAX condition with AVGAS did not represent maximum fuel flow, though the fuel flow rate (21,000 lbm/hr) was comparable to that with JP-4. Considerable instability activity could be audibly detected during the AVGAS tests, but the recorded signal levels were quite low.

High lead deposition on the augmentor hot parts and fuel injectors limited the duration of AVGAS testing; consequently, following each AVGAS test, 20 to 30 minutes of additional running with JP-4 fuel was conducted to clear away the bulk of the lead deposits.

During Test 10 a back-to-back AVGAS/JP-4 test was conducted at essentially the same operating conditions. Stability data were taken first with the AVGAS fuel at the highest Z8 condition possible. The augmentor was then changed to a JP-4 fuel supply, and the same Z8 condition was repeated. This provided a back-to-back comparison of the two fuels. The maximum amplitude level observed was essentially the same with either fuel in these tests (1.22 per cent with AVGAS and 1.27 per cent with JP-4), but the levels in question were so low that no salient conclusion could be drawn.

MODELLING THE FUELS IN THE INSTABILITY ANALYSIS

Two parameters in NREC's combustion instability model are directly dependent on the properties of the augmentor fuel: E, the chemical energy content of the fluid (per unit mass) entering the combustion zone; and τ, the characteristic time required for combustion of a fluid particle. Both of these parameters are treated in terms of their mean and oscillatory components in the model:

$$E = \bar{E} + E' e^{j\omega t}$$

$$\tau = \bar{\tau} + \tau' e^{j\omega t}$$

The oscillatory components are in turn functionally related to the pressure and velocity oscillations

$$E' = f_{E'}(p', \mu', \bar{E})$$

$$\tau' = f_{\tau'}(p', \mu', \bar{\tau})$$

Both the mean components and the functions defining the oscillatory components are dependent on fuel properties. These are discussed separately below.

The mean energy content of the fluid varies linearly with the net heat of combustion of the fuel and with the local mixture ratio. The difference in the heat of combustion of AVGAS and that of JP-4 was assumed to be negligible in the current study. Thus $\bar{E}$ remained the same in the JP-4 and the AVGAS solutions.

The other three model parameters (E', τ', and $\bar{\tau}$) are sensitive to the vaporization characteristics of the fuel used. They will be discussed below. First, however, it is important to recognize the differences in the vaporization properties of AVGAS and JP-4. Figure 45 shows vapor pressure versus temperature for JP-4 and AVGAS (for 10 per cent distillation). At two atmospheres, the condition of the TF-30 augmentor, the boiling temperature of AVGAS is 180 degrees F, and that of JP-4 is 260 degrees F. The distillation band of JP-4 is also much wider than that of AVGAS. Figure 46 shows the distillation bands of AVGAS and JP-4 for atmospheric conditions. The table below indicates how much wider the JP-4 distillation band is:

	AVGAS	JP-4	
10 per cent distillation	150	210	deg F
50 per cent distillation	215	300	deg F
90 per cent distillation	245	410	deg F

The fan discharge temperature in the TF-30 tests ranged from a low of 178 degrees F (cold day) to 240 degrees F (hot day); Tests 6 and 10, corresponding to the standard engine geometry, represent the principal comparison between AVGAS and JP-4, and in these the fan discharge temperature ranged from 210 to 212 degrees F. The fan stream temperature at the flameholders is, of course, somewhat higher because of heating from the turbine casing and from mixing with the turbine exhaust stream. For Tests 6 and 10, with the 210 degrees F fan discharge temperature, it was assumed that fuel from Zones 3 and 4 in the fan stream was 90 per cent vaporized at the flameholders in the case of AVGAS, and 40 per cent in the case of JP-4. In the case of the cold day tests, with a 178 degrees F fan discharge temperature, it was assumed that the JP-4 from Zones 3 and 4 was entirely in liquid form at the flameholders.

The basic parameter which relates to the volatility of the fuel is a, the fraction of the fuel remaining in droplet form at the flameholders. Assuming that the droplet motion is not influenced by oscillations in the flow, then oscillations in the energy content of the fluid at the flame-front can be defined as follows:

$$\frac{E'}{\bar{E}} = -\frac{a}{\gamma}\left(\frac{P'}{\bar{P}}\right) - \frac{1-a}{2}\left(\frac{\mu_2'}{\mu_2} + \frac{1}{\gamma}\frac{P'}{\bar{P}}\right)_{INJECTOR}$$

The first term represents fluctuations in fuel-air ratio which result from air density fluctuations. The second term reflects the dependence of droplet vaporization rate on the local Reynolds number raised to the one-half power (vaporization is assumed to occur instantaneously at the fuel injectors).

The time required for combustion in an augmentor is assumed to result from the characteristic times of the mechanisms controlling the combustion process. In general, the processes controlling the rate of combustion include turbulent mixing, droplet burning, and chemical kinetics. Assuming these processes occur essentially in series, the over-all combustion characteristic time is as follows:

$$\tau = \tau_T + \tau_E + \tau_c$$

where τ_T = characteristic time of turbulent mixing
τ_E = characteristic time for evaporation of burning fuel spray
τ_c = characteristic time for chemical reaction.

When the fuel is partially evaporated, with a fraction a in liquid droplet form, the pre-evaporated fuel will miss the evaporation step in the above process. Thus, a properly weighted characteristic time of combustion is defined as follows:

$$\tau = \tau_T + a\,\tau_e + \tau_c$$

where τ_e = droplet evaporation characteristic time
a = fraction of fuel in liquid form at the flame-front.

These four parameters (τ_T , a, τ_e , and τ_c) can vary with the different properties of the fuel. In the current study, however, it was assumed that τ_T , τ_e , and τ_c do not change when AVGAS is used instead of JP-4. Thus, only a changes, and the specific values, as described above, are 0.1 for AVGAS, 0.6 for JP-4 on a hot day, and 1.0 for JP-4 on a cold day in the Zone 3 and 4 fan stream; in the core stream and in Zone 2 the value of a assumed in all tests was 0.0.

APPENDIX V

AUGMENTOR OPERATING CONDITIONS: FUEL ZONE COMBINATIONS

FUEL ZONE COMBINATIONS TESTED

The stability testing conducted on the TF-30 augmentor during the course of this program followed a specific test plan. A matrix of test conditions was defined for each augmentor test configuration to be examined. Common to nearly all tests was a sequence of afterburner fuel distribution schedules based on the five (5) zones of fuel injection within the afterburner or on combinations thereof. The fuel distribution schedules were identified as follows:

Z0	Max Military Power, Nonafterburning
Z4	Fuel zones 1, 2, 3, and 4 on
Z5	Fuel zones 1, 2, 3, 4, and 5 on (Max Afterburning)
Z6	Fuel zones 1, 3, 4, and 5 only (zone 2 off)
Z7	Fuel zones 1 and 3 only (zone 2 off)
Z8MIN	Fuel zones 1, 3, and 4 only with min fuel flow to zone 4
Z8MAX	Fuel zones 1, 3, and 4 only with max fuel flow to zone 4 (zone 2 and 5 off)

An example of this fuel distribution matrix can be illustrated by observing the conditions of Test 6. This test required an examination of a conventional TF-30 augmentor (standard screech liner, standard flameholder assembly, no inlet distortion and fueled with JP-4). The fuel distribution matrix for this test was as follows:

Run	Condition	Procedure
#1	Z0	Trim the engine to the maximum military power setting in accordance with the TF-30-P1 engine Technical Order; allow five minutes for thermal and performance stability; record all steady-state and dynamic operating and performance parameters
#2	Z4	Advance throttle to position providing fuel zones 1, 2, 3, and 4. Zone 5 is to remain off; allow five minutes for stabilization; record all steady-state and dynamic operating and performance parameters

Run	Condition	Procedure
#3	Z5	Advance throttle to full afterburning--zones 1, 2, 3, 4, and 5 on. Allow for stabilization and make full recording as described above
#4	Z6	Same as Run #3 except zone 2 fuel is cut-off
#5	Z7	Same as Run #3 except only fuel zones 1 and 3 are on
#6	Z8MIN	With fuel zone 2 cut-off, advance throttle to position providing minimum fuel flow to zone 4 (i.e., zones 1, 3, and min 4 on). Repeat stabilization and recording procedure
#7	Z8MAX	Same as Run #6 except throttle is positioned to provide maximum fuel flow to zone 4 as allowed by afterburner fuel control schedule, zone 5 off

Because continuous afterburning imposed a high heat load to much of the internal hardware (i.e., flameholders, nozzle flaps, etc.), a cool-down period was often allowed between runs. Afterburner titanium case temperatures were never allowed to progress above 150 degrees F as monitored by skin thermocouples.

It was noted that during those runs when intermediate fuel zones were cut-off (i.e., zone 2 at Z8MAX condition), the afterburner fuel control would automatically adjust fuel schedules permitting greater fuel flows in the operating zones. This occasionally resulted in apparent improved thermodynamics within the afterburner; i.e., during one such test an intermediate fuel zone was cut-off, a fuel shift occurred in the remaining zones, and although total fuel flow had been reduced, engine thrust achieved approximately the same level as existed with the intermediate zone on.

The basic fuel distribution schedule described herein was used for each afterburner configuration tested. The matrix was altered only during the AVGAS testing due to supply tank fuel pump flow limitations. During the AVGAS tests (9 and 10), the highest possible fuel flow permitted testing only to Z8. Maximum afterburning could not be examined.

ANALYTICAL MODELS OF THE FUEL ZONE COMBINATIONS

Three variables in the combustion instability analysis depend explicitly on the amount and the distribution of the fuel: the mean sonic velocity in the combustion chamber, the distribution of the through-flow velocity downstream of the flame-front, and the magnitude and distribution of the energy content of the fluid (E) entering the combustion zone. The assumptions made in

calculating values for these variables in the study of the TF-30-P1 augmentor are discussed below, and the specific input values are summarized.

As mentioned above, cutting-off intermediate fuel zones caused a redistribution of fuel in the operating zones because of an automatic fuel schedule adjustment made by the augmentor fuel control system. The total fuel flow observed in different tests during operation with different combinations of fuel zones is shown in Table XV. This table indicates that a simple deduction of the amount of fuel supplied in each zone individually is not possible: for example, the total ab fuel flow is greater with Zone 2 off than with Zone 2 on, but this, of course, does not entail that the Zone 2 fuel flow rate is negative. Fuel manifold pressures for each zone were recorded throughout the test program, and these were used to estimate the amount of fuel in each zone.

Table XVI shows the specific fuel split assumed in the analyses. The same fuel splits were assumed regardless of the fuel used on the engine geometry being analyzed. The total fuel flow for each zone combination, as shown in Table XVI, is accordingly a representative value from Table XV. Using representative values of total fuel flow in the analyses rather than changing the total fuel flow when, for example, studying the modified flameholder not only reduced the computational effort involved, but more importantly was considered to be more instructive.

The fuel flow in the individual zones mixes with different air streams. The analyses assumed that all of the Zones 1 and 5 fuel mixed with the turbine discharge stream, while Zones 2, 3, and 4 mix with the fan stream. Zone 2 fuel, which is pre-mixed with compressor discharge air, was assumed to be entirely pre-vaporized prior to injection into the fan stream.

CALCULATION OF SONIC VELOCITIES

Two assumptions were made in arriving at values of sonic velocity in the combustion chamber:

1. The average value of sonic velocity throughout the combustion chamber corresponds to 80 per cent of the total temperature rise produced by combustion.

2. In the case of the cylindrical afterburner model, the average sonic velocity corresponds to the numerical average of the average sonic velocity in the fan stream and that in the core stream.

Upstream of the flame-front a sonic velocity of 1600 ft/sec was assumed in the cylindrical afterburner solutions, and a value of 1260 ft/sec was assumed in the annular ductburner solutions. The sonic velocities and nozzle total temperatures (100 per cent of ΔT) in the combustion chamber for various zone combinations are summarized in Table XVII.

THROUGH-FLOW VELOCITY DISTRIBUTIONS

The combustion instability analysis, as presently constituted, recognizes only the axial component of the through-flow velocity. Thus the very complicated velocity distribution in the mixed-flow augmentor was simplified in the present study. Specifically, it was assumed that the fan and core streams could be evaluated one-dimensionally separately (no mixing across streams), but that the inner radius of the fan stream varied so that the static pressure in the two streams remains the same. Then, in calculating the through-flow velocity for the afterburner analyses, the fan and core stream values were averaged.

The one-dimensional analysis of each stream assumed constant area heating (Table B.4 of Reference 6) in two steps: the first involving 80 per cent of the temperature rise, and the second the remaining 20 per cent. An isentropic flow analysis was made before and after the second step of heating to determine the value of the radius between fan and core streams for which the static pressures would be the same. In calculating the rapid velocity rise across the flameholders, it was further assumed that the velocities corresponding to 80 per cent of the temperature rise occur at a distance of 15 inches downstream of the flame-front plane.

The input values of through-flow velocity distribution used in the afterburner analyses are shown in Figure 47, and those in the ductburner analyses are shown in Figure 48. The mean convection velocity, governing combustion, was assumed to be the value 15 inches downstream of the flame-front.

ENERGY CONTENT DISTRIBUTION

The dynamics of the fuel mixing upstream of the flame-front are quite complicated. In the combustion instability analyses estimates were made of the radial variation of the fuel-to-air ratio for the various fuel zone combinations. These estimates, based on Table XVI, assumed radial diffusion except across the (fictional) interface between the fan and core streams: all of Zones 1 and 5 fuel were confined to the core stream, and all of Zones 2, 3, and 4 were confined to the fan stream. Once the fuel-to-air ratios in each stream were stipulated, values of $\bar{E}$ (energy content of fluid per unit mass) as a function of radius were determined from the following equation:

$$\bar{E} = q_c \left[\frac{\dot{m}_f}{\dot{m}_f + \dot{m}_a} \right]$$

where q_c is the net heat of combustion of fuel, and the bracketed mixture ratio term varies radially (essentially from zone to zone). Plots of $\bar{E}$ versus radius (with $\bar{E}$ in units of sonic velocity squared) are shown in Figure 57 for each of the six fuel zone combinations examined in the study. The "dividing line" between the fan and core streams is at 70 per cent of the outer radius. The fan stream fuel distribution, by itself, was used in the ductburner solutions.

APPENDIX VI

INSTRUMENTATION

The main objective of the test program was to investigate the combustion stability characteristics of the augmentor using conventional high response pressure instrumentation. The main engine was also instrumented with steady-state pressure and temperature instrumentation to permit a continuous evaluation of basic engine performance throughout the test program. Much of the steady-state instrumentation was required to define the flow field conditions (both fan and core streams) entering the augmentor.

STEADY-STATE INSTRUMENTATION

Figure 50 illustrates the approximate axial and circumferential locations of all steady-state instrumentation installed on the test engine. Chromal-alumel thermocouples were installed in the bellmouth inlet screen to monitor inlet air temperature to the engine and to detect exhaust recirculation, a test cell problem described in Chapter III. Chromal-alumel thermocouples were also employed in all downstream temperature rakes and probes, the outputs of which were recorded by the NLS data acquisition system. All pressures (both static and total) were sensed with C.E.C. pressure transducers and recorded by the NLS system. In addition to this basic flow path instrumentation, several on-board engine sense points were monitored, such as interspool pressure (PS3), compressor discharge pressure (PS4), combustor exit temperature[1] (TT5) and afterburner fuel zone manifold pressures. Fuel flow to the main engine and the augmentor were monitored independently using turbine-type flow meters.

The engine test stand was a floating, parallel rail thrust stand equipped with dual 20,000 pound load cells. The basic stand is designed for engines employing parallel thrust support mounts; however, the TF-30 mounting system, as required by the airframe, is one-side only resulting in a nonparallel loading of the thrust cells. Although thrust was not a critical parameter during this test program, the stand was calibrated prior to test initiation to permit approximate thrust monitoring. General thrust levels were consistent with engine specifications at most operating points.

DYNAMIC INSTRUMENTATION

The dynamic instrumentation consisted of eight high response pressure transducers, four at each of two axial locations on the augmentor case--

---

[1] Combustor exit temperature on the TF-30-P1 is determined indirectly as a function of turbine discharge temperature, compressor discharge temperature and engine inlet temperature as measured by on-board thermocouples.

flameholder plane and screech liner exit plane. Figure 50 illustrates the circumferential location of the instrumentation. Kistler Model 603L, acceleration compensated transducers where used. Each transducer was installed in a special water cooled housing; however, early in the test program a water cooling requirement for the transducer was eliminated when it was found that maximum case temperatures at full afterburning never exceeded 150 degrees F. This was within the thermal limits of the transducers.

A first resonance analysis of the sensing tube to the transducer was made prior to its installation in the afterburner. The first resonant frequency of the sense tube was found to be two times higher than the highest frequency of interest (5000 Hz) and was considered acceptable for the purposes of this program.

As illustrated in Figure 50, eight Kistler transducers were installed at the augmentor case locations identified. Two of the eight transducers, one at each axial station, were capped in order to monitor vibration and background noise levels at each station. The transducer sensing tubes were mounted in a sliding sleeve plate attached to the inner afterburner cooling/screech liner permitting lateral movement resulting from normal vibration and thermal growth during augmentor operation.

High temperature Microdot cabling was used to connect the transducers to the Kistler Model 504A charge amplifiers (see Figure 32). Since small movements in the Microdot cabling can cause a signal shift, care was taken to secure firmly the cabling to structural members of the engine and stand, thus minimizing such movements. Unfortunately, the charge amplifiers had to be located as near the engine as possible to minimize Microdot cable length. As a result, the charge amplifiers were continuously subjected to intense noise and stand vibration during augmentor operation. The charge amplifiers were mounted in a specially insulated, thermally controlled, and shock-mounted case to minimize amplifier performance deterioration and damage. The severe environment, however, still caused an average of two amplifier failures out of the eight used during each augmentor test. Consequently, a full calibration of all dynamic instrumentation was conducted before and after each test. If the pretest calibration of the amplifiers shifted, a retest was accomplished.

The output signals from the charge amplifiers were transmitted via coax cable to DANA Model 2000 DC amplifiers to provide a more accurate control of the low charge amplifier output signal and to insure signal compatibility with the AMPEX FR 1300 Analog Recorder. A schematic of the analog circuitry as described herein is given in Figure 51. An oscilloscope was used with each analog signal to monitor amplitude levels and permit appropriate gain adjustments prior to recording on the AMPEX Recorder. In addition, 5000 Hz Kistler Filters Model 544A5 were used between the charge and DANA amplifiers to eliminate all signal activity above the frequency of interest.

The AMPEX FR 1300 Analog Recorder identified above was a 14 channel FM system permitting both record and play-back of the high response pressure

signals. Consequently, the same system could be used for recording each test and later reducing the data through the spectrum analysis equipment described in Appendix VII.

HIGH SPEED PHOTOGRAPHY

A Fastax camera was installed in the exhaust ejector of the test cell to record instabilities in the augmentor. The camera can be seen clearly in Figure 35. The high speed film obtained displayed the tangential characteristics of the 400 Hz oscillation.

APPENDIX VII

DATA REDUCTION

During the course of this program two basic data acquisition systems were used to record steady-state and high response performance information at each test condition. The input instrumentation used with these recording systems is described in Appendix VI.

STEADY-STATE INFORMATION

The millivolt output signals from the steady-state pressure and temperature sensors on the engine were recorded on a Non-Linear Systems (NLS) Data Acquisition System. The NLS system is a medium speed continuous scanning recorder capable of recording up to a rate of 15 channels per second. For this test a total of 54 channels of test data were recorded on each scan. Between recordings, continuous single channel monitoring was used to note signal drift and instrument response time during engine power level changes. The allowable input voltage range to the recorder was ± 10 millivolts to ± 10 volts permitting the use of conventional nonamplified pressure and temperature instrumentation. When required, gain changes internal to the recorder could be made to improve readout quality and accuracy. To assure recording accuracy on the magnetic tape system, a fixed input nal of +1.57 volts was used throughout the program for first channel identification. The data tape was processed with a special reduction program using a CDC 6600 computer converting the recorded information to engineering units.

Occasionally, the cross-bar scanner of the recorder would fail to register the first channel, resulting in a record error. To preclude the possibility of losing a complete data run, the more important steady-state parameters were displayed on the engine operator's control panel. These parameters were hand recorded during each run. However, the automatic recorder, when functioning properly, provided more accurate information because of its instant response capability.

DYNAMIC INFORMATION

The high response pressure information from the Kistler Transducers was recorded, following signal amplification and conditioning, on a 14 track AMPEX FR 1300 Analog Recorder. The tape was then reduced to a graphic presentation of pressure oscillation amplitude in volts (RMS) versus oscillation frequency. The frequency range of interest was 5 Hz to 5000 Hz. The following equipment was used to reduce the analog tape information to the plotted information described above:

To assess the significance of an analog signal prior to initiating a full reduction, an occassional oscillograph recording was made from selected channels of a particular run. If the oscillation characteristics appeared significant, then a full spectral analysis was conducted.

3. Spectral Dynamics Corporation SD112-1 Voltmeter/Frequency Log Converter.

4. Hewlett-Packard 7000A X-Y Recorder.

5. AMPEX Bin Loop Recorder (FB-400).

The analog reduction system layout is illustrated in Figure 52. The following important settings were made to the spectral analysis equipment prior to initiating an analog data plot to insure an optimum analysis of the recorded signals:

1. Filter Select Switch on the SD101B: In all cases, the band pass filter had a bandwidth of 5Hz.

2. AC Response Switch on the SD112-1: This switch was placed in the slow response position (8 db/sec nominal) to give a more readable plot by eliminating much of the small but rapid oscillations of the plotter pen and to minimize pen overshoot.

3. Sweep Speed on SD104A-5: A sweep speed of 0.5 decade/minute was used. This was considered slow enough to identify all amplitude peaks; however, the sweep speed was decreased by a factor of 10 in the immediate vicinity of those points of greatest interest to provide more accuracy and to minimize pen undershoot.

OSCILLOGRAPH REDUCTION

To assess the significance of an analog signal prior to initiating a full reduction using the equipment described in 2. above, an occassional oscillograph recording was made from selected channels of a particular run. If the oscillation characteristics appeared significant, then a full spectral analysis was conducted.

APPENDIX VIII

A SUMMARY OF THE COMBUSTION INSTABILITY MODEL

NREC's instability model has been described in various detail in References 1 through 4. This appendix presents a skeletal summary of the principal equations and their solutions. The reasons for constructing the model in the way we did are best found in Reference 4, and systematic derivations are in References 1 and 2.

THE BASIC MODEL

Combustion instability is a self-excited acoustic resonance. The general governing equation is therefore a variant of the standard wave equation:

$$\nabla \cdot \frac{C_o^2}{R_o^2} \nabla \eta + \omega^2 \eta = h\left(\underline{x}, \eta, \omega\right) \qquad \text{(VIII-1)}$$

where C_o is the sonic velocity, R_o is the outer radius, ω is the angular velocity of the oscillation, and η is a nondimensionalized pressure oscillation:

$$\eta = p' / \bar{P} \qquad \text{(VIII-2)}$$

where

$$P = \bar{P} + p' e^{-j\omega t} \qquad \text{(VIII-3)}$$

For simplicity it is assumed that the only significant variation in sonic velocity in an augmentor can be approximated as a step-change at a flame-front. In other words, the augmentor is assumed to be separated axially into two chambers, in each of which the sonic velocity remains uniform. The general governing equation can then be put in a more manageable form:

$$\nabla^2 \eta_i + k_i^2 \eta_i = \frac{R_o^2}{C_{oi}^2} h\left(\underline{x}_i, \eta_i, k_i\right) \qquad \text{(VIII-4)}$$

where the subscript i designates the augmentor chamber, and k_i is a nondimensional wave number:

$$k_i = \frac{R_o \omega}{C_{oi}} \qquad \text{(VIII-5)}$$

The eigenvalue problem is completed by appropriate boundary equations. At the upstream and downstream ends, respectively:

$$\frac{1}{\eta}\frac{\partial \eta}{\partial z} = -j k_1 \left(A_o - \frac{M_o}{k_1^2}\frac{1}{\eta}\frac{\partial^2 \eta}{\partial z^2} \right)$$

$$\frac{1}{\eta}\frac{\partial \eta}{\partial z} = j k_2 \left(A_\ell + \frac{M_\ell}{k_2^2}\frac{1}{\eta}\frac{\partial^2 \eta}{\partial z^2} \right) \qquad \text{(VIII-6)}$$

where A is the acoustic admittance ratio, M is the Mach number, and o and ℓ correspond to the upstream and nozzle ends, respectively. At the outer and inner walls of the annulus, respectively:

$$\frac{1}{\eta}\frac{\partial \eta}{\partial r} = j k_i A_{a_i}$$

$$\frac{1}{\eta}\frac{\partial \eta}{\partial r} = -j k_i A_{b_i} \qquad \text{(VIII-7)}$$

where the subscripts a and b pertain to the outer and inner boundaries. In the case of a cylindrical afterburner, there is no inner boundary.

Finally, the function h in the general governing equation treats unsteady heat release, through-flow, and unusual boundary effects. Formally, the function is defined as follows:

$$h(\underline{x}, \eta, \omega) = j\frac{(\gamma-1)}{\bar{p}}\omega \mu \dot{w}_c'(\underline{x}_2, \eta_2, \omega) - \cdots$$

$$-\sum_{i=1}^{2}\frac{j\omega}{R_o}\mathcal{U}'(\underline{x}_i, \eta_i, \omega) + \qquad \text{(VIII-8)}$$

$$+\sum_{i=1}^{2}\frac{c_{o_i}^2}{R_o^2}\mathcal{B}'(\underline{x}_i, \eta_i, \omega)$$

where $\mu\dot{w}_c'$ is the oscillatory component of the local heat release rate per unit volume, and the functions $\mathcal{B}'$ and $\mathcal{U}'$ pertain to boundary and through-flow effects, respectively.

Equations VIII-4 through VIII-8 define a complex-valued eigenvalue problem in terms of ω, with eigenfunctions or mode shapes η defining the distribution of the pressure wave in the augmentor.

FORMAL SOLUTION OF THE MODEL

NREC uses a perturbation method to develop a first order approximation to the eigenvalue ω. Consider first the standard acoustics problem ($h = 0$) with the same boundary equations:

$$\nabla^2 \eta_i^\circ + (k_i^\circ)^2 \eta_i^\circ = 0 \qquad \text{(VIII-9)}$$

The solution of this problem by separation of variables is straightforward, so that the acoustic eigenvalue ω° and the normalized acoustic mode shape η° can be determined explicitly. Normalization here entails:

$$\sum_{i=1}^{2} \iiint \hat{\eta}_i^\circ \eta_i^\circ \, dV_i = 0 \qquad \text{(VIII-10)}$$

where $\hat{}$ indicates complex conjugation. Substitution of the acoustics solution into the right-hand side of the governing equation then produces a non-homogeneous wave equation in terms of ω' and η':

$$\nabla^2 \eta_i' + (k_i')^2 \eta_i' = \frac{R_o^2}{C_{o_i}^2} h\left(\underline{x}_i, \eta_i^\circ, k_i^\circ\right) \qquad \text{(VIII-11)}$$

The equation is readily solvable by Green's function techniques. In particular

$$(\omega')^2 = (\omega^\circ)^2 + \sum_{i=1}^{2} \iiint \hat{\eta}_i^\circ h\left(\underline{x}_i, \eta_i^\circ, k_i^\circ\right) dV_i \qquad \text{(VIII-12)}$$

NREC accepts ω' as an adequate approximation of the eigenvalue ω.

The real part of ω defines a frequency of oscillation and the imaginary part, a logarithmic decrement:

$$f = \text{REAL}\{\omega\} / 2\pi \qquad \text{(VIII-13)}$$

$$\delta = -2\pi \cdot \text{IMAG}\{\omega\} / \text{REAL}\{\omega\} \qquad \text{(VIII-14)}$$

Distinct values are determined for each mode-- i.e., for each eigenvalue ω.

The eigenvalue ω of each mode suffices to determine an oscillation frequency and decrement. The function h, however, and some of the

boundary admittances vary nonlinearly with the fluid oscillation amplitude. Thus, by assuming different values of amplitude, one can obtain a sequence of solutions for frequency and decrement, as plotted in the sketch. In the example shown the decrement is positive for small amplitudes, so that the mode in question is damped until an initial disturbance component in excess of the indicated threshold occurs. Once the threshold is exceeded, the oscillations grow (the decrement is negative) until equilibrium is reached at the self-sustaining amplitude, corresponding to which is a distinct frequency. When the decrement never becomes negative, the mode is simply stable.

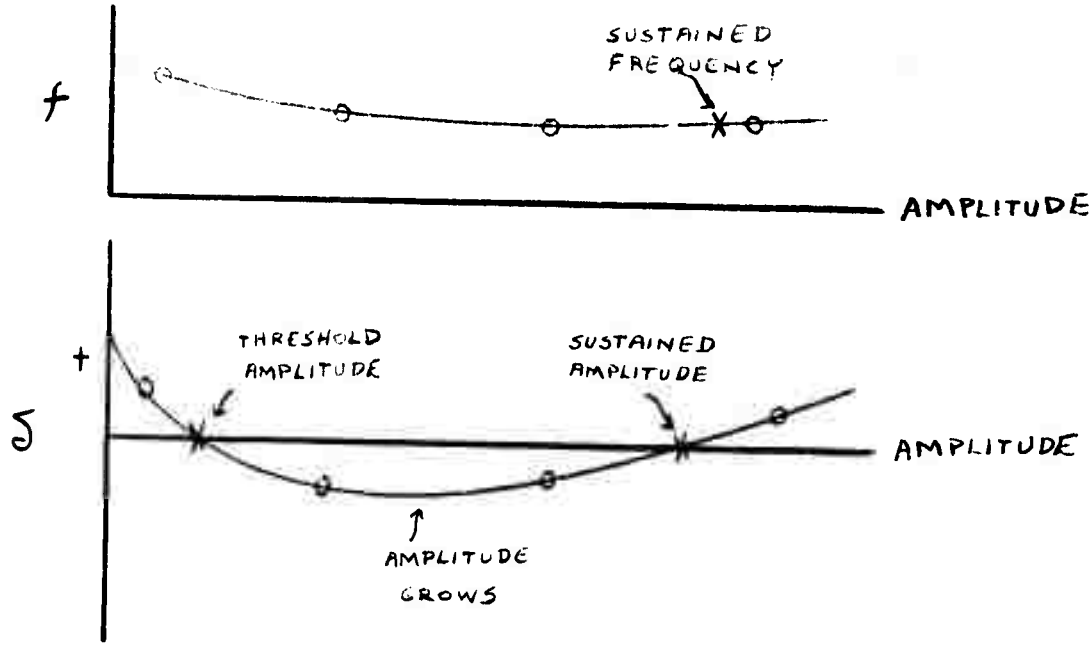

The ultimate solution of the combustion instability model, then, is the graphically determined threshold and self-sustained amplitudes and frequencies of each mode.

THE HEAT RELEASE MODEL

The local heat release rate is assumed to consist of a mean and of an oscillatory component:

$$\dot{w}_c(\underline{x}) = \bar{\dot{w}}_c(\underline{x}) + \dot{w}_c'(\underline{x})e^{-j\omega t} \qquad \text{(VIII-15)}$$

NREC's major contribution is to construct a model of the heat release rate in terms of physically interpretable variables, which can hence be examined experimentally.

The central assumption in the heat release analysis is that the local energy release occurs at a rate proportional to the local concentration of unburned fuel. It is also assumed that the mean combustion is governed by a single characteristic rate (or, inversely, a

characteristic time), which may however be sensitive to fluctuations in thermodynamic properties. This phenomenological approach leads to an intuitively satisfying expression for the local value of the mean volumetric heat release rate:

$$\bar{\omega}_c = \frac{\bar{\rho}\,\bar{E}(r,\theta)}{\bar{\tau}} \exp\left(-R_o z_2/\bar{u}_c\bar{\tau}\right) \qquad \text{(VIII-16)}$$

where $\bar{\rho}$ is the mean fluid density, $\bar{u}_c$ is the mean axial convection velocity, $\bar{\tau}$ is the mean characteristic time required for combustion of a fluid particle, and $\bar{E}$ is the mean chemical energy content per unit mass of the fluid entering the combustion chamber. The spatial distribution of the fuel is accounted for by radial and circumferential variations of $\bar{E}$.

The oscillatory heat release rate is then defined in terms of the mean heat release rate via a perturbation of Equation VIII-16:

$$\begin{aligned}\frac{\omega_c'}{\bar{\omega}_c}(r,\theta,z_2,t) = {} & \frac{\rho'}{\bar{\rho}}(r,\theta,z_2,t) - \\ & - \frac{\tau'}{\bar{\tau}}(r,\theta,z_2,t) + \\ & + \frac{E'}{\bar{E}}\left(r,\theta,0,t-\frac{R_o z_2}{\bar{u}_c}\right) + \\ & + \int_0^{z_2} \frac{\tau'}{\bar{\tau}}\left(r,\theta,\xi,t-\frac{R_o z_2}{\bar{u}_c}+\frac{R_o\xi}{\bar{u}_c}\right)\frac{R_o\,d\xi}{\bar{u}_c\bar{\tau}} + \\ & + \int_0^{z_2} \frac{u_c'}{\bar{u}_c}\left(r,\theta,\xi,t-\frac{R_o z_2}{\bar{u}_c}+\frac{R_o\xi}{\bar{u}_c}\right)\frac{R_o\,d\xi}{\bar{u}_c\bar{\tau}}\end{aligned} \qquad \text{(VIII-17)}$$

The key attribute of the model is its accounting for the cumulative effects of oscillatory combustion upstream of each point of interest. Also, the quantity of ultimate concern, ω_c', depends on the spatial distribution of the mean heat release rate, $\bar{\omega}_c$.

COUPLING MECHANISM MODELS

The two variables $\bar{E}$ and $\bar{\tau}$ are physically interpretable, but assigning values to them for a specific augmentor is not a simple theoretical exercise. It is recognized that pressure and velocity fluctuations affect $\bar{E}$ and $\bar{\tau}$, so that what is needed to complete the combustion instability model are functions of the following form:

$$\frac{\tau'}{\bar{\tau}} = f_{\tau'}\left(\frac{p'}{\bar{p}}, \frac{\mu'}{\bar{\mu}}\right) \qquad \text{(VIII-18)}$$

$$\bar{\tau} = f_{\bar{\tau}}\left(\frac{p'}{\bar{p}}, \frac{\mu'}{\bar{\mu}}, \bar{p}, \bar{\mu}\right) \qquad \text{(VIII-19)}$$

$$\frac{E'}{\bar{E}} = f_{E'}\left(\frac{p'}{\bar{p}}, \frac{\mu'}{\bar{\mu}}\right) \qquad \text{(VIII-20)}$$

The physical mechanisms thought to govern these functions in augmentors are turbulent mixing, chemical kinetics, and droplet atomization, vaporiation, and burning. The effects of such mechanisms on τ and E must be defined via appropriate experiments. The above functions are not considered amenable to a purely theoretical treatment.

To generate solutions from NREC's model, some specification is needed of the above coupling mechanism functions. Without an experimental program, any such choice must be crude. NREC's programs have been constructed with provision for the following functional forms:

$$\frac{E'}{\bar{E}} = \tilde{C}_3 \frac{p'}{\bar{p}} + \tilde{C}_4 \left(\frac{p'}{\bar{p}}\right)_{INJECTOR} + \tilde{C}_5 \left(\frac{\mu'}{\bar{\mu}}\right)_{INJECTOR} \qquad \text{(VIII-21)}$$

$$\bar{\tau} = \tilde{C}_7 \tau_d \qquad \text{(VIII-22)}$$

$$\frac{\tau'}{\bar{\tau}} = \tilde{C}_1 \frac{p'}{\bar{p}} + \tilde{C}_6 \left(\frac{\mu_3'}{\bar{\mu}_3}\right)_{FLAMEHOLDER} \qquad \text{(VIII-23)}$$

where τ_d is the "design" characteristic time, in the absence of fluid oscillations.

As discussed in detail in Chapters IV and V of the report, a very simple model of droplet vaporization was used to assign values to $\tilde{C}_1$, $\tilde{C}_3$, $\tilde{C}_4$, $\tilde{C}_5$, and $\tilde{C}_7$ (see, for example, Equations 3 through 7 of Chapter IV). In an effort to predict sustained amplitude levels, a numerical definition of $\tilde{C}_6$ was also devised, with an interpretation of the values stated in terms of turbulent mixing. Developing correct functions (or coefficients) for the coupling mechanisms remains a task for the future. What light has been cast on the problem in the current study's comparisons of predicted and observed instabilities is examined in the main text.

APPENDIX IX

MODIFICATIONS OF PROGRAMS HLMHLT AND REFINE

Several modifications of the previously developed computer programs were made during the current effort. Five of these represent corrections of errors, and the remainder provide either ease of use or more accurate modelling. The changes are described below, and updated Fortran listings are given in Appendix X.

PROGRAM HLMHLT

1. CYFUN: Calculation of the derivative of the Bessel function of the second kind (Y) was erroneous in the original program. Two cards have been modified:

   a. Statement defining FNP just before Statement 100.

   b. Statement defining FNP just before Statement 600.

   Only ductburner results are affected by the change.

2. AXFUN: An error in AXFUN was discovered, again in a derivative formula, which had the effect of preventing convergence in some Newton-Raphson iterations. Both of the definitions of F2P are correctly functions of Q2, not of G2 as in the original program.

3. HLMHLT: Statements from 6600 to 6800 have been added to provide the additional print-out of the correct value of the Chamber 2 mode shape coefficient. In the original program this coefficient was hand calculated, using the chamber-to-chamber amplification coefficient. The new output coefficient is defined by the following product:

$$\frac{C'_{\beta_2,L,K}}{C_{\beta_1,L,K}} = \left(\frac{C'_{\beta_1,L,K}}{C_{\beta_2,L,K}}\right)\cdot\left(\frac{C_{\beta_2,L,K}}{C_{\beta_1,L,K}}\right)$$

   Thus when $C_{\beta_1,L,K} = 1.0$, as is standard in most cases, all input data required by REFINE is now defined by HLMHLT.

4. HLMHLT: The sign of the radial mode shape coefficient, CIQ, was wrong in the original program. The card shortly before Statement 6050 has been corrected accordingly. Equation I-30 of Reference 2 should also be corrected to read:

$$\frac{C'_{r_{i,l,k}}}{C_{r_{i,l,k}}} = - \frac{J_m(\alpha_{i,l,k}, \bar{A}_{a\,i,l,k})}{Y_m(\alpha_{i,l,k}, \bar{A}_{a\,i,l,k})}$$

This error affects only the annular ductburner results.

PROGRAM REFINE

1. The major change is to input the radial component of $\bar{E}$ not as a parabola, but as a table of values at the end of the complete REFINE input. The table is input as follows:

Line	Location	Type	Input Item	Description
16	1-6	I	NMUQ	Number of entries in input table: $2 \leq NMUQ \leq 21$
17	1-12	R	RMUQ(1)	The smallest value of $r = R/R_0$ at which $\bar{E}$ has a non-zero value
	13-24	R	XMUQ(1)	The value of μ_q at RMUQ(1)
	25-36	R	RMUQ(1)	
	37-48	R	XMUQ(1)	

etc., until all input values are accounted for. The values of $\bar{E}_r$ are then calculated as follows:

$$\bar{E}_r = \mu_q(r) \cdot (\mu_1 r^2 + \mu_2 r + \mu_3)$$

where $\mu_q(r)$ is defined by linear interpolation in the table. This addition to REFINE permits a far more accurate representation of the radial distribution of the fuel than in the original program.

Three subroutines were modified in effectuating this change:

a. REFINE:

(1) a new COMMON block, /MUQ/, was added

(2) new I/O cards were introduced shortly after Statement 500

b. FUNGEN:

(1) a new COMMON block, /MUQ/, was added

(2) Statement 230 was replaced as follows:

```
230 CONTINUE

    CALL INTERP (R, Q)
```

c. INTERP: A new subroutine was added to the program for linearly interpolating in the μ_1 input table.

2. A second change, made in REFINE, was to restrict the optimal dump output of the various functions so that it will include only the axial mode shape. This restricted form of the dump output is obtained only when KDUMP=2; when KDUMP=0, no dump output occurs, and when KDUMP=1, all dump output occurs. Six cards have been added to the REFINE source deck, and another card has been modified, as follows:

```
      L1=1

      L2=28

      IF (KDUMP .NE. 2) GO TO 1195

      L1=13

      L2=14

1195  CONTINUE

      DO 1200 L=L1, L2                                (modified)
```

3. A third change eliminates the need to repeat mode shape input when only the assumed amplitude level is changing. When KONTRL $\geq$ 21, the program requires only two lines of input as follows:

Line	
3	Same as Line 7 when KONTRL $\leq$ 20
4	Same as Line 8 when KONTRL $\leq$ 20

The formats remain the same as on pages 70 and 71 of Reference 3. The change is accomplished by by-passing the two mode shape input statements, just before Statements 380 and 410, respectively.

4. QYFUN: Three cards immediately preceding Statement 100 have been corrected. The original program calculated an erroneous radial distribution of the mode shape in the case of annular ductburners. With these corrections the radial component of the mode shape satisfies the boundary conditions properly.

5. FUNGEN and NTGRAT: The correct equation for the unsteady heat release rate is given below (see Ref 4, Equation 20):

$$\frac{\mu r_c'}{\mu \bar{r}_c}(r,\theta,z_2,t) = \frac{\rho'}{\bar{\rho}}(r,\theta,z_2,t) -$$

$$- \frac{T'}{\bar{T}}(r,\theta,z_2,t) +$$

$$+ \frac{E'}{\bar{E}}\left(r,\theta,0,t-\frac{R_0 z_2}{\bar{\mu}_c}\right) +$$

$$+ \int_0^{z_2} \frac{T'}{\bar{T}}\left(r,\theta,\xi,t-\frac{R_0 z_2}{\bar{\mu}_c}+\frac{R_0\xi}{\bar{\mu}_c}\right)\frac{R_0 d\xi}{\bar{\mu}_c \bar{T}} +$$

$$+ \int_0^{z_2} \frac{\mu_c'}{\bar{\mu}_c}\left(r,\theta,\xi,t-\frac{R_0 z^2}{\bar{\mu}_c}+\frac{R_0\xi}{\bar{\mu}_c}\right)\frac{R_0 d\xi}{\bar{\mu}_c \bar{T}}$$

In the original program the $E'/\bar{E}$ term was treated erroneously as a local value rather than as a convected value. That is, the program used

$$\frac{E'}{E}(r,\theta,z,t)$$

rather than

$$\frac{E'}{\bar{E}}\left(r,\theta,0,t-\frac{R_0 z_2}{\bar{\mu}_c}\right)$$

This error has been corrected by changing the following cards:

a. In FUNGEN, just after Statement 310, the cards defining H3F(J), HEFP(J), HEPP(J), have been modified to account for a convected effect of E' at the flame-front.

b. In NTGRAT, before Statement 300, the cards defining OMEG2E have been revised to eliminate reference to QNHRF (now clearly incorporated in the above functions).

This correction appears to have only a minor effect on results. Specifically, it mostly changes the phase relation between E' and $\mu r_c'$ at every point downstream of the flame-front.

APPENDIX X

COMPUTER PROGRAM LISTING

```
ON 2.3 --PSR LEVEL 298--

      PROGRAM HLMHLT(INPUT,OUTPUT,TAPE5=INPUT,TAPE6=OUTPUT)
      COMPLEX QAO,QAL,QAA(2),QAB(2),QQFF,QQFP,QQGF,QQGP,QQKP(5,5,2)
      COMPLEX XJ
      COMPLEX AO,AL,AA,AB,QFF,QFP,QGF,QGP,ALP,QNP,QKP
      COMPLEX QFL1,QFL2
       COMPLEX FN,FNP,C1Q(5,5,2),C2Q(5,5,2),C3Q(5,5)
      DIMENSION UO(2)
      DIMENSION TITLE(12)
      DIMENSION XLD(2)
      COMMON/DIM/RO(2),RI(2),XL(2),CO(2),INRAD
      COMMON/BOUN/AO(5,5),AL(5,5),AA(5,5,2),AB(5,5,2),QFF(5,5),QFP(5,5),
     1  QGF(5,5),QGP(5,5)
      COMMON/WAVE/M,ALP(5,5,2),QNP(5,5,2),QKP(5,5,2)
      COMMON/RANGE/ALPAN(3,2),XNRAN(3),KST,KXQ,KSTP,LST,LRQ,LSTP,NRQ
   10 DO 100 L=1,5
      DO 100 K=1,5
      DO 100 I=1,2
       ALP(L,K,I)=(0.0,0.0)
      QNP(L,K,I)=(0.0,0.0)
      QKP(L,K,I)=(0.0,0.0)
      QQKP(L,K,I)=(0.0,0.0)
  100 CONTINUE
      READ (5,9000) TITLE
      READ (5,9010) M,KST,KSTP,KXQ,LST,LSTP,LRQ,NRQ,ITER,ITYPE
      IF(KXQ+LRQ+M  .LE.  0) STOP
      WRITE (6,9200) TITLE
      DO 200 I=1,2
      READ (5,9020) RO(I),RI(I),XLD(I),CO(I),UO(I),INRAD
       WRITE (6,9210) I,RO(I),RI(I),XLD(I),CO(I),UO(I)
      UO(I)=UO(I)/CO(I)
      XL(I)=XLD(I)/RO(I)
  200 CONTINUE
      WRITE(6,9220)
      IF(ITYPE .GE. 0) GO TO 250
      WRITE (6,9225)
      QAO=(0.0,0.0)
      QAL=(0.0,0.0)
       DO 220 I=1,2
      QAA(I)=(0.0,0.0)
      QAB(I)=(0.0,0.0)
  220 CONTINUE
      QQFF=(1.0,0.0)
      QQFP=(0.0,0.0)
       QQGF=(0.0,0.0)
      QQGP=(RO(2)/RO(1))*(CO(1)/CO(2))**2
      IADMIT=0
      GO TO 280
  250 READ (5,9030) QAO,QAL
      WRITE (6,9230) QAO,QAL
      READ(5,9030)QAA(1),QAB(1)
      WRITE (6,9240) QAA(1),QAB(1)
      READ(5,9030) QAA(2),QAB(2)
      WRITE (6,9250) QAA(2),QAB(2)
      WRITE (6,9260)
```

```
      READ (5,9010) IADMIT
      IF (IADMIT .GT. 0) WRITE (6,9270)
      READ(5,9030) QQFF,QQFP
      WRITE(6,9280) QQFF,QQFP
      READ(5,9030)QQGF,QQGP
      WRITE (6,9290) QQGF,QQGP
  280 B=(RO(2)*CO(1)/(RO(1)*CO(2)))**2
      BP=SQRT(B)
      IF (ITYPE .LE. 0) GO TO 500
      DO 300 I=1,2
       DO 300 L=LSTP,LRQ
      READ (5,9030)(ALP(L,K,I),K=KSTP,KXQ)
  300 CONTINUE
      DO 350 L=LSTP,LRQ
      READ (5,9030) (QNP(L,K,2),K=KSTP,KXQ)
      DO 350 K=KSTP,KXQ
      QNP(L,K,1)=CSQRT((QNP(L,K,2)**2+ALP(L,K,2)**2)/B-ALP(L,K,1)**2)
  350 CONTINUE
      DO 400 I=1,2
      DO 400 L=LSTP,LRQ
      DO 400 K=KSTP,KXQ
      QQKP(L,K,I)=CSQRT(ALP(L,K,I)**2+QNP(L,K,I)**2)
      QKP(L,K,I)=QQKP(L,K,I)
  400 CONTINUE
      GO TO 650
  500 DO 550 I=1,2
      READ (5,9030) (ALRAN(K,I),K=1,3)
  550 CONTINUE
      READ (5,9030)(XNRAN(K),K=1,3)
      IF (ITYPE .LT. 0) GO TO 650
      DO 600 L=LSTP,LRQ
      READ (5,9030) (QQKP(L,K,2),K=KSTP,KXQ)
      DO 600 K=KSTP,KXQ
      QQKP(L,K,1)=QQKP(L,K,2)/BP
  600 CONTINUE
  650 XJ=CMPLX(0.0,1.0)
      ITERQP=0
  660 DO 700 L=LSTP,LRQ
      DO 700 K=KSTP,KXQ
      IF (ITYPE .GE. 0) GO TO 665
      QFL1=0.0
      QFL2=0.0
      GO TO 668
  665 CONTINUE
      QFL1=QNP(L,K,1)/QQKP(L,K,1)
      QFL2=QNP(L,K,2)/QQKP(L,K,2)
      IF (UO(1) .EQ. 0.0) QFL1=0.0
      IF (UO(2) .EQ. 0.0) QFL2=0.0
  668 CONTINUE
      AO(L,K)=XJ*QQKP(L,K,1)*(-QAO-UO(1)*QFL1**2)
      AL(L,K)=XJ*QQKP(L,K,2)*(QAL-UO(2)*QFL2**2)
      IF (ITYPE .EQ. 0 .AND. ITERQP .EQ. 0)
     1QNP(L,K,2)=CMPLX(0.0,-AIMAG((AO(L,K)+AL(L,K))/10.0)    )
      QFF(L,K)=QQFF
      QFP(L,K)=QQFP
```

```
      QGF(L,K)=QQGF
      QGP(L,K)=QQGP
      IF (IADMIT .LE. 0) GO TO 670
      QFP(L,K)=-QFP(L,K)*XJ*CO(1)/(1.4*QQKP(L,K,1))
      QGF(L,K)=XJ*QQKP(L,K,2)*1.4*QGF(L,K)/CO(2)
      QGP(L,K)=QGP(L,K)*(RO(2)/RO(1))*(CO(1)/CO(2))**2
  670 CONTINUE
      DO 700 I=1,2
      AA(L,K,I)=XJ*QQKP(L,K,I)*QAA(I)
      AB(L,K,I)=-XJ*QQKP(L,K,I)*QAB(I)
      IF (ITYPE .EQ. 0 .AND. ITERQP .EQ. 0)
     1ALP(L,K,I)=CMPLX(0.0,-AIMAG((AA(L,K,I)+AB(L,K,I))/5.)  )
  700 CONTINUE
      IF (ITYPE .GT. 0 .OR. ITERQP .GT. ITER/4) GO TO 2000
 1000 CALL ACUSTK(0,0)
      GO TO 3000
 2000 CALL ACUSTK(1,1)
 3000 DO 3100 I=1,2
      DO 3100 L=LSTP,LRQ
      DO 3100 K=KSTP,KXQ
      QKP(L,K,I)=CSQRT(ALP(L,K,I)**2+QNP(L,K,I)**2)
 3100 CONTINUE
      IF(ITYPE.GT.0.OR.(ITERQP.GT.1.AND.ITERQP.LT.ITER-2))GO TO 3950
 3200 WRITE (6,9300) M,ITERQP
      DO 3300 I=1,2
      WRITE (6,9310) I,(K,K=KSTP,KXQ)
      DO 3300 L=LSTP,LRQ
      WRITE (6,9320) L,(ALP(L,K,I),K=KSTP,KXQ)
 3300 CONTINUE
      WRITE (6,9330)
      DO 3400 I=1,2
      WRITE (6,9310) I,(K,K=KSTP,KXQ)
      DO 3400 L=LSTP,LRQ
      WRITE (6,9320) L,(QNP(L,K,I),K=KSTP,KXQ)
 3400 CONTINUE
      WRITE (6,9340)
      DO 3500 I=1,2
      WRITE (6,9310) I,(K,K=KSTP,KXQ)
      DO 3500 L=LSTP,LRQ
      WRITE (6,9320) L, (QKP(L,K,I),K=KSTP,KXQ)
 3500 CONTINUE
      IF (ITYPE .GE. 0 .AND. ITERQP .LT. ITER) GO TO 4000
      IF (ITYPE .LT. 0) WRITE (6,9350) ITERQP
      IF (ITERQP .GE. ITER) WRITE (6,9360) ITERQP
      GO TO 6000
 3950 IF (ITERQP .EQ. 2) WRITE (6,9380)
      WRITE (6,9370) ITERQP
 4000 ITERQP=ITERQP+1
      IF (ITERQP .GT. ITER) GO TO 3200
      DO 4500 I=1,2
      DO 4500 K=KSTP,KXQ
      DO 4500 L=LSTP,LRQ
      IF (CABS(QQKP(L,K,I)-QKP(L,K,I)).GT. 1.0E-3) GO TO 4600
 4500 CONTINUE
      ITYPE=-1
```

```
      ITERQP=ITERQP-1
      GO TO 3200
 4600 C=ITERQP*5
      DO 4700 I=1,2
      DO 4700 K=KSTP,KXQ
      DO 4700 L=LSTP,LRQ
      QQKP(L,K,I)=QQKP(L,K,I)/C+(C-1.0)*QKP(L,K,I)/C
 4700 CONTINUE
      GO TO 660
 6000 CONTINUE
      WRITE (6,9390) M
      DO 6100 L=LSTP,LRQ
      DO 6100 K=KSTP,KXQ
      IF (RI(1) .LE. 0.0) GO TO 6050
      CALL CJFUN (FN,FNP,ALP(L,K,1),AA(L,K,1),M)
      C1Q(L,K,1)=FN
      CALL CYFUN(FN,FNP,ALP(L,K,1),AA(L,K,1),M)
      IF (CABS(FN) .EQ. 0.0 ) FN=(1.0E-20,0.0)
      C1Q(L,K,1)=-C1Q(L,K,1)/FN
      GO TO 6100
 6050 C1Q(L,K,1)=(0.0,0.0)
 6100 CONTINUE
      I=1
      WRITE(6,9310)I,(K,K=KSTP,KXQ)
      DO 6200 L=LSTP,LRQ
      WRITE (6,9420) L,(C1Q(L,K,1),K=KSTP,KXQ)
 6200 CONTINUE
      WRITE (6,9400)
      DO 6300 L=LSTP,LRQ
      DO 6300 K=KSTP,KXQ
       C2Q(L,K,1)=AO(L,K)
      FN=CCOS(QNP(L,K,2)*XL(2))
      FNP=CSIN(QNP(L,K,2)*XL(2))
      IF (CABS(QNP(L,K,2)).LE. 0.0) GO TO 6230
      FNP=FNP/QNP(L,K,2)
      GO TO 6240
 6230 FNP=(1.0,0.0)
 6240 C2Q(L,K,2)=FN-AL(L,K)*FNP
      IF (CABS(AL(L,K)) .GT. 1.0E5) C2Q(L,K,2)=FN/AL(L,K)-FNP
      IF (CABS(C2Q(L,K,2)).EQ. 0.0) C2Q(L,K,2)=(1.0E-20,0.0)
      IF (CABS(AL(L,K)) .GT. 1.0E5) C2Q(L,K,2)=(QNP(L,K,2)**2*FNP/AL(L,K)
     1  )+FN)/C2Q(L,K,2)
      IF (CABS(AL(L,K)).GT. 1.0E5) GO TO 6300
      C2Q(L,K,2)=(QNP(L,K,2)**2*FNP+AL(L,K)*FN)/C2Q(L,K,2)
 6300 CONTINUE
      DO 6400 I=1,2
      WRITE (6,9310) I,(K,K=KSTP,KXQ)
      DO 6400 L=LSTP,LRQ
      WRITE (6,9420) L,(C2Q(L,K,I),K=KSTP,KXQ)
 6400 CONTINUE
      I=2
      WRITE(6,9410)
      DO 6500 L=LSTP,LRQ
      DO 6500 K=KSTP,KXQ
      FN=CCOS(QNP(L,K,1)*XL(1))
```

```
      FNP=CSIN(QNP(L,K,1)*XL(1))
      IF (CABS(QNP(L,K,1)) .LE. 0.0) GO TO 6430
      FNP=FNP/QNP(L,K,1)
      GO TO 6440
 6430 FNP=(1.0,0.0)
 6440 C3Q(L,K)=FN*(QFF(L,K)+AO(L,K)*QFP(L,K))+FNP*(QFF(L,K)*AO(L,K)-
     1 QFP(L,K)*QNP(L,K,1)**2)
      IF (CABS(AO(L,K)) .GT. 1.0E5) C3Q(L,K)=AO(L,K)*(FN*(QFF(L,K)/
     1  AO(L,K)+QFP(L,K))+FNP*(QFF(L,K)-QFP(L,K)*QNP(L,K,1)**2/AO))
 6500 CONTINUE
      WRITE (6,9310) I,(K,K=KSTP,KXQ)
      DO 6600 L=LSTP,LRQ
      WRITE (6,9420) L, (C3Q(L,K),K=KSTP,KXQ)
 6600 CONTINUE
      DO 6700 L=LSTP,LRQ
      DO 6700 K=KSTP,KXQ
      C3Q(L,K)=C3Q(L,K)*C2Q(L,K,2)
 6700 CONTINUE
      I=2
      WRITE(6,9430)
      WRITE(6,9310) I,(K,K=KSTP,KXQ)
      DO 6800 L=LSTP,LRQ
      WRITE(6,9420)L,(C3Q(L,K),K=KSTP,KXQ)
 6800 CONTINUE
      GO TO 10
 9000 FORMAT(12A6)
 9010 FORMAT(10I6)
 9200 FORMAT(1H1,30X,65HAN ACOUSTIC ANALYSIS OF ANNULAR DUCTS WITH AN AXIAL
     1IAL DISCONTINUITY  , ////,30X,12A6,///////,20X,15HDUCT DIMENSIONS,/
     2 ///,1X,7HCHAMBER,6X,12HOUTER RADIUS,5X,12HINNER RADIUS,5X,12HAXIA
     3L LENGTH,5X,13HSPEED O SOUND,4X,13H END VELOCITY )
 9020 FORMAT (5E12.0,I6)
 9210 FORMAT(/,5X,I1,8X,E12.5,5X,E12.5,5X,E12.5,5X,E12.5,5X,E12.5)
 9220 FORMAT (////,20X,34HSURFACE ACOUSTIC ADMITTANCE RATIOS ,//)
 9030 FORMAT(6E12.0)
 9230 FORMAT(10X,9HINLET A= ,F12.5,3H , ,E12.5,20X,9HEXIT A=  ,E12.5,3H
     1, ,E12.5//)
 9240 FORMAT(10X,9HOUTER A= ,E12.5,3H , ,E12.5,20X,9HINNER A= ,E12.5,
     1 3H , ,E12.5,10X,16HIN FIRST CHAMBER , //)
 9250 FORMAT(10X,9HOUTER A= ,E12.5,3H , ,E12.5, 20X,9HINNER A= ,E12.5,
     1 3H , , E12.5,10X,17HIN SECOND CHAMBER , //)
 9260 FORMAT(////,20X,26HDISCONTINUITY COEFFICIENTS ,  //)
 9270 FORMAT(30X,92HCOEFFICIENTS FP AND G RELATE PRESSURES AND VELOCITIE
     1S AND ARE THUS MODIFIED BY (J*K) FACTORS ,//)
 9280 FORMAT(10X,2HF=,E12.5,3H , ,E12.5,25X,3HFP=,E12.5,3H , ,E12.5,//)
 9290 FORMAT(10X,2HG=,E12.5,3H , ,E12.5,25X,3HGP=,E12.5,3H , ,E12.5,//)
 9300 FORMAT(1H1,30X,29HEIGENVALUE SOLUTIONS FOR THE ,I1,     26HTH TANG
     1ENTIAL MODE ON THE ,I2,12HTH ITERATION,////,20X,19HRADIAL WAVE NUM
     2BERS ,  )
 9310 FORMAT(//50X,11HIN CHAMBER  ,I1,//7X,5(9X,2HK=,I1,13X)//)
 9320 FORMAT(1X,2HL=,I1,3X,5(F9.4,3H , , F9.4,4X)//)
 9330 FORMAT(///,20X,18HAXIAL WAVE NUMBERS ,    )
 9340 FORMAT(///,20X,21HCOMBINED WAVE NUMBERS,    )
 9350 FORMAT(1H1,30X,29HSOLUTION HAS CONVERGED AFTER I2,11H ITERATIONS ,
     1 //)
```

```
9360 FORMAT(1H1,30X,56HITERATION HAS BEEN TERMINATED WITHOUT CONVERGENC
    1E AFTER  ,I2, 11H ITERATIONS, //)
9225 FORMAT(20X,88HBOTH CHAMBERS HAVE ACOUSTICALLY RIGID SURFACES AND T
    1HE FLAME-FRONT IS ACOUSTICALLY IDEAL ,///)
9370 FORMAT (30X,10HITERATION ,I2,//)
9380 FORMAT(1H1)
9390 FORMAT (1H1,30X,32HMODE SHAPE COEFFICIENTS FOR THE ,I1,18HTH TANGE
    1NTIAL MODE  ,////,20X,18HRADIAL COEFFICIENT  ,)
9400 FORMAT(///,20X,17HAXIAL COEFFICIENT  ,)
9410 FORMAT(///,20X,44HCHAMBER TO CHAMBER AMPLIFICATION COEFFICIENT ,)
9420 FORMAT(1X,2HL=,I1,2X,5(F1).4,1H,,E11.4,2X))
9430 FORMAT(///,20X,49H(AXIAL COEFFICIENT) * (AMPLIFICATION COEFFICIENT
    1)   ,)
     END
```

```
ON 2.3 --PSR LEVEL 29A--

      SUBROUTINE ACUSTK(INDIC1,INDIC2)
      COMPLEX AO,AL,AA,AB,QFF,QFP,QGF,QGP,ALP,QNP,QKP,AQ,FN,FNP,
     1    ZDEL, QN1,QN2
      COMPLEX FQN,FQNP,AQP,QNP1,QNP2
      COMMON/DIM/RO(2),RI(2),XL(2),CO(2),INRAD
      COMMON/BOUN/AO(5,5),AL(5,5),AA(5,5,2),AB(5,5,2),QFF(5,5),QFP(5,5),
     1  QGF(5,5),QGP(5,5)
      COMMON/WAVE/M,ALP(5,5,2),QNP(5,5,2),QKP(5,5,2)
      COMMON/RANGE/ALRAN(3,2),XNRAN(3),KST,KXQ,KSTP,LST,LRQ,LSTP,NRQ
      NFRN=NRQ/4
      IF (INDIC1) 3000,1000,2000
 1000 I=1
      IF (LST .GT. LRQ) GO TO 3000
 1050 B=RI(I)/RO(I)
      K=1
 1100 L=LST
 1110 LP=LST
      FNTST=0.0
      AQ=CMPLX(ALRAN(1,I),AIMAG(ALP(L,K,I)))
 1150 CALL ANFUN(FN,FNP,AQ,AA(L,K,I),AB(L,K,I),B,M)
      IF (REAL(FN) .NE. 0.0) GO TO 1170
      FNTST=1.0
      GO TO 1175
 1170 CONTINUE
      IF (FNTST/REAL(FN) .GE. 0.0) GO TO 1200
 1175 CONTINUE
      AQP=AQ+ALRAN(3,I)*REAL(FN)/(FNTST-REAL(FN))
      DO 1185 N=1,NFRN
      CALL ANFUN(FQN,FQNP,AQP,AA(L,K,I),AB(L,K,I),B,M)
      IF(CABS(FQN).LE.1.0E-5)GO TO 1195
      IF(CABS(FQNP).EQ.0.0) GO TO 1200
      XR=REAL(FQN)
      XI=AIMAG(FQN)
      XPR=REAL(FQNP)
      XPI=AIMAG(FQNP)
      ZDEL=CMPLX(-XPI*XI-XPR*XR,XPI*XR-XPR*XI)/(XPR**2+XPI**2)
      IF(CABS(ZDEL).GT.5.*CABS(FQN))ZDEL=ZDEL*CABS(FQN)/(2.*CABS(ZDEL))
      AQP=AQP+ZDEL
      IF(REAL(AQP).LT.0.0)AQP=CMPLX(0.0,AIMAG(AQP))
      IF (CABS(ZDEL) .LE. .01 .OR. CABS(FQN) .LE. .1) GO TO 1195
 1185 CONTINUE
      GO TO 1200
 1195 LP=LP+1
      IF (LP .LE. L) GO TO 1200
      ALP(L,K,I)=AQP
      L=L+1
      IF (L .GT. LRQ)  GO TO 1300
      GO TO 1110
 1200 FNTST=REAL(FN)
      AQ=AQ+ALRAN(3,I)
      IF (REAL(AQ) .LE. ALRAN(2,I)) GO TO 1150
 1300 LRQ=L-1
      IF (LRQ .LE. LSTP)  LRQ=LSTP
      K=K+1
```

```
      IF (K .LE. KXQ) GO TO 1100
      IF (I .GE. 2)  GO TO 2000
      I=2
      IF (INRAD) 1050,1050,1350
 1350 DO 1400  L=LST,LRQ
      DO 1400  K=1,KXQ
      ALP(L,K,2)=ALP(L,K,1)
 1400 CONTINUE
 2000 I=1
      IF (LST .GT. LRQ) GO TO 3000
 2050 R=RT(I)/RO(I)
      K=KSTP
 2100 L=LST
 2150 AQ=ALP(L,K,I)
      N=1
 2200 CALL ANFUN(FN,FNP,AQ,AA(L,K,I),AB(L,K,I),R,M)
      IF (CABS(FN) .LE. 1.0E-5)  GO TO 2300
      IF (CABS(FNP).EQ.0.0) GO TO 2290
      XR=REAL(FN)
      XI=AIMAG(FN)
      XPR=REAL(FNP)
      XPI=AIMAG(FNP)
      ZDEL=CMPLX(-XPI*XI-XPR*XR,XPI*XR-XPR*XI)/(XPR**2+XPI**2)
      IF(CABS(ZDEL).GT.5.*CABS(FN ))ZDEL=ZDEL*CABS(FN )/(2.*CABS(ZDEL))
      AQ=AQ+ZDEL
      IF (CABS(ZDEL) .LE. 1.0E-5 .OR. CABS(FN) .LE. 1.0E-5) GO TO 2300
      N=N+1
      IF (N .LE. NRQ) GO TO 2200
 2290 CONTINUE
      WRITE (6,9050) L,K,I,XR,XI,XPR,XPI
 2300 ALP(L,K,I)=AQ
      L=L+1
      IF (L .LE. LRQ) GO TO 2150
      K=K+1
      IF (K .LE. KXQ) GO TO 2100
      IF (I .GE. 2) GO TO 3000
      I=2
      IF (INRAD) 2050,2050,2350
 2350 DO 2400 L=LST,LRQ
       DO 2400 K=KSTP,KXQ
      ALP(L,K,2)=ALP(L,K,1 )
 2400 CONTINUE
 3000 IF(INDIC2) 5000,3100,4000
 3100 L=1
      IF (KST .GT. KXQ) GO TO 5000
      R=(RO(2)*CO(1)/(RO(1)*CO(2)))**2
 3150 K=KST
 3160 KP=KST
      FNTST=0.0
      QN2=CMPLX(XNRAN(1),AIMAG(QNP(L,K,2)))
 3200 QN1         =CSQRT((QN2         **2+ALP(L,K,2)**2)/R-ALP(L,K,1)**2)
      CALL AXFUN(FN,FNP,QN1,QN2,AO(L,K),AL(L,K),QFF(L,K),QFP(L,K),
     1   QGF(L,K),QGP(L,K),R)
       IF (REAL(FN) .NE. 0.0) GOTO 3240
      FNTST=1.0
```

```
      GO TO 3250
 3240 CONTINUE
      IF (FNTST/REAL(FN) .GE. 0.0) GO TO 3300
 3250 CONTINUE
      QNP2=QN2+XNRAN(3)*REAL(FN)/(FNTST-REAL(FN))
      QNP1=CSQRT((QNP2**2+ALP(L,K,2)**2)/B-ALP(L,K,1)**2)
      DO 3260 N=1,NFRN
      CALL AXFUN(FQN,FQNP,QNP1,QNP2,AO(L,K),AL(L,K),QFF(L,K),QFP(L,K),
     1 QGF(L,K),QGP(L,K),B)
      IF (CABS(FQN).LE.1.0E-5)GO TO 3270
      IF(CABS(FQNP).EQ.0.0)GO TO 3300
      XR=REAL(FQN)
      XI=AIMAG(FQN)
      XPR=REAL(FQNP)
      XPI=AIMAG(FQNP)
      ZDEL=CMPLX(-XPI*XI-XPR*XR,XPI*XR-XPR*XI)/(XPR**2+XPI**2)
      IF(CABS(ZDEL).GT.5.*CABS(FQN))ZDEL=ZDEL*CABS(FQN)/(2.*CABS(ZDEL))
      QNP2=QNP2+ZDEL
      IF(REAL(QNP2).LT.0.0)QNP2=CMPLX(0.0,AIMAG(QNP2))
      IF (CABS(ZDEL).LE. .01 .OR. CABS(FQN) .LE. .1) GO TO 3270
 3260 CONTINUE
      GO TO 3300
 3270 KP=KP+1
      IF (KP .LE. K) GO TO 3300
      QNP(L,K,2)=QNP2
      QNP(L,K,1)=CSQRT((QNP(L,K,2)**2+ALP(L,K,2)**2)/B-ALP(L,K,1)**2)
      K=K+1
      IF (K.GT. KXQ) GO TO 3400
      GO TO 3160
 3300 FNTST=REAL(FN)
      QN2=QN2+XNRAN(3)
      IF (REAL(QN2) .LE. XNRAN(2)) GO TO 3200
 3400 KXQ=K-1
      IF (KXQ .LE. KSTP)  KXQ=KSTP
      L=L+1
      IF (L .LE. LRQ) GO TO 3150
 4000 L=LSTP
      IF (KST .GT. KXQ) GO TO 5000
      B=(RO(2)*CO(1)/(RO(1)*CO(2)))**2
 4100 K=KST
 4200 QN2=QNP(L,K,2)
      N=1
 4300 QN1        =CSQRT((QN2        **2+ALP(L,K,2)**2)/B-ALP(L,K,1)**2)
      CALL AXFUN(FN,FNP,QN1,QN2,AO(L,K),AL(L,K),QFF(L,K),QFP(L,K),
     1  QGF(L,K),QGP(L,K),B)
      IF (CABS(FN) .LE. 1.0E-5)  GO TO 4400
      IF (CABS(FNP).EQ.0.0) GO TO 4390
      XR=REAL(FN)
      XI=AIMAG(FN)
      XPR=REAL(FNP)
      XPI=AIMAG(FNP)
      ZDEL=CMPLX(-XPI*XI-XPR*XR,XPI*XR-XPR*XI)/(XPR**2+XPI**2)
      IF(CABS(ZDEL).GT.5.*CABS(FN ))ZDEL=ZDEL*CABS(FN )/(2.*CABS(ZDEL))
      QN2=QN2+ZDEL
      IF (CABS(ZDEL) .LE. 1.0E-5 .OR. CABS(FN) .LE. 1.0E-5) GO TO 4400
```

```
      N=N+1
      IF (N .LE. NRQ) GO TO 4300
 4390 CONTINUE
      WRITE (6,9060) I,K,XR,XI,XPR,XPI
 4400 QNP(L,K,2)=QN2
      QNP(L,K,1)=CSQRT((QNP(L,K,2)**2+ALP(L,K,2)**2)/B-ALP(L,K,1)**2)
      K=K+1
      IF (K .LE. KXQ) GO TO 4200
      L=L+1
      IF (L .LE. LRQ) GO TO 4100
      IF (KSTP .GE. KST)  GO TO 5000
      KP=KST-1
      DO 4700 K=KSTP,KP
       DO 4700 L=1,LRQ
      QNP(L,K,1)=CSQRT((QNP(L,K,2)**2+ALP(L,K,2)**2)/B-ALP(L,K,1)**2)
 4700 CONTINUE
 5000 RETURN
 9050 FORMAT(3X,59HNEWTON-RAPHSON ITERATION HAS EXCEEDED LIMIT FOR RADIA
     1L MODE  , // 3X,2HL=,I2,5X,2HK=,I2,5X,2HI=,I2,5X,2HF=,E14.5,3H , ,
     2 E14.5,5X,3HFP=,E14.5,3H , ,E14.5,//)
 9060 FORMAT(3X,58HNEWTON-RAPHSON ITERATION HAS EXCEEDED LIMIT FOR AXIAL
     1 MODE, // 3X,2HL=,I2,5X,2HK=,I2,5X,2HF=,E14.5,3H , ,E14.5,5X,3HFP=
     2 ,E14.5,3H , ,E14.5,//)
      END
```

```
TON 2.3 --PSR LEVEL 29A--

      SUBROUTINE ANFUN(FN,FNP,Z,AA,AB,B,M)
      COMPLEX FN,FNP,Z,AA,AB,FQ1,FQP1,FQ2,FQP2,YQ1,YQP1,YQ2,YQP2
      CALL CJFUN(FQ1,FQP1,Z,AA,M)
      IF (B .GT. 0.0) GO TO 50
      FN=FQ1
      FNP=FQP1
      RETURN
   50 CALL CJFUN(FQ2,FQP2,B*Z,B*AB,M)
      CALL CYFUN(YQ1,YQP1,Z,AA,M)
      CALL CYFUN(YQ2,YQP2,B*Z,B*AB,M)
      FN=FQ2*YQ1-FQ1*YQ2
      FNP=FQ2*YQP1+FQP2*YQ1*B-FQP1*YQ2-FQ1*YQP2*B
      RETURN
      END
```

```
.TON 2.3 --PSR LEVEL 298--

      SUBROUTINE CJFUN(FN,FNP,Z,A,M)
      COMPLEX FN,FNP,Z,A,ZD2,ZD2S,S,T,Q1,Q2,Q3
      ZD2=Z/2.0
      ZD2S=ZD2**2
      IF (M .EQ. 0)  GO TO 500
      XM =M
      S=1.0/FACT(M)
      T=ZD2
      IF (CABS(T) .EQ. 0.0) T=(1.0,0.0)
      TST=CABS((A+XM+1.0)/(T**M))
      XK=1.0
      FN=(A-XM)*S
      FNP=FN*(XM/2.0)
  100 S=S*ZD2S/(XK*(XK+XM))
      T=ZD2S/((XK+1.0)*(XM+XK+1.0))
      Q3=A-XM-2.0*XK
      Q1=T*(Q3-2.0)
      Q2=Q1*(XK+1.0+XM/2.0)
      Q1=(Q1-Q3)*S
       Q2=(Q2-(XK+XM/2.0)*Q3)*S
      FN=FN+Q1
      FNP=FNP+Q2
      IF (CABS(Q1)/TST .LT. 1.0E-8 .AND. CABS(Q2)/TST .LT. 1.0E-8)
     1  GO TO 200
      XK=XK+2.0
      S=S*T
       GO TO 100
  200 FN=FN*ZD2**M
      IF (M .EQ. 1) RETURN
      FNP=FNP*ZD2**(M-1)
      RETURN
  500 TST=CABS(A+1.0)
      S=1.0
      XK=1.0
      FNP=2.0*ZD2S
      FN=A+FNP
  600 S=S*ZD2S/(XK*XK)
       T=ZD2S/((XK+1.0)*(XK+1.0))
      Q3=2.0*ZD2S+XK*A
       Q2=((Q3+A)*T-Q3)*S
       Q1=(T*(2.0*ZD2S/(XK+2.0)+A)-(2.0*ZD2S/(XK+1.0)+A))*S
      FN=FN+Q1
      FNP=FNP+Q2
      IF (CABS(Q1)/TST .LT. 1.0E-8 .AND. CABS(Q2)/TST .LT. 1.0E-8)
     1  GO TO 700
      XK=XK+2.0
      S=S*T
       GO TO 600
  700 IF (CABS(ZD2).EQ. 0.0) GO TO 750
      FNP=FNP/ZD2
  750 RETURN
      END
```

```
      SUBROUTINE CYFUN(FN,FNP,Z,A,M)
      COMPLEX FN,FNP,Z,A,ZD2,ZD2S,S,T,Q1,Q2,Q3,Q4,GN,GNP
      IF (CABS(Z).GT. 1.0E-5) GO TO 10
      FN=1.0E30
      FNP=1.0E30
      RETURN
   10 ZD2=Z/2.0
      ZD2S=ZD2**2
      IF (M.EQ.0) GO TO 500
       Q4= CLOG(ZD2)*2.0
       FN=0.0
      FNP=0.0
      XM=M
      S=ZD2**(-M)
      DO 50 L=1,M
       K=L-1
       XK=K
      Q1=2.0*ZD2S*FACT(M-K-2)
      Q2=(A+XM)*FACT(M-K-1)
      Q3=S/FACT(K)
      FN=FN+(Q1-Q2)*Q3
      FNP=FNP+(Q1*(XK+1.0-XM/2.0)-Q2*(XK-XM/2.0))*Q3
      S=S*ZD2S
   50 CONTINUE
      GN=FN
      GNP=FNP/ZD2
      PSI1=-.5772156649
      PSI2=PSI1
      DO 60 L=1,M
      XL=L
      PSI2=PSI2+1.0/XL
   60 CONTINUE
      S=1.0/FACT(M)
      XK=1.0
      TST=CABS((A+XM+1.0)/(ZD2)**M)
      Q4=Q4-PSI1-PSI2
      FNP=(A-XM)*Q4
      FN=(FNP-2.0)*S
      FNP=(FNP*XM/2.0+A-2.0*XM)*S
  100 Q4=Q4-(1.0/XK+1.0/(XK+XM))
      T=ZD2S/((XK+1.)*(XM+XK+1.))
      S=S*ZD2S/(XK*(XK+XM))
      PSI1=(1.0/(XM+XK+1.)+1./(XK+1.))
      Q3=A-XM-2.0*XK
      Q1=(Q4*(T*(Q3-2.0)-Q3)+2.0*(1.0-T)-(Q3-2.0)*T*PSI1)*S
      Q2=(Q4*(((Q3-2.0)*(XK+XM/2.+1.)*T)-Q3*(XK+XM/2.))-PSI1*((Q3-2.)*
     1     (XK+XM/2.+1.)*T)+(2.*Q3-A)*(T-1.)-4.*T)*S
      FN=FN+Q1
      FNP=FNP+Q2
      IF (CABS(Q1)/TST .LT. 1.0E-8 .AND. CABS(Q2)/TST .LT. 1.0E-8)
     1  GO TO 200
      Q4=Q4-PSI1
      S=S*T
      XK=XK+2.
```

```
      GO TO 100
  200 FN=(FN*ZD2**M+GN)/3.14159265
      FNP=(FNP*ZD2**(M-1)+GNP)/3.14159265
      RETURN
  500 TST=CABS(A+1.)
      S=1.
      Q4=CLOG(ZD2)+.5772156649
      XK=1.
      FN=(A+2.*ZD2S)
      FNP=A/2.0+Q4*ZD2S*2.0
      FN=FN*Q4    -ZD2S
  600 Q4=Q4-1./XK
      T=ZD2S/((XK+1.)**2)
      S=S*ZD2S/(XK*XK)
      PSI1=1./(XK+1.)
      Q3=2.*ZD2S
      Q1=(Q4*(A*(T-1.)+Q3*(T/(XK+2.)-PSI1))-PSI1*T*(A+Q3/(XK+2.))+
     1    ZD2S*(PSI1**2-T/((XK+2.)**2)))*S
      Q2=(A*(T-1.)/2.                          +Q4*((T-1.)*(Q3+XK*A)+T*A)-
     1       T*PSI1*(Q3+(XK*A)+A))*S
      FN=FN+Q1
      FNP=FNP+Q2
      IF (CABS(Q1)/TST .LT. 1.0E-8 .AND. CABS(Q2)/TST .LT. 1.0E-8)
     1  GO TO 700
      XK=XK+2.
      S=S*T
      Q4=Q4-PSI1
      GO TO 600
  700 FN=(FN-1.)/1.57079632
      FNP=(FNP/ZD2)/1.57079632
      RETURN
      END
```

```
TON 2.3 --PSR LEVEL 298--

      FUNCTION FACT(N)
       DIMENSION G(20)
      DATA (G(I),I=1,20)/1.,2.,6.,24.,120.,720.,5040.,40320.,362880.,
     1    3628800.,3.99168E7,4.790016E8,6.2270208E9,8.71782912E10,
     2     1.30767437E12,2.09227899E13,3.55687428E14,6.4023737E15,
     3      1.216451E17,2.432902E18/
       IF (N) 10,20,30
   10 FACT=0.0
      RETURN
   20 FACT=1.
      RETURN
   30 IF (N .GT. 20) GO TO 40
      FACT=G(N)
      RETURN
   40 X=N
      FACT=SQRT(6.2831853*X)*(X/2.71828)**N
      RETURN
      END
```

```
TON 2.3 --PSR LEVEL 298--

      SUBROUTINE AXFUN(FN,FNP,QN1,QN2,A0,AL,QFF,QFP,QGF,QGP,B)
      COMPLEX FN,FNP,QN1,QN2,A0,AL,QFF,QFP,QGF,QGP,XJ,Q1,E1,Q2,E2,DN,
     1  F1,F2,G1,G2,F1P,F2P,G1P,G2P
      COMMON/DIM/R0(2),RI(2),XL(2),CO(2),INRAD
      COMPLEX E1P,E2P
      DATA XJ/(0.0,1.0)/
      Q1=CCOS(QN1*XL(1))
      Q2=CCOS(QN2*XL(2))
      IF (CABS(QN1)) 20,20,30
   20 E1=XL(1)
      E1P=0.0
      DN=1.0E20
      GO TO 40
   30 E1=CSIN(QN1*XL(1))/QN1
      E1P=(XL(1)*Q1-E1)/QN1
      DN=QN2/(B*QN1)
   40 CONTINUE
      IF (CABS(QN2)) 50,50,60
   50 E2=XL(2)
      E2P=0.0
      GO TO 70
   60 E2=CSIN(QN2*XL(2))/QN2
      E2P=(XL(2)*Q2-E2)/QN2
   70 CONTINUE
      F1=(QFF+A0*QFP)*Q1+(A0*QFF-QFP*QN1**2)*E1
      G1=(QGF+A0*QGP)*Q1+(A0*QGF-QGP*QN1**2)*E1
      F2=F2*QN2**2+Q2*AL
      G2=Q2-AL*E2
      F1P=F1*QN1*(-XL(1)*QFF-(XL(1)*A0+2.0)*QFP)+(QFF*A0-QFP*QN1**2)*E1P
      G1P=E1*QN1*(-XL(1)*QGF-(XL(1)*A0+2.0)*QGP)+(QGF*A0-QGP*QN1**2)*E1P
      F2P=QN2*(E2*(1.0-XL(2)*AL)+XL(2)*Q2)
      G2P=-QN2*XL(2)*F2-AL*E2P
       IF (CABS(A0) .LE. 1.0E5) GO TO 80
      F1=(QFF/A0+QFP)*Q1+(QFF-QFP*QN1**2/A0)*F1
      G1=(QGF/A0+QGP)*Q1+(QGF-QGP*QN1**2/A0)*E1
      F1P=E1*QN1*(-XL(1)*QFF/A0-(XL(1)+2.0/A0)*QFP)+(QFF-QFP*QN1**2/A0)
     1  *F1P
      G1P=E1*QN1*(-XL(1)*QGF/A0-(XL(1)+2.0/A0)*QGP)+(QGF-QGP*QN1**2/A0)
     1  *F1P
   80 CONTINUE
      IF (CABS(AL) .LE. 1.0E5) GO TO 90
      F2=E2*QN2**2/AL+Q2
      G2=Q2/AL-E2
      F2P=QN2*(E2*(1.0/AL-XL(2))+XL(2)*Q2/AL)
      G2P=-QN2*XL(2)*F2/AL-E2P
   90 CONTINUE
      FN=F1*F2-G1*G2
      FNP=F2*F1P*DN+F2P*F1-G1P*G2*DN-G1*G2P
      RETURN
      END
```

```
SION 2.3 --PSR LEVEL 294--

      PROGRAM REFINE(INPUT,OUTPUT,TAPE5=INPUT,TAPE6=OUTPUT)
      COMMON/FUN/FT,FTP,ETF,ETFP,FR,FRP,RFR,ERF2,ERF2P,FZ,FZP,GF,GFP,
     1  HRF,H3F,H4F,HEFP,HTPP,HUPP,HEPP,ALHTPP,G3,HRHOB,HUB,SQRM1
      COMMON/QINT/QNEFT,QNEFTP,QNRFR,QNERFR,QNERFP,QNEFR,QNFZ,QNGFZ,
     1QNGFZP,QNHRF,QNH3F,QNH4F,QNHEFP,QNHTPP,QNHUPP,QNHEPP,QNHTQQ,QNFT
      COMMON/DIM/RO(2),RI(2),XL(2),CO(2),UO(2),INRAD,DR(2),DZ(2),DTHET,
     1  XI1(2),XI2(2),XI3(2),INTEG,LIM
      COMMON/WAVE/M,ALP,QNP,QKP,RTN,INDIC1,CRAD1,CRAD2,CAXL1,CAXL2,
     1 QKPNEW
      COMMON/EIGEN/OMEG0,OMEG1,OMEG1F,OMEG1T,OMEG1U,OMEG1R,OMEG1E,
     1 OMEG1B,OMG1BO,OMG1BL,OMG1BA,OMG1BB,OMEG3A,OMEG3
      COMMON/EIGEN2/OMEG02,OMEG2,OMEG2F,OMEG2T,OMEG2U,OMEG2R,OMEG2E,
     1  OMEG2B,OMG2BO,OMG2BL,OMG2BA,OMG2BB,OMEG2A
      COMMON/COMB/CBAR1,CBAR2T,CBAR2R,CBAR2Z,CBAR3,CBAR4,CBAR5,GAMMA,
     1 UBAR,TAUBAR,XNU1,XNU2,XNU3,XMU1,XMU2,XMU3,INDIC2,ZS,CBAR6
      COMMON/BOUN/INDICO,INDICL,AO,AL,AA,AB,BFFA,BFFB
      COMMON /MUQ/ RMUQ(21),XMUQ(21),NMUQ,LASINT
      COMPLEX BFFA(101,2),BFFB(101,2)
      COMPLEX FT(101),FTP(101),ETF(101),ETFP(101),FR(101,2),FRP(101,2),
     1 RFR(101,2),ERF2(101),ERF2P(101),FZ(101,2),FZP(101,2),GF(101,2),
     2 GFP(101,2),HRF(101),H3F(101),H4F(101),HEFP(101),HTPP(101),
     3 HUPP(101),HEPP(101),ALHTPP(101),G3,HRHOB,HUB,SQRM1
      COMPLEX QNEFT,QNEFTP,QNRFR(2),QNERFR,QNERFP,QNEFR,QNFZ(2),QNGFZ(2)
     1,QNGFZP(2),QNHRF,QNH3F,QNH4F,QNHEFP,QNHTPP,QNHUPP,QNHEPP,QNHTQQ,
     2 QNFT
      COMPLEX ALP(2),QNP(2),QKP(2),RTN,CRAD1(2),CRAD2(2),CAXL1(2),
     1  CAXL2(2),QKPNEW(2)
      COMPLEX       OMEG0,OMEG1,OMEG1F,OMEG1T,OMEG1U,OMEG1R,OMEG1E,
     1 OMEG1B,OMG1BO,OMG1BL,OMG1BA,OMG1BB,OMEG3A,OMEG3
       COMPLEX       OMEG02,OMEG2,OMEG2F,OMEG2T,OMEG2U,OMEG2R,OMEG2E,
     1  OMEG2B,OMG2BO,OMG2BL,OMG2BA,OMG2BB,OMEG2A
      COMPLEX AO,AL,AA(2),AB(2)
      COMPLEX FUNOM,OM
      DIMENSION TITLE(12),XLO(2)
      DIMENSION LIN1(2),LIN2(2)
      COMPLEX BLKFUN(101,28),BLKOM(14),BLKOM2(12),BLKINT(22)
      EQUIVALENCE (BLKFUN,FT),(BLKOM,OMEG0),(BLKOM2,OMEG02),
     1  (BLKINT,QNEFT)
      COMPLEX QAO,QAL,QAA(2),QAB(2)
      COMPLEX VEC(12)
      SQRM1=(0.0,1.0)
  100 READ(5,9000) TITLE
      READ (5,9010)M,INDIC1,INTEG,INDIC2,INDICB,INDICO,INDICL,KONTRL,
     1  KDUMP
      LASINT=1
      INTEG=2*(INTEG/2)
      IF (INTEG .LE. 0) STOP
      LIM=INTEG+1
      WRITE (6,9200) TITLE
      RTN=(1.0,0.0)
      IF(KONTRL .GT. 0) GO TO 350
      DO 200 I=1,2
      READ(5,9020)RO(I),RI(I),XLO(I),CO(I),UO(I),INRAD
      WRITE(6,9210)I,RO(I),RI(I),XLO(I),CO(I),UO(I)
```

```
      AL(I)=XLD(I)/RO(I)
  200 CONTINUE
      READ(5,9030)(XI1(I),XI2(I),XI3(I),I=1,2)
      WRITE (6,9215)
      DO 300 I=1,2
      IF (XI1(I) .EQ. 0.0 .AND. XI2(I) .EQ. 0.0 .AND. XI3(I) .EQ. 0.0)
     1   XI3(I)=UO(I)
      WRITE(6,9216) I,XI1(I),I,XI2(I),I,XI3(I)
  300 CONTINUE
      WRITE(6,9220)
      READ(5,9030)AO,AL
      WRITE(6,9230)AO,AL
      READ (5,9040)  AA(1),AB(1),LIN1(1),LIN2(1)
      IF (LIN1(1) .EQ. 0) LIN1(1)=1
      IF (LIN2(1) .EQ. 0) LIN2(1)=LIM
      WRITE(6,9240)AA(1),AB(1)
      READ (5,9040)  AA(2),AB(2),LIN1(2),LIN2(2)
      IF (LIN1(2) .EQ. 0) LIN1(2)=1
      IF (LIN2(2) .EQ. 0) LIN2(2)=LIM
      WRITE(6,9250)AA(2),AB(2)
      QAO=AO
      QAL=AL
      DO 320 I=1,2
      QAA(I)=AA(I)
      QAB(I)=AB(I)
  320 CONTINUE
      IF (INDICB .LE. 0) WRITE(6,9260)
      IF (INDICB .GT. 0) WRITE(6,9270)
      WRITE (6,9275) LIN1(1),LIN2(1),LIN1(2),LIN2(2)
  350 CONTINUE
       WRITE(6,9280)
      IF (INDIC1 .GT. 0) WRITE(6,9300)M
      IF (INDIC1 .LE. 0) WRITE(6,9290)M
      WRITE(6,9310)
      DO 400 I=1,2
      IF(KONTRL .GE. 21) GO TO 380
      READ(5,9030) ALP(I),CRAD1(I),CRAD2(I)
  380 CONTINUE
      WRITE(6,9320)  I,ALP(I),CRAD1(I),CRAD2(I)
  400 CONTINUE
      WRITE (6,9330)
      DO 500 I=1,2
      IF (KONTRL .GE. 21) GO TO 410
      READ(5,9030)QNP(I),CAXL1(I),CAXL2(I)
  410 CONTINUE
      WRITE(6,9320) I,QNP(I),CAXL1(I),CAXL2(I)
  500 CONTINUE
      IF (KONTRL .GT. 0) GO TO 540
      READ(5,9030) GAMMA,UBAR,TAUBAR,ZS,CHAR1,CHAR6
      READ(5,9030)CHAR21,CHAR2R,CHAR22,CHAR3,CHAR4,CHAR5
      READ(5,9030)XNU1,XNU2,XMU3,XMU1,XMU2,XMU3
      IF(XMU1.EQ.0.0.AND.XMU2.EQ.0.0.AND.XMU3.EQ.0.0) XMU1=1.0
      READ(5,9010) NMUQ
      READ(5,9030)(RMUQ(I),XMUQ(I), I=1,NMUQ)
      WRITE(6,9340)GAMMA,UBAR,TAUBAR
```

```
      WRITE (6,9340) XNU1,XNU3,XNU2,XNU3
      WRITE(6,9370)CBAR1
      WRITE (6,9375) CBAR6
      WRITE(6,9380)CBAR2T
      WRITE(6,9390)CBAR2R
      WRITE(6,9400)CBAR2Z
      WRITE(6,9410)CBAR3
      WRITE(6,9420)CBAR4
      WRITE(6,9430)CBAR5
      WRITE(6,9440)ZS
      WRITE(6,9350)
      DO 510 I=1,NMUQ
      XMUQ(I)=XMUQ(I)*(XMU1*RMUQ(I)**2+XMU2*RMUQ(I)+XMU3)
      WRITE (6,9355) RMUQ(I),XMUQ(I)
  510 CONTINUE
      ZS=ZS/R0(1)
      IF (INDIC2 .LT. 0) WRITE(6,9450)
      GO TO 545
  540 CONTINUE
      IF (KONTRL .LT. 5) GO TO 541
      READ(5,9030) TAUBAR,CBAR1,CBAR6
      WRITE (6,9340)  GAMMA,UBAR,TAUBAR
      WRITE(6,9370) CBAR1
      WRITE (6,9375) CBAR6
  541 CONTINUE
      IF (KONTRL .GT.10) READ (5,9030) QAA(1),QAA(2)
      A0=QA0
      AL=QAL
      DO 542 I=1,2
      AA(I)= QAA(I)
      AB(I)=QAB(I)
  542 CONTINUE
      IF (KONTRL .GT. 10) WRITE(6,9220)
      IF (KONTRL .GT. 10) WRITE(6,9240)AA(1),AB(1)
      IF (KONTRL .GT. 10) WRITE(6,9250)AA(2),AB(2)
  545 CONTINUE
      WRITE(6,9460) TITLE
      QKP(1)=CSQRT(ALP(1)**2+QNP(1)**2)
      QKP(2)=CSQRT(ALP(2)**2+QNP(2)**2)
      OMEG0=QKP(1)*C0(1)/R0(1)
      OMEG02=OMEG0**2
      IF (INDICR .LE. 0) GO TO 600
      A0=SQRM1*QKP(1)*(-A0-U0(1)/C0(1)*(QNP(1)/QKP(1))**2)
      AL=SQRM1*QKP(2)*(AL-U0(2)/C0(2)*(QNP(2)/QKP(2))**2)
      DO 550 I=1,2
      AA(I)=SQRM1*QKP(I)*AA(I)
      AB(I)=-SQRM1*QKP(I)*AB(I)
  550  CONTINUE
  600 CONTINUE
      CALL FUNGEN
      DO 700 I=1,2
      DO 700 J=1,LIM
      BFFA(J,I)=(0.0,0.0)
      BFFB(J,I)=(0.0,0.0)
      IF (J .LT. LIN1(I) .OR. J .GT. LIN2(I)) GO TO 700
```

```
      BFFA(J,I)=FZ(J,I)*AA(I)
      BFFB(J,I)=FZ(J,I)*AB(I)
  700 CONTINUE
       CALL NTGRAT
      DO 1050 L=1,14
      BLKOM(L)=FUNOM(BLKOM(L))
 1050 CONTINUE
      WRITE (6,9470)
      DO 1100 I=1,2
      WRITE (6,9480) I,OKP(I),OKPNEW(I)
 1100 CONTINUE
      WRITE (6,9490) OMEG1
      DO 1150 L=1,12
      VEC(L)=BLKOM2(L)
 1150 CONTINUE
      OMEG2=OMEG1-OMEG0
       DO 1180 L=3,12
      BLKOM2(L)=OMEG1-BLKOM(L)
 1180 CONTINUE
      WRITE(6,9500)
      WRITE (6,9510) OMEG0,OMEG2
      WRITE (6,9520) OMEG1F,OMEG2F
      WRITE (6,9530) OMEG1T,OMEG2T
       WRITE (6,9540) OMEG1U,OMEG2U
      WRITE (6,9550) OMEG1R,OMEG2R
      WRITE (6,9560) OMEG1E,OMEG2E
      WRITE (6,9570) OMEG1B,OMEG2B
      WRITE (6,9580) OMG1B0,OMG2B0
      WRITE (6,9590) OMG1BL,OMG2BL
      WRITE (6,9600) OMG1BA,OMG2BA
      WRITE (6,9610) OMG1BB,OMG2BB
      IF (INDIC2 .LE. 0) GO TO 100
      OMEG2=OMEG3-OMEG3A
      WRITE (6,9620) OMEG3,OMEG3A,OMEG2
      IF(KDUMP .EQ. 0)  GO TO 1300
      WRITE(6,9710)
 9710 FORMAT(1H1)
      DO 1190 I=1,2
      CALL SIMSON(   AA(I),FZP(1,I),FZ(1,I),DZ(I),INTEG)
 1190 CONTINUE
         AB(1)=FZP(LIM,2)/(FZ(LIM,2)*SQOM1*OKP(2))
         AB(2)=FRP(LIM,2)/(FR(LIM,2)*SQOM1*OKP(2))
      WRITE(6,9700) AA(1),AA(2),AB(1),AB(2)
      WRITE(6,9700) BIN,HKHOB,HUB,G3
 9700 FORMAT(8(4X,E12.5))
      L1=1
      L2=28
      IF (KDUMP .NE. 2) GO TO 1195
      L1=13
      L2=14
 1195 CONTINUE
      DO 1200 L=L1,L2
       WRITE (6,9720) L
 9720 FORMAT(//,1X,I2)
      WRITE(6,9700)(BLKFUN(I,L),I=1,LIM)
```

```
 1200 CONTINUE
      WRITE (6,9730)
 9730 FORMAT(//,1X,6HBLKOM2)
      WRITE (6,9700) (VEC(I), I=1,12)
      WRITE(6,9740)
 9740 FORMAT(//,1X,6HBLKINT)
      WRITE(6,9700)(BLKINT(I),I=1,22)
 1300 CONTINUE
      IF (INDIC1 .NE. 2 .OR. M .EQ. 0)  GO TO 100
      BTN=(1.0,0.0)
      INDIC1=0
      KONTRL=0
      WRITE(6,9280)
      WRITE (6,9290) M
      GO TO 540
 9000 FORMAT(12A6)
 9010 FORMAT(12I6)
 9200 FORMAT(1H1,30X,74HA STABILITY EVALUATION OF ANNULAR DUCT BURNERS WITH
     1ITH AN AXIAL DISCONTINUITY ,////,30X,12A6,////////,20X,15HDUCT DIME
     2NSIONS , ///,1X,7HCHAMBER,6X,12HOUTER RADIUS, 5X, 12HINNER RADIUS,5X,
     35X,12HAXIAL LENGTH, 5X,13HSPEED O SOUND, 5X, 12HEND VELOCITY )
 9020 FORMAT(5E12.0,I5)
 9210 FORMAT(/,5X,I1,8X,E12.5,4(5X,E12.5))
 9030 FORMAT(6E12.0)
 9215 FORMAT(////,20X,34HTHROUGH FLOW VELOCITY COEFFICIENTS ,//)
 9216 FORMAT(10X,11HIN CHAMBER ,I1,2X,6HUO = (,F8.3,3H)*Z,I1,7H**2 + (,
     1F8.3,3H)*Z,I1,4H + (,F8.3,1H),//)
 9220 FORMAT(////,20X,47HSURFACE PROPERTIES USED IN BOUNDARY REFINEMENTS
     1  ,//)
 9230 FORMAT(10X,10HINLET AP= ,E12.5,3H , ,E12.5,20X,10HEXIT AP=  ,E12.5,
     1, 3H , ,E12.5,//)
 9240 FORMAT(10X,10HOUTER AP= ,E12.5,3H , ,E12.5,20X,10HINNER AP= ,E12.5,3H
     1,3H , ,E12.5,10X,16HIN FIRST CHAMBER ,//)
 9250 FORMAT(10X,10HOUTER AP= ,E12.5,3H , ,E12.5,20X,10HINNER AP= ,E12.5
     1,3H , ,E12.5,10X,17HIN SECOND CHAMBER ,//)
 9260 FORMAT(15X,76HABOVE VALUES RELATE (DETA/DNORMAL) TO ETA, AND ARE T
     1HUS MODIFIED ADMITTANCES  )
 9270 FORMAT(15X,84HABOVE VALUES RELATE VELOCITY TO PRESSURE, AND ARE TH
     1US ACOUSTIC ADMITTANCE RATIOS  )
 9275 FORMAT (///,15X,43HINNER AND OUTER ACOUSTIC LINERS EXTEND FROM ,
     1 //,20X,8HSTATION ,I3, 12H TO STATION ,I3,21H IN THE FIRST CHAMBER
     1  ,//,20X,8HSTATION ,I3,12H TO STATION ,I3,22H IN THE SECOND CHAMB
     1ER  )
 9280 FORMAT(1H1,20X,31HACOUSTIC MODE UNDER EXAMINATION ,////)
 9290 FORMAT(10X,44HSTANDING MODE WITH TANGENTIAL WAVE NUMBER = ,I2 )
 9300 FORMAT(10X,44HSPINNING MODE WITH TANGENTIAL WAVE NUMBER = ,I2)
 9310 FORMAT(///,1X,7HCHAMBER,8X,18HRADIAL WAVE NUMBER,10X,25HCOEFFICIEN
     1T OF J FUNCTION ,10X,25HCOEFFICIENT OF Y FUNCTION )
 9320 FORMAT(/5X,I1,8X,F9.4,3H , ,F9.4,8X,E12.5,3H , ,E12.5,9X,E12.5,
     1 3H , ,E12.5)
 9330 FORMAT(///,1X,7HCHAMBER,8X,17HAXIAL WAVE NUMBER, 10X,27HCOEFFICIEN
     1T OF COS FUNCTION,8X,27HCOEFFICIENT OF SIN FUNCTION)
 9340 FORMAT(1H1,20X,21HCOMBUSTION PARAMETERS ,///,10X,7HGAMMA =,F7.4,
     110X,7HUBAR = ,E12.5, 10X,9HTAUBAR =  ,E12.5)
 9350 FORMAT(///,30X,11HRADIAL EBAR,//,23X,4HR/RO,16X,5HREBAR,//)
```

```
 9355 FORMAT(22X,F7.4,10X,E11.4)
 9360 FORMAT(/,10X,19HTANGENTIAL EBAR = (,E11.4,6H)*COS(,F6.3,11H*THETA)
     1 + (,E11.4,5H)*SIN(,F6.3,13H*THETA) + 1.0  )
 9370 FORMAT(///,20X,33HCOEFFICIENT OF P/PO IN TAU/TAU = ,F8.5)
 9375 FORMAT(/,32X,24HOF UZ/UBAR IN TAU/TAU = ,F8.5)
 9380 FORMAT(/,32X,20HOF UT/UBAR IN E/E = ,F8.5)
 9390 FORMAT(/,32X,20HOF UR/UBAR IN E/E = ,F8.5)
 9400 FORMAT(/,32X,20HOF UZ/UBAR IN E/E = ,F8.5)
 9410 FORMAT(/,32X,17HOF P/PO IN E/E = ,F8.5)
 9420 FORMAT(/,32X,26HOF UZ/UBAR SPRAY IN E/E = ,F8.5)
 9430 FORMAT(/,32X,23HOF P/PO SPRAY IN E/E = ,F8.5)
 9440 FORMAT(/,25X,15HWHERE ZSPRAY = ,F4.5)
 9450 FORMAT(//,30X,74HCHARACTERISTIC TIME FLUCTUATION FIXED BY INITIAL
     1CONDITIONS AT FLAME FRONT)
 9460 FORMAT(1H1,30X,43HRESULTS OF THE REFINED STABILITY EVALUATION ,////,30
     1/,30X,12A6,//////)
 9470 FORMAT(20X,21HCOMBINED WAVE NUMBERS ,///,8X,7HCHAMBER,9X,8HACOUSTI
     1C,19X,7HREFINED )
 9480 FORMAT(/,11X,I1,6X,F9.4,3H + ,F9.4,5X,F9.4,3H + ,F9.4)
 9490 FORMAT(/////,20X,38HNATURAL MODE STABILITY CHARACTERISTICS,///,
     1 35X,9HFREQUENCY, 11X, 9HDECREMENT,//,10X,11HFINAL VALUE,14X,F9.4,
     2,11X,F9.4,//,35X,9H*********,11X,9H**********,)
 9500 FORMAT(1H1,20X,54HSTABILITY CHARACTERISTICS WITHOUT VARIOUS REFIN
     1EMENTS,///,35X,9HFREQUENCY,11X,9HDECREMENT,11X,9HDELTA FRQ,11X,
     2 9HDELTA DEC,/,37X,5H(CPS),35X,5H(CPS),)
 9510 FORMAT(//,10X,21HPURELY ACOUSTIC VALUE,4X,4(F9.4,11X))
 9520 FORMAT(//,10X,19HFINAL W/O THRU-FLOW ,6X,4(F9.4,11X))
 9530 FORMAT(/,10X,20HFINAL W/O TAU/TAUBAR,5X,4(F9.4,11X))
 9540 FORMAT(/,10X,17HFINAL W/O UZ/UBAR,8X,4(F9.4,11X))
 9550 FORMAT(/,10X,20HFINAL W/O RHO/RHOBAR,5X,4(F9.4,11X))
 9560 FORMAT(/,10X,16HFINAL W/O E/EBAR,9X,4(F9.4,11X))
 9570 FORMAT(//10X,22HFINAL W/O ANY BOUNDARY, 3X,4(F9.4,11X))
 9580 FORMAT(/,12X,17HW/O UPSTREAM ONLY ,6X,4(F9.4,11X))
 9590 FORMAT(/,12X,19HW/O DOWNSTREAM ONLY ,4X,4(F9.4,11X))
 9600 FORMAT(/,12X,19HW/O OUTER DIAM ONLY,4X,4(F9.4,11X))
 9610 FORMAT(/,12X,19HW/O INNER DIAM ONLY, 4X,4(F9.4,11X))
 9620 FORMAT(/////,20X,103HSTABILITY CHARACTERISTICS IF CHARACTERISTIC T
     1IME FLUCTUATION FIXED BY INITIAL CONDITIONS AT FLAME FRONT ,///,
     235X,9HFREQUENCY,11X,9HDECREMENT,11X,9HDELTA FRQ, 11X,9HDELTA DEC,
     3 /,37X,5H(CPS),35X,5H(CPS),//,10X,11HFINAL VALUE,14X,F9.4,11X,
     4 F9.4,//,10X,20HFINAL W/O TAU/TAUBAR,5X,4(F9.4,11X))
 9040 FORMAT(4E12.0,2I6)
      END
```

```
SION 2.3 --PSR LEVEL 298--

      COMPLEX FUNCTION FUNOM(OM)
      COMPLEX FUNOM,OM
*********************************
      A=REAL(OM)/6.28318531
      B=-AIMAG(OM)/A
      FUNOM=CMPLX(A,B)
      RETURN
      END
```

```
SION 2.3 --PSR LEVEL 277--

      SUBROUTINE FUNGEN
      COMMON/FUN/FT,FTP,ETF,ETFP,FR,FRP,HFR,ERF2,HRF2P,FZ,FZP,GF,GFP,
     1  HRF,H3F,H4F,HEFP,HTPP,HUPP,HEPP,ALHTPP,G3,HRHOR,HUB,SQRM1
      COMMON/DINT/QNEFT,QNEFTP,QNHFR,QNEHFR,QNEHFP,QNEFR,QNFZ,QN3FZ,
     1QNGFZP,QNHRF,QNH3F,QNH4F,QNHEFP,QNHTPP,QNHUPP,QNHEPP,QNHTQQ,QNFT
      COMMON/DIM/RO(2),RI(2),XL(2),CO(2),UO(2),INRAD,DR(2),DZ(2),DTHET,
     1  XI1(2),XI2(2),XI3(2),INTEG,LIM
      COMMON/WAVE/M,ALP,QNP,QKP,BTN,INDIC1,CRAD1,CRAD2,CAXL1,CAXL2,
     1 QKPNEW
      COMMON/EIGEN/OMEG0,OMEG1,OMEG1F,OMEG1T,OMEG1U,OMEG1R,OMEG1E,
     1 OMEG1B,OMG1BO,OMG1BL,OMG1BA,OMG1BB,OMEG3A,OMEG3
      COMMON/EIGEN2/OMEG02,OMEG2,OMEG2F,OMEG2T,OMEG2J,OMEG2R,OMEG2E,
     1  OMEG2H,OMG2BO,OMG2BL,OMG2BA,OMG2BB,OMEG2A
      COMMON/COMB/CBAR1,CBAR2T,CBAR2R,CBAR2Z,CBAR3,CBAR4,CBAR5,GAMMA,
     1 UBAR,TAUBAR,XNU1,XNU2,XNU3,XMU1,XMU2,XMU3,INDIC2,ZS,CBAR6
      COMMON/BOUN/INDICO,INDICL,AO,AL,AA,AB,BFFA,BFFB
      COMMON /MUQ/ RMUQ(21),XMUQ(21),NMUQ,LASINT
      COMPLEX BFFA(101,2),BFFB(101,2)
      COMPLEX FT(101),FTP(101),ETF(101),ETFP(101),FR(101,2),FRP(101,2),
     1 HFR(101,2),ERF2(101),ERF2P(101),FZ(101,2),FZP(101,2),GF(101,2),
     2 GFP(101,2),HRF(101),H3F(101),H4F(101),HEFP(101),HTPP(101),
     3 HUPP(101),HEPP(101),ALHTPP(101),G3,HRHOR,HUB,SQRM1
      COMPLEX QNEFT,QNEFTP,QNHFR(2),QNEHFR,QNEHFP,QNEFR,QNFZ(2),QNGFZ(2)
     1,QNGFZP(2),QNHRF,QNH3F,QNH4F,QNHEFP,QNHTPP,QNHUPP,QNHEPP,QNHTQQ,
     2 QNFT
      COMPLEX ALP(2),QNP(2),QKP(2),BTN,CRAD1(2),CRAD2(2),CAXL1(2),
     1  CAXL2(2),QKPNEW(2)
      COMPLEX       OMEG0,OMEG1,OMEG1F,OMEG1T,OMEG1U,OMEG1R,OMEG1E,
     1 OMEG1B,OMG1BO,OMG1BL,OMG1BA,OMG1BB,OMEG3A,OMEG3
      COMPLEX       OMEG02,OMEG2,OMEG2F,OMEG2T,OMEG2J,OMEG2R,OMEG2E,
     1  OMEG2H,OMG2BO,OMG2BL,OMG2BA,OMG2BB,OMEG2A
      COMPLEX AO,AL,AA(2),AB(2)
      COMPLEX QCBAR,QJBAR,QSUM,QSUMP,QF(11),QFP(11),QTERM(11),QINTS
      XINTEG=INTEG
      DO 10 I=1,2
      DZ(I)=XL(I)/XINTEG
      DR(I)=(1.0-RI(I)/RO(I))/XINTEG
   10 CONTINUE
      IF (INRAD .GT. 0) DR(2)=DR(1)
      THET=0.0
      DTHET=6.28318531/XINTEG
      DO 120 J=1,LIM
      CALL TNGIAL(FT(J),FTP(J),THET,M,BTN,INDIC1)
      Q=XNU1*COS(XNU3*THET)+XNU2*SIN(XNU3*THET)  +1.0
      ETF(J)=Q*FT(J)
      ETFP(J)=Q*FTP(J)
      THET=THET+DTHET
  120 CONTINUE
      ASSIGN 240 TO IMPAS
      IF (INRAD .GT. 0) ASSIGN 220 TO IMPAS
      DO 260 I=1,2
      R=RI(I)/RO(I)
      DO 250 J=1,LIM
      CALL RADIAL(FR(J,I),FRP(J,I),R,ALP(I),CRAD1(I),CRAD2(I),M)
```

```
      RFR(J,I)=R*FR(J,I)
      GO TO IBIPAS,(220,230,240)
  220 FR(J,2)=FR(J,1)
      RFR(J,2)=RFR(J,1)
      FRP(J,2)=FRP(J,1)
  230 CONTINUE
      CALL INTERP(R,Q)
      ERF2(J)=FR(J,2)*Q
      ERF2P(J)=FRP(J,2)*Q
  240 R=R*DR(I)
  250 CONTINUE
      IF(INRAD .GT. 0) GO TO 300
      ASSIGN 230 TO IBIPAS
  260 CONTINUE
  300 CONTINUE
      CALL AXIAL(QSUM,QSUMP,ZS,QNP(1),CAXL1(1),CAXL2(1))
      QFFUB=(XI1(1)*ZS+XI2(1))*ZS+XI3(1)
      QCBAR=CBAR5*QSUM+CBAR4*QSUMP*CO(1)/(SQRM1*QKP(1)*GAMMA*QFFUB)
      QSUM=(0.0,0.0)
      QSUMP=(0.0,0.0)
      QJBAR=SQRM1*RO(2)*OMEGO/UBAR
      Q=UBAR*TAUBAR
      ASSIGN 390 TO JBIPAS
      DO 400 I=1,2
      Z=0.0
      DO 395 J=1,LIM
      CALL AXIAL(FZ(J,I),FZP(J,I),Z,QNP(I),CAXL1(I),CAXL2(I))
      QU=(XI1(I)*Z+XI2(I))*Z+XI3(I)
      QUP=2.0*XI1(I)*Z+XI2(I)
      QUPP=2.0*XI1(I)
      GF(J,I)=FZ(J,I)*(-SQRM1*OMEGO/RO(I)*QUP*(GAMMA+2.0)*(QNP(I)/QKP(I))
     1    **2))
      GFP(J,I)=FZP(J,I)*(-SQRM1*OMEGO/RO(I)*(2.0*QU-QUPP/QKP(I)**2))
      GO TO JBIPAS,(310,390)
  310 QE=EXP(-RO(I)*Z/Q)
      HRF(J)=FZ(J,I)*QE
      H3F(J)=(GAMMA-1.0)/(Q*RO(I))   *QE *FZ(1,I)*CEXP(QJBAR*Z)
      H4F(J)=H3F(J)*CBAR2I
      H3F(J)=H3F(J)*CBAR2R
      HEFP(J)=(CBAR3*FZ(1,I)+CBAR2Z*FZP(1,I)*CO(I)/(SQRM1*QNP(1)*GAMMA*
     1    UBAR))   * QE*CEXP(QJBAR*Z)
      HEPP(J)=QCBAR*QE*CEXP(QJBAR*(Z-UBAR*(XL(1)-ZS)*RO(1)/(QFFUB*RO(2)
     1   )))
      ALHTPP(J)=(RO(I)*Z/Q-1.0)*QE*CEXP(QJBAR*Z)*(CBAR1*FZ(1,I) +
     1   CBAR6*CO(I)*FZP(1,I)/(SQRM1*QKP(I)*GAMMA*UBAR))
      IF (J.GT. 1) GO TO 330
      LP=11
      QF(LP)=FZ(J,I)
      QFP(LP)=FZP(J,I)
      HTPP(1)=-CBAR6*CO(I)*FZP(1,I)/(SQRM1*QKP(I)*GAMMA*UBAR)
      HUPP(1)=(0.0,0.0)
      QTEM(1)=CONJG(CEXP(QJBAR*DZ(I)))
      GO TO 390
  330 QF(1)=QF(LP)
      QFP(1)=QFP(LP)
```

```
      JP=10-2*(J/5)
      IF (JP .LT. 4) JP=4
      LP=JP+1
      QJP=JP
      DZP=DZ(I)/QJP
      ZP=Z-DZ(I)+DZP
      DO 340 K=2,LP
      CALL AXIAL(QF(K),QFP(K),ZP,QJP(I),CAXL1(I),CAXL2(I))
      QTEM(K)=CONJG(CEXP(QJBAR*(Z-ZP)) )
      ZP=ZP+DZP
  340 CONTINUE
      CALL SIMSON(QINTS,QF,QTEM,DZP,JP)
      QSUM=QTEM(1)*QSUM+QINTS
      CALL SIMSON(QINTS,QFP,QTEM,DZP,JP)
      QSUMP=QTEM(1)*QSUMP+QINTS
      HTPP(J)=RO(I)*CBAR1*QE*QSUM/Q+(RO(I)*Z/Q-1.0)*QE*(EXP(QJBAR*Z)*
     1 CBAR6*CO(I)*PZP(1,I)/(SQRM1*QKP(I)*GAMMA*UBAR)
      HUPP(J)=QE*QSUMP/Q
  390 Z=Z+DZ(I)
  395 CONTINUE
      ASSIGN 310 TO JUMPAS
  400 CONTINUE
      QU=(XI1(1)*XL(1)+XI2(1))*AL(1)+XI3(1)
      G3=-(SQRM1*OMEGO/RO(2))*GAMMA*(XI3(2)*PZ(1,2)-QU*PZ(LIM,1))
      HRHOB=SQRM1*OMEGO*(GAMMA-1.0)/(TAUBAR*CO(2)**2)
      HOB=(GAMMA-1.0)/Q
      RETURN
      END
```

```
SION 2.3 --PSR LEVEL 294--

      SUBROUTINE GTGRAT
      COMMON/FUN/FT,FTP,ETF,ETFP,FR,FRP,RFR,ERF2,FRF2P,FZ,FZP,GF,GFP,
     1  HRF,H3F,H4F,HEFP,HTPP,HUPP,HEPP,ALHTPP,G3,HRHOB,HUB,SQRM1
      COMMON/DINT/QNEFT,QNEFTP,QNRFR,QNERFR,QNERFP,QNEFR,QNFZ,QNGFZ,
     1QNGFZP,QNHRF,QNH3F,QNH4F,QNHEFP,QNHTPP,QNHUPP,QNHEPP,QNHTQQ,QNFT
      COMMON/DIM/RO(2),RI(2),XL(2),CO(2),UO(2),INRAD,DR(2),DZ(2),DTHET,
     1  XI1(2),XI2(2),XI3(2),INTEG,LIM
      COMMON/WAVE/M,ALP,QNP,QKP,BTN,INDICI,CRAD1,CRAD2,CAXL1,CAXL2,
     1 QKPNEW
      COMMON/EIGEN/OMEG0,OMEG1,OMEG1F,OMEG1T,OMEG1U,OMEG1R,OMEG1E,
     1 OMEG1B,OMG1BO,OMG1BL,OMG1BA,OMG1BB,OMEG3A,OMEG3
      COMMON/EIGEN2/OMEG02,OMEG2,OMEG2F,OMEG2T,OMEG2U,OMEG2R,OMEG2E,
     1  OMEG2B,OMG2BO,OMG2BL,OMG2BA,OMG2BB,OMEG2A
      COMMON/COMB/CBAR1,CBAR2T,CBAR2R,CBAR2Z,CBAR3,CBAR4,CBAR5,GAMMA,
     1 UBAR,TAUBAR,XNU1,XNU2,XNU3,XMU1,XMU2,XMU3,INDIC2,ZS,CBAR6
      COMMON/BOUN/INDICO,INDICL,AO,AL,AA,AB,BFFA,BFFB
      COMPLEX BFFA(101,2),BFFB(101,2)
      COMPLEX FT(101),FTP(101),ETF(101),ETFP(101),FR(101,2),FRP(101,2),
     1 RFR(101,2),ERF2(101),ERF2P(101),FZ(101,2),FZP(101,2),GF(101,2),
     2 GFP(101,2),HRF(101),H3F(101),H4F(101),HEFP(101),HTPP(101),
     3 HUPP(101),HEPP(101),ALHTPP(101),G3,HRHOB,HUB,SQRM1
      COMPLEX QNEFT,QNEFTP,QNRFR(2),QNERFR,QNERFP,QNEFR,QNFZ(2),QNGFZ(2)
     1,QNGFZP(2),QNHRF,QNH3F,QNH4F,QNHEFP,QNHTPP,QNHUPP,QNHEPP,QNHTQQ,
     2 QNFT
      COMPLEX ALP(2),QNP(2),QKP(2),BTN,CRAD1(2),CRAD2(2),CAXL1(2),
     1  CAXL2(2),QKPNEW(2)
      COMPLEX       OMEG0,OMEG1,OMEG1F,OMEG1T,OMEG1U,OMEG1R,OMEG1E,
     1 OMEG1B,OMG1BO,OMG1BL,OMG1BA,OMG1BB,OMEG3A,OMEG3
       COMPLEX       OMEG02,OMEG2,OMEG2F,OMEG2T,OMEG2U,OMEG2R,OMEG2E,
     1  OMEG2B,OMG2BO,OMG2BL,OMG2BA,OMG2BB,OMEG2A
      COMPLEX AO,AL,AA(2),AB(2)
      CALL SIMSON(QNFT,FT,FT,DTHET,INTEG)
      CALL SIMSON(QNRFR(1),RFR(1,1),FR(1,1),DR(1),INTEG)
      QNRFR(2)=QNRFR(1)
      IF (INRAD .LE. 1) CALL SIMSON(QNRFR(2),RFR(1,2),FR(1,2),DR(2),
     1 INTEG)
      CALL SIMSON(QNFZ(1),FZ(1,1),FZ(1,1),DZ(1),INTEG)
      CALL SIMSON(QNFZ(2),FZ(1,2),FZ(1,2),DZ(2),INTEG)
      BTN=CSQRT(QNFT*(QNRFR(1)*QNFZ(1)+QNRFR(2)*QNFZ(2)))
      BTN=1.0/BTN
      DO 100 J=1,LIM
      FT(J)=BTN*FT(J)
      FTP(J)=BTN*FTP(J)
      ETF(J)=BTN*ETF(J)
      ETFP(J)=BTN*ETFP(J)
  100 CONTINUE
      QNFT=QNFT*BTN**2
      CALL SIMSON(QNEFT,ETF,FT,DTHET,INTEG)
      CALL SIMSON(QNEFTP,ETFP,FT,DTHET,INTEG)
      CALL SIMSON(QNERFR,ERF2,RFR(1,2),DR(2),INTEG)
      CALL SIMSON(QNERFP,ERF2P,RFR(1,2),DR(2),INTEG)
      CALL SIMSON(QNEFR,ERF2,FR(1,2),DR(2),INTEG)
      DO 200 I=1,2
      CALL SIMSON(QNGFZ(I),GF(1,I),FZ(1,I),DZ(I),INTEG)
```

```
STON 2.3 --PSR LEVEL 29<--                                        NTGRAT

      CALL SIMSON(QNGFZP(I),GFP(1,I),FZ(1,I),DZ(I),INTEG)
      CALL SIMSON(AA(I),BFFA(1,I),FZ(1,I),DZ(I),INTEG)
      CALL SIMSON (AB(I),BFFB(1,I),FZ(1,I),DZ(I),INTEG)
  200 CONTINUE
      CALL SIMSON(QNHRF,HRF,FZ(1,2),DZ(2),INTEG)
      CALL SIMSON(QNH3F,H3F,FZ(1,2),DZ(2),INTEG)
      CALL SIMSON(QNH4F,H4F,FZ(1,2),DZ(2),INTEG)
      CALL SIMSON(QNHEFP,HEFP,FZ(1,2),DZ(2),INTEG)
      CALL SIMSON(QNHTPP,HTPP,FZ(1,2),DZ(2),INTEG)
      CALL SIMSON(QNHUPP,HUPP,FZ(1,2),DZ(2),INTEG)
      CALL SIMSON(QNHEPP,HEPP,FZ(1,2),DZ(2),INTEG)
      CALL SIMSON(QNHTQQ,ALHTPP,FZ(1,2),DZ(2),INTEG)
      OMEG2F=QNFT*(QNRFR(1)*(QNGFZ(1)+QNGFZP(1))+QNRFR(2)*(QNGFZ(2)+
     1   G3*CONJG(FZ(LIM,1)*FZ(1,2))/2.0 +QNGFZP(2)))
      OMEG2T=QNFFT*QNFRFR*GAMMA*HRHOR*(QNHTPP-CHAR1*QNHRF)
      OMEG2U=QNFFT*QNFRFR*HUH*QNHUPP
      OMEG2R=QNFFT*QNFRFR*HRHOR*QNHRF
      OMEG2E=QNFFT*QNFRFR*(GAMMA*HRHOR)*(                    QNHEFP+QNHEPP)+
     1  QNFFT*QNFRFP*QNH3F+QNFFR*QNFFTP*QNH4F
      OMEG2A=QNFFT*QNFRFR*GAMMA*HRHOR*QNHTQQ
      OMG2BA=(0.0,0.0)
      OMG2BB=(0.0,0.0)
      DO 300 I=1,2
      OMG2BA=OMG2BA-(CO(I)/RO(I))**2*AA(I)*QNFT*FZP(LIM,I)*CONJG(FR(LIM,
     1 I))
      OMG2BB=OMG2BB+(CO(I)/RO(I))**2*AB(I)*QNFT*FZ(1,I)*CONJG(FR(1,I))
  300 CONTINUE
      OMG2BO=A0*FZ(1,1)*CONJG(FZ(1,1))
      IF(INDICO .GT. 0)OMG2BO=(QNP(1)**2*FZ(1,1)*CONJG(FZ(1,1))
     1   -FZP(1,1)*CONJG(FZP(1,1)))/A0
      OMG2BO=OMG2BO*QNFT*QNRFR(1)*(CO(1)/RO(1))**2
      OMG2BL=AL*FZ(LIM,2)*CONJG(FZ(LIM,2))
      IF (INDICL .GT. 0) OMG2BL=(-FZP(LIM,2)*CONJG(FZP(LIM,2))+
     1   QNP(2)**2*CONJG(FZ(LIM,2))*FZ(LIM,2))/AL
      OMG2BL=-OMG2BL*QNFT*QNRFR(2)*(CO(2)/RO(2))**2
      OMEG2B=OMG2BO+OMG2BL+OMG2BA+OMG2BB
      OMEG2=OMEG0**2+ OMEG2F+OMEG2T+OMEG2U+OMEG2R+OMEG2E+OMEG2B
      OMEG1=CSQRT(OMEG2)
      OMEG3=CSQRT(OMEG2-OMEG2T+OMEG2A)
      IF (INDIC2 .LT. 0) OMEG3=OMEG3**2
      OMEG1F=CSQRT(OMEG2-OMEG2F)
      OMEG1T=CSQRT(OMEG2-OMEG2T)
      OMEG1U=CSQRT(OMEG2-OMEG2U)
      OMEG1R=CSQRT(OMEG2-OMEG2R)
      OMEG1E=CSQRT(OMEG2-OMEG2E)
      OMEG1B=CSQRT(OMEG2-OMEG2B)
      OMG1BO=CSQRT(OMEG2-OMG2BO)
      OMG1BL=CSQRT(OMEG2-OMG2BL)
      OMG1BA=CSQRT(OMEG2-OMG2BA)
      OMG1BB=CSQRT(OMEG2-OMG2BB)
      OMEG3A=CSQRT(OMEG3**2-OMEG2A)
      IF (INDIC2 .LT. 0) OMEG1T=OMEG3A
      IF (INDIC2 .LT. 0) OMEG1=OMEG3
      QKPNEW(1)=OMEG1*RO(1)/CO(1)
      QKPNEW(2)=OMEG1*RO(2)/CO(2)
```

SION 2.3 --PSR LEVEL 29H--

```
      SUBROUTINE SIMSON(QN,V1,V2,DV,INT)
      DIMENSION V1(1),V2(1)
      COMPLEX QN,V1,V2,S
      S=V1(1)*CONJG(V2(1))+V1(INT+1)*CONJG(V2(INT+1))
      K=INT
      DO 100 I=2,K,2
      S=S+4.0*V1(I)*CONJG(V2(I))
  100 CONTINUE
      K=K-1
      IF (K .LT. 3) GO TO 300
      DO 200 I=3,K,2
      S=S+2.0*V1(I)*CONJG(V2(I))
  200 CONTINUE
  300 QN=S*DV/3.0
      RETURN
      END
```

SION 2.3 --PSR LEVEL 294--

```
      SUBROUTINE AXIAL(FN,FNP,Z,QN,C1,C2)
      COMPLEX FN,FNP,QN,C1,C2,Q1,Q2
      Q1=CCOS(Z*QN)
      Q2=CSIN(Z*QN)
      IF (CABS(QN) .EQ. 0.0) GO TO 20
      Q2=Q2/QN
      GO TO 30
   20 Q2=(1.0,0.0)
   30 FN=C1*Q1+C2*Q2
      FNP=-C1*Q2*QN**2+C2*Q1
      RETURN
       END
```

```
ISION 2.3 --PSR LEVEL 298--

      SUBROUTINE TNGIAL(FN,FNP,THET,M,C1,INDIC1)
      COMPLEX FN,FNP,C1
      XM=M
      IF (INDIC1 .GT. 0) GO TO 50
      FN=C1*COS(XM*THET)
      FNP=-C1*XM*SIN(XM*THET)
      RETURN
   50 FN=C1*CEXP(CMPLX(0.0,XM*THET))
      FNP=CMPLX(0.0,XM)*FN
      RETURN
      END
```

```
RSION 2.3 --PSR LEVEL 29H--

      SUBROUTINE RADIAL (FN,FNP,R,ALP,C1,C2,M)
      COMPLEX FN,FNP,ALP,C1,C2,Q1,Q2,Q3,Q4
      Q3=(0.0,0.0)
      Q4=(0.0,0.0)
      CALL QJFUN(Q2,Q1,R*ALP,M)
      IF(CABS(C2) .NE. 0.0) CALL QYFUN(Q4,Q3,R*ALP,M)
      FN=C1*Q1+C2*Q3
      IF (R .EQ. 0.0) GO TO 50
      FNP=-Q2*C1/R-Q4*C2/R
      RETURN
   50 IF (M .EQ. 1) FNP=ALP/2.0 *C1
      IF (M .NE. 1) FNP=(0.0,0.0)
      RETURN
      END
```

```
ISTON 2.3 --PSR LEVEL 29R--

      SUBROUTINE OJFUN(FN,FNP,Z,M)
      COMPLEX FN,FNP,Z,A,ZD2,ZD2S,S,T,Q1,Q2,Q3
      A=(0.0,0.0)
      ZD2=Z/2.0
      ZD2S=ZD2**2
      IF (M .EQ. 0)  GO TO 500
      XM =M
      S=1.0/FACT(M)
      T=ZD2
      IF (CABS(T) .EQ. 0.0) T=(1.0,0.0)
      TST=CABS((A+XM+1.0)/(T**M))
      XK=1.0
      FN=(A-XM)*S
      FNP=S
  100 S=S*ZD2S/(XK*(XK+XM))
      T=ZD2S/((XK+1.0)*(XM+XK+1.0))
      Q3=A-XM-2.0*XK
      Q1=T*(Q3-2.0)
      Q2=Q1*(XK+1.0+XM/2.0)
      Q1=(Q1-Q3)*S
      Q2=(T-1.0)*S
      FN=FN+Q1
      FNP=FNP+Q2
      IF (CABS(Q1)/TST .LT. 1.0E-8 .AND. CABS(Q2)/TST .LT. 1.0E-8)
     1  GO TO 200
      XK=XK+2.0
      S=S*T
       GO TO 100
  200 FN=FN*ZD2**M
      FNP=FNP*ZD2**M
      RETURN
  500 TST=CABS(A+1.0)
      S=1.0
      XK=1.0
      FNP=2.0*ZD2S
      FN=A+FNP
      FNP=S
  600 S=S*ZD2S/(XK*XK)
       T=ZD2S/((XK+1.0)*(XK+1.0))
      Q3=2.0*ZD2S+XK*A
       Q2=((Q3+A)*T-Q3)*S
       Q1=(T*(2.0*ZD2S/(XK+2.0)+A)-(2.0*ZD2S/(XK+1.0)+A))*S
      Q2=(T-1.0)*S
      FN=FN+Q1
      FNP=FNP+Q2
      IF (CABS(Q1)/TST .LT. 1.0E-8 .AND. CABS(Q2)/TST .LT. 1.0E-8)
     1  GO TO 700
      XK=XK+2.0
      S=S*T
      GO TO 600
  700 CONTINUE
  750 RETURN
      END
```

```
RSION 2.3 --PSR LEVEL 29B--

      SUBROUTINE CYFUN(FN,FNP,Z,M)
      COMPLEX FN,FNP,Z,A,Z02,Z02S,S,T,Q1,Q2,Q3,Q4,GN,GNP
      A=(0.0,0.0)
      IF (CABS(Z).GT. 1.0E-5) GO TO 10
      FN=1.0E30
      FNP=1.0E30
      RETURN
   10 Z02=Z/2.0
      Z02S=Z02**2
      IF (M.EQ.0) GO TO 500
       Q4= CLOG(Z02)*2.0
       FN=0.0
      FNP=0.0
      XM=M
      S=Z02**(-M)
      DO 50 L=1,M
       K=L-1
       XK=K
      Q1=2.0*Z02S*FACT(M-K-2)
      Q2=(A+XM)*FACT(M-K-1)
      Q3=S/FACT(K)
      FN=FN+(Q1-Q2)*Q3
      FNP=FNP-FACT(M-K-1)*Q3
      S=S*Z02S
   50 CONTINUE
      GN=FN
      GNP=FNP
      PSI1=-.5772156649
      PSI2=PSI1
      DO 60 L=1,M
      XL=L
      PSI2=PSI2+1.0/XL
   60 CONTINUE
      S=1.0/FACT(M)
      XK=1.0
      TST=CABS((A+XM+1.0)/(Z02)**M)
      Q4=Q4-PSI1-PSI2
      FNP=(A-XM)*Q4
      FN=(FNP-2.0)*S
      FNP=Q4*S
  100 Q4=Q4-(1.0/XK+1.0/(AK+XM))
      T=Z02S/((XK+1.)*(AM+XK+1.))
      S=S*Z02S/(XK*(XK+XM))
      PSI1=(1.0/(XM+XK+1.)+1./(XK+1.))
      Q3=A-XM-2.0*XK
      Q1=(Q4*(T*(Q3-2.0)-Q3)+2.0*(1.0-T)-(Q3-2.0)*T*PSI1)*S
      Q2=S*(Q4*(T-1.0)-T*PSI1)
      FN=FN+Q1
      FNP=FNP+Q2
      IF (CABS(Q1)/TST .LT. 1.0E-8 .AND. CABS(Q2)/TST .LT. 1.0E-8)
     1  GO TO 200
      Q4=Q4-PSI1
      S=S*T
      AK=XK+2.
```

```
      GO TO 100
  200 FN=(FN*ZD2**M+GN)/3.14159265
      FNP=(FNP*ZD2**M+GNP)/3.14159265
      RETURN
  500 TST=CABS(A+1.)
      S=1.
      Q4=CLOG(ZD2)+.5772156649
      XK=1.
      FN=(A+2.*ZD2S)
      FNP=Q4
      FN=FN*Q4    -ZD2S
  600 Q4=Q4-1./XK
      T=ZD2S/((XK+1.)**2)
      S=S*ZD2S/(XK*XK)
      PSI1=1./(XK+1.)
      Q3=2.*ZD2S
      Q1=(Q4*(A*(T-1.)+Q3*(T/(XK+2.)-PSI1))-PSI1*T*(A+Q3/(XK+2.))+
     1    ZD2S*(PSI1**2-T/((XK+2.)**2)))*S
      Q2=S*(Q4*(T-1.0)-T*PSI1)
      FN=FN+Q1
      FNP=FNP+Q2
      IF (CABS(Q1)/TST .LT. 1.0E-8 .AND. CABS(Q2)/TST .LT. 1.0E-8)
     1  GO TO 700
      XK=XK+2.
      S=S*T
      Q4=Q4-PSI1
      GO TO 600
  700 FN=(FN-1.)/1.57079632
      FNP=FNP/1.57079632
      RETURN
      END
```

```
RSION 2.3 --PSR LEVEL 294--

      FUNCTION FACT(N)
       DIMENSION G(20)
      DATA (G(I),I=1,20)/1.,2.,6.,24.,120.,720.,5040.,40320.,362880.,
     1    3628800.,3.991680E7,4.790016E8,6.227020E9,8.717829I2E10,
     2     1.3076743?E12,2.092278?99E13,3.556874?8E14,6.4023737E15,
     3      1.216451E17,2.432902E18/
       IF (N) 10,20,30
   10 FACT=0.0
      RETURN
   20 FACT=1.
      RETURN
   30 IF (N .GT. 20) GO TO 40
      FACT=G(N)
      RETURN
   40 X=N
      FACT=SQRT(6.2831853*X)*(X/2.71828)**N
      RETURN
      END
```

```
      SUBROUTINE INTERP(R,Q)
      COMMON /MUQ/ RMUQ(21),XMUQ(21),NMUQ,LASINT
      IF(R .LT. RMUQ(1) .OR. R .GT. RMUQ(NMUQ)) GO TO 500
      K=MOD(LASINT,NMUQ)
      IF (K .LE. 0) K=1
   20 IF (K .EQ. 0) K=NMUQ-1
      IF(R .GT. RMUQ(K+1) .OR. R .LT. RMUQ(K)) GO TO 50
      J=K
      GO TO 200
   50 CONTINUE
      K=MOD(K+1,NMUQ)
      IF (K .EQ. LASINT) GO TO 500
      GO TO 20
  200 LASINT=J
      DR=(R-RMUQ(J))/(RMUQ(J+1)-RMUQ(J))
      Q=XMUQ(J)+DR*(XMUQ(J+1)-XMUQ(J))
      RETURN
  500 Q=0.0
      LASINT=1
      RETURN
      END
```

REFERENCES

1. Dix, D. M., Duffield, P. L., and Smith, J. E., Propulsion System Flow Stability Program (Dynamic), Part XII - Unsteady Combustion in Duct Burners and Afterburners (AFAPL-TR-68-142), Air Force Aero Propulsion Laboratory, Air Force Systems Command, Wright-Patterson Air Force Base, Ohio, December, 1968.

2. Dix, D. M. and Smith, G. E., Propulsion System Flow Stability Program (Dynamic), Part IX - Combustion Instability Model Program Description and Parametric Study Results (AFAPL-TR-69-113), Air Force Aero Propulsion Laboratory, Air Force Systems Command, Wright-Patterson Air Force Base, Ohio, February, 1970.

3. Smith, G. E. and Bastress, E. K., Propulsion System Flow Stability Program (Dynamic), Part X - Combustion Instability Model Program User's Manual (AFAPL-TR-69-113), Air Force Aero Propulsion Laboratory, Air Force Systems Command, Wright-Patterson Air Force Base, Ohio, February, 1970.

4. Dix, D. M. and Smith, G. E., Analysis of Combustion Instability in Aircraft Engine Augmenters (AIAA Paper No. 71-700), American Institute of Aeronautics and Astronautics, New York.

5. Marino, P. A., et al, A Study of the Suppression of Combustion Oscillations with Mechanical Damping Devices (PWA FR-2596), Pratt & Whitney Aircraft, Florida Research and Development Center, November, 1967.

6. Shapiro, A. H., The Dynamics and Thermodynamics of Compressible Fluid Flow, The Ronald Press Company, N. Y., Volume I, 1953.

UNCLASSIFIED
Security Classification

DOCUMENT CONTROL DATA - R & D

(Security classification of title, body of abstract and indexing annotation must be entered when the overall report is classified)

1. ORIGINATING ACTIVITY *(Corporate author)*
Northern Research and Engineering Corporation (NREC)
219 Vassar Street
Cambridge, Mass. 02139

2a. REPORT SECURITY CLASSIFICATION
UNCLASSIFIED

2b. GROUP
—

3. REPORT TITLE
INVESTIGATION OF COMBUSTION INSTABILITY IN A TURBOFAN MIXED-FLOW AUGMENTOR

4. DESCRIPTIVE NOTES *(Type of report and inclusive dates)*
Final Technical Report (70 June 30 to 72 February 29)

5. AUTHOR(S) *(First name, middle initial, last name)*
George E. Smith (NREC) and Robert E. Henderson (USAF-APL)

6. REPORT DATE	7a. TOTAL NO. OF PAGES	7b. NO. OF REFS
April 1972	201	6

8a. CONTRACT OR GRANT NO.	9a. ORIGINATOR'S REPORT NUMBER(S)
F33615-70-C-1669 NEW b. PROJECT NO. 3066	1161-1
c.	9b. OTHER REPORT NO(S) *(Any other numbers that may be assigned this report)*
d.	AFAPL-TR-72-4

10. DISTRIBUTION STATEMENT Distribution limited to U. S. Government agencies only; Test and Evaluation: February 1972. Other requests for this document must be referred to the Air Force Aero Propulsion Laboratory (AFAPL/TBC), Wright-Patterson Air Force Base, Ohio 45433.

11. SUPPLEMENTARY NOTES	12. SPONSORING MILITARY ACTIVITY
—	Air Force Aero Propulsion Laboratory Air Force Systems Command Wright-Patterson Air Force Base, Ohio 45433

13. ABSTRACT

An analytical and experimental investigation was conducted of combustion instability in a TF-30-P1 augmentor. A sustained oscillation was observed with a fuel zone combination which does not occur during normal engine operation. On cold days oscillation amplitudes above 35 per cent (peak-to-mean) were observed, but on hot days the amplitudes dropped below 10 per cent. NREC's previously developed combustion instability model correctly predicted an instability with the same frequency as that observed. Once the individual zones of combustion of the TF-30-P1 augmentor were modelled properly, the analysis correctly indicated the fuel zone combination during which the oscillation becomes most severe. The analytical model also correctly predicted the trends which were observed when engine geometry was modified, when AVGAS replaced JP-4, and when the engine inlet temperature was low. But to correlate predicted and observed amplitude levels, a stabilizing turbulent mixing effect had to be hypothesized to supplement the droplet vaporization effects which excite the instability.

DD FORM 1 NOV 68 1473 REPLACES DD FORM 1473, 1 JAN 64, WHICH IS OBSOLETE FOR ARMY USE.

UNCLASSIFIED
Security Classification

14 KEY WORDS	LINK A		LINK B		LINK C	
	ROLE	WT	ROLE	WT	ROLE	WT
Afterburners						
Augmentors						
Turbofans						
Combustion						
Combustion Instability						
Oscillatory Combustion						